VLÁKNA a TEXTIL

4

Volume 25.
December
2018

FIBRES AND TEXTILES

STU FCHPT

TECHNICAL UNIVERSITY OF LIBEREC
Faculty of Textile Engineering

Trenčianska univerzita Alexandra Dubčeka v Trenčíne
Fakulta priemyselných technológií v Púchove

VÚCHV

VÚTCH CHEMITEX

Spoločnosť priemyselnej chémie ZSVTS

CHEMOSVIT FIBROCHEM

Indexed in:
SCOPUS
Chemical Abstracts
World Textiles

ISSN 1335-0617
print version

ISSN 2585-8890
online version

Fibres and Textiles
Vlákna a textil

Published by	*Vydáva*
• Slovak University of Technology in Bratislava, Faculty of Chemical and Food Technology	• Slovenská technická univerzita v Bratislave, Fakulta chemickej a potravinárskej technológie
• Technical University of Liberec, Faculty of Textile Engineering	• Technická univerzita v Liberci, Fakulta textilní
• Alexander Dubček University of Trenčín, Faculty of Industrial Technologies	• Trenčianska univerzita Alexandra Dubčeka v Trenčíne, Fakulta priemyselných technológií
• Slovak Society of Industrial Chemistry, Bratislava	• Slovenská spoločnosť priemyselnej chémie, Bratislava
• Research Institute of Man-Made Fibres, JSC, Svit	• Výskumný ústav chemických vlákien, a.s. Svit
• VÚTCH – CHEMITEX, Ltd., Žilina	• VÚTCH – CHEMITEX, spol. s r.o., Žilina
• Chemosvit Fibrochem, JSC, Svit	• Chemosvit Fibrochem, a.s., Svit

Editorial office and distribution of the journal
(Redakcia a distribúcia časopisu)

Ústav prírodných a syntetických polymérov
Fakulta chemickej a potravinárskej technológie
Slovenská technická univerzita v Bratislave
Radlinského 9, 812 37 Bratislava, SK
Tel: 00 421 2 59 325 575
e-mail: marcela.hricova@stuba.sk

Order and advertisement of the journal
(Objednávka a inzercia časopisu)

Slovenská spoločnosť priemyselnej chémie,
člen Zväzu vedecko-technických spoločností
Radlinského 9, 812 37 Bratislava, SK
Tel: 00 421 2 59 325 575
e-mail: marcela.hricova@stuba.sk

Order of the journal from abroad – excepting Czech Republic
Objednávka časopisu zo zahraničia – okrem Českej Republiky

SLOVART G.T.G, s.r.o. EXPORT-IMPORT
Krupinská 4, P.O.Box 152, 852 99 Bratislava, SK
Tel: 00421 2 839 471-3, Fax: 00421 2 839 485
e-mail: info@slovart-gtg.sk

Typeset and printing *(Sadzba a tlač)*

FOART, s.r.o., Bratislava

Journal is published 4x per year
Subscription 60 EUR

Časopis vychádza 4x ročne
Ročné predplatné 60 EUR

Evidenčné číslo MKCR SR Bratislava EV 4006/10

Fibres and Textiles (4) 2018
Vlákna a textil (4) 2018
December 2018

Content

ROLE OF CARBON MICROFIBERS ON ELEVATED TEMPERATURE PROPERTIES OF GEOPOLYMERS

Promoda Behera[1], Vijay Baheti[1], Jiri Militky[1], Petr Louda[2] and Salman Naeem[1]

[1]Department of Material Engineering, Faculty of Textile Engineering, Technical University of Liberec
[2]Department of Material Science, Faculty of Mechanical Engineering, Technical University of Liberec
Studentska 2, Liberec 46117, Czech Republic
vijaykumar.baheti@tul.cz

Abstract: *The present work deals with the effect of carbon microfiber addition on the development of microstructure and mechanical properties of geopolymers at elevated temperature. The carbon microfibers were prepared from recycled inexpensive carbon fibrous wastes by ball milling and then subsequently incorporated under 5, 10 and 15 wt.% loading into metakaoline based geopolymers. The addition of carbon microfibers was found to produce compact structure of geopolymers due to their pore filling characteristics and formation of additional calcium silicate or calcium alumino-silicate and sodium alumino-silicate hydrates. The geopolymer composite of 15 wt.% carbon microfiber was found to maintain the residual compressive strengths of 33.55 and 23.96 MPa at 400 and 800°C, respectively and thus recording a minimum strength loss of 19 and 42%, respectively. This behavior was attributed to decreased thermal stresses and restricted swelling of unreacted geopolymer phases after addition of carbon microfibers.*

Keywords: *Carbon microfibers; geopolymer; thermal stability; mechanical strength; microstructure analysis.*

1 INTRODUCTION

In recent years, geopolymers have received considerable attention for their cost efficiency, chemical stability, corrosion resistance, rapid strength gain rate, low density, low permeability, low shrinkage and freeze-thaw resistance [1, 2]. In addition, geopolymers are considered as an attractive replacement to ordinary Portland cement due to reduced energy consumption and less CO_2 emission during their manufacture [3-5]. The geopolymers are amorphous cementitious binders having cross-link chain of silica, oxygen and alumina (Si-O-Al) [6, 7]. They are synthesized by reacting aluminosilicate source materials (i.e. fly ash, slag, metakaoline, etc.) with highly alkaline activators. Despite many benefits, geopolymers still have certain limitations over ordinary Portland cement. Due to their cross-linked structure, geopolymers tend to be more brittle, susceptible to crack formation and undergo catastrophic failure as compared to ordinary Portland cement [8, 9]. Previous studies have reported their fracture energy about 40% of that of ordinary Portland cement [10]. Therefore, for further improvements of performance and durability, the improvement in fracture properties of geopolymers is extremely necessary. Although incorporation of different fibers (steel, polypropylene, polyvinyl chloride, and basalt fibers) have been found to be effective in controlling crack propagation and enhancing the fracture energy of geopolymers, the mechanical properties of geopolymers were found non-consistent and inadequate when exposed to elevated temperatures [11-13]. During fire accidents, many of these fibers fail in providing effective reinforcements due to lack of structural strength and durability at higher temperature[14]. Therefore, further research is required to identify alternative fibers which possess good thermal resistance and maintain higher residual mechanical properties when exposed to elevated temperature. The present work deals with the effect of carbon microfiber addition on the development of microstructure and mechanical properties of geopolymers at elevated temperature. The carbon microfibers were prepared from recycled inexpensive carbon fibrous wastes by ball milling, and then subsequently incorporated under 5, 10 and 15 wt.% loading into metakaoline based geopolymers. Further, the composites were examined for change in microstructure, mechanical properties and toughening mechanisms after exposure to the elevated temperatures of 200, 400, and 800°C. To the best of the authors' knowledge, this is the first study on elevated temperature properties of geopolymers filled with carbon microfibers obtained from carbon fibrous wastes.

2 EXPERIMENTAL METHODS

2.1 Materials

The recycled carbon materials under trade name carbiso mil 100 μ were purchased from Easy composites, UK. The Baucis L110 alumino-silicate geopolymer binder based on metakaoline was obtained from Ceske Lupkove Zavody, Czech Republic along with sodium alkali activator. The chemical composition of the kaolin was as follows [wt.%]: SiO_2 47, Al_2O_3 24, LOI 0.5, Fe_2O_3 0.50, TiO_2 0.8, MgO 3.5, K_2O 0.40, CaO 17.5. The mean particle size (d50) was 5 µm. The alkali activator was mixture of Na_2SiO_3/NaOH in mass ratio of 2.0.

2.2 Preparation of carbon microfibers (CMF)

The size of carbiso mil 100 µ particles was further refined to the micro-scale using ball milling based on previous research experience [15, 16]. The 30 min grinding was carried out by high-energy planetary ball mill (Fritsch Pulverisette 7, Germany) in a sintered corundum container of 80 ml capacity using zirconium balls of 10 mm diameter. The ball to material ratio was kept at 10:1 and the speed was kept at 850 rpm. Later, Malvern zetasizer nano series based on dynamic light scattering principle of Brownian motion of particles was employed to characterize the particle size distribution of dry milled carbon particles. Deionized water was used as dispersion medium and it was ultrasonicated for 5 min with bandelin ultrasonic probe before characterization. In addition, microstructure of carbon particles was observed on scanning electron microscope (SEM) of Hitachi–model TM-3000 at accelerated voltage of 15 kV.

2.3 Preparation of carbon microfiber/ /geopolymer composites (CMF+G)

The geopolymer (G) was synthesized from calcined kaolin and shale clay residues with Si/Al ratio of 2.0. The four parts of sodium alkali activator and five parts of metakaoline based geopolymer were manually mixed for 10 min to ensure homogeneous preparation of geopolymer binders. For preparation of geopolymer composites, the carbon microfibers were initially pre-dried for 60 min at 70°C in an oven. Next, the carbon microfibers were added into the prepared geopolymer binder at 5 wt.% (5% CMF+G), 10 wt.% (10% CMF+G) and 15 wt.% (15% CMF+G) loading. The mixing was homogeneously done in Hobart mixer for 5 min. Subsequently, the fresh prepared composite mortar was poured into 40 mm cubic-shaped moulds, vibrated for 2 minutes on the vibration table to remove air voids and wrapped using a thin plastic sheet to prevent water evaporation. The wrapped samples were demolded after 24 h of casting and then cured at room temperature (20±2°C) and a relative humidity of (70±10%) for 28 days.

2.4 Exposure to elevated temperature

The prepared geopolymer composites were exposed to elevated temperatures of 200, 400 and 800°C at age of 28 days. The specimens were placed into a furnace (Elektrické Pece Svoboda, Czech Republic) and heated at fixed heating rate of 5°C/min. As soon as the target temperature was attained, it was maintained for an additional 60 min. The furnace was then shut down to allow the specimens in the furnace to cool down to room temperature. Meanwhile, the unexposed specimens were left undisturbed at ambient condition.

2.5 Characterization of carbon microfiber/ /geopolymer composites

Physical properties: The hardness of geopolymer composites was measured on the Rockwell H scale using an Avery Rockwell hardness tester. The samples were polished with emery paper to achieve flat and smooth surfaces before the measurement. Furthermore, the values of bulk density was determined in accordance with the ASTM Standard (C-20) and calculated using the Eq. (1). The test was repeated for 5 samples and an average of measurements was taken.

$$Bulk\ density = \frac{W_d}{W_a - W_w} \tag{1}$$

where W_d is weight of the dried sample, W_w is weight of the sample suspended in water and W_a is weight of sample saturated in air.

Microstructure analysis: The low vacuum scanning electron microscopy (SEM) of Hitachi–model TM-3000, coupled with X-rays microanalysis system of energy dispersive spectroscopy was employed to investigate the microstructure of geopolymer composites. It was carried out at 15 kV accelerated voltage. The samples were directly observed under the SEM without metallic coating due to low vacuum operations. The images were formed by acquisition of backscattered electrons at different magnifications.

Compression strength: The geopolymer composites were tested for compression testing using LaborTech universal testing machine, Czech Republic, with load cell capacity of 2000 kN. The 40 mm cubes were tested for the determination of compression strength according to ASTM C109 standard. The test was repeated for 5 specimens and an average of measurements was taken.

3 RESULTS AND DISCUSSION

3.1 Microstructure analysis

The CMF particles of around 10 µm diameter were obtained after the ball milling of carbiso particles. The SEM micrographs of neat geopolymer and geopolymer composites at different temperature exposure are shown in Figure 1. The microstructure of dense and homogeneous matrix consisting mainly of alumino-silicate gel can be observed for all samples before exposure to the elevated temperatures. The smooth surfaces of carbon fibers in the geopolymer matrix indicated no degradation of carbon fibers under action of alkali in the activating solution. The strong adhesion between the geopolymer gel and the surface of the fiber can be confirmed based on presence of geopolymer layer on fiber ends pulled out from the matrix and more striations on fiber surfaces. When the samples exposed to elevated temperatures, the geopolymer composites showed lower micro structural deterioration than neat geopolymers due to mechanical percolation along with pore filling effects of carbon microfibers [17]. The carbon microfibers did not exhibit any observable degradation after elevated temperature exposure. This indicated the thermal resistance characteristics of carbon microfibers that can continue to provide the reinforcement to geopolymers when exposed to higher temperatures and therefore less strength loss.

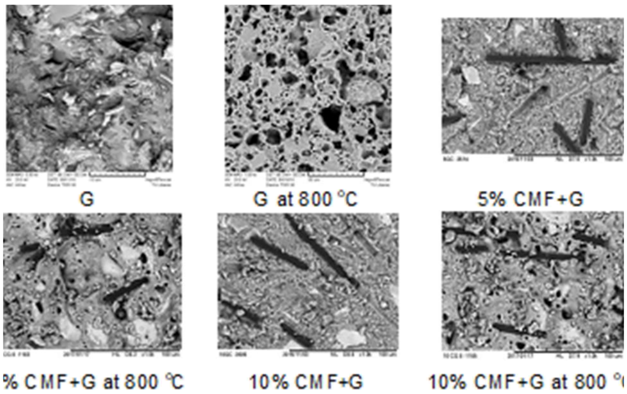

Figure 1 Microstructure of geopolymer composites

3.2 Physical properties

Table 1 illustrates the physical properties (i.e. hardness Vickers Pyramid Number HV and bulk density [g/cm^3]) of the neat geopolymer and its composites before and after exposure to elevated temperature. The density was found to reduce with increase in carbon microfiber loading. The carbon microfiber filled geopolymers exhibited significant increase in viscosity due to high aspect ratio and smooth light surfaces of microfibers. This subsequently resulted into the entrapment of more air and thus possible reduction in density of geopolymer composites than neat geopolymers [18]. The higher hardness of geopolymer composites over neat geopolymers can be ascribed to the extra precipitation of Calcium Alumina Silicate hydrates formation due to nucleating sites present on carbon microfibers [19]. When exposed to elevated temperature of 200, 400 and 800°C, all the samples showed reduction in bulk density and hardness values. The neat geopolymers became more porous than geopolymer composites when exposed to elevated temperatures. This behavior can be attributed to evaporation of water and increase in Si/Al ratio as temperature increased [20, 21]. A similar phenomenon was observed previously which resulted in foam like structures by formation and growth of bubbles with increasing the Si/Al ratio [22]. The intact structure of geopolymer composites at elevated temperatures can be attributed to the pore-filling effect of carbon microfibers.

Table 1 Physical properties of geopolymer composites

Temperature [°C]	G		5% CMF+G		10% CMF+G		15% CMF+G	
	HV	ρ [g/cm^3]	HV	ρ [g/cm^3]	HV	ρ [g/cm^3]	HV	ρ [g/cm^3]
30	536	1.51	558	1.48	569	1.49	562	1.48
200	395	1.49	489	1.44	494	1.51	482	1.48
400	290	1.42	435	1.40	482	1.36	577	1.35
800	330	1.31	367	1.27	371	1.26	379	1.22

3.3 Compression strength

Table 2 shows the compression strength [MPa] results of geopolymer and geopolymer composites before and after exposure to elevated temperatures. The geopolymer composites showed higher compression strength than neat geopolymers over all range of temperature exposures. The neat geopolymer indicated a typical brittle failure mode, whereas geopolymer composites exhibited an extended period of plastic deformation (i.e. pseudoplastic behavior) unlike short drop at the point of maximum load. This non-linear behavior of geopolymer composites can be explained from the fiber-bridging and sliding after debonding and pulling-out of carbon fibers from the geopolymer matrix. This further indicated more favorable interaction between carbon microfibers and the matrix possibly due to a combination of physical and chemical bonding. With increase in temperature till 200°C, all samples showed increase in compression strength. This behavior was attributed to the formation of discontinuous nano-pores and dehydration shrinkage of geopolymers due to expel of free water at 200°C. However, the compression strength deteriorated for all samples at 400 and 800°C. This behavior can be attributed to thermal incompatibility (i.e. differential thermal expansion between geopolymer and carbon microfibers), pore pressure effects (i.e. movement of free water and hydroxyls) and possible phase transition in geopolymers at elevated temperature. The less deterioration for geopolymer composites indicated the thermal resistance characteristics of geopolymers after the addition of carbon microfibers, which further decreased the thermal stresses and restricted the swelling of unreacted geopolymer phases.

Table 2 Compression strength [MPa] at elevated temperature

Temperature [°C]	G	5% CMF+G	10% CMF+G	15% CMF+G
30	28±3	39±4	44±4	41±4
200	37±4	44±5	49±5	45±5
400	15±3	24±3	30±3	34±4
800	11±5	20±4	21±4	24±4

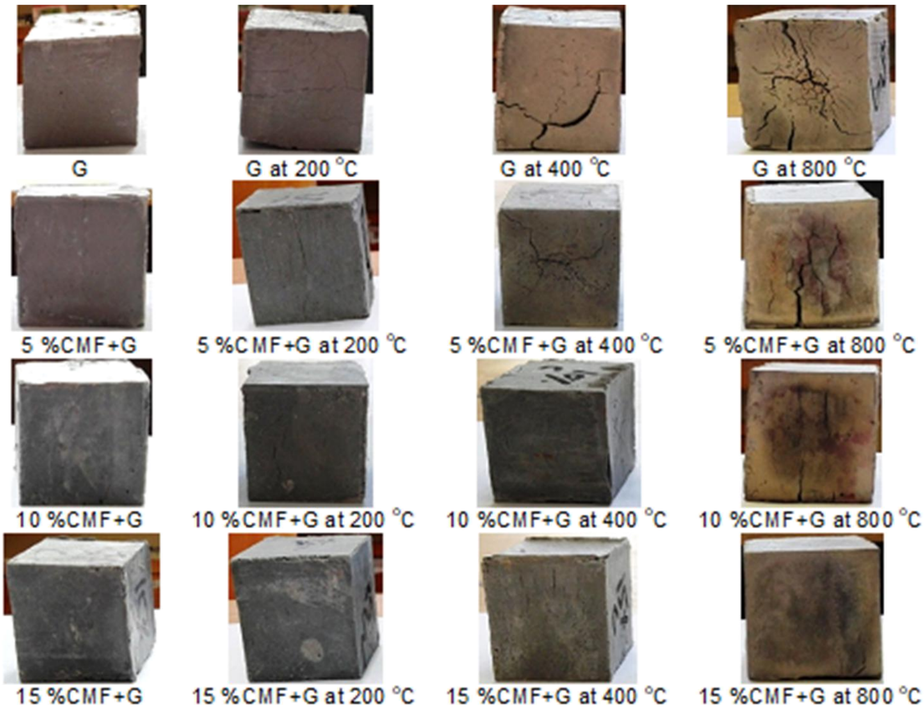

Figure 2 Physical observations of composites after exposure to elevated temperature

3.4 Physical observations

Figure 2 illustrates photographs of the physical observation of the neat geopolymers and geopolymer composites when exposed to the elevated temperatures of 200, 400, and 800°C, respectively. The neat geopolymers showed increased amount, width and length of thermal cracks than geopolymer composites. The cracks further increased with increasing the elevated temperatures. The development of cracks at higher temperature exposure can be explained from dehydration/ dehydroxylation of the geopolymers and the volumetric expansion of unreacted silicon dioxide [23]. The intact original structural characteristics with minimum development of thermal cracks in case of geopolymer composites were found due to the presence of high thermal resistant thin carbon microfibers which possibly bridged the cracks when exposed to the elevated temperatures [24].

4 CONCLUSIONS

In present study, the role of carbon microfibers for improvement in elevated temperature properties of geopolymer composites was studied. The carbon microfibers were produced by 30 min dry pulverization of short carbon fibrous wastes in high energy planetary ball milling. The geopolymer composites were prepared by addition of 5, 10 and 15 wt.% of carbon microfibers and later exposed to the elevated temperatures of 200, 400, and 800°C. Further, the carbon microfiber/geopolymer composites were evaluated for physical properties, microstructural analysis and compression strength. The addition of carbon microfibers was found to produce compact structure of geopolymers due to their pore filling characteristics and formation of additional calcium silicate or calcium alumino-silicate and sodium alumino-silicate hydrates. The presence of geopolymer layer on surface of fiber ends pulled out from matrix indicated strong adhesion between the geopolymer and the carbon microfibers. The carbon microfibers did not exhibit any observable degradation after elevated temperature exposure, which indicated their thermal resistance characteristics. Furthermore, more number of curvilinear small cracks was found in case of geopolymer composites due to crack deflections by carbon microfibers. Therefore, the addition of carbon microfibers ensured the effective toughening mechanism to prevent the catastrophic fracture of geopolymers. When samples exposed to elevated temperatures, the compression strength deteriorated for all samples at 400 and 800°C. This behavior was attributed to thermal incompatibility (i.e. differential thermal expansion between geopolymer and carbon microfibers), pore pressure effects (i.e. movement of free water and hydroxyls) and possible phase transition in geopolymers at elevated temperature. The less deterioration for geopolymer composites indicated the thermal resistance characteristics of geopolymers after the addition of carbon micro fibers, which further decreased the thermal stresses and restricted the swelling of unreacted geopolymer phases. In this way, the carbon microfibers filled geopolymers could be suitable for high temperature applications in thermal barrier coatings and panels.

5 REFERENCES

1. Suwan T., Fan M., Braimah N.: Micro-mechanisms and compressive strength of Geopolymer-Portland cementitious system under various curing temperatures, Material Chemistry and Physics180(1), 2016, pp. 219-225, doi: 10.1016/j.matchemphys.2016.05.069
2. Zhou W., Yan C., Duan P., Liu Y., Zhang Z., Qiu X., et al.: A comparative study of high- and low-Al_2O_3 fly ash based-geopolymers: The role of mix proportion factors and curing temperature, Materials & Design 95, 2016, pp. 63-74, doi: 10.1016/j.matdes.2016.01.084
3. Alomayri T., Shaikh F.U.A., Low I.M.: Effect of fabric orientation on mechanical properties of cotton fabric reinforced geopolymer composites, Materials & Design 57, 2014, pp. 360-365, doi: 10.1016/j.matdes.2014.01.036
4. Aliabdo A.A., Abd Elmoaty A.E.M., Salem H.A.: Effect of water addition, plasticizer and alkaline solution constitution on fly ash based geopolymer concrete performance, Construction and Building Materials 121, 2016, pp. 694-703, doi: 10.1016/j.conbuildmat.2016.06.062
5. Kong D.L.Y., Sanjayan J.G.: Damage behavior of geopolymer composites exposed to elevated temperatures, Cement and Concrete Composites 30(10), 2008, pp. 986-991, doi: 10.1016/j.cemconcomp.2008.08.001
6. Su H., Xu J., Ren W.: Mechanical properties of geopolymer concrete exposed to dynamic compression under elevated temperatures, Ceramics International 42(3), 2015, pp. 3888-98, doi: 10.1016/j.ceramint.2015.11.055
7. Zhang H.Y., Kodur V., Wu B., Cao L., Wang F.: Thermal behavior and mechanical properties of geopolymer mortar after exposure to elevated temperatures, Construction and Building Materials 109, 2016, pp. 17-24, doi: 10.1016/j.conbuildmat.2016.01.043
8. Shaikh F.U.A, Hosan A.: Mechanical properties of steel fibre reinforced geopolymer concretes at elevated temperatures, Construction and Building Materials 114, 2016, pp. 15-28, doi: 10.1016/j.conbuildmat.2016.03.158
9. Sarker P.K., Kelly S., Yao Z.: Effect of fire exposure on cracking, spalling and residual strength of fly ash geopolymer concrete, Materials & Design 63, 2014, pp. 584-592, doi: 10.1016/j.matdes.2014.06.059
10. Saafi M., Andrew K., Tang P.L., McGhon D., Taylor S., Rahman M., et al.: Multifunctional properties of carbon nanotube/fly ash geopolymeric nano-composites, Construction and Building Materials 49, 2013, pp. 46-55, doi: 10.1016/j.conbuildmat.2013.08.007
11. Abbasi S.M., Ahmadi H., Khalaj G., Ghasemi B.: Microstructure and mechanical properties of a metakaolinite-based geopolymer nanocomposite reinforced with carbon nanotubes, Ceramics International 42(14), 2016, pp. 15171-15176, doi: 10.1016/j.ceramint.2016.06.080
12. Yuan J., He P., Jia D., Yang C., Zhang Y., Yan S., et al.: Effect of curing temperature and SiO_2/K_2O molar ratio on the performance of metakaolin-based geopolymers, Ceramics International 42(14), 2016, pp. 16184-16190, doi: 10.1016/j.ceramint.2016.07.139
13. Abdulkareem O.A., Mustafa Al., Bakri A.M., Kamarudin H., Khairul Nizar I., Saif A.A.: Effects of elevated temperatures on the thermal behavior and mechanical performance of fly ash geopolymer paste, mortar and lightweight concrete, Construction and Building Materials 50, 2014, pp. 377-387, doi: 10.1016/j.conbuildmat.2013.09.047
14. Kong D.L.Y., Sanjayan J.G.: Effect of elevated temperatures on geopolymer paste, mortar and concrete, Cement and Concrete Research 40(2), 2010, pp. 334-339, doi: 10.1016/j.cemconres.2009.10.017
15. Baheti V., Marsalkova M., Abbasi R., Militky J.: Comparison of wet milling action for fibrous and solid materials, Vlakna a Textil (Fibres and Textiles) 19(1), 2012, pp. 3-7
16. Baheti V., Naeem S., Militky J., Okrasa M., Tomkova B.: Optimized preparation of activated carbon nanoparticles from acrylic fibrous wastes, Fibers and Polymers 16(10), 2015, pp. 2193-2201, doi: 10.1007/s12221-015-5364-0
17. Behera P., Baheti V., Militky J., Louda P.: Elevated temperature properties of basalt microfibril filled geopolymer composites, Construction and Building Materials 163, 2018, pp. 850-860, doi: 10.1016/j.conbuildmat.2017.12.152
18. Masi G., Rickard W.D.A., Bignozzi M.C., Van Riessen A.: The effect of organic and inorganic fibres on the mechanical and thermal properties of aluminate activated geopolymers, Composites Part B Engineering 76, 2015, pp. 218-228, doi: 10.1016/j.compositesb.2015.02.023
19. Khater H.M., Abd El Gawaad H.A.: Characterization of alkali activated geopolymer mortar doped with MWCNT, Construction and Building Mater 102, 2016, pp. 329-337, doi: 10.1016/j.conbuildmat.2015.10.121
20. Omer S.A., Demirboga R., Khushefati W.H.: Relationship between compressive strength and UPV of GGBFS based geopolymer mortars exposed to elevated temperatures, Construction and Building Materials 94, 2015, pp. 189-195, doi: 10.1016/j.conbuildmat.2015.07.006
21. Ranjbar N., Mehrali M., Alengaram U.J., Metselaar H.S.C., Jumaat M.Z.: Compressive strength and microstructural analysis of fly ash/palm oil fuel ash based geopolymer mortar under elevated temperatures, Construction and Building Materials 65, 2014, pp. 114-121, doi: 10.1016/j.conbuildmat.2014.04.064
22. Rovnaník P., Bayer P., Rovnaníková P.: Characterization of alkali activated slag paste after exposure to high temperatures, Construction and Building Materials 47, 2013, pp. 1479-1487, doi: 10.1016/j.conbuildmat.2013.06.070
23. Ye J., Zhang W., Shi D.: Effect of elevated temperature on the properties of geopolymer synthesized from calcined ore-dressing tailing of bauxite and ground-granulated blast furnace slag, Construction and Building Materials 69, 2014, pp. 41-48, doi: 10.1016/j.conbuildmat.2014.07.002
24. Zhang H.Y., Kodur V., Qi S.L., Wu B.: Characterizing the bond strength of geopolymers at ambient and elevated temperatures, Cement and Concrete Composites 58, 2015, pp. 40-49, doi: 10.1016/j.cemconcomp.2015.01.006

THE EVOLUTION OF THE MICROSTRUCTURE OF CANE CELLULOSE MICROFIBRILS DURING COLD CAUSTIC EXTRACTION

Yurii Budash, Yelyzaveta Kucherenko and Viktoriia Plavan

Ku4erenko_Elizaveta@i.ua; yubudash@gmail.com; plavan@live.ru

Abstract: *The cellulose yield depending on NaOH concentration, as well as time of cold caustic extraction (CCE) of cane has been investigated. Modeling of the extraction process has been carried out by the method of bivariate interpolation of the received dependence. Optimal NaOH solution concentration (12-13%) and time of extraction (3.5-4 days) have been defined. Behavior of cellulose fibers allocation in transversal dimension, depending on the CCE process conditions has been determined. At the parameters near to optimal, microfibrillar fibers with the average transverse dimension ~11 µm have been received. The decrease of this index to 9 µm may be due to an increase in the concentration of NaOH to 18 mass %. Increase of the process duration from 4 to 7 days does not affect the average transverse dimension of the fibers, but increases the homogeneity of their distribution at this indicator.*

Keywords: *cellulose, cane, microfibrils, extraction, morphology, modeling, image analysis.*

1 INTRODUCTION

The use of renewable natural resources is one of the strategic directions of the development of modern technologies, which is connected with the environmental problems of the present, as well as with the necessity to create environmentally safe materials [1-3]. The most commonly used eco-friendly filler for synthetic polymers is cellulose, which is traditionally derived from wood of different breeds. Nowadays, other "non-wood" sources of fiber cellulose semi-finished products, including kenaf, jute, ramie, straw of cereal crops, etc., are intensively investigated [4].

One of the popular areas of these studies is the use of bamboo (*Bambúsa*) as a rapidly recovering resource of fibrillar cellulose with high stress-strain properties [5-8]. The cane (*Phragmites australis*), like bamboo, belongs to the grass family (*Gramíneae*). This cosmopolitan plant is widespread throughout Europe, forming large array of thickets in the deltas and floodplains of rivers, on the banks of lakes and swamps. The biological feature of the cane is a perennial root system, from which annual annulus grow up to 5-6 m in height [9]. Stems that die in autumn accumulate in aquatic ecosystems, which eventually lead to a deterioration of the ecological situation of reservoirs. Harvesting the cane in winter can be an important component of the rational use of ecosystem resources and an important regulatory mechanism [10].

The above stipulates the feasibility of conducting research in the use of cane as a raw material for the production of environmentally safe microfibrillary cellulosic fillers of various applications, in particular for the production of polymer biocomposite materials.

There are a few chemical methods of cellulose selection which are based on the treatment by different reagents. A method of "cold" delignification is traditional and widely used for the selection of bast fibres from plant row material such as flax, hemp, linen, etc. [11]. Its essence lies in the presoaking of raw materials in water (as a rule, for a few weeks) at an ordinary temperature, which results in destruction of microfibrillar connections under the effect of physical and biological factors. It is possible to force the cold delignification process using caustic water solutions. This method is known as "cold caustic extraction" (CCE), and due to its environmental friendliness and energy efficiency attracted attention of the researchers [12-14].

The aim of the research was the study of influence of "cold caustic extraction" parameters process on the structure and dimension properties of microfibrillar cellulose fibres from cane.

2 MATERIALS AND METHODS

The main research object is a cellulose-based plant – cane (phragmites australis). There was used the middle part of the dry stem collected in the winter after the end of the growing season.

After longitudinal crushing (~30x2 mm), the weight (~1-2 g) of the plant stem was dried to constant mass. After that, 100 gr. weight was filled with aqueous solution of NaOH (20°C) at a given concentration. The extraction time lasted for 1-7 days. The concentration of aqueous solutions of NaOH was in the range of 2-18%. After the extraction process was completed, the obtained fibers were washed with a weak (1%) solution of H_2SO_4, then with distilled water to neutralize and dried to permanent weight.

The morphology of the samples was studied by optical polarization microscopy (Biolam S-11). Registration of digital images was carried out using a special eyepiece nozzle. To determine the dimensional characteristics of the fibers, a method for analyzing digital images was used, followed by a statistical processing of the data obtained.

To simulate the extraction process, the method of bivariate interpolation of Akima IMSL was used to calculate the values of the interpolation function at the points of the regular network by the values of irregularly distributed data points [15].

3 RESULTS AND DISCUSSION

The main technological parameters influencing the CCE process are the caustic concentration as well as the extraction time. The influence of these parameters on cellulose output, structure and dimensional characteristics of fibers were investigated.

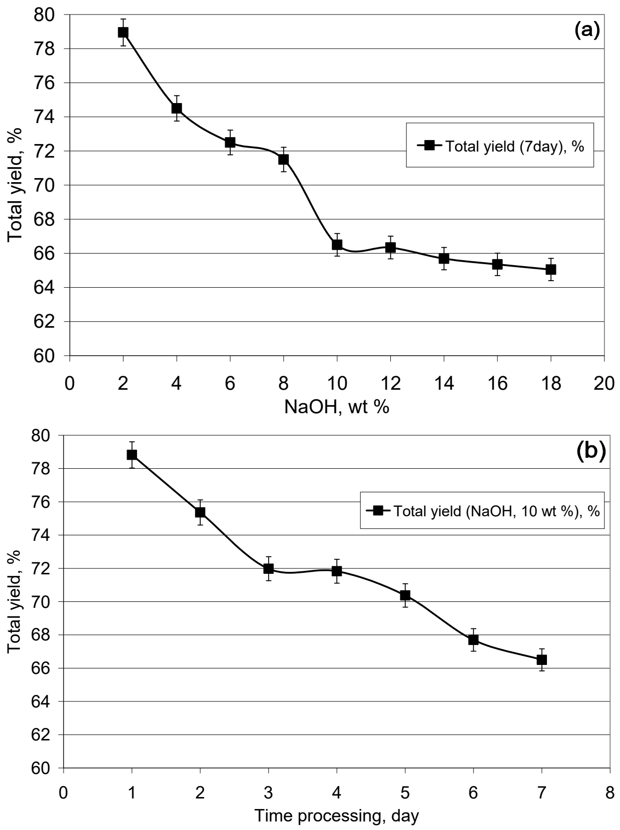

Figure 1 Dependence of the yield of cellulose on the concentration of NaOH (20°C, 7 days) (a), and time of processing (20°C, 10% NaOH) (b)

On the 2nd day of the CCE process one could observe a change in the color of the working solution from the transparent to the light brown, indicating that the extraction process proceeded. The results of the study of the caustic concentration influence in the working solution (from 2 to 18%) at a fixed time of the process (7 days) on the yield of cellulose are presented in Figure 1a.

It should be noted that the lower value of cellulose output indicates a greater completeness of the delignification process. From Figure 1, it can be seen that an increase in the concentration of caustic from 2 to 10% leads to a virtually linear decrease in the yield of cellulose from 79 to 66.5%. With a further increase in concentration from 10 to 18%, the change in the yield of cellulose is not significant. Thus, the rational concentration of NaOH solution, at given conditions of the CCE process, corresponds to the interval of 10-12%.

The study results of the influence on the effect of the cane extraction time on cellulose output at a fixed (10%) concentration of NaOH solution are shown in Figure 1b. The data shows that an increase in the extraction time from 1 to 7 days leads to almost linear decrease in the yield of cellulose from 78.8 to 66.5%. It is interesting to note that on the 3-4th day of the research, the cane yield is practically the same. This may be due to the complicated step-by-step process of simultaneous extraction of several substances from natural raw materials.

The experimental dependences of the cellulose yield on the concentration of NaOH and the time of the process allow us to construct a general approximation model that binds these indices.

The result of interpolation modeling of cellulose yield from caustic concentration and extraction time is shown in Figure 2.

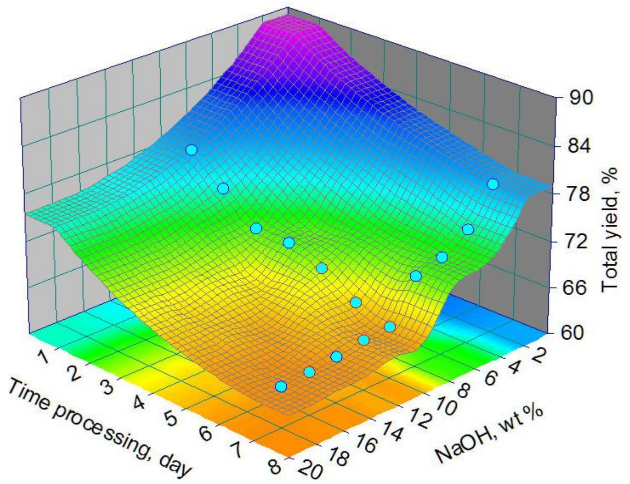

Figure 2 The 3D surface diagram obtained by the method of interpolation simulation of the dependence of cellulose yield on concentration and time of processing. The points are marked with experimental data

The approximation of the experimental data by the surface and the subsequent design of the surface to the plane allows to obtain a map of the lines which is presented for the investigated systems in Figure 3.

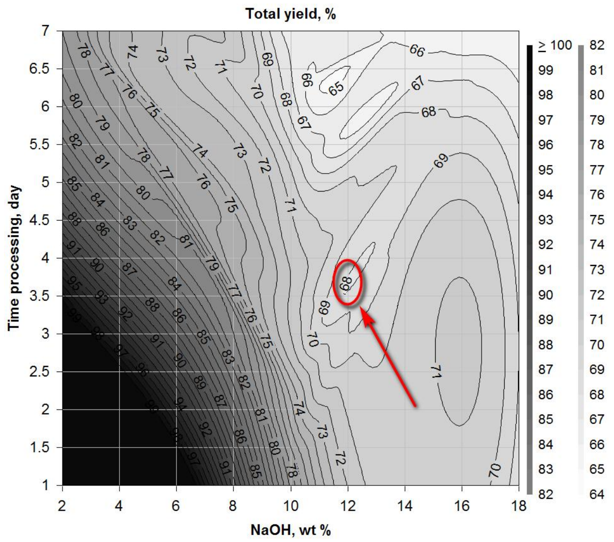

Figure 3 Map of the line levels of the interpolation model for cellulose yield from caustic concentration and time of processing

This map shows that the effect on the yield of cellulose concentration of NaOH in the working solution is more significant than the effect of the extraction process time. The optimization of process parameters is possible based on the need to achieve a satisfactory yield of cellulose at the lowest values of the concentration of caustic and the duration of the process. The given simulation results allow to predict that the optimal values (indicated by the ellipse in Figure 3) of NaOH concentration and process duration, which provide satisfactory (68-69%) yield of cellulose, make up 12-13% and 3.5-4 days respectively. The experimental testing of cellulose yield at the specified parameters of the delignification process showed that the obtained value (67.8%) is well consistent with the model representations.

The image analysis method defines the average transverse dimensions and the distribution of this index of fibers (Figure 4).

The results of the studies indicate that an increase in the concentration of NaOH in the working solution from 2 to 10% causes a decrease in the following distribution parameters (shown in the histogram heading):

- average transverse dimension of fibers (from 14.2 to 11.4 μm);
- an interval corresponding to the largest fraction of fibers (from 10-12 to 8-10 μm);
- standard deviation (from 6.5 to 4.4 μm);
- scale of distribution (from 3-50 to 3-34 μm).

According to the calculations, the coefficients of variation (~7%) and oscillations (~59%) of the aggregate also decrease. Thus, as a result of an increase in the concentration of NaOH in the working solution from 2 to 10%, the displacement of the distribution of the transverse dimension of fibers towards the lower values and their narrowing occurs.

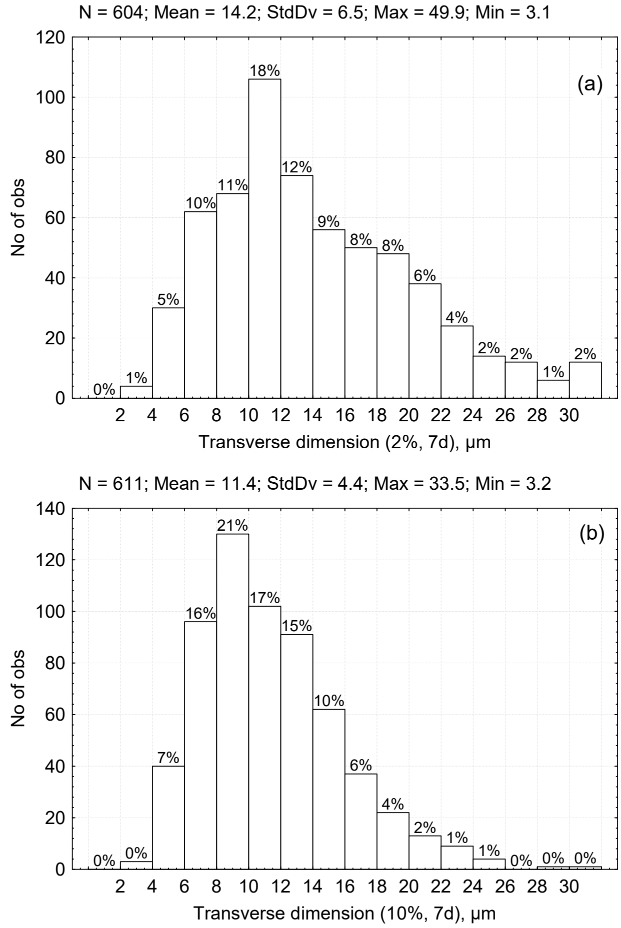

Figure 4 Histogram of transverse size distribution of cellulose microfibrils, isolated from cane by treatment with NaOH (a) 2 wt.%; (b) 10 wt.% (20°C, 7 days)

At the highest (from the investigated) concentration of caustic in the working solution (18%), the mean value of the transverse dimension of the fibers is reduced to 9.3 μm, while maintaining the values of the standard deviation of the distribution (Figure 5).

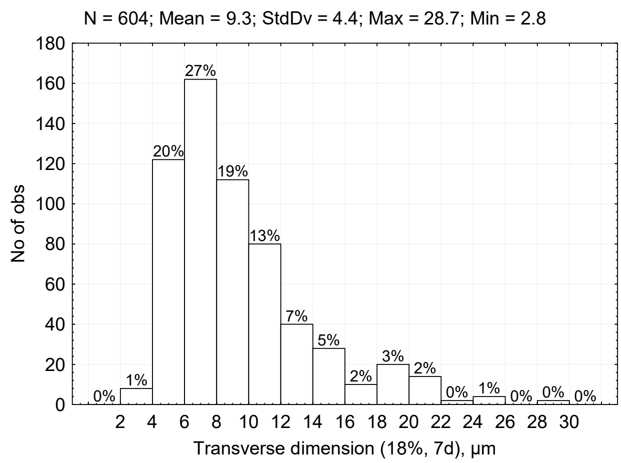

Figure 5 Histogram of transverse size distribution of cellulose microfibrils, isolated from cane by treatment with NaOH (18 wt.%; 20°C, 7 days)

Compared with the previous case (Figure 4b), the largest proportion of fibers increases from 21 to 27% and the interval corresponding to it decreases to 6-8 μm.

It should be noted that with increasing caustic concentration in the working solution from 10 to 18 wt.%, the yield of cellulose decreases slightly (~2%), while the decrease in the average transverse dimension of fibers is quite significant (by 18%). Extremely (~3 times) increases the proportion of fibers with transverse dimensions >6 μm. These results may indicate that at 10% caustic concentration, the equilibrium completeness of the delignification process of the raw material is achieved. At the same time, increasing the concentration of NaOH in the working solution to 18%, stimulates further defibrillation of fibers and reduce their transverse dimensions.

Figure 6 shows microphotographs of cellulose microfibrils obtained by cold caustic extraction in 10 wt.% of NaOH solution at different times of this process.

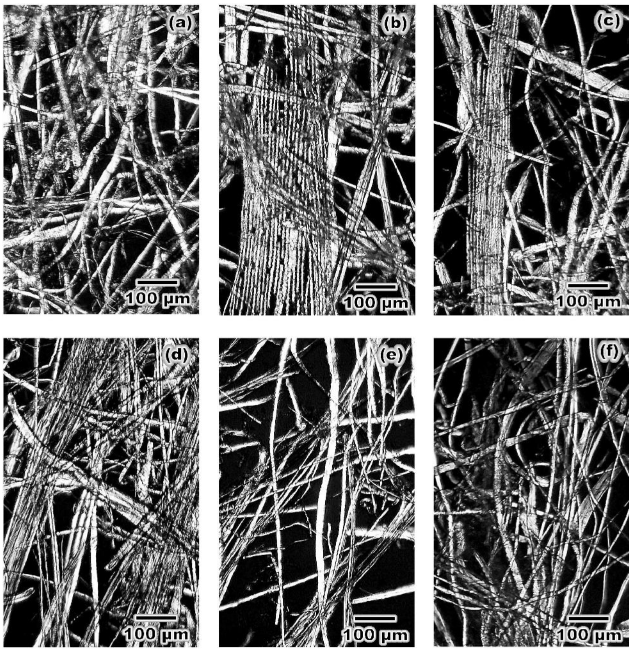

Figure 6 PLM image with crossed polars of cane cellulose microfibrils, extracted from cane by treatment with NaOH (20°C, 10 wt.%). Time of processing (a) 1 day; (b) 2 days; (c) 3 days; (d) 4 days; (e) 5 days; (f) 6 days

One can see that increasing of extraction time leads to a change in dimensional characteristics of cellulose fibers and their uniform distribution according to this indicator. This is especially noticeable for samples with extraction time >4 days (Figure 6e-f).

Figure 7 shows distribution histograms for the transverse dimension of cellulose microfibrils obtained by extraction in 10 wt.% of NaOH solution at different time of the process. They show that after the first day of the extraction process (a) the largest proportion of fibers (27%) has a dimension of 10-12 μm. The proportion of fibers with a transverse dimension <10 μm and >12 μm is respectively 32 and 40%. It should be noted, however, that in the latter case, the fiber share >12 μm refers to a much wider range of dimension (12-30 μm) than for fibers with a transverse dimension <10 μm (2-10 μm). A substantial proportion of fibers larger than the average may indicate incompleteness of the delignification of the raw material at such a time of the CCE process.

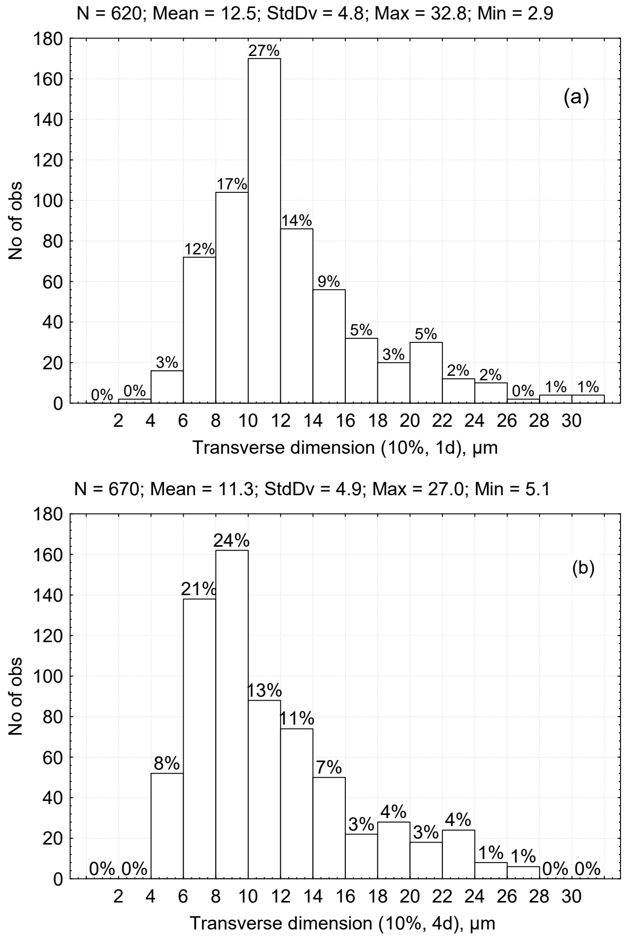

Figure 7 Histogram of transverse size distribution of cellulose microfibrils, isolated from cane by treatment with NaOH (20°C, 10 wt.%). Time of processing (a) 1 day; (b) 4 days

Increasing the extraction time up to 4 days (which approximates the optimal parameters of the model) leads to a decrease in the average transverse dimension of the fibers from 12.5 to 11.3 μm while maintaining the values of the standard deviation of the distribution (Figure 7b). At the same time, the interval corresponding to the largest (24%) fraction of fibers decreases to 8-10 μm. The transverse dimension of more than half of all fibers (53%) does not exceed 10 μm. The proportion of fibers with a transverse dimension >12 μm decreases to 34%. Thus, as a result of an increase in the time of the process, the bias of the distribution towards the lower values occurs, which leads to a decrease in the average value of the transverse dimension of the fibers by ~10%.

The comparison of the obtained distribution data shown in Figures 4b and 7b makes it possible to constant that increasing the length of the extraction process in 10% solution of NaOH from 4 to 7 days does not affect the average fiber dimension. At that time, the standard deviation of the distribution and the coefficient of variation are reduced (from 4.9 to 4.4 and 4.8% respectively), which indicates an increase in the homogeneity of the distribution at this indicator.

4 CONCLUSIONS

Dependences of the yield of cellulose on the concentration of NaOH and the time of the process of cold caustic extraction (CCE) of the cellulosic plant cane. The modeling of the extraction process has been performed by the method of bivariate interpolation of the obtained dependences. This allowed to establish the optimal concentration of NaOH solution (12-13%) and the time of processing (3.5-4 days). The experimental testing of cellulose yield at the specified parameters of the delignification process showed that the obtained value (67.8%) is well consistent with the model representations.

There has been established the nature of the change in the distribution of cellulose microfibrils in transverse dimensions, depending on the conditions of the CCE process. At parameters close to optimal, fibers have been obtained with average transverse dimensions of ~11 µm. The decrease of this index to 9 µm may be due to an increase in the concentration of NaOH to 18 wt.%. Increasing the duration of the process from 4 to 7 days does not affect the average transverse dimension of the fibers, but increases the uniformity of their distribution at this indicator.

5 REFERENCES

1. Kalia S., Avérous L. (Eds.): Biodegradable and Biobased Polymers for Environmental and Biomedical Applications, Hoboken: John Wiley & Sons, 2016
2. Thakur V.K., Thakur M.K. (Eds.): Handbook of Polymers for Pharmaceutical Technologies, Volume 3, Biodegradable Polymers, Hoboken: John Wiley & Sons, 2015
3. Bastioli C. (Ed.): Handbook of Biodegradable Polymers, Akron: iSmithers Rapra Publishing, 2005
4. Thakur V.K., Thakur M.K.: Processing and characterization of natural cellulose fibers/thermoset polymer composites, Carbohydrate Polymers 109, 2014, pp. 102-117, doi: 10.1016/j.carbpol.2014.03.039
5. Deepak V., Siddharth J., Zhang X., Gope P.Ch.: Green Approaches to Biocomposite Materials Science and Engineering, Hershey: IGI Global, 2016
6. Kartal S.N., Aysal S., Terzi E., Yılgör N., Yoshimura T., Tsunoda K.: Wood and bamboo-PP composites: Fungal and termite resistance, water absorption, and FT-IR analyses, BioResources 8(1), 2013, pp. 1222-1244
7. Li Y., Du L., Kai. Ch., Huang R., Wu Q.: Bamboo and high density polyethylene composite with heat-treated bamboo fiber: thermal decomposition properties, BioResources 8(1), 2013, pp. 900-912
8. Phong N.T., Fujii T., Chuong B., Okubo K.: Study on how to effectively extract bamboo fibers from raw bamboo and wastewater treatment, Journal of Materials Science Research 1(1), 2012, pp. 144-155, doi:10.5539/jmsr.v1n1p144
9. Prokudyn Y.N.: Zlaky Ukrayny. Cereals of Ukraine, Naukova dumka, 1977
10. Jhmud O.I.: Syngenetic and exogenous vegetation changes in the Danube Biosphere Reserve (Synhenetychni i ekzohenni zminy roslynnosti Dunayskoho biosfernoho) Ph.D. Dissertation, National Academy of Sciences of Ukraine, National botanic garden named after M.M.Hryshko, Kyiv, Ukraine, 2001
11. Kozłowski R. (Ed.): Handbook of Natural Fibres: Types, properties and factors affecting breeding and cultivation, New York: Elsevier, 2012
12. Arnoul-Jarriault B., Lachenal D., Chirat C., Heux L.: Upgrading softwood bleached kraft pulp to dissolving pulp by cold caustic treatment and acid-hot caustic treatment, Industrial Crops and Products 65, 2015, pp. 565-571, doi: 10.1016/j.indcrop.2014.09.051
13. Li J., Liu Y., Duan C., Zhang H., Ni Y.: Mechanical pretreatment improving hemicelluloses removal from cellulosic fibers during cold caustic extraction, Bioresource Technology 192, 2015, pp. 501-506, doi: 10.1016/j.biortech.2015.06.011
14. Li J., Hu H., Huang L., Chen L., Ni Y., Li H.: Kinetics and mechanism of hemicelluloses removal from cellulosic fibers during the cold caustic extraction process, Bioresource Technology 234, 2017, pp. 61-66, doi: 10.1016/j.biortech.2017.03.026
15. Akima H.: A method of bivariate interpolation and smooth surface fitting for irregularly distributed data points, ACM Transactions on Mathematical Software 4(2), 1978, pp. 148-159, doi: 10.1145/355780.355786

DYNAMIC MOISTURE SORPTION BEHAVIOUR OF DEVELOPING COTTON FIBRES

Özgür Ceylan[1] and Karen De Clerck[2]

[1]*Anadolu University, Faculty of Architecture and Design, Department of Fashion and Textile Design, Yunusemre Campus 26470 Eskişehir, Turkey*
[2]*Department of Materials, Textiles and Chemical Engineering, Ghent University, Technologiepark 907, 9052 Ghent, Belgium*
ozgurceylan@anadolu.edu.tr, karen.declerck@ugent.be

Abstract: *Dynamic vapour sorption is used to gain valuable information concerning the sorption behaviour of cotton fibres during their development. Moisture sorption isotherms for cotton fibres are obtained through dynamic vapour sorption analyser during their development stages. The developing cotton fibres exhibited variable dynamic moisture sorption behaviour. The sorption rate is found to be closely related to the structural and compositional changes in cotton fibres during their maturation process. This study provides valuable insights into the driving principles of the moisture sorption process of cotton fibres may aid to develop ways to improve the moisture management properties in general.*

Keywords: *moisture sorption, cotton, dynamic vapour sorption, sorption rate.*

1 INTRODUCTION

Cotton is the premier natural fibre for textile applications mainly because of its biodegradable and renewable nature with a high-water absorption potential and light weight properties. Besides the traditional use as a textile material, cotton fits also in today's challenge to search for biopolymers or composites based on sustainable resources.

Water sorption is expressed as moisture content and/or water retention value of textile fibres [1]. Water content in the fibre has a profound effect on almost all the mechanical properties (tensile strength, stiffness, ultimate elongation, etc.) as well as the physical (electric and thermal conductivity, isolation against UV radiation solubility, etc.) and chemical ones (chemical reactivity, resistance to microbes, etc.) [2]. Thus, a study on the moisture sorption is also of high interest for cotton fibres.

Previous research reported on the sorption behaviour of cotton fibres harvested at different stages in their development process. The moisture sorption profiles as well as the hysteresis behaviour were studied for the developing cotton fibres [3]. This knowledge will be further deepened in the present paper.

The main objective of this study is to examine the dynamic sorption behaviour of developing cotton fibres. Thus, the total running time of the sorption process and sorption rate for the developing fibres are studied extensively. The aim is to provide valuable insights in the moisture sorption mechanisms of the cotton fibre during their development process which may aid to develop ways to improve the moisture management properties in general.

2 MATERIALS AND METHODS

2.1 Materials

Cotton cultivar ST457 (Gossypium hirsutum) was grown in a green-house at 23°C and 15 kLux, with a 16 h/8 h day/night cycle). Flowers were tagged at anthesis and a few bolls were harvested at 15, 21, 36 and 80 days post anthesis (DPA).

2.2 Methods

Dynamic vapour sorption measurements were conducted in a Q-5000SA instrument (TA-instruments, Zellik, Belgium). All measurements were performed at 23±0.1°C. Deliquescent salts (sodium bromide and potassium chloride) were used to verify the humidity of the instrument.

Four milligrams of cotton fibres, harvested at different stages during their development process, were rolled into a small ball and placed in the quartz sample pans. The humidity was increased stepwise, with steps of 10% relative humidity (RH) from 5 till 95%. The desorption isotherm, from 95 till 5%, was recorded as well. At every RH, the equilibrium moisture content (EMC) is monitored after reaching equilibrium, or thus when the weight change is less than 0.05% over a time period of 15 minutes.

3 RESULTS AND DISCUSSION

The response of the cotton fibre samples to a step change in RH in the sample chamber produces an asymptotic curve when plotted as moisture content against time, Figure1. The total running time of sorption process for fibres with higher DPA is noticeably lower than those of the lower DPA ones. This may be explained by the differences in availability of sorption sites due to structural and compositional changes in cotton fibres during their maturation process. At the early stages of development fibre growth is characterized by the synthesis of the primary cell wall and an increase in fibre length [4]. Ones this phase is passed, around 21 DPA, the secondary cell wall growth initiates and the amount of cellulose increases quickly. This results in more structural organization thus less accessibility of water to the fibres. The variation in the total running time is closely related to the sorption ability, with higher levels of moisture sorption results in increases in the total run time [5].

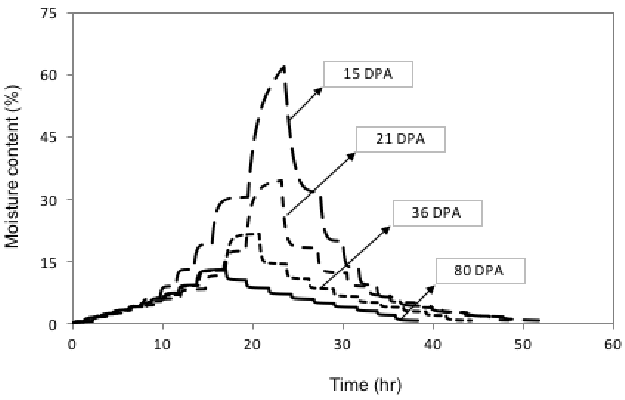

Figure 1 Change in moisture content as a function of time for developing cotton fibres

Increasing the RH, in each step of the sorption cycle, results in a new equilibrium condition within a specific time period for every sample. Dividing the increment or decrement of the moisture content at any RH by the time taken to reach the new EMC gives the sorption rate of materials [6].

At the lowest RH, similar sorption rates were observed for developing cotton fibres. At the higher end of the hygroscopic range, however, the differences in sorption rates were more pronounced, being higher for fibres with low DPA, and lower for fibres with high DPA. The higher sorption rate of the fibres with low DPA can mainly be attributed to the hygroscopic nature of the fibre components at this stage of development. The immature fibres contain next to 15-20% cellulose, also pectins, lignin, hemicelluloses and proteins [7]. This results in a loose and more open arrangement of micro fibrils thus a higher number of accessible OH groups per unit volume. A high proportion of non-cellulosic and the less crystalline cellulose content results in a loose and more open arrangements of the micro fibrils thus a more accessible structure for moisture sorption.

Also, the isotherm shape for low DPA fibres is found to be different from other natural fibres with it showing a rather type III isotherm instead of type II according to IUPAC classification [3]. Materials exhibit type III isotherms, due to lack of cross-linking, can swell significantly at higher RH [8].

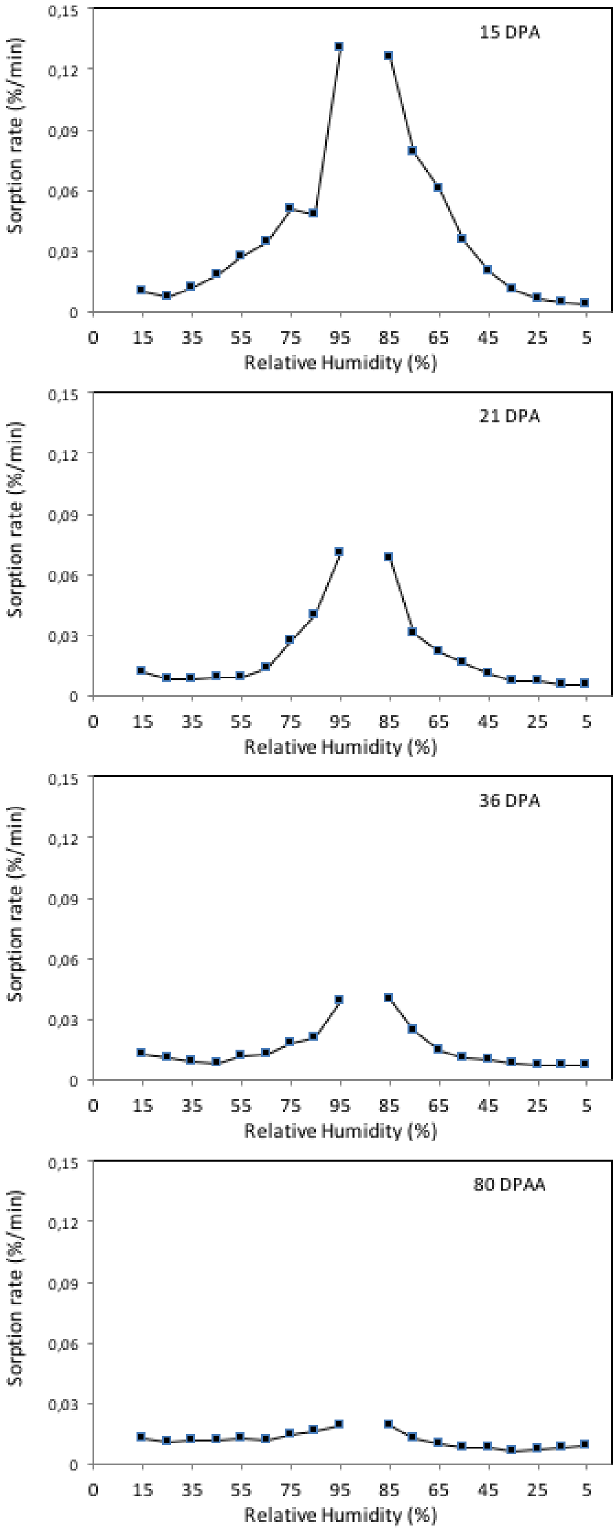

Figure 2 Sorption rate within a set of relative humidity during sorption process for developing cotton fibres

4 CONCLUSIONS

Dynamic vapour sorption can be used to gain valuable information concerning the dynamic moisture sorption behaviour of cotton fibres. Significant differences were observed in sorption time and sorption rate of developing cotton fibres. It is likely that these differences are closely related to the ratio between the cellulose crystalline and the amorphous zones as well as to the structural composition of the fibres. This study provides valuable insights to develop ways to improve the moisture management properties of cotton fibres in general. These improvements can lead further areas of application for cotton fibres such as composites due to the increasing demand on renewable sources, recyclability or biodegradability.

5 REFERENCES

1. Pušić T., Boban A., Dekanić T., Soljačić I.: The sorption ability of textile fibres, Vlakna a Textil (Fibres and Textiles) 18(1), 2011, pp. 7-15
2. Okubayashi S., Griesser U.J., Bechtold T.: A kinetic study of moisture sorption and desorption on lyocell fibers, Carbohydrate Polymers 58(3), 2004, pp. 293-299, doi: 10.1016/j.carbpol.2004.07.004
3. Ceylan Ö., Van Landuyt L., Meulewaeter F., et al.: Moisture sorption in developing cotton fibers, Cellulose 19(5), 2012, pp. 1517-1526, doi: 10.1007/s10570-012-9737-x
4. Abidi N., Hequet E., Cabrales L.: Applications of Fourier transform infrared spectroscopy to study cotton fibers. In Fourier transforms-new analytical approaches and FTIR strategies, 2011, Goran Nikolic (Ed.), London: InTech. ISBN: 978-953-307-232-6
5. Xie Y., Hill C.A.S., Jalaludin Z., et al.: The water vapour sorption behaviour of three celluloses: analysis using parallel exponential kinetics and interpretation using the Kelvin-Voigt viscoelastic model, Cellulose 18(3), 2011, pp. 517-530, doi: 10.1007/s10570-011-9512-4
6. Xie Y., Hill C.A.S., Xiao Z., et al.: Water vapor sorption kinetics of wood modified with glutaraldehyde, Journal of Applied Polymer Sciences 117(3), 2010, pp. 1674-1682, doi: 10.1002/app.32054
7. Hill C.A.S., Norton A., Newman G.: The water vapor sorption behavior of natural fibers, Journal of Applied Polymer Science 112(3), 2009, pp. 1524-1537, doi: 10.1002/app.29725
8. Xie Y., Hill C.A.S., Jalaludin Z., et al.: The dynamic water vapor sorption behaviour of natural fibres and kinetic analysis using the parallel exponential kinetics model, Journal of Material Science 46(2), 2010, pp. 479-489, doi: 10.1007/s10853-010-4935-0

IMMOBILIZATION OF PROTEOLYTIC ENZYMES ONTO SILICA NANOFIBERS

Iveta Danilová and Irena Lovětinská-Šlamborová

Technical University of Liberec, Studentská 1402/2, 461 17 Liberec 1, Czech Republic
iveta.danilova@tul.cz, irena.slamborova@tul.cz

Abstract: *Even in modern medicine, it is still necessary to remove necrotic tissue from burns in a very painful method – by using surgical instruments. It is possible to replace the surgical method with application of proteolytic enzymes directly to the wound, which removes the necrotic tissue completely painlessly. However, most enzymes are active only for a short time and under the specific conditions. The catalytic activity of enzymes can be increased e.g. by immobilization of enzymes onto the biocompatible silica nanofibers. The nanofibers must be functionalized by suitable reagents to form a ligand between silica nanofibers and amino groups of proteolytic enzymes. In our research, the nanofibers surface was modified by 3-Aminopropyl triethoxysilane firstly, than functionalization by succinic anhydride and N-Hydroxysuccinimide ester was done. As the next step, 7 different proteolytic enzymes were immobilized to the silica nanofibers surface. Proteolytic activity of enzymes was tested under conditions simulated skin burns environment (temperature of 37°C and pH 4.6).*

Keywords: *burns, immobilization, proteolytic enzymes, silica nanofibers.*

1 INTRODUCTION

Painless removal of necrotic tissue is called an enzymatic debridement. The necrosis occurs especially in deep skin burns; it appears in the second and the third degree burns, when the tissue is damaged and skin tissue recovery is not possible. Therefore, removal of the damaged tissue is necessary step before beginning of the granulation and re-epithelization phase of healthy tissue. Especially proteolytic enzymes are chosen for the enzymatic debridement for their ability to catalyze the proteolytic reactions (hydrolysis of the peptide bonds that link amino acids together in a polypeptide chain). In other words, proteolytic enzymes provide a digestion of necrotic tissue. For example bromelain [1], collagenase [2], or papain-urea [3] are already used in the treatment of burns, however, they are usually mixed in gels or ointments. Unfortunately, application of enzymes in this form may cause the infection formation by using wet wound dressing. Native enzymes are unstable, have a short lifetime, and high temperature and pH dependence. The solution of this problem is to immobilize the enzyme onto a suitable material. Silica nanofibers appear to be a very good supporting material for the immobilization of enzymes, because they are biocompatible, biodegradable and they have a number of active functional groups for covalent binding of enzymes.

The aim of the research is to develop a method for the immobilization of enzymes on silica nanofibers that can be used in healthcare (without toxic ligands). Furthermore, it was tested the proteolytic activity of seven immobilized enzymes to determine which enzymes would be the most suitable for these purposes. For this reason, proteolytic activity of enzymes was tested under conditions simulated skin burns environment and pH and thermal dependence were monitored.

2 EXPERIMENT

2.1 Material

Nanofibers were prepared from tetraethyl orthosilicate (TEOS, Sigma-Aldrich, 98 wt.%) and propan-2-ol (Penta CZ, p.a. 99.9 wt.%).

For functionalization of the nanofibers were used: ethanol absolute (Penta), 3-Aminopropyl triethoxysilane (APTES, 98 wt.%), succinic anhydride (SU, 99 wt.%), N-(3-Dimethylaminopropyl)-N′-ethylcarbodiimide hydrochloride (EDC, 98 wt.%), N-Hydroxy-succinimide (NHS, 98 wt.%), 4-Morpholineethane-sulfonic acid monohydrate (MES, 99 wt.%), Tris(hydroxymethyl)aminomethane (TRIS, 99,8 wt.%) (all from Sigma-Aldrich).

Trypsin from hog pancreas was purchased in Fluka, other proteolytic enzymes: protease from bovine pancreas, protease from *Aspergillus oryzae*, protease from *Bacillus licheniformis*, bromelain from pineapple stem, trypsin from bovine pancreas and α-chymotrypsin from bovine pancreas were from Sigma-Aldrich. For enzyme activity assay was used casein from bovine milk and trichloroacetic acid (TCA, 99 wt.%) were used, both from Sigma-Aldrich too.

Table 1 Characteristic of immobilized enzymes

Designation	Name	Source	Optimum pH	Optimum temperature	Reference
P1	Protease type I	bovine pancreas	6.5-7.5	35-55°C	[6]
P2	Protease type XXIII	*Aspergillus oryzae*	4.5-5.5	55-60°C	[7]
P3	Protease type XXIV	*Bacillus licheniformis*	6-5-8.5	65-70°C	[8]
BR	Bromelain	pineapple stem	6.5-7.5	55°C	[9]
T1	Trypsin type I	bovine pancreas	7-9	40°C	[10]
T2	Trypsin type V-S	hog pancreas	7-9	40-45°C	[11]
CH	α-Chymotrypsin type II	bovine pancreas	7-9	40°C	[12]

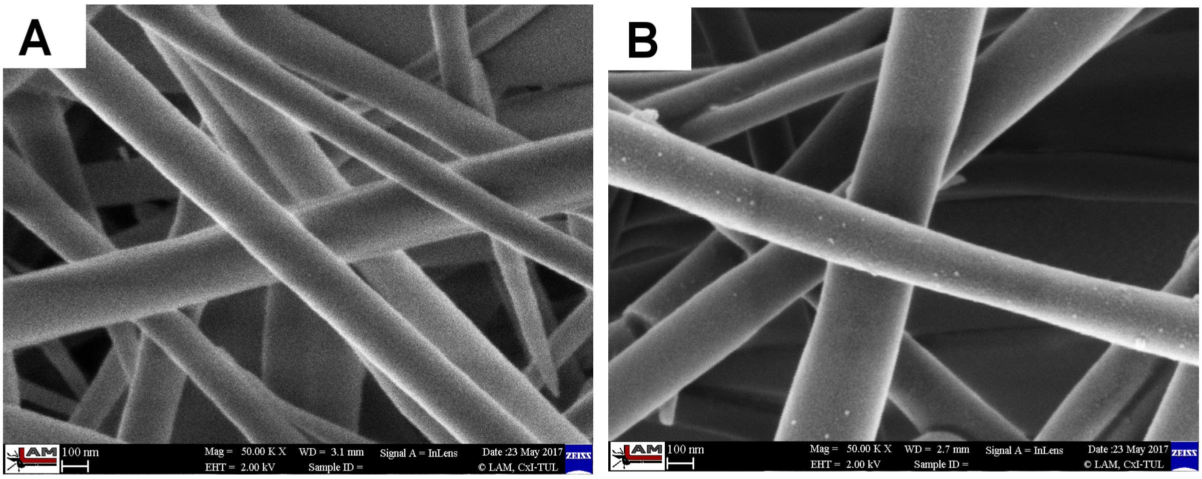

Figure 1 SEM images of non-modified silica nanofibers (A) and silica nanofibers with immobilized trypsin from hog pancreas (B)

2.1 Preparation of silica nanofibers

Silica nanofibers were prepared according to [4] by sol-gel method and subsequently electrospun on the needleless NanospiderTM device (Elmarco). Silica nanofibers were electrospun from free liquid surface under standardized conditions [5]. The nanofibers were thermally stabilized at 260°C for 2 hours.

2.2 Immobilization of enzymes onto nanofibers

For immobilization of proteolytic enzyme, it is necessary to functionalized silica nanofibers surface. As a silanization reagent, 3-Aminopropyl triethoxysilane (APTES) was chosen. For carboxylation of APTES amino groups, succinic anhydride was used.

The final step was the reaction of mentioned chemicals with N-Hydroxysuccinimide ester created using N-(3-Dimethyl-aminopropyl)-N′-ethylcarbo-diimide hydrochloride and N-Hydroxysuccinimide. After functionalization of silica nanofibers, 7 different proteolytic enzymes were covalently bonded to the nanofibers surface. Full characteristics of used enzymes are in Table 1.

3 RESULTS AND DISCUSSION

3.1 Visualization and characterization of nanofibers

Visualization of nanofibers was taken by scanning electron microscope Carl Zeiss ULTRA Plus. Samples were gold-dusted in advance and observed in the form of secondary electrons SE1 (Figure 1). According to the procedure described above, silica nanofibers with specific weight ~40 g.m^{-2} and mean fiber diameter 222±97nm were produces. The histogram of the nanofibers diameter is shown in Figure 2.

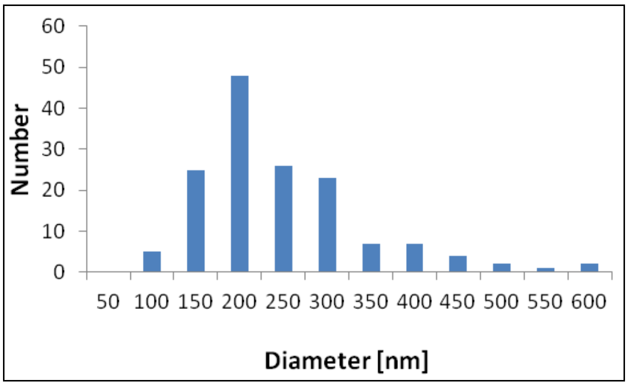

Figure 2 Histogram of the nanofibers diameter

3.2 Enzyme activity assay

Protease activity assay was measured by casein as a substrate. When proteolytic enzyme catalyses a digestion of this substrate, the amino acid tyrosine and peptide fragments are separated from casein. Free tyrosine reacts with Folin & Ciocalteu reagent to produce a blue coloured chromophore. The chromophore can be spectrophotometrically quantified as an absorbance value at wavelength 750 nm. 1 unit of activity is defined as the amount of tyrosine equivalents in micromoles released from casein per minute. In testing of immobilized enzyme, the activity units refer to mg of nanofibers. Activity of three types of proteases, bromelain, 2 types of trypsins and α-chymotrypsin immobilized on the nanofibers was tested at 37°C and pH value of 4.6 (Figure 3). By analysis of variance (one-factor ANOVA test) was found that the measured enzyme activity values differ from one another at a significance level of 5% – F (6.42)=232.18 p=2.32. By sequential testing of the measured enzyme activity values (2-sample t-test, 5% significance level) it was found that the activity values of BR, P1 and CH enzymes do not differ from each other and activity value of P2, P3 and T1 do not differ from each other too. Thus, the lowest activity was measured for the T2 enzyme, the higher activity was measured for the enzymes P1, BR and CH and the highest for P2, P3 and T1.

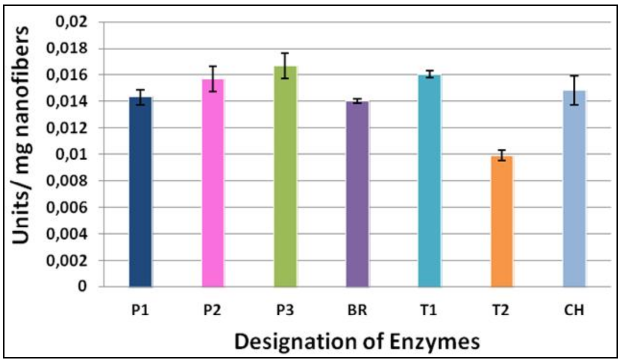

Figure 3 Proteolytic activity of protease from bovine pankreas (P1), protease from *Aspergillus oryzae* (P2), protease from *Bacillus licheniformis* (P3), bromelain from pineapple stem (BR), trypsin from bovine pancreas (T1), trypsin from hog pancreas (T2) and α-chymotrypsin from bovine pancreas

The highest activities were detected for P3 enzyme (protease from *Bacillus licheniformis*) and T1 enzyme (trypsin from bovine pancreas). P2 (protease from *Aspergillus oryzae*) and CH (α-chymotrypsin from bovine pancreas) had high proteolytic activity too. The immobilized enzymes activity was compared with the activity of free enzymes under the same conditions. Activity of enzymes in percent was determined as a ratio of proteolytic activity of immobilized enzyme to proteolytic activity of soluble enzyme (Figure 4).

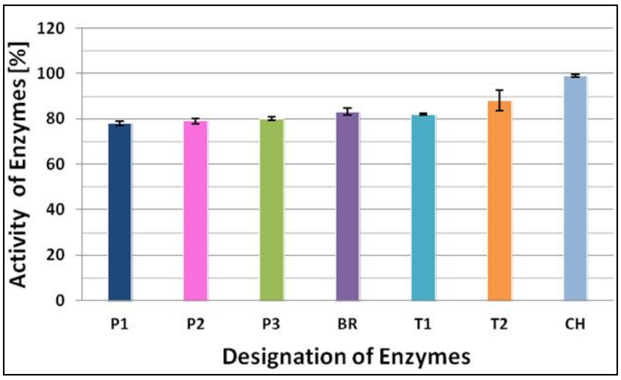

Figure 4 Immobilized enzyme activity to soluble enzyme activity ratio in percent

The ratio of proteolytic activity of immobilized enzyme to proteolytic activity of soluble enzyme was at least 76%. The results show that α-chymotrypsin has a relatively high activity compared to other proteolytic enzymes; and its activity did not decrease after immobilization onto silica nanofibers. Therefore, less concentration of the α-chymotrypsin enzyme would be required to maintain efficiency in comparison with other tested enzymes. 98% efficiency of the enzyme immobilized onto the nanofibers is a great success and it is a sign of high quality of enzyme binding and selection of ligands because the amount of immobilized enzyme is significantly limited by the number of functional groups on the nanofibers surface.

The highest success rate of α-chymotrypsin immobilization is very closely related to the temperature at which the tests were performed (37°C). Table 1 shows that the α-chymotrypsin has an optimum temperature at 40°C. But proteases and bromelain have its optimum temperature at higher temperatures. This can be one of the reasons why ratio of proteolytic activity of immobilized α-chymotrypsin to proteolytic activity of soluble α-chymotrypsin is almost 100 %.

Proteolytic activity of protease from *Aspergillus oryzae* (P2), bromelain from pineapple stem (BR), trypsin from bovine pancreas (T1) and α-chymotrypsin from bovine pancreas was measured at three different temperatures: 4, 23 and 37°C. The results are shown in Figure 5 (pH value was 4.6 too). Effect of temperature on enzyme activity was observed most in the case of protease from *Aspergillus oryzae* (P2). Conversely, bromelain seemed to be temperature independent in this temperature range. An analysis of variance (one-factor ANOVA test, significance level of 5%) found that temperature dependence was demonstrated in the case of P2, T1 and CH enzymes. This was not confirmed for the BR enzyme.

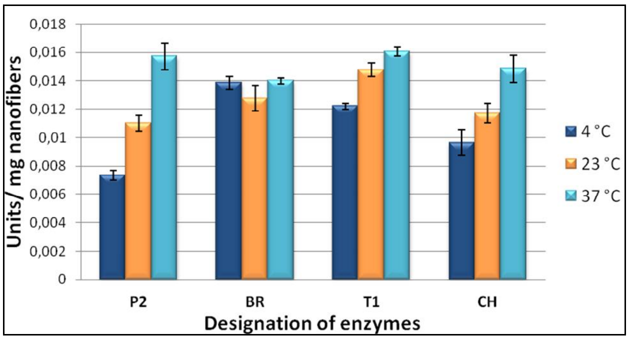

Figure 5 Activity of immobilized protease from *Aspergillus oryzae* (P2), bromelain from pineapple stem (BR), trypsin from bovine pancreas (T1) and α-chymotrypsin from bovine pancreas at the different temperatures

4 CONCLUSION

Suitable enzymes for immobilization onto silica nanofibers appear to be the α-chymotrypsin from bovine pancreas, protease from *Aspergillus oryzae*, bromelain from pineapple stem and trypsin from bovine pancreas. These enzymes were selected for further testing – the long-term stability of silica nanofibers with immobilized enzymes and cytotoxicity tests.

5 REFERENCES

1. Sheridan R.L.: Comprehensive treatment of burns, Current Problems in Surgery 38(9), 2001, pp. 657-756, doi: 10.1016/S0011-3840(01)70019-6
2. Erdel I.: Iruxol mono in preparation of chronic wound for transplantation, Journal of the European Academy of Dermatology and Venereology 11(2), 1998, pp. S214, doi: 10.1016/S0926-9959(98)95365-X
3. Langer V., Bhandari P.S., Rajagopalan S. et al.: Enzymatic debridement of large burn wounds with papain–urea: Is it safe? Medical Journal Armed Forces India 69(2), 2013, pp. 144-150, doi: 10.1016/j.mjafi.2012.09.001
4. Šlamborová I., Zajícová V., Exnar P. et al.: Nanofiber structure with immobilized organic agens and the method of its preparation, WO 2014026656 A1, 9.4. 2014
5. Danilová I., Lovětinská-Šlamborová I., Zajícová V., et al.: Immobilization of esterase enzyme onto silica nanofibers for biomedical applications, Vlakna a textil (Fibres and Textiles) 21(2), 2014, pp. 3-11
6. Rawlings N.D., Salvesen G.: Handbook of proteolytic enzymes, Third edition, 2013, ISBN 978-0-12-382219-2
7. Soares de Castro R.J., Sato H.H.: Protease from Aspergillus oryzae: Biochemical characterization and application as a potential biocatalyst for production of protein hydrolysates with antioxidant activities, Journal of Food Processing 2014, pp.1-12, doi: 10.1155/2014/372352
8. Sellami-Kamoun A., Haddar A., Ali N.H. et al.: Stability of thermostable alkaline protease from Bacillus licheniformis RP1 in commercial solid laundry detergent formulations, Microbiological Research 163(3), 2008, pp. 299-306, doi: 10.1016/j.micres.2006.06.001
9. Silveira E., Souza J., Santana M.E. et al.: Expanded bed adsorption of bromelain (EC 3.4.22.33) from Ananas comosus crude extract, Brazilian Journal of Chemical Engineering 26(1), 2009, pp. 149-157, doi: 10.1590/S0104-66322009000100014
10. Sipos T., Merkel J.R.: An effect of calcium ions on the activity, heat stability, and structure of trypsin, Biochemistry 9(14), 1970, pp. 2766-2775, doi: 10.1021/bi00816a003
11. Buck F.F., Vithayathil A.J., Bier M., et al.: On the mechanism of enzyme action. LXXII. Studies on trypsins from beef, sheep, and pig pancreas, Archives of Biochemistry and Biophysics 97(2), 1962, pp. 417-424, doi: 10.1016/0003-9861(62)90099-1
12. Walsh G.: Proteins: biochemistry and biotechnology, New York: J. Wiley, 2002, 547 p. ISBN 04-718-9907-0

MEDICAL TEXTILE EQUIPMENTS FOR CLASS ONE WITH A NON-INVASIVE CHARACTER

Antonín Havelka, Ladislav Nagy and Adnan Ahmed Mazari

Technical University of Liberec, Faculty of Textile Engineering, Department of Clothing Technology
Studentská 2, Liberec, Czech Republic
antonin.havelka@tul.cz

Abstract: *The research work is focused on the CLASS 1 medical textiles like clothes, linen, towel and other medical items for professionals and patients. These medical items are defined by the relevant technical standards and EU requirements. The requirements for the textile fabrics in the healthcare sector are determined in terms of the end use according to its purpose and usage. Basic requirements for medical items are specified in Government Regulation of the Czech Republic no. 268/2014 Coll. [1], which determines technical requirements for medical items in accordance with European Directive 93/42/EEC. This directive specifies the basic parameters of these products from the point of view of their safety and lays down classification of medical devices into classes' I-III according to the risk of use. The theme of this research is to show the characteristics of medical textiles products under Class I. Products in this class present a low risk of use from the point of view of the user's health. These are mostly non-sterile, non-invasive products that are not subject to the pre-market approval process. On the basis of a survey of the Czech market, these products are used as textile products in healthcare, rehabilitation, spa and after-care and long-term care facilities. Based on the findings and information, it is apparent from the point of view of the material composition what kind of the fabrics is commonly used in these facilities. The material composition of 36.9% of the total products consumed consist of 100% Cotton (CO) in mercerized treatment, 24.1% of the material was made of 100% Polyester (PES), material composition 65% PES / 35% CO is represented by 20.2% of products, material composition 50% PES / 50% CO is represented by 16.7% of products from offered assortment, other types of material composition and use of special fibers is represented in the assortment of medical products of Czech suppliers only Marginal 2.1% of products. It is clear that there is a need for research and development of new types of textiles in mixtures with new, functional fibers in order to achieve the special utility properties of the products. One of the key objectives was to find a suitable solution for achieving the special utility properties of the fabrics for the manufacture of medical items according to their purpose and usage. The utility value of these items are then defined in terms of the useful properties like vapour resistance, antibacterial treatment, active protection of the health of workers in the environment affected by infectious and toxic influences, better user comfort of employees and clients in terms of improvement of personal feelings and work performance, and economic product relations and easy maintenance of products with respect to environmental protection. In the field of health care, the thermo-physiological properties of clothing and the characteristics of air transport, water vapour and moisture are an essential component of comfort. Secondly, the feeling of comfort is influenced by a good make of clothing, a practical and aesthetic design. Requirements for properties are governed by ČSN P ENV 14 237 "Textiles in Health Care". This standard defines the basic properties and methods of textile testing for health care to ensure the suitability of the product for the intended use. It sets minimum requirements to meet acceptable usability.*

Keywords: *medical textiles, utility properties, comfort.*

1 HEALTHCARE TEXTILES

On the basis of a survey of the Czech market, information was obtained on the textile products used in health care, rehabilitation, spa and after-care and long-term care facilities [2]. Each of these environments has its own specifics that govern the use of personal and patient clothing, bedding and medical devices with an emphasis on minimizing health security risks.

From a view of material composition, it has been found that, in these facilities are used fabrics where:

- The material composition of 100% CO in sanforized or mercerized treatment is represented by 36.9% of products from the offered assortment of Czech manufacturers.
- The material composition of 100% PES is represented in 24.1% of the products from the offer of Czech manufacturers.
- The material composition 65% PES / 35% CO represents 20.2% of products from the offered range of Czech suppliers,

- The material composition of 50% PES / 50% CO represents 16.7% of the products from the offered assortment.
- Other types of material composition and use of special fibers are only 2.1% of products in the range of Czech products [2].

From the above, there is a need for application research and development of new types of textiles in mixtures with new, functional fibers in order to achieve the special utility properties of the products. The object of the invention is therefore the textile fabrics for the production of professional and patient clothes, bed linen, towels, drapes and other textile medical devices whose requirements for utility properties are defined by legislation and other technical standards. The aim of the solution is to achieve the special utility properties of the fabrics for the production of medical devices according to their purpose and use.

1.1 Basic requirements for medical textiles and devices

The basic requirements for medical devices are laid down in Government Decree No. 268/2014 Coll., laying down technical requirements for medical devices in accordance with Directive 93/42/EEC [1]. It specifies the basic parameters of these products from the point of view of their safety and lists the classification rules for the inclusion of medical devices in classes according to the risk of use. Class I presents a low risk of use from the point of view of the user's health safety. These products are mostly non-sterile, non-invasive, not subject to the pre-market approval process. For Class I medical devices (sterile) and for all Class IIa, IIb, III devices, the Authorized Person is required to participate in the conformity assessment. For the class I medical devices (non-sterile), the manufacturer carries out the conformity assessment itself without the participation of an authorized person.

The aim of the solution is to achieve the special utility properties of the textile fabrics for the manufacture of medical devices according to the purpose and the method of use by using:

- sophisticated intelligent fiber blends,
- special yarns,
- improved textile and clothing technology.

2 TEXTILES FABRIC IN HEALTHCARE

The requirements for the textile fabrics in the health sector are determined with regard to the end use of the product according to the:

- purpose of use,
- type of usage.

The purpose of the application characterizes the function of the product in the set of medical devices used in terms of its determination due to its interaction with the human organism and the environment (first layer, second layer of clothing). Method of use is defined by the terms of use due to the characteristics of the user's working environment and separated products at once and repeatedly used [3].

The set of utility properties of the fabric is divided according to the following scheme into properties characterizing the user's requirements in terms of

- clothing comfort,
- the appearance,
- durability,
- functional protection.

The set of these requirements is a criterion of quality of a product that is controlled by both the manufacturer and the customer by measuring output properties according to the valid standards.

3 COMFORT FEATURES

Comfort is defined as the state of the organism where all physiological functions are optimal [4]. In the field of health care, the thermos-physiological properties of clothing and the characteristics of air permeability, water vapor and moisture transports are an essential component of comfort. If these properties are not consistent, there is a disturbing perception of clothing comfort. For a feeling of comfort are also important others utility properties as of the hand touch of fabric from the mechanical-comfort viewpoint the THV (Total Hand Value) and heat capacity and thermal conductivity of fabrics represented by the effusivity.

Many factors influence the comfort of clothing from yarn properties to structure of fabric and there are multiple methods how to measure the comfort objectively [5-8]. Last but not least, the feeling of comfort is influenced by the good fitting of garments and a practical and aesthetic design [9]. The medical environment places specific requirements on clothing and textiles. Apparel must be suitable in a relatively warm environment, but at the same time it must cover the skin and avoid contamination of the clean, sterile environment with the human organism, through skin bacterial flora, skin and hair scalp.

3.1 Selected utility properties and other specification

Clothes and generally textiles for use in healthcare are tested for user comfort using the methods they list see Table 1.

Table 1 Selected methods for determining the functional properties of garment comfort [9]

FUNCTIONAL PROPERTIES OF CLOTHING COMFORT	
Utility property	**Air permeability**
Method of determination	ČSN EN ISO 9237- Determination of the permeability of fabrics to air
Measuring equipment	SDL M021S
Result	Speed of air flow
Physical unit	$mm.s^{-1}$
Utility property	**Thermal resistance**
Method of determination	ISO 11092:2014 Physiological effects - Measurement of thermal and water-vapour resistance under steady-state conditions (sweating guarded-hotplate test)
Measuring equipment	SGHP 8.2 Skin Model
Result	Thermal resistance - Rct
Physical unit	$m^2.K.W^{-1}$
Utility property	**Resistance to water vapour**
Method of determination	ISO 11092:2014 Physiological effects - Measurement of thermal and water-vapour resistance under steady-state conditions (sweating guarded-hotplate test)
Measuring equipment	SGHP 8.2 Skin Model
Result	Resistance to water vapour - Ret
Physical unit	$m^2.Pa.W^{-1}$
Utility property	**Thermal conductivity, thermal effusivity**
Method of determination	ASTM D7984 - 16 Standard Test Method for Measurement of Thermal Effusivity of Fabrics Using a Modified Transient Plane Source (MTPS) Instrument
Measuring equipment	FOX 314, TCi
Result	Coefficient of thermal conductivity, thermal effusivity
Physical unit	$W.m^{-1}.K^{-1}$, $W^2.s.m^{-4}K^{-2}$
Utility property	**THV-Total Hand Value**
Method of determination	Internal regulation IP KOD 01-2004
Measuring equipment	Kawabata system
Result	HV, THV
Physical unit	Degree [-]
Utility property	**Integral transport of moisture**
Method of determination	AATCC 195-2011 Liquid Moisture Management Properties of Textile Fabrics
Measuring equipment	MMT - Moisture management tester
Result	Wetting time [s], Absorption [%/s], Maximum wetting radius [mm],Textile solution spreading rate [mm/s], OWTC [%] - The cumulative unidirectional fluid transmission index, OMMC -Index overall indicator of moisture management fabric

3.2 Functional characteristics of medical protective clothing and equipment

The functional and protective properties of medical clothing include the bacteriostatic efficacy of clothing and reduced flammability. Both protective properties can be achieved by:

- special treatments applied,
- addition of fibers with a special function to the material composition.

3.3 Lifetime of medical clothing and equipment

The lifespan of the garment is characterized by the use time which has not resulted in any limitations on the durability of the wear properties. In the case of textile products in the health sector, the lifetime is measured by the number of washing maintenance cycles which are usually performed after one-day use. In Czech health care, the use time of 100 to 150 maintenance cycles is generally recognized until the removal of work clothes. This represents approximately 800 to 1200 hours of wearing [10].

On the basis of a current statistical data and a survey of the needs of the health sector, a consumption of textile fabrics of Class I (non-sterile) in the following years was estimated (see Table 2) [9].

Table 2 Estimation of the volume of textiles for healthcare in the Czech Republic, assuming the durability of 150 washing cycles and daily change of laundry [9]

VOLUMES OF FLAT TEXTILES FOR HEALTH CARE AND AFTER-CARE		
User	**Assortment Kind**	**Estimation of the volume of textiles [m^2/year]**
Patients	Beddings	2 072 596
	Apparel for patient examination	212 130
	Garments for a patients	20 039 010
Dressed for a medical professionals	Clothes	2 229 776
	Other garments	1 114 888
Total together		25 668 400

3.4 Durability properties of medical clothing

Durability properties include tensile strength, seam strength, abrasion resistance, but also a change in dimensions after washing and ironing. The Table 3 presents an overview of evaluation methods and their characteristics.

3.5 Selected utility properties for health protection

Table 4 provides an overview of laboratory methods by which healthcare products can be tested for flame retardancy and bacteriostatic effectiveness.

Table 3 Methods of determination of selected durable utility properties [9]

DURABILITY	
Utility property	**Determination of tensile strength and elongation**
Method of determination	ČSN EN 29073-3
Measuring equipment	Dynamometer LabTest 2.050
Result	Maximum force and elongation
Physical unit	N, %
Utility property	**Seam tensile properties of fabrics**
Method of determination	ČSN EN ISO 13935-1,2
Measuring equipment	Dynamometr LabTest 2.050
Result	Maximum force and elongation
Physical unit	N, %
Utility property	**Determination of the abrasion resistance of fabrics by the Martindale method**
Method of determination	ČSN EN ISO 12947
Measuring equipment	SDL M235 Martindale
Result	Number of cycles to abrasion
Physical unit	Number of cycles
Utility property	**Determination of dimensional change in washing and drying**
Method of determination	ČSN EN ISO 5077
Measuring equipment	Laboratory washing machine
Result	Dimensional change in the longitudinal and transverse directions
Physical unit	%

Table 4 Methods of determination of selected protective utility properties [9]

PROTECTIVE PROPERTIES	
Utility property	**Burning behavior of textile fabrics**
Method of determination	ČSN EN ISO 6940 - Burning behaviour - Determination of ease of ignition of vertically oriented specimens
Measuring equipment	SDL Atlas M233M
Result	Length, firing rate
Physical unit	s, $mm.s^{-1}$
Utility property	**Inflammability - ignition source by the smouldering cigarette**
Method of determination	ČSN EN 1021-1, 2 Furniture. Assessment of the ignitability of upholstered furniture. Ignition source smouldering cigarette
Measuring equipment	SDL Atlas M233P1
Result	Ignition time
Physical unit	s
Utility property	**Antimicrobial efficacy**
Method of determination	ČSN EN ISO 20645 - Textile fabrics - Determination of antibacterial activity - Agar diffusion plate test
Measuring equipment	Petri dish, climatic chamber
Result	Number of bacteria colonies
Physical unit	Verbal description, number
Utility property	**Antimicrobial efficacy**
Method of determination	AATCC Test Method: 147-2004 - Antibacterial Activity Assessment of Textile materials: Parallel Streak Method
Measuring equipment	Petri dish, climatic chamber
Result	Number of bacteria colonies
Physical unit	Verbal description, number
Utility property	**Antimicrobial efficacy**
Method of determination	AATCC Test Method: 100-2004 - Antibacterial Finishes on Textile Materials: Assessment of
Measuring equipment	Petri dish, climatic chamber
Result	Reduction of bacteria
Physical unit	%
Utility property	**Antimicrobial efficacy**
Method of determination	ČSN EN ISO 20743 - Textiles - Determination of antibacterial activity of textile products
Measuring equipment	Petri dish, climatic chamber
Result	Antimicrobial efficacy
Physical unit	Number of CFU bacteria
Utility property	**Antimicrobial efficacy**
Method of determination	ASTM E 2149 – Standard Test Method for Determining the Antimicrobial Activity of Immobilized Antimicrobial Agents Under Dynamic Contact Condition
Measuring equipment	Laboratory shaker
Result	Bacterial reduction
Physical unit	%

4 MATERIALS, METHODS AND ANALYSIS

Standard ČSN P CEN/TS 14 237 "Textiles for healthcare and social services facilities" distinguishes the requirements in terms of described utility properties for two-use textile fabrics [11].

- Bedding
- Clothes

Based on those requirements, a selection was recommended for the design of the final product.

- Fibers and mixtures
- Mixed yarns
- Production textile technology
- Special finishing

4.1 Advised methods for evaluation comfort

Some of basic advised methods for an evaluation of comfort of garments, which are connected to a physiological comfort, are listed up in the Table 1. All of these properties and methods for their evaluation have a direct connection to a comfort of garments. Some of selected of them which are the most important were chosen (see list below).

- MMT - Moisture Management Tester. A method to characterize fabric properties in multi-dimensions liquid transfer.
- Thermography - for a tracking and recording of speed and an area of a liquid spreading in the textile surface can be used the thermal imaging techniques.
- SGHP - Skin model - for an evaluation a heat and water vapour resistance.
- Kawabata system KES – for an objective measurements of hand properties.
- C-Therm Tci – for an objective evaluation of thermal effusivity.

Other advised method for determine an important property of textile material used in medical textiles is 3D scan of porosity of textile materials by using a μCT system like is device SkyScan 1174.

Porosity represents one of the basic parameters of textile fabrics, which significantly affects air permeability and thus the overall physiological comfort of garment [12].

Table 5 Suggested threads, yarns, finishes and properties for a medical textiles used as a beddings [9]

Bedding			Utility properties
Component	**Commercial name**	**Default polymer, reagent**	**Comfort / Health / Safety / Durability**
Threads	Trevon	PP	thermo/ antimicrobial/ reduced flammability / excellent
	Lenzing FR	regenerated cellulose	touch feeling / - / reduced flammability / good
	Dante	regenerated cellulose	touch feeling / - / reduced flammability / good
Yarn	Tepar	PP	thermos / - / reduced flammability / excellent
Finish	Proban	crosslinking agents on the basis of phosphorus compounds using the synergism of nitrogen	- / non-toxic / reduced flammability / good
	Spolapret OS	crosslinking agents on the basis of phosphorus compounds using the synergism of nitrogen	- / non-toxic / reduced flammability / good

Table 6 Suggested threads, yarns, finishes and properties for a medical textiles used as a garments [9]

Garments			Utility properties
Component	**Commercial name**	**Default polymer, reagent**	**Comfort/Health/Safety/Durability**
Threads	Tencel C	regenerated cellulose	touch felling, hydrophilic / hemostatic support healing / antimicrobial / good
	Tencel	regenerated cellulose	touch felling, low friction coefficient, hydrophilic / healing support / - / good
	Sea-Cell	regenerated cellulose	touch felling, hydrophilic / healing support / - / good
	Trevira Bioactive	man-made, PES	- / - / antimicrobial / excellent
	Prolen	man-made , PP	- / - / antimicrobial / excellent
	Siltex	man-made, PP	- / - / antimicrobial / excellent
	Trevon	man-made, PP	- / - / antimicrobial / excellent
Yarn	Coolmax fresh FX	man-made, PES	thermal insulation / - / antimicrobial / excellent
	Tepar	man-made, PES	thermal insulation / - / antimicrobial, flame-retardant / excellent
	Climawell	man-made, PP	thermal insulation / - / antimicrobial / excellent
	Bio Silver	man-made, PP	thermal insulation / - / antimicrobial / excellent
	Multitech	man-made, PA	touch felling, softness / - / antimicrobial / excellent
	Lenzing Modal	regenerated cellulose	touch felling / hemostatic / antibacterial hemostatic / good
	Lenzing Promodal	regenerated cellulose	touch / support healing / - / good
Finish	SANITIZ*ED*® SILVER	ionty Ag	- / support healing / antibacterial / good
	NBK SANLIC		- / support healing / antibacterial / good

4.2 Required utility properties of medical textiles

From the point of view of the use value of the bedding, the components according to Table 5 can be considered as an optimal option for ensuring protection, comfort and durability.

From the point of view of utility value of the healthcare clothing, the components according to Table 6 can be considered as an optimal variant for ensuring protection, comfort and durability.

As is shown in the tables above, the recommended bedding properties include the protective function of reduced flammability, comfort, durability and health promotion. Recommended utility properties for a patients and medical workwear which are preferred for them is a protective function antimicrobial and bacteriostatic and also a comfort and durability properties of clothing.

5 CONCLUSION

The design of textile fabrics for healthcare according to purpose and usage is based on the legal requirements for application in terms of their protective, comfortable and durable function. The estimated consumption of different types of medical textiles in the next years in the Czech Republic at the level of 25 million m^2 of a textile per year clearly demonstrates the importance and necessity of research in this area of the textile industry.

Work activities in the health sector have a risk character. There are many biological, chemical, cytostatic and other factors that can negatively affect employee health and cause occupational disease.

To ensure better properties of medical devices and to achieve antibacterial, anti-inflammatory, thermoregulatory and other active functions, new fibers have been identified. These new fibers and yarns made are the main bearers of the desired functions in designing fabrics with a prognosis of expected utility properties. The resulting mixed functional yarns are thus output from the first phase of the fiber processing into the fabric. Depending on the type of yarn used and the yarn construction, special functional properties of the sheet can be achieved, which are then evaluated according to selected methods for assessing the physiological comfort during their use, especially the most important utility properties - the evaporation resistance *Ret*. The required bedding properties are defined by ČSN P CEN/TS 14 237 "Textiles for healthcare and social services facilities", where the resistance value for water vapor *Ret* ≤ 6 [m^2.Pa.W^{-1}] is also recommended. Therefore, the result from the evaluation of the vapour resistance is strongly recommended to carry out by a various methods which are advised in this paper. Suggested threads, yarns, finishes and properties for used as medical textiles for garments and also for beddings are a part of results of this article. Water vapour resistance depends mainly on the structure of the fabric influenced by the yarn construction and the technology used by in a fabric production. The result also affects the finishing of the fabric, which can significantly change this utility property.

ACKNOWLEDGEMENT: *This research work is supported by Project MPO FV10098 – MediTex.*

6 REFERENCES

1. Zákon č. 268/2014 Sb., o zdravotnických prostředidcích a o změně zákona č. 634/2004 Sb., o správních poplatcích, ve znění pozdějších předpisů. In: Sbírka zákonů České republiky, 2014. Dostupné z: https://esipa.cz/sbirka/sbsrv.dll/sb?DR=SB&CP=2014s268
2. Ditrichová E: Pracovní oděvy ve zdravotnictví - aktivizace povrchů antibakteriální úpravou (Proffesional clothing in health care – activation of surfaces through antibacterial treatment), Liberec, Technical University of Liberec, 2015
3. Bartels V., Volkmar T.: Part I - Types and properties of medical textiles, ed. Handbook of medical textiles. Philadelphia: Woodhead, 2011, ISBN 978-1-84569-691-7
4. Hes L., Sluka P.: Úvod do komfortu textilií (Introduction to Comfort of Textiles), Liberec, Technical University of Liberec, 2005
5. Mazari F.B., Mazari A., Havelka A., et al.: Novel portable device to analyze the moisture permeability of car seat, Industria Textila 69(3), 2018, pp. 183-189
6. Mangat A.E., Hes L., Bajzik V., et. al.: Thermal absorptivity model of knitted rib fabric and its experimental verification, Autex Research Journal 18(1), 2018, pp. 20-27, doi: 10.1515/aut-2017-0003
7. Naeem J., Mazari A., Akcagun E., et al.: $SI0_2$ aerogels and its application in firefighter protective clothing, Industria Textila 69(1), 2018, pp. 50-54
8. Iqbal S., Eldeeb M., Ahmad Z., et al.: Comparative study on viscose yarn and knitted fabric made from open end and Rieter airjet spinning system, Tekstil ve Konfeksiyon 27(3), 2017, pp. 234-240
9. Koldinska M., Kolinova M.: Plošné textilie využívané ve zdravotnictvi a následné dlouhodobé péči (Woven fabrics used in healthcare and subsequent long-term care), Studies for a project No FV 10098 MEDITEX, FT-TUL, Liberec, 2017
10. Zdravotnictví ČR 2015 ve statistických údajích. In: ÚZIS ČR: Ústav zdravotnických informací a statistiky ČR, 2015. Dostupné z: http:// www.uzis.cz/node/7693 [online] [cit. 2017-06-07]
11. ČSN P CEN/TS 14237 (80 4110): Textiles for healthcare and social services facilities
12. Doczyova K., Glombikova V., Komarkova P.: Application of microtomography in textile metrology, Tekstilec 57(1), 2014, pp. 4−11, doi: 10.14502/Tekstilec2014.57.4-11

APPLICATION OF HYBRID HEATING TEXTILE STRUCTURES IN CLOTHING FOR SENIORS

Antonín Havelka[1], Miroslav Tichý[2], Radek Soukup[3] and Ladislav Nagy[1]

[1]Technical University of Liberec, Faculty of Textile Engineering, Department of Clothing Technology, Studentska 2, Liberec, Czech Republic,
[2]VUB a.s., Na Ostrove 1165, Usti nad Orlici, Czech Republic,
[3]University of West Bohemia, Faculty of Electrical Engineering, Department of Technologies and Measurement, Univerzitni 8, Pilsen, Czech Republic
antonin.havelka@tul.cz, tichy@vubas.cz, rsoukup@ket.zcu.cz

Abstract: *Active integral electronic elements in smart clothes can increase the utility value of the garment and the user's comfort. This article is primarily focuses on the comfort of clothing designed especially for the elderly, or people with impaired thermoregulatory capabilities. The research part is focuses on the possibilities of increasing clothing comfort of application a smart electronic textile element into garments. It deals especially with the possibilities of application of electric heating built directly into clothing for seniors, especially for clothes designed for cold environment. The proposed heating system based on embroidery with using hybrid threads can be use especially in winter clothing, but can also be used for home-use clothing or everywhere it is disadvantageous or inappropriately to increase the ambient temperature. The main goal is to improve physiological comfort and ensure thermal comfort in the winter months. From the textile point of view, it is important to ensure that the integration of the heating structure into the garment in order to fulfil its function as best as possible and allow the normal maintenance of the garment by the user and have no impair to the physiological comfort and other utility properties which are also important for the garment. In the case of seniors, the electronics must contain safety features to prevent tampering and avoid the risk of injury to the user. The textile part must therefore comply with both the textile and maintenance requirements as well as the electrical properties. When using active elements in clothing, we need to address the issue of safety, routine clothing maintenance, battery placement, electronics interconnection, durability and other aspects of textile and electronic character. This paper describes the possibilities of creating heating elements using an embroidery machine and the possibility of their integration into selected types of clothing. A practical example then demonstrates the use of hybrid threads that are applied by embroidering the heating structure directly onto a suitable textile backing, demonstrating their potential for increasing the utility properties of the garment.*

Keywords: *thermoregulation, clothing, comfort, heating, smart textiles.*

1 INTRODUCTION

With an influence of various factors on the human organism, it is a crucial ensures that a human body should be in a thermal optimum, called thermal comfort [1]. The determination of thermal comfort and its optimization is given considerable attention form a researchers, sellers and companies especially for the younger and middle generation, which is more active than older population. Research is also focused on the relaxing athletes and especially to the top athletes. Scientific research is focuses than mainly on a medical, military and sports. Interest of a clothing manufacturers and their research has less focusing an older population at this area, because the older people are not for them their typically customers. This group of people is enough big but has a different clothing requirements and also expectation from a clothing comfort.

2 SUBJECT OF RESEARCH

The research part described in this article focuses on the area of a comfort of clothing designed especially for the elderly with the possibility to increasing of garment comfort by using a hybrid textile structure integrated into garment.

2.1 Comfort of clothing for seniors

Thermal comfort, or a thermal well-being, it is the achievement of such thermal ratios, when is a person in balance without any unpleasant feelings as cold, or warm feelings [1-2]. The properties of clothing significantly affect heat transfer and feelings of user. We can conclude that for a good thermal comfort is the most important characteristic the thermal resistance of the garment. The heat resistance of the garment is based on the layering of the material and the air layers between them.

Other properties important for clothing include air permeability, water-vapor permeability, type of a textile structure, resistance to water penetration, resistance to surface wetting, sweating management, etc. and they has to be also consider in a design of clothes [3].

2.2 Specifics of clothing comfort in the age group of seniors - utility of clothing

Elderly and consumers with diseases prefer to buy clothes with high levels of comfort that can meet their physiological, hygienic and health needs. Clothing requirements for seniors are based on physico-mechanical properties of garment comfort. Utility value is a set of utility features that meet the demands of clothing in terms of appearance, durability, easy maintenance and user-friendliness. The process of aging affects every living creature. It affects all the tissues of the organism and is characterized by a different speed. This also applies to human skin, which is an extremely important organ that provides contact with the external environment and represents a mirror, respectively is a monitor of both physiological and pathological phenomena outside and within the body. Therefore, it is important to keep the skin at optimum temperature.

3 EXPERIMENT – PREPARING OF SAMPLES EMBROIDERED BY USING A SPECIAL HYBRID THREADS FOR HEATING

Next text is describing simplified procedure of preparing and embroidering of samples and their basic characteristics.

3.1 A simplified procedure for a creating a draft of embroidery

On the beginning it was necessary to design embroidery pattern suitable for their purpose of use. Proposed embroidery topology was after that transferred to a vector by using SW AutoCAD. Subsequently, these vectors were imported into Tajima program. In this program was carried out their optimization and was prepared program for an automatic embroidery machine TEJT-C1501, on which specimens were have been made.

For embroidering we have used two types of conductive hybrid threads, which were made for this purpose in company VÚB a.s. First hybrid thread contains a Cu/Ag wires a second contains a brass wires (Msx), see Table 1 for detailed specification of hybrid thread. Hybrid thread for embroidering was used on the top and on the bottom of embroidery. Sewing speed of embroidery machine was set to 350 stitches per minute. For a sewing had been tested different types of needles which have been chosen from two companies. One was Groz-Beckert® and second one Schmetz® company. A needle which had been used for sewing was from the Schmetz® company type DBxK5 TN, size 14. Threads were for eliminating a friction and getting the right tension for sewing were lubricated by using a silicon spray.

3.2 Preparing, modification and embroidering textile hybrid heating structures

For a real testing were prepare four different type of textile hybrid heating pad. Differences and their basic properties are in the Table 2. As a underlying fabric for embroidering was used a canvas and for a special embroidery sample model with knitted fabric with a reflecting coating which should be able to reflect a heat flow to a human body.

As is it evident from the Table 2 a different type of hybrid thread and different length and shapes of embroidery lead to a variety electrical resistance of embroideries. All these changes lead to on the basis of that to the different heating performance of pads. It has to be consider before next step a proposal of power supply and electronic parts and conductive textile wires which have to be able to manage lead an electric current till 2 amperes. Samples of embroidery A, B, C are showing on the Figure 1. Sample A is at the end of the embroidery terminated by a sewing spots, which are ready to application a metal connectors or textile poppers. Samples B, C are connected with metal poppers and wired via textile conductive wire called “Ribbon”. It is a conductive textile ribbon, which combines thin metal wires (30 strands) made from Cu with Ag coating with a textile braiding with resistance 0.30 [Ω/m].

Table 1 Basic characteristics of hybrid threads used for embroidering

Type	Yarn fineness [tex]	Composition	Resistance [Ω/m]
Hybrid thread no. 53	50	47% PESh / 53% Cu/Ag wire	6.50
Hybrid thread no. 25A	72	31% PESh / 69% Msx brass wire	8.90

Table 2 Realized embroidered textile heating samples and their basic characteristics

Sample (type)	Dimensions of embroidery [mm]	Thread consumption top + bottom [m]	Electrical resistance of embroideries R [Ω]	Type of used hybrid thread	Underlying material
A1 (Meander)	125 x 283	9.2 + 3.1	5.36	Hybrid thread no. 53	Canvas (PES/Co)
A2 (Meander)	125 x 283	9.2 + 3.1	6.53	Hybrid thread no. 25A	Canvas (PES/Co)
B (Kidney)	190 x 186	12.2 + 4.1	23.56	Hybrid thread no. 53	Canvas (PES/Co)
C (Kidney)	190 x 186	12.2 + 4.1	20.86	Hybrid thread no. 53	Special knitted fabric with a reflecting coating

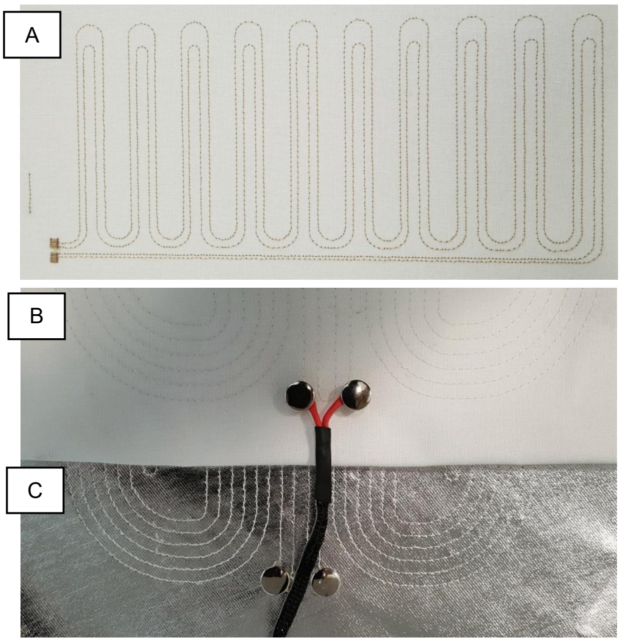

Figure 1 Textile hybrid heating pads, samples B, C are connected with metal poppers and wired via textile conductive wire called "Ribbon"

One of the most important and a difficult part of preparing hybrid textile heating pads was made an improving of automatic embroidery machine which consist with several steps. Basic machine for embroidering is not ready for using a hybrid threads with metal components. List of adaptations which have to be done to reach reasonable quality of embroidery: right size of a needle with titanium or ceramic surface finishing with bigger eye, reduction and normalization friction of a sewing thread, removing the jump change of friction in the sewing thread, adjustment of leading the sewing thread in the machine (reduction of bends), using removable oil to improving a friction.

Inappropriate machine settings or using a wrong type of needle leads to a poor quality of the embroidery, or to violation of sewing thread see Figure 2. This leads to a malfunction of the electrical circuit and it is necessary to repeat the process of embroidering.

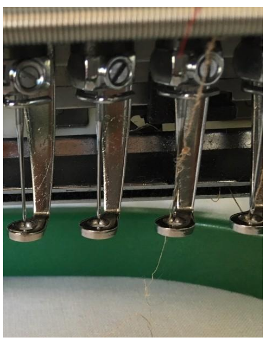

Figure 2 Violation of sewing hybrid thread in the middle of embroidering process

4 THEORY – ELECTRICAL POWER IN RESISTIVE CIRCUITS

In physics, power is the rate of doing work, the amount of energy transferred per unit time. The SI unit of power *P* is the watt [W], which is equal to one joule per second [J/s].

In the case of resistive (linear) loads as our textile heating structure, Joule's law can be combined with Ohm's law (see equation 1) to produce alternative expressions for the amount of power that is dissipated and can be expressed by equation 2:

$$U\ [V] = I\ [A]*R\ [\Omega] \quad (1)$$

$$P = dW/dt = U.I = R.I^2 = U^2/R\ [W] \quad (2)$$

For each type of textile heating structure (heating pad A1, A2, B, C) was according equation 2 calculated theoretical electrical power *P** in watt from known resistance and expectation of voltage on input to circuit. Changes in the internal energy of the wires, caused by the passage of the current, lead to an increase of their temperature and exchange heat flow between the wires and the surroundings [4].

4.1 Experiment – measuring electrical power in closed resistive circuits based on textile heating structures

Methodology

All types of samples were placed into climate room with standards textile condition where is a temperature 21±1°C, relative humidity 60±10%. After acclimatization a heating pad was connected via textiles metal poppers with the laboratory power supply EA-PS 3016-10 B, which is able to precisely set and measure current and voltage at the power source output. Voltage was set step by step (5, 10, 12 and 16 V) and after 5 minutes of stabilization for every step was taken a thermogram and data of a current in the electrical circuit.

4.2 Results

Results with theoretical calculated power and based on the measurement of electrical power from experiment are shown in the Table 3.

4.3 Evaluation of an embroidered heating pads made by using a hybrid threads

For a qualitatively evaluation of embroidering process is a good to use a thermography. The following thermograms were taking by using a thermocamera system Flir S60 in a room with climate control where is a temperature 21±1°C, relative humidity 60±10%, wind circulate 1 m/s. Pads were set to a maximum heating power see Table 3. On the thermogram (see Figure 3) is easily to recognize o spot where is a temperature extreme, which can lead in o long time to make circuit breaks and a dysfunction of heating pad.

Table 3 Measured electrical properties and calculated electrical power P in a comparison with theoretical electrical power P*

Sample (type)	Power P [W] (measured value)	Electric current I [A]	Electrical voltage U [V]	Power P* [W] (calculated value)
A1 (Meander)	4.0	0.8	5.0	4.7
A1 (Meander)	16.0	1.6	10.0	18.7
A1 (Meander)	22.8	1.9	12.0	26.9
A2 (Meander)	3.5	0.7	5.0	3.8
A2 (Meander)	15.0	1.5	10.0	15.3
A2 (Meander)	21.6	1.8	12.0	22.1
B (Kidney)	3.0	0.3	10.0	4.2
B (Kidney)	4.8	0.4	12.0	6.1
B (Kidney)	9.6	0.6	16.0	10.9
C (Kidney)	4.0	0.4	10.0	4.8
C (Kidney)	6.0	0.5	12.0	6.9
C (Kidney)	9.6	0.6	16.0	12.3

Places with lower resistance, which better lead of electric current, can be identify on thermograms as points with a higher local temperature. These locations may indicate a problem with the quality of the embroidering. From the look of functionality and durability of heating pad, this local overheat can leads to malfunction of heating pad in long term of use.

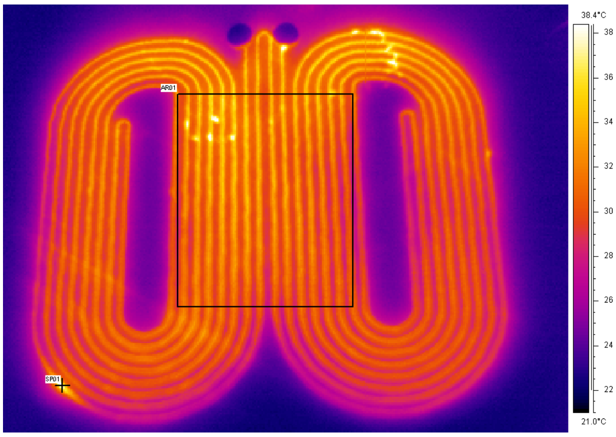

Figure 3 Thermogram of a sample C with an analysis of temperature: Area - AR01: Min. 27.5°C, Max. 40.3°C, Avg. 31.1°C, Spot - SP01: 38.1°C

Thermograms can be also used for a detailed analysis of linking stitch and analysis of flowing of heat direction and spreading in a background material and to the other layers of clothing see Figure 4. The heating pad should to be near to the human skin, but also we need to be ensuring that the temperature in contact points does not to exceed 40°C. Temperature higher than 40°C in a bigger heating area could be unpleasant for a sensitive people and it can leads to bad feelings from a wearing garment.

Whit this technique we can also visualization of the most critical spots for each part of embroider which are place for connectors to join a power supply or other electronics like a logic board. In this case we used textile poppers for a connection to power supply. This article is not focused on other important parts as electronic parts and power wires or durability.

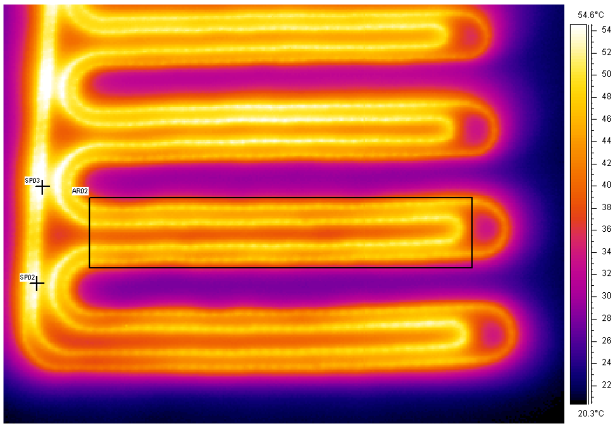

Figure 4 Thermogram of a sample A1 in detail with an analysis of temperature: Area - AR02: Min. 34.0°C, Max. 52.2°C, Avg. 45.1°C, Spots - SP02: 55.0°C, SP03: 57.1°C. (e = 0.95 [-], Temp. refl. = 20°C)

5 DISCUSSION AND CONCLUSION

Improving of thermal comfort of garment and ensuring a good thermal comfort is important for the older people and for people with an impaired thermoregulation. This can be achieved by using a textile hybrid structure like is a heating pad made by embroidering directly on the surface of a clothing, or as a separated par of textile, which can be inserted into a clothing. This article describes in two parts the procedure for the preparing of embroideries with a special hybrid threads and the evaluation of embroidered heating pads. For a using special hybrid threads with a metal parts to embroidering it is important to make some changes in setting of automatic sewing machine to achieve a good quality of embroidery. It is also important to use a lubricant to reach a right tension of sewing threads. If there is a possible to use for yours embroidery system a special needles, which has been designed for sewing with hybrid threads it is recommended to use them. These special needles for sewing with hybrid threads have improved shape, coating and bigger eye of needle. For an analysis of results it is also is important to use a thermography to discover problematic spots and improve a technology of sewing means change a needle, speed of sewing, lubricate, improve of friction of a thread and so on, or also improve a topology of embroidery. Results from experimental part are promising and mainly hybrid thread with Cu/Ag wires which have better sewing properties than hybrid thread with brass wires is suitable for next research and application as a heating textile structure in smart clothing. The use a technology of embroidering of a heating structure in the garment allows us to make a design of an optimal shape according to the location and type of clothing where will be used. Second option how to create a heating area integrated in textile is insert a hybrid threads directly into fabric to the desired area. This area of using a special hybrid heating fabric made by weaving fabric with a special hybrid threads will be close described in our next contribution.

***Acknowledgement**: This work was supported by the Ministry of Industry and Trade of the Czech Republic, Programme Trio - project "Senior Tex - Smart Modular Clothing and Textile Products with Integrated Electronic Microsystems for Improving the Health Care of the Aging Population and Handicap People", reg. no. FV10111.*

6 REFERENCES

1. Hes L., Sluka P.: Introduction to the comfort of textiles (Úvod do komfortu textilií), Skriptum, Liberec: Technical University of Liberec, 2005
2. Apurba D., Alagirusamy R.: Science in clothing comfort, 1st pub., New Delhi: New Delhi Cambridge Oxford: Woodhead Publishing, India, 2010. p. 175, ISBN 978-18-456-9789-1
3. Tao Xiaoming, (Ed.): Handbook of smart textiles: with 565 figures and 66 tables, Singapore: SpringerReference, 2015, ISBN 978-981-4451-44-4
4. Wagner J.: Physics: Summary for Textile Faculty (Přehled pro textilní fakultu), Liberec: Technical University of Liberec, 1989

EVALUATION OF THERMAL PROPERTIES OF TEXTILE STRUCTURES UNDER FAST FLOWING AIR CONDITIONS

Eva Hercikova, Petra Komarkova, Viera Glombikova, Antonin Havelka and Zdenek Kus

Technical University of Liberec, Faculty of Textile Engineering, Department of Clothing Technology, Studentská 1402/2, 461 17 Liberec 1, Czech Republic
eva.hercikova@tul.cz

Abstract: *The subject of this article is the evaluation of thermophysiological comfort of clothing under influence of flowing air. For this purpose a special device has been created, which is capable of generating an air flow of variable velocities. Under these conditions the values characterizing thermal insulating properties of the textile material sample are recorded on a human arm model which is placed in the wind tunnel.*

Keywords: *thermophysiological comfort, thermal insulation, aerodynamic tunnel, fast flowing air.*

1 INTRODUCTION

Nowadays, consumers evaluate not only the visual aspect of clothing, but also its functional properties. As the protection against cold is inherently essential among the basic functional properties, the thermal insulation capability is one of the most important qualities. Therefore, these properties are repeatedly investigated and requested. Thermal comfort is often defined as that condition of mind which expresses satisfaction with the thermal environment. It depends on the heat transfer between the body and the environment [1]. Thermal insulating properties of fabrics can be evaluated by several methods and devices. The individual methods differ from another in terms of measurement, measured values, sample size and for example ambient climatic conditions.

Methods for evaluation of thermal insulation properties are governed by international standards and can be described by basic physical quantities. Internationally recognized methods for evaluation are for example The Sweating Guarded Hotplate, which describes thermal properties using heat resistance R_{ct} [$m^2.K.W^{-1}$], or FOX 314, which describes heat insulating properties using thermal conductivity λ [$W.m^{-1}.K^{-1}$] and thermal resistance R [$m^2.K.W^{-1}$], [2-4]. When searching thoroughly, we can find many other methods and devices for evaluation of thermoisulation of clothing, but all of them observe static ambient conditions. To maintain objectivity when evaluating thermal insulation properties under realistic conditions, it is important to observe as many parameters as possible from a real environment. No one has ever been able to combine all aspects. However, there are many scientific groups that have dealt with partial problems.

The evaluation of materials designed to isolate the human body in extremely cold conditions is therefore more interesting when done at temperatures close to zero or below zero than under normal climatic conditions.

If we deal with performance verification of thermal insulation fillings that are used for outer clothes for cold environments, it is necessary to test thermal properties of batting materials (down and three sophisticated battings) under conditions approaching real weather conditions in Central Europe, where these materials are intended for usage [5]. It has been found, that the thermal insulation of clothes is also very closely related to water vapor permeability [1, 3, 6, 7].

It can be verified that movement of air influences the rate of heat loss from the human body. A moderate breeze can increase the rate of cooling so much that a cool day seems bitterly cold. The concept of "wind chill" was already proven in 1939 to describe the combined effects of wind and temperature. Siple and Passel (1945) later conducted experiments and obtained an equation to predict the rate of cooling as a function of temperature and wind speed [8]. Certain differences were also found when assessing thermal insulation properties at different positions such as siting, walking, etc. This is, of course, also dependent on the precise fit of the garment used [9]. Recent research has been carried out mostly using different models of body parts and also methods using air flow. However, the flow rate it is not possible to change during the measurement [5, 7, 10-12].

The purpose of this paper is the evaluation of thermophysiological comfort of clothing under influence of flowing air. For measuring a special wind tunnel was used, where the intensity of wind can be changed during the measurement without interfering with other set conditions.

2 MEASURING DEVICE

2.1 Description of the measuring device

As can be seen in Figure 1, the measuring system consists of two basic components, the aerodynamic tunnel and the human arm model.

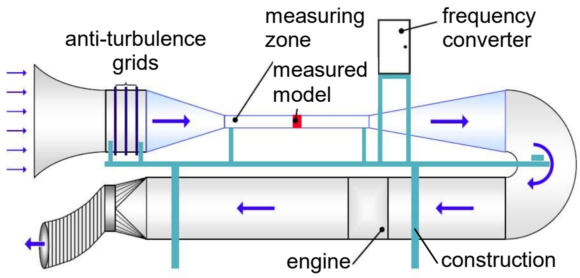

Figure 1 Diagram of the measuring device

The wind tunnel is five meters long. The measurement is carried out in the upper section of the tunnel, which is one meter long, where the required measurement conditions are set and the air flow is adjusted. In the middle of the measuring zone a cylindrical measuring module, representing the human arm, is placed. The model is composed of a heated cylinder, surface of which simulates the surface temperature of the human arm. Around the measured model the sensors are placed at regular intervals to detect the thermal resistance of the fabric.

2.2 Adjusting measurement conditions

The device is controlled by a program built in the LabVIEW programming environment. Thanks to flexibility of the program it is possible to set several important parameters of the air flow specification in the wind tunnel even in course of measurement, which is unique for our model.

The air flow rate is continually controlled and adjusted to maintain the desired value thus obtain more accurate data.

2.3 Model of human arm

The human arm model has a form of cylinder (diameter is 8 cm). In its core is a heater that heats the surface to the temperature of the human body skin. The temperature on the surface of cylinder is 32±0.5°C. Around the cylinder are eight uniformly distributed alphameters (A0-A7). Alphameter is a heat flow density sensor [W/m^2] that can measure the thermal insulation properties of the measured materials. The alphameter A0 is located directly against the air flow (on the windward side of the measured model), alphameter A4 is located on the other side of the cylinder (on the leeward side of the model). The other sensors are distributed at angles of 45 degrees, see Figure 2.

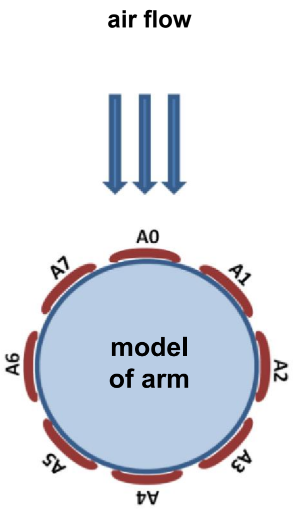

Figure 2 Human arm model with alphameters A0-A7

2.4 Air flow in aerodynamic tunnel

The air flow, which viscosity is very low, becomes quickly turbulent at higher speeds, and such a character is also exposed to a swollen (or flowed) human body.

Within the measurement, an experiment was performed for airflow visualization and human arm model wrapping, as shown in Figure 3. Special smoke was used to visualize the air flowing.

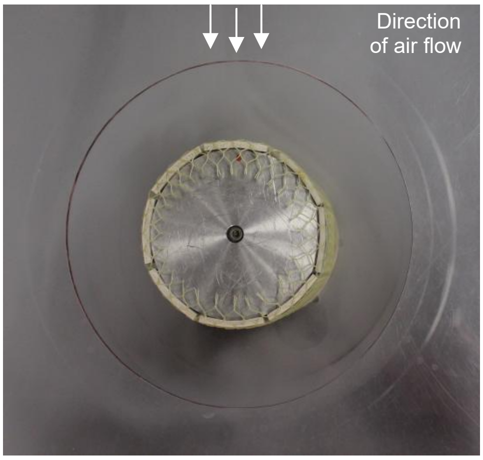

Figure 3 Visualization of air flow in velocity 10 m/s

Figure 3 shows the direction of air flow that affects the individual heat air density sensors. In front of the arm model and on its sides, it is apparent that the air flow is linear at the beginning. By contrast, the A3, A4 and A5 sensors are affected by the turbulence occurring behind the measured model.

3 MATERIALS

Four different types of fabrics were used in experiment. The first one is cotton woven fabric, designed as the working clothes. The material is highly air permeable. The second fabric is fleece knit fabric as a second layer of clothing. Air permeable of this fabric is also high. Third and fourth fabrics are used as outer layers of garments. Their air permeability is insignificant. Table 1 presents the specification of used fabrics.

Table 1 Specification of used fabrics

Sample	Fabric structure	Raw material	Weight [g/m^2]
M1	Woven fabric	100% CO	240
M2	Fleece fabric	100% PES	300
M3	Neoshell barrier fabric	100% PAD; 100% PES	129
M4	Softshell Power Shield barrier fabric	50%PES, 38% PAD, 2% Spandex;100% PES	292

4 METHODS

Thermal insulation properties of our group of textile fabrics were measured on the human arm model in the wind tunnel. The airflow intensity in the wind tunnel was changing during the measurement. It was possible to discern differences in heat loss depending on the angle position in the air flow. The positions of the individual sensors in Figures 4, 5 and 6 correspond to the real positions on the model.

Figure 4 shows the variation of the heat flux on the sample M2 at different velocities of the flowing air.

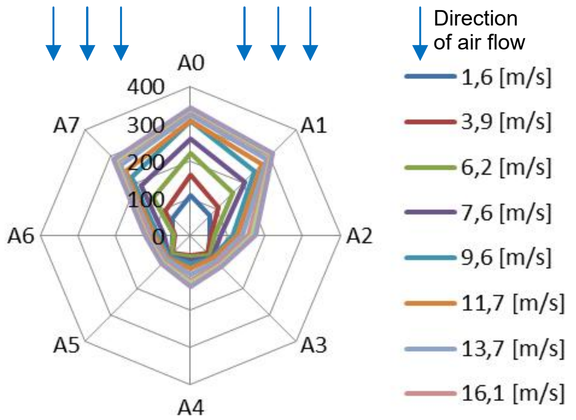

Figure 4 Measuring the variation of the heat flow on the sample M2 at different velocities of the flowing air

Figure 4 shows the difference in the behavior of the heat flux on one material at different velocities of the flowing air. In contrast, Figures 5 and 6 show the difference in thermal insulation properties of all used materials (M1-M4). While Figure 5 was measured at low speed of air flow (2 m/s), Figure 6 was measured at high speed of air flow (18 m/s). It can be deduced from Figures 5 and 6 that while at lower airflow rates the differences in heat loss are not noticeable, at higher speeds, these differences are striking. Behavior of fabrics with a membrane and without differs significantly.

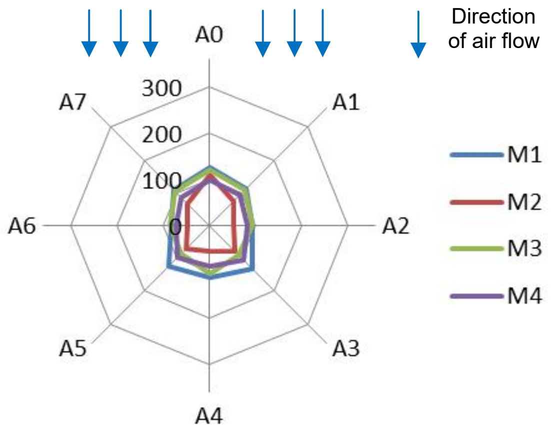

Figure 5 Heat flux at airflow velocity 2 m/s

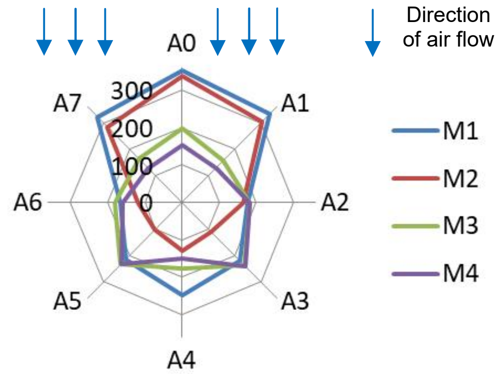

Figure 6 Heat flux at airflow velocity 18 m/s

Figure 7 shows the influence of velocity on the heat flux on the windward side of the measured model.

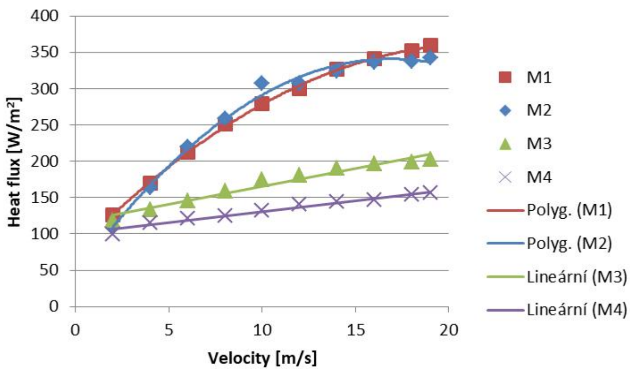

Figure 7 The influence of velocity on the heat flux for windward side (A0)

It can be seen from the Figure 7 that while fabric M1 and M2 behave with polynomial dependence, the values of heat flux and velocity for M3 and M4 show almost linear dependence. For samples M1 and M2 with increasing velocity the sensed heat flux increases much more significantly than the M3 and M4 values. This means that M3 and M4 have passed much less heat away from the arm model to the surroundings. Thus, the body is much less cooled than with M1 and M2 materials even at high airflow. This difference can be explained by the fact that while M3 and M4 materials are designed to protect the body against weather conditions (third layer), the material M1 is intended for the first layer of clothing and the M2 material for the second layer of clothing. Neither M1 nor M2 material does have any wind barrier to keep its breathability as high as possible. The difference between the M3 and M4 materials is due to the fact that the M4 material has an additional thermal insulating layer, whereas the M3 material is only a barrier fabric.

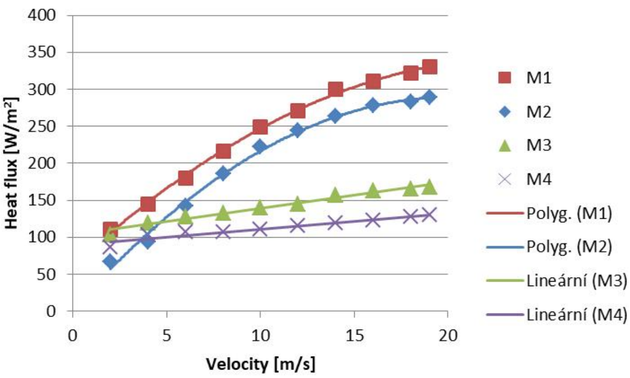

Figure 8 The influence of velocity on the heat flux for alphamether (A7)

As can be seen on Figure 8 the heat flux sensors A1 and A7, which are the first next to the windward sensor (45 degrees), show almost the same course of measurement as the direct windward sensor A0.

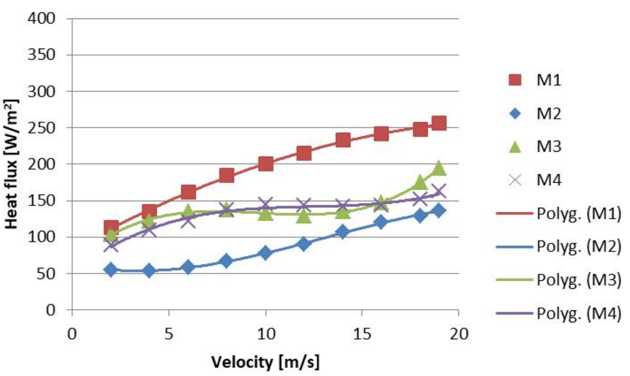

Figure 9 The influence of velocity on the heat flux for leeward side (alphamether A4)

To the contrary, the leeward side of the model (Figure 9) does not show any linear dependence at all. It is apparent on this side of the model that mainly with the barrier textiles (M3 and M4) turbulence caused on the leeward side of the cylinder influences the insulating properties significantly (as was already mentioned in the above chapter).

5 CONCLUSION

Standard methods for measurement of thermal insulation properties can only simulate the perpendicular direction of airflow to the fabric and only one concrete speed of airflow. Our wind tunnel with the human arm model allows an airflow direction which simulates real conditions when wearing clothes. This device also allows to monitor heat loss changes depending on varying airflow speed and depending on the angle of airflow to the fabric.

6 REFERENCES

1. Huang J.: Thermal parameters for assessing thermal properties of clothing, Journal of Thermal Biology 31(6), 2006, pp. 461-466, doi: 10.1016/j.jtherbio.2006.03.001
2. Švecová J., Havelka A., Nagy L.: Measurement of physiological properties of military clothing in simulation of climatic conditions in selected areas of the world, Vlakna a Textil 24(4), 2017, pp. 3-8
3. Havelka A., Nagy L., Kůs Z.: Possibilities of testing and evaluation of functional membrane textiles, Vlakna a Textil 23(4), 2016, pp. 42-46
4. ASTM F1868. Standard Test Method for Thermal and Evaporative Resistance of Clothing Materials Using a Sweating Hot Plate, 2014
5. Havelka A., Glombikova V., Chotebor M., et al.: The thermal insulation properties of hightech sportswear fillings, International Journal of Clothing Science and Technology 27(4), 2015, pp. 549-560, doi:10.1108/IJCST-03-2014-0038
6. Gizem C., Mehmet E.Y.: Comparison of thermal comfort properties of single jersey fabrics produced by hollow yarns with different hollowness ratio, The Journal of the Textile Institute 108(2), 2017, pp. 165-171, doi:10.1080/00405000.2016.1160763
7. Parsons K.C.: Human Thermal Environments, London: Taylor&Francis, 2003, ISBN 0-203-34618-1
8. Kohler J.T.: The meaning, derivation and usefulness of wind chill tables, Online: http://www.kohlerandlewis.com/pdf/windchill.pdf, March 2001, citation: 20.6.2017
9. Havenith G, Heus R, Lotens W.: Resultant clothing insulation: a function of body movement, posture, wind, clothing fit and ensemble thickness, Ergonomics 33, 1990, pp. 67-84
10. Morrissey M.P., Rossi R.M.: The effect of wind, body movement and garment adjustments on the effective thermal resistance of clothing with low and high air permeability insulation, Textile Research Journal 84(6), 2013, pp. 583-592, doi:10.1177/0040517513499431
11. Koelblen B., Psikuta A., Bogdan A., et al.: Thermal sensation models: a systematic comparison, Indoor Air 27(3), 2017, pp. 680-689, doi:10.1111/ina.12329
12. Kind R.J., Jenkins J.M., Broughton C.A.: Measurements and prediction of wind-induced heat transfer through permeable cold-weather clothing, Cold Regions Science and Technology 23, 1995, pp. 305-316

SIZE DETERMINATION OF SHOCK-ABSORBING PACKAGES OF COSTUME ELEMENT MATERIALS FOR PROTECTION AGAINST IMPACT LOADS

Mariia Ivasenko, Svitlana Garkavenko, Viktoriia Kernesh and Natalia Borshchevska

Kyiv National University of Technologies and Design, Nemirovich-Danchenko Street 2, Kyiv, Ukraine
Ivasenko.mv@knutd.com.ua

Abstract: *The article defines the directions for the optimization of shock-absorbing parameters of sports and dance costume elements. The specific body movements, topography of damage and wearing were taken into account. The theoretical and practical research and substantiation of the design features of a protective costume were done on the basis of the concept about an athlete as a biomechanical system. As a result, the dimensions of the package of materials for knee pads were calculated and the recommendations concerning the design features of shock-absorbing packages for various sports and dance directions were given.*

Keywords: *sports and dance costume, biomechanical system, topography of damage, shock absorbing material packages.*

1 INTRODUCTION

Mass fashion for a healthy lifestyle increases the interest in physical activity in various kinds of sports and dances. The sports and dances where the level of dynamic loads is correlated with the level of benefit and injury prevention are gaining popularity as well as the light ones. Among such dances are Hip-Hop, Popping, Dancehall and House. In sports, these are skating, roller sports, cycling/motor sports (and acrobatic variations), skiing, marathon racing, etc. The dance sport culture is also displayed in a special costume, but in most cases injury prevention is not taken into account.

2 EXPERIMENTAL

The aim of the article is to highlight the results of calculating the parameters of universal shock-absorbing material packages for the use in designing an ergonomic and safety costume for athletes and dancers.

Biomechanical peculiarities of the human motor apparatus and a number of influential factors are determined and taken into account in the course of the studies: typical positions and movements, types of safety-designed surfaces, topography of damage and wearing of a costume during sports and dance movements.

The object of study is the design process of universal shock-absorbing elements of a costume for sports and dances.

3 RESULTS AND DISCUSSION

3.1 Preliminary analysis of the source data for calculating the parameters of shock-absorbing packages

Each of sports and dance kinds has its own peculiarities of typical body movements and positions. Choosing the main movements that characterize the biomechanics of the athlete/ dancer's body, the most traumatic are the following: the frontal fall on one or both knees with different distances between the knee joints, abrupt half-splits, rotation on the shoulders, jumping on one/two feet.

When comparing static and dynamic loads on the athlete/dancer's musculoskeletal system, it has been established that the most traumatic are dynamic knee-joint loads:

- dynamic load when running (vertical component) (Figures 1 and 2): $F_{push\text{-}off}$ ≈ 1.3-2.8 kN; $F_{landing}$ ≈ 2.94 kN;
- dynamic load when falling on knee joints F ≤ 13.3 kN.

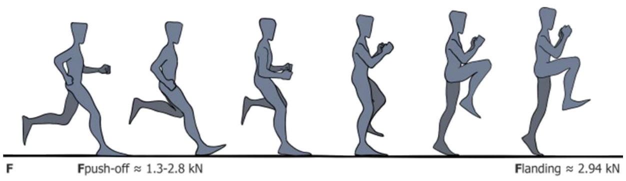

Figure 1 The forces acting on the support during push-off and landing when running

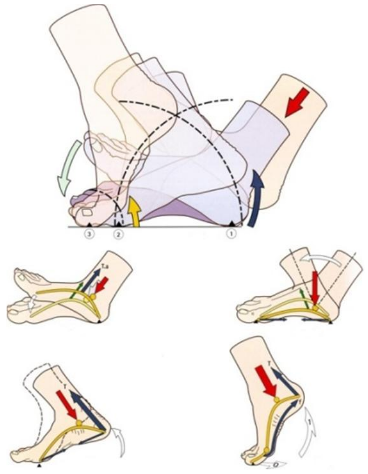

Figure 2 Four phases of the foot push-off

The types of working surfaces are of the same importance. The main of them are the following: scenic and portable sports linoleum, wooden and dance floor, vinyl surface, asphalt and concrete. Any surface can be traumatic, as each of them, depending on the type of coating, can cause different injuries. For example, the dance floor has the lowest slip friction coefficient, which in practice can lead to increased slipping and, as a result, falling of a dancer/athlete, while asphalt, with the highest slip friction coefficient, contacting with the bare areas of the athlete/dancer's body can cause skin injury.

Based on the analyzed characteristic movements and conditions of use, the topography of the athlete/dancer's body injuries and the topography of the wear of sports and dance costumes materials have been developed, and they are shown in Figures 3 and 4.

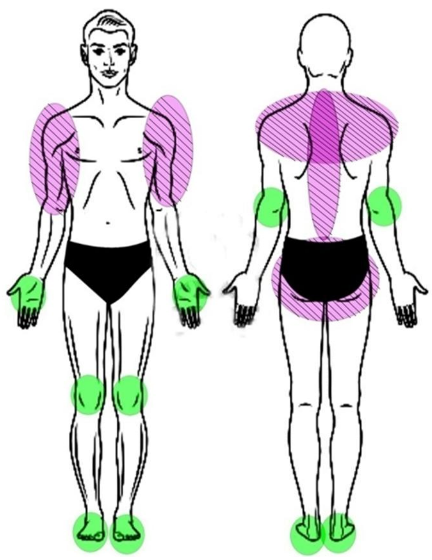

Figure 3 Topography of the athlete/dancer's body injuries

blows (hematomas, dislocations, fractures)

frictions (scratches, hematomas)

From the considered topographies of injuries, it has been found that the most injuried areas of the body are the shoulder girdle, spine, and especially, knee and elbow joints. Based on this, athletes/dancers use knee and elbow pads with an embossed surface as separate personal protective equipment (PPE) to reduce the supporting surface and impact force. When studying the special sports/dance costume design, in this work the attention is focused on the areas of knee joints as the most traumatic area.

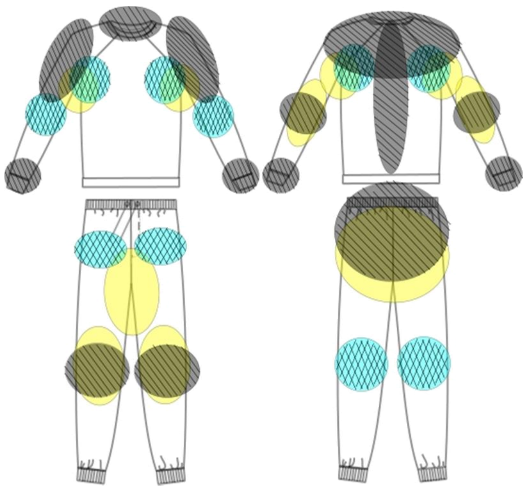

Figure 4 Topography of sports/dance costume materials wear

stretching

bending

abrasion

3.2 *Biomechanical indices of knee joints*

The study of conditions for the functioning of the human musculoskeletal system during sports and dance activities involves the identification of factors that can lead to the destruction of biomechanical systems: the study of mechanisms for improving the safety of bones, joints, muscles, ligaments, tendons; determination of the safety margin of biomechanical systems; study of adaptive mechanisms for solving specific engineering or medical problems.

The bone is a frame-mounted composite material. The mechanical properties of bone tissue depend on many factors: age, disease and individual growth conditions. The tensile strength of the bone tissue under tension σtens is 100 MPa, the relative deformation reaches 1%. In different methods of deformation (load), the bone behaves in different ways. The strength under compression is higher than while bending or stretching. Thus, the tibia in the longitudinal direction can withstand the load of 45000 N, and while bending - 2500 N. The mechanical strength of the bone is quite significant and significantly exceeds the load with which it occurs in usual living conditions.

When walking and running, during working movements of bones, gristles and joints, muscles and tendons are subjected to loading, but load in bones rarely exceeds 50 MPa. The load on the joints depends on the total weight of the body. The estimated load on the joints is expressed by the ratio of the load force to the weight of the body. At a walking speed of only 1 m/s, the load in the hip joint can reach 6 kN, which is way above the weight of the body. In sports, such acceleration is much higher, which can lead to significant, albeit short-term, loads on biomechanical systems. Thus, in time of running, the acceleration of the ankle reaches 500 m/s^2, and at the end of the impact, when performing, for example, karate tricks, even 4000 m/s^2.

It has been established that impact loads are the most injurious to the knee joint. The duration of the impact is usually 50-150 msec. In studying the process of transferring the energy of the impact through the knee joint to the thigh, it was determined that the longitudinal impact force, at which the tibia is destroyed, is from 10.6±2.7 kN (hard impact) to 18.3±6.9 kN (impact through the shock-absorbing lining).

Consequently, for sufficient protection, it is necessary to gain time and use elastic-viscous systems of supporting organs to maximize the use of shock-absorbing properties not only of technical means of protection but also of human tissues. In conventional technical materials with increased strength, as a rule, the elastic module also increases. In biological materials, all major mechanisms for increasing strength are associated with increased energy absorption. The maximum bearing capacity of bones is achieved by increasing the flexibility and raising the gradient of deformation energy growth as the load increases. Under the load above the physiological maximum, there is a significant increase in the gradient of energy gain of bone deformation.

Among the knee joint injuries, as a research object, in sports and dances, the following are common:

- injury of the collateral ligaments: elongation, partial or complete breakage of the collateral ligaments of the knee joint;

- injury of cruciate ligaments: force impact on the tibia appendages or thigh and torsion appendages (motor sports, ice hockey, football, skiing, etc.), in which the anterior cruciate ligament is 30 times more often injured than the posterior one;

- articular cartilage injury (at any joint fracture, in case of injuries with counter and compression action);

- supraclavicle fracture: as a result of direct falling on the knee or hit to the supraclavicle, less often due to excessive tension of the quadriceps muscle (transverse, less often bursting, stellate, etc. [1]).

3.3 Calculation of the parameters of shock-absorbing packages

The criterion of deformation energy density is based on two main hypotheses:

1) Destruction begins in the area where the deformation energy function has a relative constant minimum;
2) The beginning of the destruction comes at a critical for each type of material density value $(\frac{d\omega}{dv})$:

$$(\frac{d\omega}{dv})_c = \frac{S_1}{r_1} = \frac{S_2}{r_2} = ... = \frac{S_c}{r_c} = const \qquad (1)$$

where S_c - the factor of the critical deformation density, which shows the impact viscosity of the material; r_c - the radius of the end of the crack, which characterizes the size of the crack, at which its rapid increase begins.

The areas in a design or material, where energy is used mainly to change the volume, but not the shape, can be identified due to this criterion. These areas are the most sensitive to the formation of cracks and, finally, the process of destruction begins in them.

Also, an important factor in the impact contact is the relative velocity (or energy) of clashing bodies, since its change during the contact determines the dependence of the contact force, local and general deformations on the time, that is, the most important characteristics of the impact in terms of mechanical and functional strength of the human body. The role of protection means against contact impact is boiled down to the reduction of these forces and deformations.

The introduction of shock-absorbing elements makes it possible to reduce the slope of the leading edge of the impact pulse, the amplitude of the contact force, and partially absorb the impact energy [2]. Consequently, research into the construction, that will ensure the safety of an athlete/dancer during training in the most dangerous cases, boils down to the determination of the type and dimensions of shock-absorbing elements to be introduced into the most damaged places.

The basis for calculating the force of the knee's impact in free fall on the flat surface and the force necessary to cause its injury is a series of developments with the simulation of cases of a person's free fall with a certain force of contact of the head with the surface, which were conducted at the Department of Forensic Medicine MGMU named after I.M. Sechenov [3, 6].

On the basis of the given calculations, the dependence of the impact force in the process of collision of the knee with the surface on the mass, the height of the knee position before the fall and the degree of surface rigidity has been obtained, which is represented by the formula:

$$F = kP\sqrt{L} \qquad (2)$$

where F - is the force of a knee blow during accidental fall [N]; k - the coefficient depending on the surface rigidity (for a rigid surface (concrete, tile, etc.) k = 7.7±0.6; semi-rigid (asphalt, wood, etc.) k = 5.6±0.7; non-rigid (linoleum, soil) k = 1.6±0.3); P - body weight [kg]; L - height of the knee position before the fall [m].

Using Newton's second law for rotation and the law of mechanical energy conservation, the angular velocity of the knee at the moment of contact with the surface can be found. Given that the initial linear velocity at accidental fall is equal to zero, we will obtain:

$$mgL = \frac{m\upsilon_x^2}{2} \qquad (3)$$

where m - weight of the body [kg]; g - acceleration of free fall of the body (9.8 m/s^2); L - height of the knee position [m]; υ_F - final linear velocity of the knee (at the moment of impact) [m/s].

For the calculation approximating to the conditions under study, we imagine the body of the athlete/ dancer as a hinge system, and in order to simplify the task, the whole mass of the body is imagined as concentrated in one place at the point A (Figure 4). The force F, with which the body continues to move, and eventually, falls on the knee (or knees), is applied to the body of the dancer. For dead reckoning of the forces of the knee joint collision with the floor, the trajectory of the body motion and the directions of all the forces concerned are schematically depicted in Figure 5.

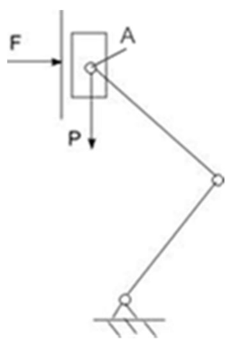

Figure 4 Scheme of fall of the athlete/dancer's body in the form of a hinge system: F - driving force [N], P - weight of the body [kg]

The following indicators were defined for solving the task: duration of falling of the athlete/dancer's body on the knee joint from the position of standing forward and sideward; duration of dancer's falling on two knee joints from th position of standing and jumping; change in the thickness of the material for inserts in the knee pads (various materials for comparison of Table 1 [4-5]); average weight of the dancer's body; height of the dancer's knee position. The necessary values for calculating the knee joint collision with the surface of the dance floor is presented in Table 2.

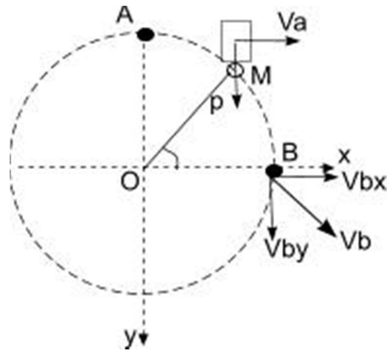

Figure 5 A diagrammatic representation of the body's fall with the distribution of forces:
A is the starting point of the body movement; M - an intermediate point on the trajectory of the body movement; B - the finishing point of the body movement; P - weight of the body [kg]; V_a - initial speed of the body movement; V_{bx}, V_{by} - projections of the body speed on the Ox and Oy axis [m/s]; V_b - terminal speed of the body movement [m/s]

Table 1 Thickness of materials for inserts in knee pads

Name of the laying material for the knee pads	Thickness of the material in its normal state X_0 [mm]
Batting (art. 89541)	5.80
Sintepon (art. 79604)	20.30
Thermosintepon	43.40
Laminate (art. 68134) (1 layer)	2.10
Laminate (art. 121845) (2 layers)	7.30
Laminate (art. 138483) (3 layers)	7.80
Laminate (art. 151353) (4 layers)	10.80

Table 2 Data for calculating the knee joint collision with the surface of the dance floor

Average speed of the dancer's body falling on the surface of the dance floor t_{max} [s]	0.21	
Height of the knee position $S = l$ [m]	0.5	
Acceleration of free fall g [m/s^2]	9.8	
Average weight of the dancer's body m [kg]	60	
Change in the materials thickness (1-7) at the load of 60 kg, $\Delta X = X_0 - X$ [mm] (X - thickness of the material when loaded)	ΔX_1	4.3
	ΔX_2	18.6
	ΔX_3	35.7
	ΔX_4	1.1
	ΔX_5	5.2
	ΔX_6	4.7
	ΔX_7	5.8

Using the values from Table 2, we calculate the forces of the knee collision with the supporting surface when falling on it. We determine the speed of the knee (p. A – Figure 5) at the beginning of the movement trajectory.

$$V_A = \frac{S}{t} = \frac{0,5}{0,21} = 2,38\, m/s \qquad (4)$$

We determine the knee speed at the moment of collision with the surface of the dance floor (p. B - Figure 5).

$$V_{Bx} = V_A = 2{,}38 m/s$$

$$V_{By} = \sqrt{\frac{2l}{g}} \tag{5}$$

$$V_B = \sqrt{V_{Bx}^2 + V_{By}^2} = \sqrt{V_{Bx}^2 + 2gl} = \sqrt{(2{,}38)^2 + 2 \cdot 9{,}8 \cdot 0{,}5} = 3{,}93 m/s \tag{6}$$

We determine the stiffness of each of the materials (c_n) proposed for insertion in the knee pads according to the formula (Table 3):

$$c = \frac{mV_B^2}{(\Delta x)^2} \tag{7}$$

We determine the elasticity strength of each of the materials (F_{str}) proposed for insertion in the knee pads according to the formula (Table 3):

$$F_{str} = c \cdot \Delta x \tag{8}$$

Table 3 Indicators of stiffness and elasticity of shock-absorbing materials

Indicators of stiffness [kN\m]	Stiffness index value [kN\m]	Force of elasticity [kN]	Elastic force value [kN]
c_1	51064.3	F_{elast1}	217.5
c_2	2675.7	F_{elast2}	49.8
c_3	727.9	F_{elast3}	26.0
c_4	725737.3	F_{elast4}	820.1
c_5	33750.0	F_{elast5}	176.9
c_6	410723.1	F_{elast6}	195.1
c_7	274522.6	F_{elast7}	159.5

We determine the force of the knee's impact when colliding with the supporting surface. The time of the interaction between the knee and the surface at the moment of collision we will take as 0.01 s:

$$F_{imp} = \frac{mV_B}{t_{collision}} = \frac{60 \cdot 3{,}93}{0{,}01} = 23580{,}0 H = 23{,}6 \kappa H \tag{9}$$

We determine the maximum permissable value of the knee collision force with the supporting surface and compare it with the force at which the knee joint breaks [3]:

$$F_{\max permis} = F_{str} - F_{imp} \rangle F_{breaks} = 10{,}6 \pm 2{,}7 \kappa H = 13300 H = 13{,}3 \kappa H$$

$$F_1 = 217{,}5 - 23{,}6 = 193{,}9 \kappa H \rangle F_{breaks}$$

$$F_2 = 49{,}8 - 23{,}6 = 26{,}2 \kappa H \rangle F_{breaks}$$

$$F_3 = 26{,}0 - 23{,}6 = 2{,}4 \kappa H \langle F_{breaks}$$

$$F_4 = 820{,}1 - 23{,}6 = 796{,}5 \kappa H \rangle F_{breaks}$$

$$F_5 = 176{,}9 - 23{,}6 = 153{,}3 \kappa H \rangle F_{breaks}$$

$$F_6 = 195{,}1 - 23{,}6 = 171{,}5 \kappa H \rangle F_{breaks}$$

$$F_7 = 159{,}5 - 23{,}6 = 135{,}9 \kappa H \rangle F_{breaks}$$

Therefore, the forces of knee joint collision with the surface using any of the suggested pads, except for Sample No. 3 (thermosintepon), will be less than the force of knee joint destruction itself. That is, for the safety of the athlete/dancer, you can use any of the selected materials for knee pads, except for thermosintepon, based on the aesthetic value only (Figure 6).

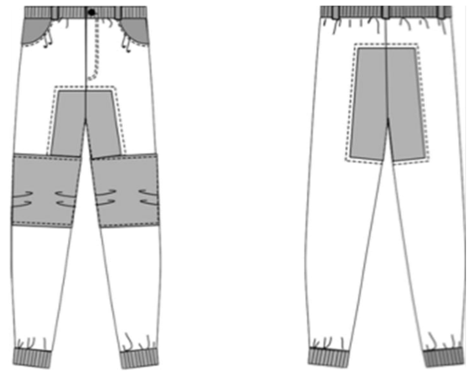

Figure 6 Design of pants with sewn-in shock-absorbing knee pads

Athletes/dancers usually use knee pads as separate personal protective equipment for workouts or performances, wearing them under their pants. However, the procedure for putting them on together with pants requires twice as much time and somewhat more efforts, moreover, separate knee pads increase the cost of the set [7-9]. Thus, in order to provide an aesthetic appearance, as well as proper safety of the dancer/athlete, it is proposed to introduce knee pads, sewn into pants, made of the material with high shock-absorbing properties and with a relatively small thickness. Laminate, which is sewn into pants in two layers, was chosen as such a material according to the research. This will allow to save time putting on supplementary PPE and reduce the cost of the set.

4 CONCLUSION

The obtained calculations can be recommended for determining the parameters of shock-absorbing overlays when designing clothes for different types of physical activity for knee and elbow joints, ischial bones, etc.

5 REFERENCES

1. Gromov A., Naumenko V.: Forensic Traumatology: a guide, Moscow, The Medicine, 1977
2. Obraztsov I., Adamovich I., Barer A.: Problems of strength in biomechanics, Textbook for technical. and biol. specialist. Universities, Moscov, The High School, 1988
3. Optimization of diagnostics of the mechanisms of head injury when falling onto a plane, Collection of plenary and poster reports of the All-Russian Scientific and Practical Conference with international participation, dedicated to 75th anniversary of the RC SME, Moscow, 2006, pp 273-278

4. Yamaguchi J., Takanishi A., Kato I., Experimental development of a foot mechanism with shock absorbing material for acquisition of landing surface position information and stabilization of dynamic biped walking, Proceedings of 1995 IEEE International Conference on Robotics and Automation, Nagoya, Japan, 1995
5. Dolzhenko M., Garkavenko S, Babich A.: Investigation of physical-mechanical characteristics of leather materials in the process of manufacture and operation of footwear, Bulletin of the Kiev National University of Technology and Design 2, 2017 http://nbuv.gov.ua/UJRN/td_2017_2_10
6. Pervaia N., Andreyeva O., Maistrenko L.: Rational use of natural polymer materials for the manufacture of footwear, Baltic Polimer Symposium 2018 (BPS 2018), Jurmala, Latvia, September 12-14, 2018, p.107
7. Gemperle F., Kasabach C., Stivoric J., Bauer, Martin R.: Design for wearability, Digest of Papers., Second International Symposium on Wearable Computers (Cat. No.98EX215), Pittsburgh, USA, 1998
8. Omelchenko G., Kolosnichenko M.: Backgrounds for the development of children's multifunctional clothes of protected dempper elements, II International Scientific and Practical Conference "The current state of the light and textile industry: innovention, efficiency, environmentality", Kherson, Ukraine, 2016, 91-93 pp
9. Ivasenko M., Ermakova M., Orenchina Ya.: Outdoor dance clothes, as part of a dancer's biomechanical system, Light industry 4, 2013, pp. 77-79

CARBONIZATION OF KEVLAR FABRICS FOR EFFECTIVE EMI SHIELDING APPLICATIONS

Daniel Karthik, Vijay Baheti, Veronika Tunakova and Jiri Militky

Department of Material Engineering, Faculty of Textile Engineering, Technical University of Liberec Studentska 2, 46117 Liberec, Czech Republic
danielkarthiktex10@gmail.com

Abstract: *In the present work, porous and electrically conductive activated carbon fabric was produced by heating Kevlar fabric wastes using novel single stage carbonization. The influence of carbonization temperature of 800, 1000 and 1200°C on physical and morphological properties of activated carbon fabric was studied from EDX and SEM analysis. Additionally, the electrical conductivity was also measured. At the end, the utility of prepared activated carbon web was investigated for electromagnetic shielding ability in high frequency (i.e. 2.45 GHz) and low frequency regions (i.e. below 1.5 GHz) using waveguide method and coaxial transition line method respectively. The activated carbon fabric produced at 1200°C showed maximum shielding effectiveness in both high and low frequency regions. For single layers of 1200°C carbon fabric, the electromagnetic shielding effectiveness of 40.5, 41.8, 45.1 and 50.9 dB was found for respective frequencies of 30 MHz, 100 MHz, 1 GHz and 1.5 GHz. This behaviour was attributed to increased absorption of electromagnetic radiations due to its higher porosity and also to increased reflections of electromagnetic radiations due to its higher electrical conductivity.*

Keywords: *Activated carbon, electrical conductivity, electromagnetic shielding, Kevlar fabric wastes, physical activation, specific surface area.*

1 INTRODUCTION

In recent years, research on electromagnetic interference (EMI) shielding materials has attracted significant attention due to an increase in electromagnetic population from widespread applications of computer and telecommunication technologies [1, 2]. Electromagnetic interference refers to the radiant electromagnetic signals emitted by electrical instruments during their operation. The emitted electromagnetic radiations are a concern since they interfere with the working of other appliances as well as causing serious health risks to the consumers [3]. The EMI shielding is related to reflection or absorption of electromagnetic radiations by shielding material. Reflection is a commonly used shielding mechanism by high electrical conductivity materials such as metals and their nanoparticles. However, high density, lack of flexibility, easy corrosion, costly processing and weak microwave absorption are main drawbacks of metals [4]. Among the continuous fibers, carbon fibers are dominant, due to their low density, high modulus, high strength, wide availability and are especially attractive in their electrical conductivity, which relates to EMI shielding effectiveness. The carbon-based shielding materials are expected to be predominant in effective shielding mechanism due to the synergetic effect of electrical conductivity and multiple reflections [6, 7]. A variety of organic precursors have been exploited for the preparation of carbonaceous materials. Aramids, particularly, Kevlar fibres have attracted much attention of researchers as a precursor for high modulus carbon fibres and high efficiency active carbon fibres because they are composed of linear single aromatic rings and no stabilization reaction in the oxygen atmosphere that is often required for the carbonization of low melting organic precursors is necessary. Moreover, if the Kevlar flocks are used as the precursor, the cheaper price may be another merit since they are the wastes from the Kevlar production process [8, 9]. In the present work, electrically conductive carbonized Kevlar fabrics were developed and analysed for their potential use in EMI shielding applications. Kevlar woven fabric wastes were collected from an industry and these flocks were carbonized under specific conditions to obtain an electrically conductive material suitable for EMI shielding applications.

2 EXPERIMENTAL METHODS

2.1 *Materials*

The Kevlar woven fabric wastes were obtained from VEBA textiles, Czech Republic. Table 1 shows the parameters of the Kevlar fabric wastes that were obtained and used in this work.

Table 1 Fabric Parameters of used Kevlar wastes

Material	Pattern	GSM	Thickness [mm]	Warp density [ends per inch]	Weft density [picks per inch]
Kevlar woven fabric	Plain weave	217.4	0.32	17.01	17.01

2.2 *Preparation of activated carbon fabric*

The Kevlar fabric waste was dipped in acetone for 24 hrs to remove surface finish and impurities. The cleaned fabric was then transferred to high temperature furnace (Elektrické Pece Svoboda, Czech Republic) for direct carbonization without any stabilization step. The single stage carbonization and physical activation in presence of air was performed at 800, 1000 and 1200°C with heating rate of 300°C.h^{-1} and without any holding time. This was achieved by controlled carbonization under the layer of charcoal.

2.3 *EMI shielding effectiveness of activated carbon web*

The electromagnetic shielding effectiveness of prepared activated carbon web was determined from two different measurement principles (i.e. waveguide method and coaxial transition line method).

Waveguide method. This method was used to determine the shielding effectiveness of samples for microwave frequency range of 2.45 GHz [14]. The device consisted of a rectangular hollow waveguide having electrically conductive walls. A receiving antenna was placed inside of this waveguide, while a sample was placed at the entrance to the waveguide. The end of the waveguide was filled with foam saturated with carbon particles to absorb the electromagnetic field passed through the sample. Transmitting antenna was placed in front of the waveguide input at 16 cm distance. A network analyser Agilent E 4991A was used to generate, and a high frequency analyser HF-38B (Gigahertz Solutions) was used to receive the electromagnetic signals. The electromagnetic shielding effectiveness *SE* [dB] was calculated based on Equation (1):

$$SE = 10\log\left(\frac{P_t}{P_i}\right) \tag{1}$$

where P_t and P_i are electromagnetic field density [W/m^2] measured in presence of sample, and without the sample respectively.

Coaxial transition line method. For more detailed electromagnetic shielding analysis, coaxial transition line method was used in frequency range of 30 MHz - 1.5 GHz according to ASTM D 4935-10. This device determined electromagnetic shielding effectiveness using the insertion-loss method. The set-up consisted of a sample holder with its input and output connected to the network analyser. A shielding effectiveness test fixture (Electro-Metrics, Inc., model EM-2107A) was used to hold the sample. The network analyser (Rohde & Schwarz ZN3) was used to generate and receive the electromagnetic signals.

3 RESULTS AND DISCUSSION

3.1 *Characterization of activated carbon web*

EDX analysis. Energy disperse x-ray spectroscopy was performed to know the relative proportion of different elements present in the activated carbon fabrics. The activated carbon web produced at 1200°C exhibited 92.35% increase in carbon content and 4.56% reduction in oxygen content (Table 2). This behavior was attributed to removal of hydrogen, sulphur, nitrogen and other elements due to decomposition at higher temperature.

Table 2 Effect of carbonization temperature on elemental composition of activated carbon fabric

AT. [%]	C	N	O	Na	S	Cl	K	Ca
1200°C	92.3	2.2	4.5	0.1	0.2	0.0	0.3	0.0
1000°C	87.6	5.1	6.1	0.2	0.2	0.0	0.5	0.0
800°C	73.8	9.1	12.2	3.3	0.9	0.1	0.2	0.0
Untreat.	69.4	14.0	15.3	0.6	0.3	0.0	0.0	0.0

Electrical conductivity. From Figure 1, the electrical volume resistivity was found to decrease with increase in carbonization temperature. The 1200°C activated carbon sample exhibited 1000 times reduction in electrical resistivity over 800°C activated carbon sample. The higher electrical conductivity of 1200°C activated carbon sample was attributed to more graphitization.

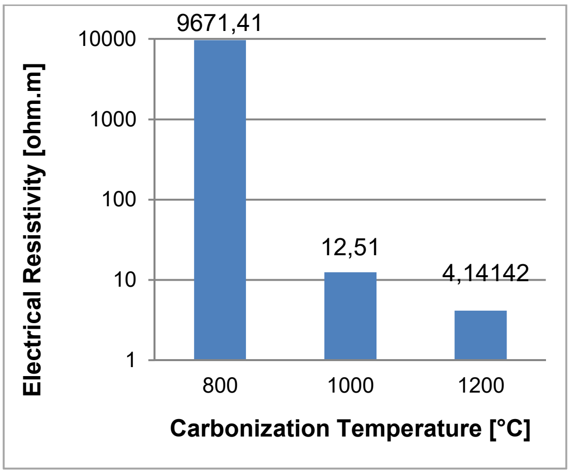

Figure 1 Effect of carbonization temperature on electrical conductivity of activated carbon web

SEM morphology. From Figure 2, the activated carbon fabric showed noticeable rough surface as compared to Kevlar fabric web. The surface roughness was found to increase with increase in carbonization temperature, which indicated the development of more porous structure after physical activation of Kevlar fabric wastes.

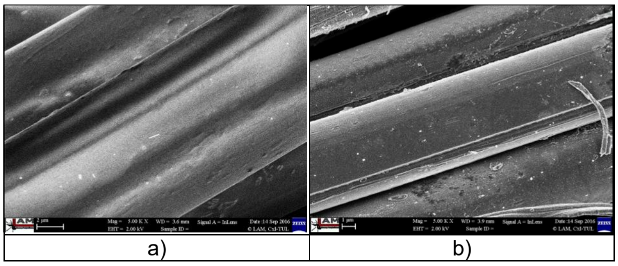

Figure 2 SEM image of (a) untreated Kevlar fabric (b) 1200°C activated carbon fabric

3.2 Electromagnetic shielding ability

Waveguide method. Figure 3 shows the average values in 95% confidence interval for electro-magnetic shielding effectiveness of prepared activated carbon web samples in single and double layers measured at 2.45 GHz frequency. The scattered data points were connected with line for easier visualization of results (i.e. there is no approximation of trend by regression analysis). The electromagnetic shielding effectiveness was found to increase with increase in number of layers and increase in carbonization temperature.

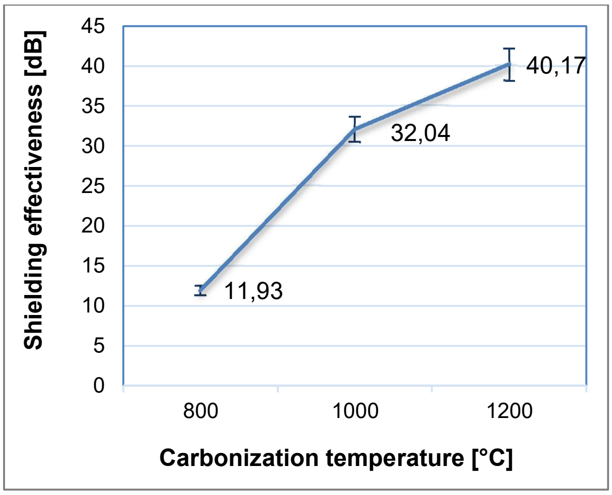

Figure 3 Effect of carbonization temperature on electromagnetic shielding effectiveness in high frequency region

Coaxial transition line method. This method was used for estimation of shielding effectiveness according to ASTM 4935-10 standard in low frequency region from 30 MHz to 1.5 GHz. Figure 4 shows the mean values of electromagnetic shielding effectiveness for single layers of different activated carbon samples in frequencies of 30 MHz, 100 MHz, 1 GHz and 1.5 GHz. The data points were connected with line as in previous figure. The increase in shielding effectiveness with increase in carbonization temperature was observed. The 1200°C activated carbon web exhibited the shielding ability of 40.51, 41.75, 45.13 and 50.90 dB for respective frequencies of 30 MHz, 100 MHz, 1 GHz and 1.5 GHz. This behavior was attributed to increased absorption of EM radiations due to its higher porosity and also to increased reflections of EM radiations due to its higher electrical conductivity.

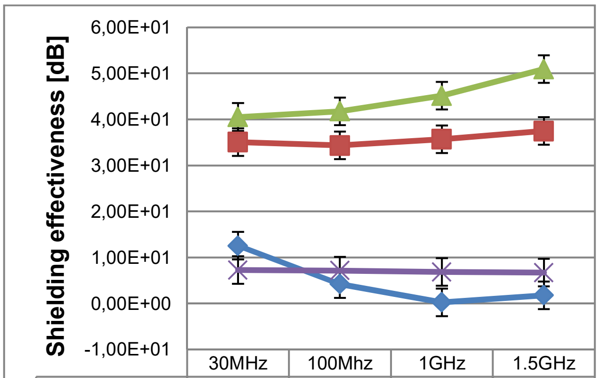

	30MHz	100Mhz	1GHz	1.5GHz
untreated	1,25E+01	4,21E+00	2,48E-01	1,76E+00
800	7,26E+00	7,14E+00	6,83E+00	6,70E+00
1000	3,51E+01	3,43E+01	3,57E+01	3,75E+01
1200	4,05E+01	4,18E+01	4,51E+01	5,09E+01

Figure 4 Effect of frequency on electromagnetic shielding effectiveness

4 CONCLUSIONS

The present study was focused on development of porous and electrically conductive carbon based electromagnetic shielding materials. This was achieved by physical activation of woven Kevlar fabric wastes into activated carbon fabric. The carbonization was performed under the layer of charcoal at 800°C, 1000°C and 1200°C with the heating rate of 300°C.h^{-1} and without any holding time. At 2.45 GHz, the electromagnetic shielding effectiveness of 40.17, 32.04 and 11.93 dB was exhibited by single layers of activated carbon fabric produced at 1200, 1000 and 800°C, respectively. On the other hand, for low frequency regions, the 1200°C activated carbon web exhibited the shielding ability of 40.51, 41.75, 45.13 and 50.90 dB for respective frequencies of 30 MHz, 100 MHz, 1 GHz and 1.5 GHz. This behavior of 1200°C activated carbon web was attributed to increased absorption of EM radiations due to its higher porosity and also to increased reflections of EM radiations due to its higher electrical conductivity.

5 REFERENCES

1. Šafářová V., Tunák M., Militký J.: Prediction of hybrid woven fabric electromagnetic shielding effectiveness. Textile Research Journal 85(7), 2015, pp. 673-686, doi: 10.1177/0040517514555802
2. Šafářová V., Militký J.: Electromagnetic shielding properties of woven fabrics made from high-performance fibers, Textile Research Journal 84(12), 2014, pp. 1255-1267, doi: 10.1177/0040517514521118

3. Chung D.D.: Electromagnetic interference shielding effectiveness of carbon materials, Carbon 39(2), 2001, pp. 279-285, doi: 10.1016/S0008-6223(00)00184-6
4. Rubežienė V., Baltušnikaitė J., Varnaitė-Žuravliova S., et al.: Development and investigation of electromagnetic shielding fabrics with different electrically conductive additives, Journal of Electrostatics 75, 2015, pp. 90-98, doi: 10.1016/j.elstat.2015.03.009
5. Wang L.L., Tay B.K., See K.Y., et al.: Electromagnetic interference shielding effectiveness of carbon-based materials prepared by screen printing, Carbon 47(8), 2009, pp. 1905-1910, doi: 10.1016/j.carbon.2009.03.033
6. Salman N., Baheti V., Tunakova V., et al.: Development of porous and electrically conductive activated carbon web for effective EMI shielding applications, Carbon 111, 2017, pp. 439-447, doi: 10.1016/j.carbon.2016.10.026
7. Junhua W., Chung D.D.: Increasing the electromagnetic interference shielding effectiveness of carbon fiber polymer–matrix composite by using activated carbon fibers, Carbon 40(3), 2002, pp. 445-467, doi: 10.1016/S0008-6223(01)00133-6
8. Ki S.K., Chul W.P., Seong-Ho Y., Seung M.O.: Preparation of Kevlar-derived carbon fibers and their anodic performances in Li secondary batteries, Carbon 39(11), 2001, pp. 1619-1625, doi: 10.1016/S0008-6223(00)00298-0
9. Giraldoa L., Ladinob Y., Pirajánc J.C.M., Rodríguezb M.P.: Synthesis and characterization of activated carbon fibers from Kevlar, Eclética Química 32(4), 2007, pp. 55-62, doi: 10.1590/S0100-46702007000400008
10. Safarova V., Tunak M., Truhlar M., Militky J.: A new method and apparatus for evaluating the electromagnetic shielding effectiveness of textiles, Textile Research Journal 86(1), 2016, pp. 44-56, doi: 10.1177/0040517515581587

RELATIVE SURFACE AREA OF NANOMATERIALS - - DREAM AND REALITY

Jiří Militký, Dana Křemenáková and Rajesh Mishra

Department of Material Engineering, Faculty of Textile Engineering, Technical University of Liberec, Studentska 2, 46117 Liberec, Czech Republic
jiri.militky@tul.cz

Abstract: *The nano fibrous assemblies (membranes) are extremely thin in the order of a few microns only. They have often relatively smaller porosity compared to micro fibrous membranes. Thus by considering their porosity as well as thickness, the nano fibrous membranes do not offer so huge real surface area as is evaluated from standard approach (surface area-to-volume or surface area-to-mass ratio) because the volume or mass are for nanofibrous materials too small. Rather the micro fibrous assemblies (membranes) provide sufficient real surface area of fibrous phase for end use applications e.g. filtration or surface activation. For estimation of relative surface area it is proposed to use surface area-to-macro surface ratio which is dimensionless and dependent on porosity as well as thickness. The advantages of this definition of relative surface area are demonstrated on the example of PA 6 nano and micro membranes.*

Keywords: *relative surface area, nano membranes, micro membranes.*

1 INTRODUCTION

The “nano“ in nanotechnology comes from the Greek word “nanos“ that means dwarf. One nanometer is one billionth i.e. 10^{-9} meter. The fundamentals of nanotechnology lie in the fact that properties of substances dramatically changes when their size is reduced to the nanometer range. When a bulk material is divided into small size particles with one or more dimension (length, width, or thickness) in the nanometer range, the individual particles exhibit unexpected properties, different from those of the bulk material. The nanometer range is characterized by the transition of a material‘s behavior from “quantum like” behavior of atoms and molecules to the “continuum like” behavior of bulk materials [1, 2].

Often, nanomaterials are defined by a size range limited by at least one of the dimensions. This range may be 1–100 nm [3, 4] (British Standards Institution 2007; ISO 2008), 0.1–100 nm [7], less than 100 nm [5], or less than 500 nm [6]. The most common and accepted definition is probably the 1–100 nm range. In addition, it is sometimes suggested that to be counted as a nanomaterial the material must have properties different from those of the bulk form of the same chemical substance [7, 8]. The European Commission released their suggested definition of nanomaterials: “‘Nanomaterial’ means a natural, incidental or manufactured material containing particles, in an unbound state or as an aggregate or as an agglomerate and where, for 50% or more of the particles in the number size distribution, one or more external dimensions is in the size range 1 nm - 100 nm” [9, 10].

The nanometer range is physically characterized by the transition of a material‘s behavior from “quantum like” behavior of atoms and molecules to the “continuum like” behavior of bulk materials. Especially for nano fibrous assemblies prepared by electrospinning is the mean fibrous elements thickness (diameter) is some hundreds of nanometers. But in general, all these fibers with a diameter below 1 μm (1000 nm) are often accepted as nanofibers [1].

One of the main advantages of nanomaterials is very huge relative surface area (surface area-to-volume ratio) [2]. This is in fact true for nanoparticles where are not limitations according to the macro geometry (unit volume).

It is widely published that by reducing fiber diameters down to the nanoscale, an enormous increase in specific surface area to the level of 1000 m^2/g or much more is possible. By reducing the fiber diameter from 10 μm to 10 nm, a million times increase in flexibility is expected. Recognizing the potential nano effect that will be created when fibers are reduced to the nanoscale, there has been an explosive growth in research efforts around the world. Specifically, the role of fiber size has been recognized in significant increase in surface area, bio-reactivity, electronic properties and mechanical properties. The enhanced reactivity and efficiency of nanofibers is based on the claim that nanofibrous membranes provide enormous availability of surface area per unit mass [3].

Limited thickness is serious limitation for volume of these objects calculation because the unit of their macro surface should be multiplied by real thickness and final macro volume is then very low. It leads to low amount of nanofibers and their low total surface area per unit of macro surface. Avoiding of this limitation leads to the unbelievable huge relative surface area values which cannot be achieved in real products. The same situation appeared when the properties as sorption capacity are calculated relatively to mass.

For estimation of relative surface area it is proposed to use surface area-to-macro surface ratio which is dimensionless and dependent of porosity as well as thickness. The advantages of this definition of relative surface area are demonstrated on the example of PA 6 nano and micro membranes.

2 NANOMATERIALS CHARACTERIZATION

Nanomaterials (nano fibrous assemblies) have some limitations for practical use because they are: too week and too sensitive to abrasion to be outer or inner part of clothing in conditions of wearing and maintenance, they have some effect on nano level only, they have low comfort (bad drape), and have serious limits for longer time use in common conditions. Their effects are often only temporarily.

There are often unprecise information oriented to highlight of „nano“ from point of view of scientific content and to suppress weakness in real conditions. Instead of seriousness there are appeared „newspaper stories“ oriented to dazzle of customers (nano layers with extremely thermal insulation, extremely surface area of nano layers, nano is equivalent to stronger, etc.). Of course, there are some big advantages of nano but the serious limitations as well.

It is well known that many properties of matters depend on the size range. In nano scale there are in some cases extra effect not following the bulk materials because the particle/wave nature of matter appears (quantum effects, tunneling, self-assembling). Nano objects are generally divided into three categories [3]:

1. Nanoparticles (3 ext. dimensions in the nanoscale)
2. Nanofibres (2 ext. dimensions in the nanoscale)
3. Nanoplates (1 ext. dimension in the nanoscale)

Plenty of characteristics are similar for all kind of nano object but simplest are derivations of relations for the case of nanoparticles. Their benefit is not limitations according to the magnitude of dimensions and therefore the properties or characteristics can be expressed in relative units (usually per unit of mass). Exclusive is relative mass expressed as density ρ where

$$\rho = m / V = m / (S\, h) \tag{1}$$

Density is then ratio between particle mass m and particle volume V as product of particle cross section area S and thickness h.

In the case of nanofibers there are real limitations due to restricted cross section area and relative mass is better expressed as fineness T_T usually in tex units. It can be simply shown that

$$\rho = T_T / S \tag{2}$$

Nanofibers are usually in the form of assemblies i.e. nanoplates.

In the case of nanoplates there are real limitations due to restricted thickness h only and better is to express relative mass as so called planar mass M_P usually in gsm (gram per square meter units) units. For this case it is:

$$\rho = M_P / h \tag{3}$$

Nanoparticles (less 100 nm) contain 1 million atoms or less (spherical particle of 1 nm radius has approximately 25 atoms) and majority of atoms are on the surface. Nanoparticles are particles with at least one dimension smaller than 1 μm, and potentially as small as atomic and molecular length scales ~0.2 nm. Nanoparticles can have amorphous or crystalline form, and their surfaces can act as carriers for liquid droplets or gases. It is very simple to compute the geometrical changes due to use of particles with smaller dimension. Simple calculations are based on the ideal cubic particles with edge length D.

The specific surface area of cubic particle of edge length D and density ρ is defined by relation:

$$S_a = \frac{S}{\rho\, V} = \frac{6\, D^2}{\rho\, D^3} = \frac{6}{\rho\, D} \tag{4}$$

The specific surface area is growing dramatically below particles of diameter 10 nm. Qualitatively similar trends are valid for related properties such as the ratio of surface/bulk atoms and the fraction of particle volume comprised by a surface layer of finite thickness.

Let the cubic particle of edge length D, with the surface area of $S = 6\, D^2$ is divided into n identical cubic particle of edge length d with total surface area $S_T = n\, 6\, d^2$. Because the volume of bigger particle $V = D^3$ is the same as sum of volumes of n smaller particles $V = n\, V_S = n\, d^3$ the number of smaller particles is simply:

$$n = \left(\frac{D}{d} \right)^3 \tag{5}$$

Relative gain of surface area S_R while maintaining the volumes is:

$$S_R = \frac{S_T - S}{S} = \left(\frac{D}{d} - 1 \right) \tag{6}$$

For example, if the particles of edge length 10 nm are produced from particle of edge length 10 mm, the number of particles is $n = 10^9$ and $S_R = 999$.

Increase of area S_n is then equal to:

$$S_n = S_T\ / S = D / d = \sqrt[3]{n} \tag{7}$$

Typical length ratio $L = D/d$ for d equal to the atom size and D equal to particles size can be simply used for computation of:

1. Number of atoms in particle $n = L^3$
2. Particle mass $M_c = M_m\ L^3 / 6.022\ 10^{23}$, where M_m is molecular mass of material.
3. Particle volume $Vp = 6\ d^2\ L^3$

Very common mistake is assumption that nano particles have better mechanical properties in comparison with more voluminous particles. In facts is cohesion energy per atom (size d) dependent on the size of particles (D) by relation:

$$E = E_b \left(1 - \frac{d}{D}\right) = E_b \left(1 - \frac{1}{L}\right) \tag{8}$$

where E_b is cohesive energy for bulk material.

For nanoparticles it is ratio d/D from 0.1 till 0.01 and cohesive energy is increasing with particle diameter. It is interesting that starting from diameter of nanoparticles around 100 nm is E practically constant. This is one natural support of definition of nano range.

Many particle and molecular clusters properties (e.g. ionization energy, electron affinity, melting temperature and cohesive energy) show a smooth variation with size in the large particle regime. The following scaling laws can be applied for a general property (G) [5]:

$$G(N) = G(\infty) + a\ N^{-b} \tag{9}$$

where N is size (number of atoms) in particle or cluster. Usually $b = 1/3$.

Large deviations (oscillations about the smooth trend) are observed for many properties in the medium and (especially) the small particle size regimes. Deviations arise due to quantum size effects (electronic shell closings) and surface effects (geometric shell closings).

Between particles generally occur gravitational and electromagnetic forces. Gravitational force is a function of mass and distance and is extraordinary weak between (low-mass) nano sized particles. Electromagnetic force on the other hand is a function of charge and distance. It is not affected by mass, so it can be very strong even when we have nano sized particles. The electromagnetic force between for example two protons is 10^{36} times stronger than the gravitational force. The stability in liquid continuous phase depends on the settling velocity v_s, which is proportional to their size squared $v_s \sim d_p^2$.

For nanoparticles is d_p very small and settling velocity is very small (sedimentation occurs after long time). For these particle sizes the diffusion is due to molecular collision i.e. Brownian motion [11-15].

3 MEMBRANES CREATED IN ELECTROSTATIC FIELDS

Traditionally high voltage electrostatic field is used for creation of nanofibrous assemblies and conditions of preparation are selected to avoid the creation of other structures (bead, solidified drops etc.). This technology, called electrospinning, is powerful in fabrication of two-dimensional (2D) or three-dimensional (3D) fibrous nanostructures [16, 17]. In fact the same technology can be used for creation of porous membranes based on electrospraying principle (deposition of droplets) or electronetting principle (see Figure 1).

The structures shown in Figure 1 can be prepared by using the same machinery (needless electrospinning of Nanospider type) by changing of properties of spinning liquid phase, voltage and machine setting. All these parameters are critically dependent on the selected polymer solvent or dispersion chemical composition, physical form and concentration. These parameters are important for tuning porosity or compactness of membranes. The Nanospider electrodes which have been developed through last ten years of optimization can give big portfolio for electrospraying as well. The nano sized structures are deposited on supporting layer which can improve functionality.

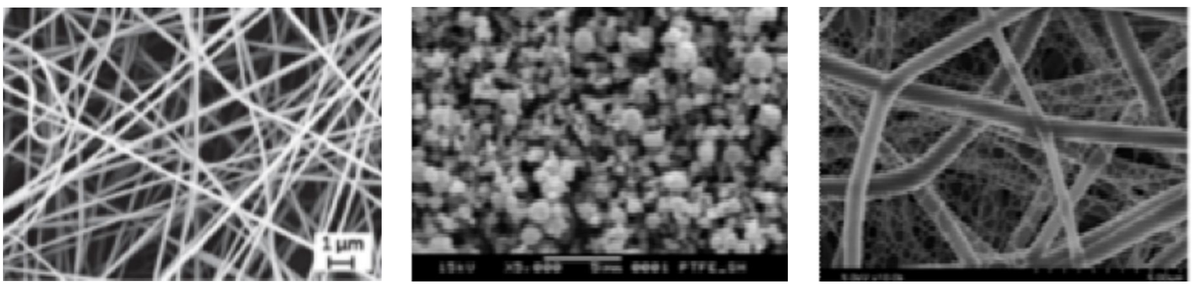

Elspun nanofiber membrane | Electrosprayed PTFE | Electronetting effect

Figure 1 Porous layers prepared in electrostatic field

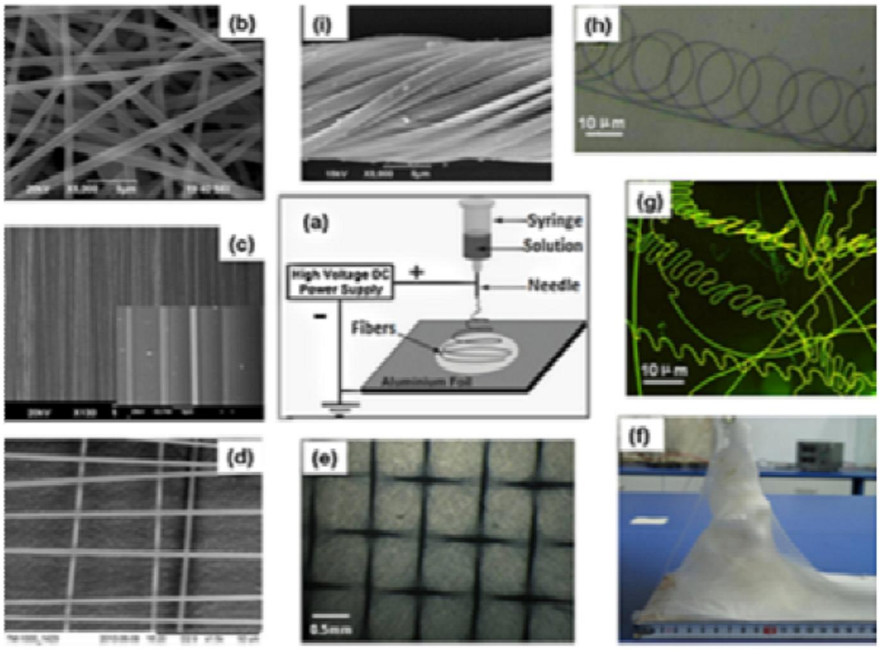

Figure 2 (a) Schematic diagram of electrospinning method, (b) electrospun polymer nanofiber mesh without orientation, (c) parallel and (d) crossed fiber array, (e) patterned fiber web, (f) 3D fibrous stack, (g) wavy and (h) helical fibers, and (i) twisted fiber yarns [18]

Electrospinning, an electrostatic fiber fabrication technique, is versatile and applicable in diverse fields. The nanoscale fibers are generated by the application of strong electric field on polymer solution, dispersion or melt [17]. The assembly of fibers produced by this process, offer various advantages like high surface area to volume ratio, changeable porosity and the ability to change composition to get desired function. Over the years, more than 200 polymers have been electrospun for various applications and the number is still increasing with time [17]. Electrospinning is superior in production and construction of ordered or more complex nanofibrous assemblies (see Figure 2).

The random orientation of fibrous mats fabricated by the conventional electrospinning may limit the potential applications, especially in the fields of electronics, photonics, photovoltaics and tissue engineering which need fast charge transfer or regular structures. To solve this problem, a variety of strategies have been proposed, such as pair electrodes collection, rotating drum or disk collection, auxiliary electric or magnetic electrospinning, double spinning, near-field electrospinning, direct-writing electrospinning, etc. Some approaches such as rotating drum collection have been used in the commercial electrospinning setup. The ability to consistently fabricate highly aligned fibers in large quantity over a large area is still a challenge [18].

Electrospraying utilizes electrical forces for liquid atomization [19]. Droplets obtained by this method are highly charged. The advantage of electrospraying is that the droplets can be extremely small (tens nanometers), and the charge and size of the droplets can be controlled to some extent by electrical means. Motion of the charged droplets can be controlled by electric field. The deposition efficiency of the charged spray on an object is usually higher than that for uncharged droplets. The membrane morphologies can be categorized into two main groups: dense and porous. The dense layer can be amorphous, crystalline (of different structures) or amorphous with incorporated particles (intrusions). The porous layer can be reticular, grainy, or fractal like. These structures are schematically shown in Figure 3. The membrane morphology depends, in general, on the temperature, the solvent used for spraying, voltage, physical properties of liquid phase (emulsion, dispersion, solution, density and surface tension), distance of collector from source, doping agents and the time of solvent evaporation. Post annealing and post treatment e.g. by plasma or microwaves can also modify the final morphology [20].

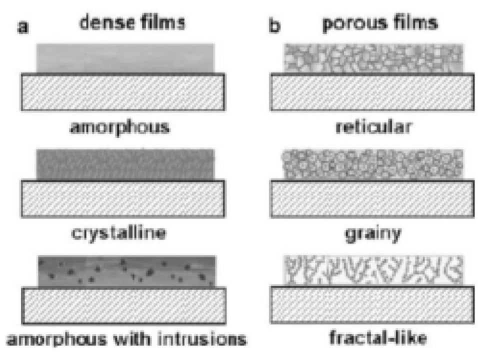

Figure 3 Typical morphologies obtained by electrospraying [20]

Electrospinning/netting or electronetting is a one-step strategy for fabricating nanofiber/net membranes comprising common electro spun nanofibers and two-dimensional (2D) soap bubble-like structured nano-nets [21]. Nano-nets, assembled from net-like structured nanowires with an ultrafine diameter (5-40 nm), exhibit several amazing characteristics, such as an extremely large specific surface area, high porosity and superior mechanical performance. The nano-net formation is connected with fast phase separation of the charged droplets [22].

4 RELATIVE SURFACE AREA OF MEMBRANES

Relative surface area of fibers is defined as surface area related to mass.

The typical membrane (layer) shown in Figure 4 has length L_F, width C_F, and thickness *h*.

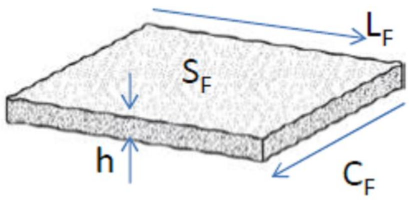

Figure 4 Membrane macroscopic dimensions

Corresponding macroscopic surface area is:

$$S_F = L_F \; C_F \tag{10}$$

Let this membrane is composed from N_v cylindrical fibers with length *l,* radius *r* and density ρ_F. The relative surface area *SR* [m^2/g] (surface area-to-mass ratio) is generally defined as:

$$S_r = \frac{2}{r\;\rho_F} \tag{11}$$

This relation is not dependent on the total fibrous assembly porosity P_o defined as:

$$P_o = 1 - \frac{w_T}{h\;\rho_F} \tag{12}$$

where w_T is planar mas (usually in gsm/1000, where gsm is grams of layer per surface area in meter squared).

The total surface area of fibers S_{FT} in membrane is simply expressed as:

$$S_{FT} = \frac{2\left(1-P_o\right)\;h\;S_F}{r} \tag{13}$$

In comparison with S_R is characteristic S_{FT} related to the thickness and overall porosity of membrane as well.

Much better characteristics of relative surface area is planar relative surface area (surface area-to-macro surface ratio) S_{SR} [-]. Quantity of S_{SR} is ratio of total surface area of fibers in layer S_{FT} and layer macroscopic surface area S_F:

$$S_{SR} = \frac{S_{FT}}{S_F} = \frac{2\;(1-P_o)\;h}{r} \tag{14}$$

The S_{SR} is connected with S_R by relation:

$$S_{SR} = S_R\;(1-P_o)\;h\;\rho_F \tag{15}$$

The dimensionless quantity planar relative surface area S_{SR} is taking in account the porosity and thickness influence on the relative surface area of fibers in membrane.

5 COMPARISON OR RELATIVE SURFACE AREAS

PA 6 nanofibrous membrane (MN) with areal density of 1.3 g/m^2 was purchased from ELMARCO s. r. o Liberec. Spunbond PA 6 nonwoven fabrics (MM) with areal density of 100 g/m^2 was provided by Asahi KASEI Fibers Corporation. The morphologies of membranes were observed by Scanning Electron Microscopy (SEM) using a JEOL JSM-6510LV (Japan) with 10-20 kV of accelerating voltage. The membrane samples were coated with Au/Pd before being mounted on SEM chamber. The fibers on the membranes were randomly selected to measure the individual fiber diameters by identifying two points at opposite ends of a fiber diameter for each sample 50 times. The membrane samples were broken in liquid nitrogen and the cross section images were taken by SEM. Thickness was measured for each sample 10 times. More details about characterization and measurements of geometrical parameters of these membranes are given in [15]. Basic characteristics of both membranes are summarized in Table 1.

Table 1 Membranes characteristics

Characteristic	Micro membrane	Nano membrane
r [nm]	1520	140
h [mm]	0.53	0.00185
gsm [g /m^2]	100	1.3
P_O [-]	0.83	0.36
S_R [m^2/kg]	1196.2	12987.1
S_{SR} [-]	119.62	16.88

The calculated relative surface areas are given in Table 1. The ratio S_{SR} micro/nano = 7.0850 indicates that real relative area of micro membrane is much higher in comparison with nano membrane. On the other side the ratio S_R micro/nano = 0.0921, i.e. relative area per mass is for micro membrane very low in comparison with nano membrane due to differences in thickness mainly.

It is interesting that for nano membrane corresponds the mass 100 g to huge real surface area 77 m^2 but for micro membrane corresponds the mass 100 g to much smaller real surface area approx. 1 m^2. Very interesting is comparison of sorptive properties characteristics [6]. Under the same conditions was sorption of Acid Blue 41 by nano membrane expressed as concentration 138 mg/g and by mico membrane 15 mg/g only. This leads to (wrong) decision about better sorptive properties of nano membranes. By using real sample sizes (membrane thickness) there was calculated concentration for nano membrane 0.017 mg/m^2 but for micro membrane much higher value 0.15 mg/m^2. From these concentrations are visible better sorption properties of micro membranes for real membranes thicknesses.

6 CONCLUSION

Definition of relative surface area S_R [m^2/g] as total surface area of fibers divided by their mass is not taking into account porosity P_o and thickness of layer h. Especially limitations due to extremely thin nano fibrous membranes in the order of a few microns only leads to over optimistic values of S_R. For the same real surface area of membranes is mass of nano membrane about two orders less in comparison with mass of micro membrane. Division of surface areas by their real mass then causes huge increase of nano membrane S_R in comparison of micro membrane S_R. By considering real thickness of both layers, the nano fibrous membranes do not offer so big real surface area as is evaluated from standard characteristic S_R (surface area-to-volume or surface area-to-mass ratio) because the real volume or mass are for nanofibrous materials too small.

For end use applications e.g. filtration, sorption or surface activation the micro fibrous layers are more beneficial providing sufficiently higher real surface area of fibrous phase.

ACKNOWLEDGEMENT: *This work was supported by the Ministry of Education, Youth and Sports of the Czech Republic, European Structural and Investment Funds in the frames of Operational Programme Research, Development and Education – project Hybrid Materials for Hierarchical Structures (HyHi, Reg. No. CZ.02.1.01/0.0/0.0/16_019/0000843).*

7 REFERENCES

1. Purushotham H.: Transfer of nanotechnologies from R&D institutions to SMEs in India, Tech. Monitor 2012, Oct-Dec: 23-33
2. Jeevani T.: Nanotextiles - a broader perspective, J. Nanomedic. Nanotechnol. 2(7), 2011, pp. 1-5, doi:10.4172/2157-7439.1000124
3. British Standards Institution. Terminology for nanomaterials. London: PAS Publicly Available Specification 136, 2007
4. ISO: Nanotechnologies - terminology and definitions for nano-objects - nanoparticle, nanofibre and nanoplate: ISO/TS 27687, 2008(E)
5. O'Brien N., Cummins E.: Recent developments in nanotechnology and risk assessment strategies for addressing public and environmental health concerns, Hum. Ecol. Risk. Assess. 14(3), 2008, pp. 568-592, doi: 10.1080/10807030802074261
6. Handy R., Von Der Kammer F., Lead J., Hassellöv M., Owen R., Crane M.: The ecotoxicology and chemistry of manufactured nanoparticles, Ecotoxicology 17(4), 2008, pp. 287-314, doi: 10.1007/s10646-008-0199-8
7. Royal Society. Nanoscience and nanotechnologies: Opportunities and uncertainties. London, 2004
8. Foss Hansen S., Larsen B.H., Olsen S.I., Baun A.: Categorization framework to aid hazard identification of nanomaterials, Nanotoxicology 1(3), 2007, pp. 243-250, doi: 10.1080/17435390701727509
9. European Commission: Commission recommendation of 18 October 2011 on the definition of nanomaterial, Brussels, 2011
10. Anonym: Nanotechnologies - terminology and definitions for nano-objects - nanoparticle, nanofibre and nanoplate: ISO/TS 80004-2:2015 (E)
11. Ko F.K., Wan Y.: Introduction to Nanofiber Materials, New York: Cambridge University Press, 2014
12. Ko F.K.: Nanofiber technology: bridging the gap between nano and macro world in Nanoengineered Nanofibrous Materials, Guceri S., et al. eds.: Dordrecht: Kluwer Academic Publishers, 2004
13. Wang Y.: Selected sorption properties of nanofibers assembly, PhD Thesis, Liberec: TU Liberec, 2016
14. Jortner J.: Cluster size effects, Zeitschrift für Physik D Atoms, Molecules and Clusters 24, 1992, pp. 247-275, doi: 10.1007/BF01425749
15. Militký J., Wang Y., Mishra R.: Comparison of membranes functionality, Original paper under preparation
16. Bhardwaj N., Kundu S.C.: Electrospinning: A fascinating fiber fabrication technique, Biotechnology Advances 28, 2010, pp. 325-347, doi: 10.1016/j.biotechadv.2010.01.004
17. Lukáš D., et al.: Physical principles of electrospinning (Electrospinning as a nano-scale technology of the twenty first century), Textile Progress 41(2), 2009, pp. 59-140, doi: 10.1080/00405160902904641
18. Sun B., et al.: Advances in three-dimensional nanofibrous macrostructures via electrospinning, Progress in Polymer Science 39(5), 2014, pp. 862-890, doi: 10.1016/j.progpolymsci.2013.06.002
19. Bock N. et al.: Electrospraying of polymers with therapeutic molecules: State of the art, Progress in Polymer Science 37(11), 2012, pp. 1510-1551, doi: 10.1016/j.progpolymsci.2012.03.002
20. Jaworek A.: Electrospray droplet sources for thin film deposition, J. Mater. Sci. 42(1), 2007, pp. 266-297, doi: 10.1007/s10853-006-0842-9
21. Hu J., et al.: One-step electro-spinning/netting technique for controllably preparing polyurethane nano-fiber/net, Macromol. Rapid Commun. 32(21), 2011, pp. 1729-1734, doi: 10.1002/marc.201100343
22. Ding B., et al.: Formation of novel 2D polymer nanowebs via electrospinning, Nanotechnology 17(15), 2006, pp. 3685-3691, doi: 10.1088/0957-4484/17/15/011

BEHAVIOR OF TWO AND THREE-FOLD TWISTED MULTIFILAMENT YARNS

Eva Moučková, Iva Mertová, Šárka Hajská and Monika Vyšanská

Technical University of Liberec, Faculty of Textile Engineering, Department of Technologies and Structures, Studentská 2, Liberec, Czech Republic
eva.mouckova@tul.cz

Abstract: *This work deals with analysis of the behavior of two and three-fold twisted multifilament yarn in dependence on twist level. The structure and consequently various parameters and properties of filament fibers bundle are changed due to twisting. For experiment, two and three-fold twisted polyamide and polyester multifilament yarns were used. Selected properties such as tenacity, breaking elongation, twist take-up and structural parameters (multifilament yarn diameter and packing density) were observed and evaluated. The experiment showed that with increasing twist coefficient the twisted multifilament yarn twist take-up increases, whereas the yarn diameter decreases and the packing density increases-up to the value of twist coefficient of 60 - 70 ktex*$^{1/2}$*m*$^{-1}$*. Tenacity showed decreasing tendency with increasing twist coefficient from the level approximately equal to 50 ktex*$^{1/2}$*m*$^{-1}$ *(which corresponds to the angle of peripheral fiber inclination of* β_D *= 12°) due to lower coefficient of fiber stress utilization in the twisted multifilament yarn. The behavior of the two and three-fold twisted multifilament yarns in terms of utilization of fiber tenacity and yarn breaking elongation was predicted using theoretical models. The significant correlation coefficients between experimental and predicted breaking elongation verified the validity of the corresponding theoretical model. The comparison between the two and three-fold twisted multifilament yarns of the same raw material at the same twist coefficient showed that observed number of single multifilament yarns in the twisted yarn has not any influence on analyzed properties except tenacity and yarn diameter. Moreover, saturated twist of multifilament yarn was discussed.*

Keywords: *multifilament yarn, twist, tenacity, breaking elongation, utilization of fibre tenacity, twist take-up, packing density.*

1 INTRODUCTION

Currently, multifilament yarns are becoming increasingly widespread not only in the field of technical or household textiles, but also in the clothing industry. Twisting multifilament yarns means either twisting raw single-end multifilament yarn, to increase yarn cohesion, or assembling and twisting of two or more multifilament yarns together to achieve the required multifilament thickness, increase cohesion, luster, handle, abrasion resistance, or improve their mechanical and physical properties to a certain extent. The process, where two or more strands of twist-less multifilament yarn are twisted in two-step operation is called also cabling.

One of the important factors which influence multifilament yarn properties is the angle of slope of the fiber to the yarn axis (called a twist angle) [1]. This angle changes with the level of multifilament yarn twist. By increasing number of twists, the diameter of multifilament yarns reduces, the individual fibrils come closer, and the elongation of multifilament yarn increases [2]. However, unlike staple yarn, twisting of multifilament yarn reduces their strength [1-3] which is an important factor in terms of their end use, and this become increasingly important particularly in the case of multifilament yarn for technical applications.

Structure and properties of twisted multifilament yarns were studied in number of works, for example, [1-10]. Huang et al. [4] derived a mathematical model for prediction of ply-yarn strength in relation to the twist coefficient using the single yarn radius, the twist angle, the tensile strain, the cohesion coefficient, the tensile modulus and shear modulus of the single yarn. The model is based on continuum mechanics theory and geometrical analysis of plied yarn. Zimliki et al. [5] predicted the mechanical properties of parallel filament bundles, twisted single-end multifilament yarns and the two-ply multifilament from single-multifilament yarn data. They derived a model for ply-yarn failure based on the statistical distribution of single filament breaks including average filament strength and coefficient of its variation. Kilby [6] discussed and theoretically studied the effect of the equalization of filament tensions on the initial modulus, tenacity, and breaking extension of mechanical properties of twisted single-end multifilament yarn. Treloar [7] theoretically modeled tensile properties (a stress-strain curve) of twisted single-end multifilament yarn based on its geometrical structure and properties of individual fibrils. His analysis was realized based on strain-energy of the system. He compared his model with experimental results and concluded their good agreement with theoretical curve except the region of small extension and high twist. He also applied his "energy-method" for derivation of the stress-strain curve of ply multifilament yarn [8] using theory of geometry of the ply fibers strand [9].

Hearle et al. [1] published, among others, experimental values of relative strength in dependence of inclination of peripheral fibers for single multifilament yarns of various raw material and count. These data was used by Neckar [2]. He verified theoretical model enabling calculation of utilization of fiber stress in yarn tenacity. Hearle [1] and later Neckar [2] also predicted twisted single-end multifilament yarn tenacity using geometrical helical model of yarn.

There is a lack of experimental works focused on two and three-fold twisted multifilament yarn behavior in relation to the yarn twist. Jones et al. [10] experimentally investigated tensile behavior of glass plied multifilament yarn in relation to yarn twist. They compared the results with the theoretical model of Hearle and Bosse [11] based on wrapped-ribbon twist geometry and also with mentioned Treloar's model. Thus, it is necessary to study properties and structural characteristic of twisted (plied) multifilament yarns made from various material and construction in relation to the twist level. Various theoretical models which were derived in last decades are very sophisticated and complicated. A lot of them are not suitable for use in practice. In this work we present models (described below) which seems to be easier to apply. It is necessary to verify its validity for two and three-fold twisted multifilament yarn and compare the models with experimental data. The knowledge of the relation between properties and structure is required also for modeling of behavior of plied multifilament yarns during next downstream manufacturing processes.

The aim of this work was to analyze the effect of number of twists on selected properties of two and three-fold multifilament yarns. These properties were observed: multifilament yarn twist take-up as a factor influencing yarn consumption; diameter and packing density of multifilament yarn which influence weaveability and bending rigidity of multifilament yarn. Simultaneously, tenacity and breaking elongation was analyzed. Based on experimental measurements, a model of utilization of fiber tenacity in the multifilament yarn was constructed and compared with the current theoretical model. The axial strain of fiber bundle was also predicted based on measured values of breaking strain of single-end multifilament yarn and values of angle of peripheral fibers. This work is based on work [3], where authors observed the influence of twist of single-end multifilament yarns on multifilament tenacity, breaking elongation, coefficient of fiber stress utilization in the yarn, angle of peripheral fibers and packing density. For experiment authors used polypropylene and polyester single-end multifilament yarns of count 10 tex and 17 tex. Author verified the known model relationships, derived decades ago based on the helical model, by comparing them with experimentally obtained data.

Moreover, this work contributes to the knowledge about behavior of twisted multifilament yarns particularly two and three-fold yarn used in the technical textile field.

2 SHORT THEORETICAL BACKGROUND

By twisting the fibrous bundle, individual fibers take the helix shape. This geometrical arrangement is possible to be described by concentric helices model [1, 2]. The helical model is the best known theoretical concept in the internal yarn geometry. This ideal helical model assumes that the axes of all fibers have the shape of a helix with the same direction of rotation; helices of all fibers have one common axis which is a multifilament yarn axis; the height of one coil of each helix is the same, and the packing density is the same at all places inside the multifilament yarn. Inside the textile fibrous assembly, there are fibers of volume V. When we mark the total volume of this body as V_c, the compactness of this body can be characterized by the ratio between these two volumes (V/V_c) and it is known as the fiber packing density μ. Evidently, the fiber packing density value must lie in the range from 0 to 1. The packing density in our case is compactness of fibers in the multifilament yarn.

In this work, twisting multifilament yarns means twisting several (two or three) single-end multifilament yarns together, where each of which is provided with only a protective twist or interlaced. We assume that during multifilament yarn twisting, a "doubly-wound" helix is not created. It means that a helix is wound around a helical axis as in the case of staple spun yarn or cabled multifilament yarn, but it is only one wound concentric helix.

From the model of concentric helix, generally known equation (1) results:

$$\tan\beta_D = \pi D Z = \frac{2\sqrt{\pi}\,\alpha}{\sqrt{\mu\rho}} \tag{1}$$

where β_D denotes angle of slope of the peripheral fiber to the linear axis of twisted fiber bundle; D is diameter of cylindrical helix of peripheral fibers axis; Z is twist (strictly speaking: number of turns per unit length of twisted fiber bundle); α is Koechlin's twist coefficient; ρ is fiber density and μ is packing density of fiber bundle.

The relationship between twist Z and fineness T of twisted fiber bundle was derived by Koechlin, as shown in equation (2):

$$Z = \frac{\alpha}{\sqrt{T}} \tag{2}$$

Due to twisting, the length of fiber bundle is contracted. Here, this shortening is expressed by the so called yarn retraction δ (or also yarn twist take-up) as a fractional reduction in length due to twisting [12] as shown in equation (3):

$$\delta = \frac{\Delta l}{l + \Delta l}.100 \qquad (3)$$

where Δl is increment of length after untwisting of twisted multifilament yarn [mm]; l is length of twisted multifilament yarn (clamping length) [mm] and δ is yarn twist take-up [%].

Based on the ideal helical model, the yarn twist take-up δ can be derived using Koechlin´s twist coefficient α, packing density μ and fiber density ρ [2], as shown in equation (4):

$$\delta = \frac{\sqrt{1 + 4\pi\alpha^2 / (\mu\rho)} - 1}{\sqrt{1 + 4\pi\alpha^2 / (\mu\rho)} + 1} \qquad (4)$$

Using formula (4) and suitable mathematical adjustment, we can express the packing density (i.e. the degree of compactness of fibrils in the multifilament yarn) depending on the Koechlin's twist coefficient [3] as shown in equation (5):

$$\mu = \frac{\pi\,\alpha^2}{\rho}\frac{(1-\delta)^2}{\delta} \qquad (5)$$

Based on the knowledge of yarn retraction δ, we can predict the angle of peripheral fiber β_D by equation (6), which Braschler derived. This equation was presented, for example, in work [2] and [3].

$$\delta = \tan^2\left(\frac{\beta_D}{2}\right) \qquad (6)$$

On the basis of ideal helical model and other assumptions, the relation between tensile force utilization coefficient in the twisted multifilament φ and angle of peripheral fiber β_D is valid as shown in equation (7).

The other assumptions of this model are: individual fibrils are straight; there is no interaction between individual fibers during fiber bundle tension; stress-strain curves of fiber are linear, small deformation is assumed and the contraction ratio η is constant. More general solution of this problematic is mentioned in [13].

$$\varphi = (1+\eta)\cos^2\beta_D + \eta\frac{\ln\cos^2\beta_D}{\tan^2\beta_D} \qquad (7)$$

where η is Poisson's contraction ratio [-].

In the case that no image analysis is available to measure the angle of inclination of the fibers, it is possible to derive the relation between yarn twist take-up δ and tensile force utilization coefficient φ using equation (1), (6) and (7).

3 EXPERIMENTAL PART

Two types of single-end flat multifilament yarns were used for experiment: polyester (PES) and polyamide 6 (PA) multifilament yarns. Their specification is mentioned in Table 1. PES multifilament yarn was slightly twisted, whereas PA multifilament yarn was interlaced. Thereinafter, these multifilament yarns are called single multifilament yarns. Multifilament yarn cross-sections are presented in Figure 1a and 1b, longitudinal view are mentioned in Figure 2a and 2b. Cross-sections were made by a method of soft slices according to the internal standard [14].

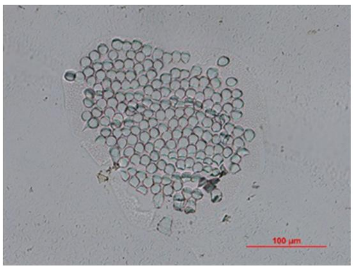

Figure 1a PES single multifilament yarn cross-section

Figure 1b PA single multifilament yarn cross-section

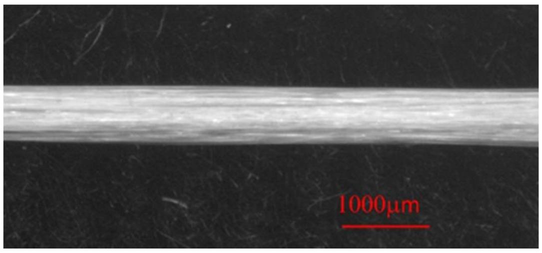

Figure 2a PES single multifilament yarn

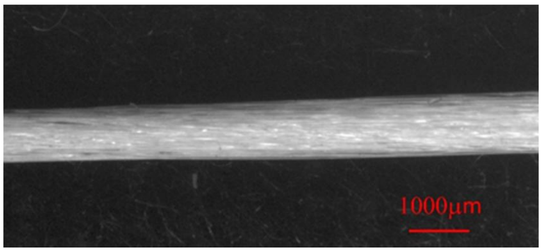

Figure 2b PA single multifilament yarn

Table 1 Parameters of multifilament yarns used for experiment

Parameter	Multifilament yarn	
	100% PES	100% PA
Nominal multifilament yarn count [dtex]	1100	1880
Number of fibrils	192	280
Fibre density [kg.m^{-3}]	1360	1140
Twist [m^{-1}]	60	-
Number of entanglements [m^{-1}]	-	17

Each type of single multifilament yarns was assembled and then twisted in Z direction using the ring twisting machine Twistec. Two folded and three folded twisted multifilament yarns with the various twist level were produced (see Table 2a and 2b). The range of twist level was selected based on the technical possibilities of twisting machine.

Actual yarn count was verified using gravimetrical method. Actual level of plied multifilament yarn twist and length of untwisted multifilament yarn were measured using a twist tester with clamping length 0.5m.

Table 2a and 2b display the nominal number of twists Z_n of twisted multifilament yarns together with values of actual number of twist Z, actual twisted yarn counts T, calculated Koechlin's twist coefficient α, and respective yarn twist take-up δ calculated according to formula (3). Only average values of observed parameters and properties are shown in Table 2a and 2b for their clarity. Differences between nominal and actual yarn twist are caused by spindle slips.

Twisted multifilament yarn diameter was measured using images analysis Nis Elements software according to the internal standard [15]. From each sample of multifilament yarn, 50 measurements were recorded. Figure 3 and Figure 4 demonstrate longitudinal views of the twisted multifilament yarns and their cross-sections. Geometrical arrangement of fibers in Figure 3 and Figure 4 verified the assumption that single multifilament yarns form flat ribbons of fibrils that are twisted around each other. Twisted multifilament yarns strength and breaking extension were measured using the tensile tester Instron under these conditions: clamping length 500 mm, cross-beam speed 500 mm/min and pre-tension 0.5 cN/tex. For each level of twist, 50 measurements were carried out. The strength and breaking extension of individual fibrils in multifilament yarns as well as single multifilament yarns were measured too. These measurements were performed under the same conditions as measurements of twisted multifilament yarns. The results are shown in Table 3. For clarification, only average values of observed parameters and properties are shown in the table.

Table 2a PES twisted multifilament yarn - results of observed parameters and measurement

Nominal twist Z_n [m^{-1}]	Twisted multifilament yarn 2 x 1100 dtex				Twisted multifilament yarn 3 x 1100 dtex			
	Actual twist Z [m^{-1}]	Actual count [dtex]	Koechlin's twist coefficient α [ktex$^{1/2}$.m^{-1}]	Yarn twist take-up δ [%]	Actual twist Z [m^{-1}]	Actual count [dtex]	Koechlin's twist coefficient α [ktex$^{1/2}$.m^{-1}]	Yarn twist take-up δ [%]
20	20	2230	9	0.120	20	3340	11	0.123
40	38	2240	18	0.292	38	3360	22	0.464
60	59	2240	28	0.388	59	3380	35	0.497
80	81	2250	39	0.573	84	3410	49	0.846
100	100	2260	47	0.794	105	3440	62	1.270
120	120	2260	57	1.081	125	3450	73	1.762
140	134	2260	64	1.309	138	3460	81	2.095
160	152	2270	72	1.768	156	3480	92	2.717
200	197	2290	94	2.723	207	3520	123	4.605
250	251	2330	121	4.213	269	3570	161	7.526

Table 2b PA twisted multifilament yarn - results of observed parameters and measurement

Nominal twist Z_n [m^{-1}]	Twisted multifilament yarn 2 x 1880 dtex				Twisted multifilament yarn 3 x 1880 dtex			
	Actual twist Z [m^{-1}]	Actual count [dtex]	Koechlin's twist coefficient α [ktex$^{1/2}$.m^{-1}]	Yarn twist take-up δ [%]	Actual twist Z [m^{-1}]	Actual count [dtex]	Koechlin's twist coefficient α [ktex$^{1/2}$.m^{-1}]	Yarn twist take-up δ [%]
20	18	3760	11	0.213	21	5650	16	0.312
40	35	3790	22	0.253	38	5680	29	0.718
60	54	3800	33	0.570	52	5700	39	0.783
80	76	3810	47	1.147	76	5760	58	1.600
100	95	3850	59	1.639	95	5790	73	2.520
120	115	3900	72	2.466	114	5810	87	3.619
140	129	3928	81	3.025	129	5880	99	4.519
160	150	3952	94	3.987	147	5940	114	5.811
200	196	4080	125	6.522	192	6250	152	8.749
250	255	4264	167	9.863	266	6570	216	15.858


a) b)

Figure 3 Twisted PA multifilament yarn 2x1880 dtex, Z = 160 m^{-1}; a) longitudinal view; b) cross-section


a) b)

Figure 4 Twisted PES multifilament yarn 2x1110 dtex, Z = 160 m^{-1}; a) longitudinal view; b) cross-section

Table 3 PES twisted multifilament yarn and PA twisted multifilament yarn - results of measurement

Nominal twist Z_n [m^{-1}]	PES twisted multifilament yarn 2 x 1100 dtex		PES twisted multifilament yarn 3 x 1100 dtex		PA twisted multifilament yarn 2 x 1880 dtex		PA twisted multifilament yarn 3 x 1880 dtex	
	Tenacity [cN/tex]	Breaking elongation [%]	Tenacity [cN/tex]	Breaking elongation [%]	Tenacity [cN/tex]	Breaking elongation [%]	Tenacity [cN/tex]	Breaking elongation [%]
0**	81.688	12.125			90.851	24.090		
0*	81.636	10.720			80.500	20.404		
20	79.262	10.964	74.092	10.712	77.202	19.982	79.812	20.130
40	79.720	11.590	73.960	10.858	77.586	21.376	80.076	20.784
60	79.738	11.752	75.272	11.657	77.296	21.531	79.506	20.938
80	80.414	11.929	75.208	11.959	77.486	21.752	78.286	21.618
100	80.648	12.502	75.657	12.514	77.759	22.654	77.174	22.540
120	80.330	12.598	74.344	12.332	75.855	23.118	74.772	23.718
140	79.900	12.466	73.748	12.618	76.082	23.706	70.518	25.045
160	79.022	12.692	72.831	12.864	74.684	24.134	69.535	25.886
200	77.856	13.812	70.542	13.552	71.564	26.439	63.862	30.414
250	73.832	13.808	63.384	12.872	67.049	30.262	56.630	33.482

Note: 0** - results of individual fibrils measurements; 0* - results of single multifilament yarn measurements

4 DISCUSSION OF RESULTS

4.1 Twisted multifilament yarn twist take-up

The dependence of the twisted multifilament yarn twist take-up on the twist coefficient is shown in Figure 5. The average values with relevant 95% confidence limit are plotted, however, the limits are not visible in the graph because they are so narrow to show up. From the results it is obvious that the yarn twist take-up increases by increasing twist coefficient. This phenomenon is logical, because the yarn gets shortened during twisting. There is not any difference in the yarn twist take-up behavior when comparing two-fold and three-fold multifilament yarns of the same raw material. This can be explained by the fact that when the twisted yarns have the same twist coefficient, they have also the same or nearly the same angle of slope of single multifilament to the twisted yarn axis, and thus the same twist take-up [3].

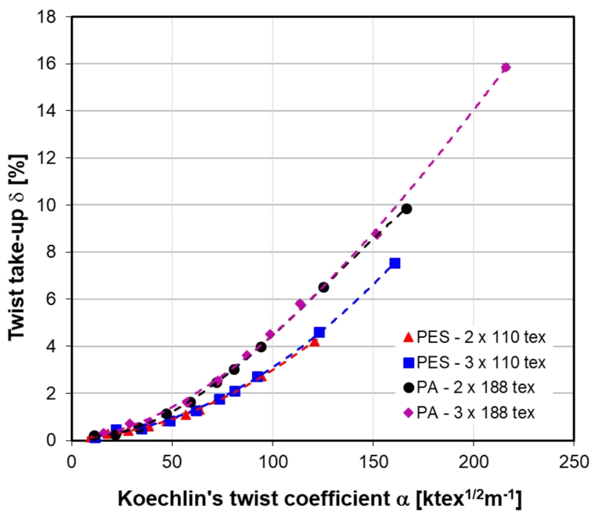

Figure 5 Influence of Koechlin's twist take-up coefficient on twisted multifilament yarn twist take-up

But when comparing PES and PA twisted multifilament yarns, the effect of raw material and structure of multifilament yarn can be observed from Figure 5. Polyamide 6 twisted multifilament yarns show higher twist take-up. It could be caused by raw material as well as the different structure of single multifilament yarn (here fibrils are mutually interlaced).

4.2 Twisted multifilament yarn diameter

By twisting, the individual filaments in the multifilament yarn get closer to each other and thus the multifilament yarn diameter decreases. Results of yarn diameter measurement confirmed this phenomenon. Figure 6 shows the dependence of average values of yarn diameter (with relevant confidence intervals with the confidence level 95%) on Koechlin's twist coefficient. Measurements of three-fold PA twisted multifilament yarns diameter at Koechlin's twist coefficient α = 216 ktex$^{1/2}$.m^{-1} were not possible to carry out by used method because of high snarling tendency of this yarn.

From the course it is obvious that the relationship is polynomial. The most decrease in diameter is visible up to the value of twist coefficient of approx. 60 ktex$^{1/2}$m^{-1}. Although the diameter has decreasing tendency, there were not recorded any statistically significant differences among average yarn diameters in the range of the twist coefficient 70-170 ktex$^{1/2}$ m^{-1} at the level of confidence 95% (according to one-way Anova).

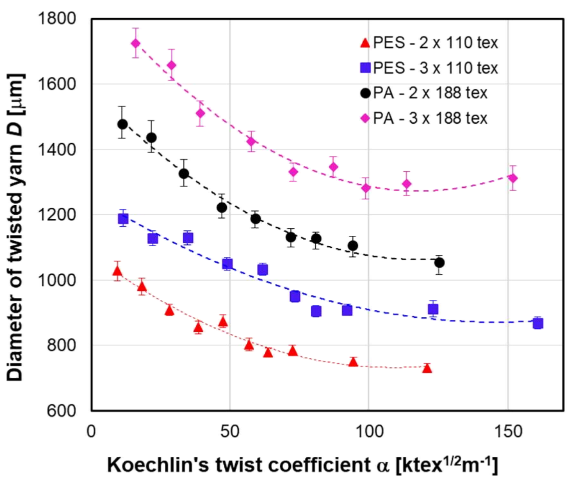

Figure 6 Influence of Koechlin's twist coefficient on twisted multifilament yarn diameter

After exceeding twist coefficient 60 ktex$^{1/2}$·m^{-1}, individual fibrils in the twisted multifilament yarn are very close to each other. During further twisting they can only mutually change their position (i.e. migrate and/or regroup between each other). That can lead to the insignificant change of yarn diameter. Insignificant fluctuation in diameter in this twist range may be also caused by small deviations in the tension of single multifilament yarns during assembling of these yarns on the twisting machine. PA6 twisted multifilament yarns have higher yarn diameter due to their higher number of fibrils in the yarn cross-section and higher diameter of fibril compared to PES twisted yarns.

4.3 Twisted multifilament yarn packing density

The dependence of twisted multifilament yarn packing density on Koechlin's twist coefficient is presented in Figure 7.

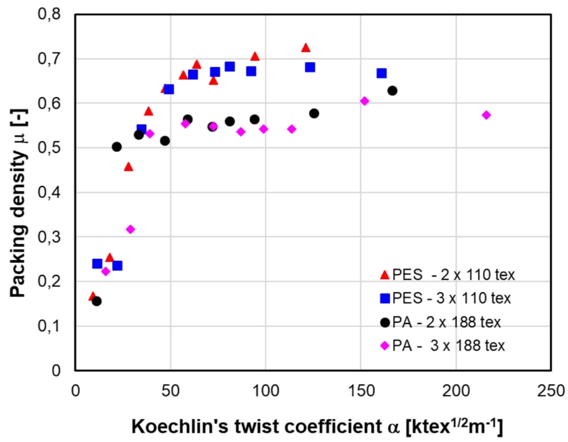

Figure 7 Dependence of twisted multifilament yarn packing density on Koechlin's twist coefficient

We can see that the multifilament yarn packing density increases with increasing Koechlin's twist coefficient because individual filaments get closer to each other during twisting. But when twist coefficient crosses the value of approx. α = 60 ktex$^{1/2}$.m^{-1}, the values of multifilament yarn packing density get stabilized. Thus, at higher twist coefficients, the packing density values are almost equal and independent of the multiplier. Fibrils can no longer be closer to each other. When being nearly constant, the level of packing density takes the value about μ = 0.68 in the case of the PES multifilament yarn and μ = 0.55 in the case of the PA multifilament yarn. The difference can be caused by internal structure of multifilament yarns. Individual fibrils in the PA single multifilament yarn are interlaced, it means that parallel arrangement of individual fibrils is worse compared to the fibrils in the PES single multifilament yarn, which has a low protective twist. The value of PES twisted multifilament yarn packing density corresponds to values of packing density of single multifilament yarn presented in [3] as well as in [2].

We can see that the multifilament yarn packing density increases with increasing Koechlin's twist coefficient because individual filaments get closer to each other during twisting. But when twist coefficient crosses the value of approx. α = 60 ktex$^{1/2}$.m^{-1}, the values of multifilament yarn packing density get stabilized. Thus, at higher twist coefficients, the packing density values are almost equal and

independent of the multiplier. Fibrils can no longer be closer to each other. When being nearly constant, the level of packing density takes the value about μ = 0.68 in the case of the PES multifilament yarn and μ = 0.55 in the case of the PA multifilament yarn. The difference can be caused by internal structure of multifilament yarns. Individual fibrils in the PA single multifilament yarn are intermingled, it means that parallel arrangement of individual fibrils is worse compared to the fibrils in the PES single multifilament yarn, which has a low protective twist. The value of PES twisted multifilament yarn packing density corresponds to values of packing density of single multifilament yarn presented in [3] as well as in [2].

4.4 Twisted multifilament yarn tenacity

Average values of twisted PES multifilament yarn tenacity depending on Koechlin's twist coefficient are plotted in Figure 8a. From this figure, we can see that when twist coefficient increases (i.e. twist level is higher), the value of tenacity decreases from the twist coefficient value approximately equal to 50 ktex$^{1/2}$.m^{-1}. Up to this value, the negligible increase in tenacity can be seen. In the range of small twist multipliers, the relationship between twisted multifilament yarn tenacity and the twist factor may be influenced by crimping of individual fibers and friction between individual fibers in consequence of twist increase. At the range of twist coefficient higher than 50 ktex$^{1/2}$.m^{-1}, the fiber arrangement become not parallel to the yarn axis, thus strength of individual fibrils is less utilized in yarn and tenacity of multifilament yarn decreases with increasing twist level. Tenacity of single multifilament PES yarn is higher than tenacity of two or three folded twisted multifilament yarn. This tendency was expected. Probably, the reason is the decomposition of tensile force in the filaments in consequence of twist because individual fibrils are not arranged in parallel to the multifilament yarn axis due to the ply twist. In the field of folded staple spun yarns, it is known that tenacity of two-ply yarn is higher than tenacity of single staple spun yarn, because plying (due to the effect of doubling) equalizes the single strand mass irregularity and compensates yarn faults (i.e. thin places, thick places). However, this relation isn't valid in the field of twisted multifilament yarn, and the tendency is different.

The dependence of PA twisted multifilament yarn tenacity on Koechlin's twist multiplier is presented in Figure 8b. We can see that behavior of two-fold PA multifilament yarns is similar to PES multifilament yarns. The three-fold PA multifilament yarns have higher values of tenacity than two-fold yarns at low multipliers, up to the twist coefficient value of approximately 70 ktex$^{1/2}$.m^{-1}. The difference can be caused by internal structure of these yarns. Individual fibrils in the PA single multifilament yarn are not slightly twisted as in the case of PES single multifilament yarn but entangled in some places. Thus, inner friction forces between individual PA fibrils probably varies more in yarn length. This phenomenon in connection with higher friction forces given by higher number of fibrils in twisted multifilament yarn cross-section may be a reason of higher tenacity of three-fold PA multifilament yarn in the small range of twist coefficient.

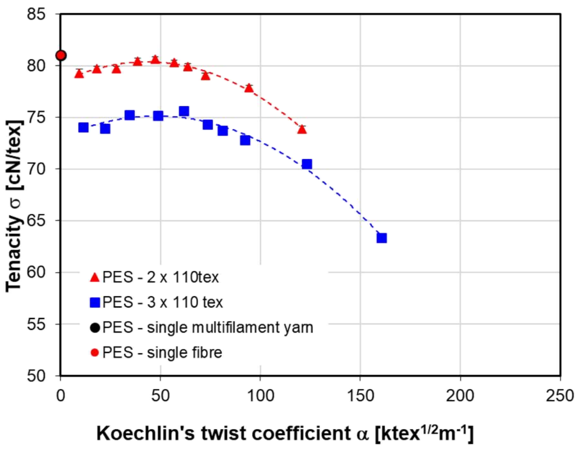

Figure 8a Dependence of PES twisted multifilament yarn tenacity on Koechlin's twist multiplier

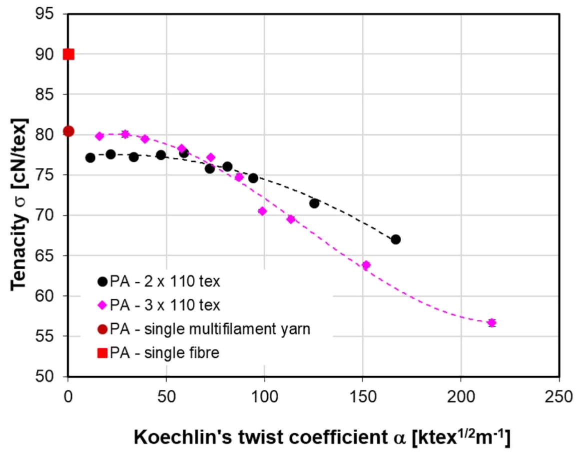

Figure 8b Dependence of PA twisted multifilament yarn tenacity on Koechlin's twist multiplier

4.5 Utilization of fibres tenacity in multifilament yarn

Low utilization of tensile forces of individual fibers causes the decreasing in the tenacity of both multifilament yarns. The coefficient of fiber stress utilization in the multifilament yarn decreases with increasing twist factor value due to higher slope of fibers to the multifilament axis. We can calculate the coefficient of fiber stress utilization in the multifilament yarn (fiber bundle) φ_{exp} based on the experimental values according to equation (8). Also, the theoretical coefficient of fiber stress utilization in the multifilament yarn can be calculated based on the helical model predicting equation (7). This model was derived by Gégauff [16] and then modified by Neckář [2].

$$\varphi_{\exp} = \frac{\sigma}{\sigma^*} \qquad (8)$$

where σ is tenacity of twisted fiber bundle and σ^* is tenacity of individual fibers.

It is necessary to know the value of Poisson's ratio for the evaluation of predicted coefficient of fiber stress utilization. But it is problematic to determine this constant. In the case that the value is unknown, it is generally set to η = 0.5. The multifilament yarn volume is not changed by this ratio value during small tension deformations [2].

The coefficients of fiber stress utilization in the multifilament yarn calculated according to equations (7) and (8) are presented in Figure 9.

The dependence of experimental and theoretical coefficient of fiber stress utilization in the multifilament yarn on the angle of peripheral fiber (see Figure 9) corresponds to results presented in works [1] and [2]. From Figure 9 it is seen that the experimentally determined coefficient of fiber stress utilization of PA fibers is lower than the predicted one and it has increasing tendency in the range of small angles (up to β_D = 20°).

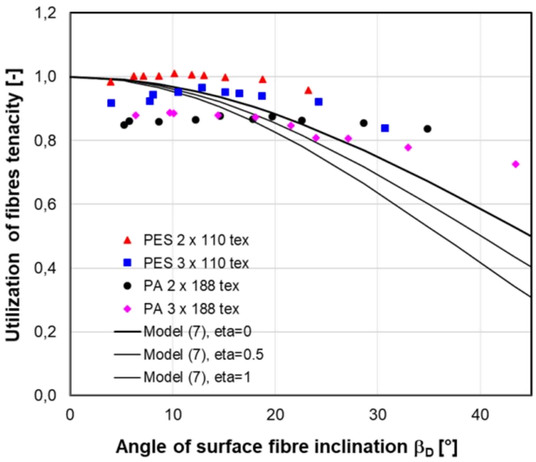

Figure 9 Dependence of coefficient of fiber stress utilization in multifilament yarn on angle of fiber inclination

The experimentally determined coefficient of stress utilization of PES fibers has increasing tendency with growing angle in the range of small angles up to β_D = 12°. The reason of this phenomenon is connected probably with different properties of individual fibers – crimping of fibers, variability of elongation at break. Thus, the average value of individual fiber tenacity is higher than tenacity of fiber bundle (the multifilament yarn), see Figure 8a and 8b. The crimping of fibers given by production technology are not identical, consequently initial lengths of individual fibers are not identical. All fibers in the fiber bundle (multifilament yarn) are loaded non-uniformly. This fact can be a cause of reduction of fiber stress utilization in the multifilament yarn. The twisting of multifilament yarn is processed under stress. Crimped fibers are straightened and interacted during this process in the range of small angles of peripheral fibers. It can lead to the increase in cohesive forces and to the increase in coefficient of fiber stress utilization in the multifilament yarn. Other reason can be the clamping (initial) length too [17], or a modification of multifilament diameter during twisting.

4.6 Twisted multifilament yarn breaking elongation

We can predict the axial strain of fiber bundle based on measured values of breaking strain of non-twisted fiber bundle (single-end multifilament yarn) and values of angle of peripheral fibers using Gégauff model [16]. This model was modified by Neckář [2] for different values of Poisson's ratio, see equation (9). The simplified assumption of this model is: all fibers have helical structure in the same direction of rotation in the fiber bundle; no deformation occurs due to twist and there is no migration of fibers.

$$\varepsilon_l = \varepsilon_a\left(\cos^2\beta - \eta\sin^2\beta\right) \qquad (9)$$

where ε_a denotes relative breaking elongation of twisted fiber bundle and ε_l is the relative breaking elongation of non-twisted fiber bundle.

Average values of breaking elongation ε along with their 95% confidence level depending on Koechlin's twist multiplier are plotted in Figure 10. It can be seen that breaking elongation increases with increasing twist. The level of breaking elongation values certainly depends on twist multiplier and probably is affected by raw material and internal structure of single multifilament yarn. The PES multifilament yarn shows lower values of breaking elongation. They also exhibit lower differences between yarn tenacity at minimum and maximum observed twist coefficients compared to PA yarns.

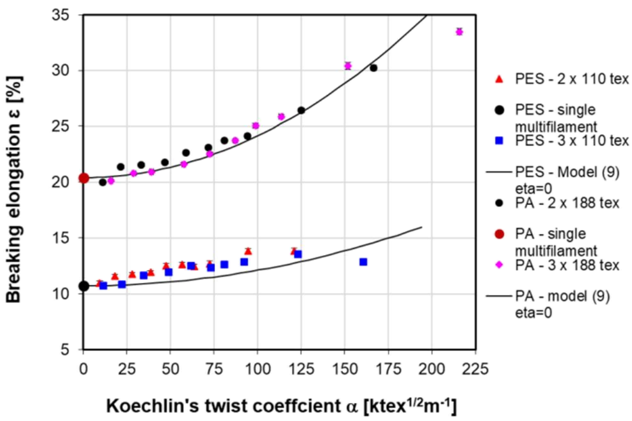

Figure 10 Dependence of PES and PA twisted multifilament yarn breaking elongation on Koechlin's twist multiplier

The comparison of experimental and predicted values of breaking elongation of twisted multifilament yarns depending on the twist coefficient is visible in Figure 10. Theoretical values of breaking elongation were calculated with Poisson's ratio η = 0. The theoretical model supposes that the dependence between the breaking strain and the twist multiplier is increasing which is evident from the diagram in Figure 10. Values of correlation coefficients, presented in Table 4, also validate this hypothesis. All correlation coefficients are statistically significant.

Table 4 Correlation coefficient between experimental and theoretical breaking elongation of multifilament yarn

Multifilament yarn	Correlation coefficient R
PA 2x 188 tex	0.989
PA 3 x188 tex	0.959
PES 2x 110 tex	0.904
PES 3 x110 tex	0.690

4.7 Saturated twist

Generally, it is possible to insert a limited number of coils into a given length of multifilament yarn. Inserting a twist higher than limited turns leads to destruction of fiber bundle and the so called twist of second order is formed [2]. Thus the optimal twist level is limited. This limit case is called saturated twist.

Based on the assumptions of helical model, the equation for calculation of twist take-up as a function of latent twist multiplier α_0 was derived [2]:

$$\delta = \frac{1}{2} - \frac{1}{2}\sqrt{1 - \frac{4\pi}{\mu}\frac{\alpha_0^2}{\rho}} \tag{10}$$

The latent twist coefficient α_0 is defined as:

$$\alpha_0 = Z_0\sqrt{T_0}\,. \tag{10a}$$

where T_0 is initial fineness of non-twisted fiber bundle, Z_0 is latent twist of fiber bundle expressed as number of turns per input length of non-twisted fiber bundle (before twisting).

It is obvious from equation (10), that the value of twist coefficient is also limited. This relation is valid only when formula (11) holds.

$$\frac{\alpha_0}{\sqrt{\mu\rho}} \le \frac{1}{\sqrt{4\pi}}\,. \tag{11}$$

In the case that $\frac{\alpha_0}{\sqrt{\mu\rho}} = \frac{1}{\sqrt{4\pi}} = 0.281$, then the theoretical twist take-up is equal to δ = 0.5 and angle of peripheral fiber is β_D = 70.5°. This is in the limit case (is referred to as saturated twist).

Figure 11 shows the course of function in equation (10) with packing density μ = 0.6; polyamide raw material was considered for the construction of the function.

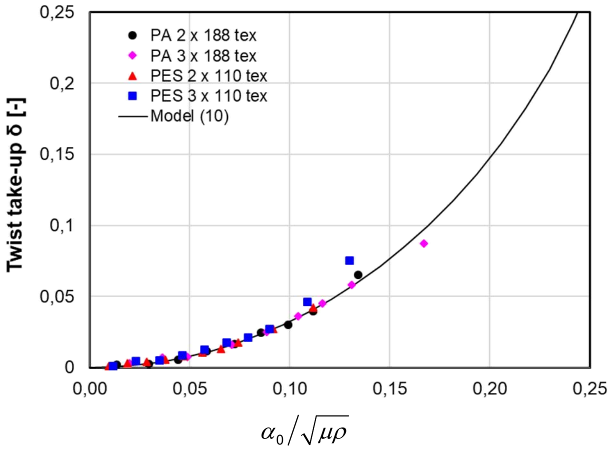

Figure 11 Dependence of twist take-up on latent twist coefficient

Such course is really observed experimentally, but for a smaller value of latent twist. Usually, the saturated twist is observed in the case of yarn twist take-up δ = 0.42, value of angle β_D lies in the range from 45° to 55° in case of multifilament yarns, or the expression $\alpha_0/\sqrt{\mu\rho}$ is approximately equal to 0.22 instead of theoretical value 0.28. Axial asymmetry of twisted yarn is the probable reason of this phenomenon [2] and [3]. If we insert a twist higher than the saturated twist to the yarn, the yarn will not able to absorb it "inside" its structure and then some turns will be placed "outside", such as the coils of the twist of second order.

5 CONCLUSION

The influence of Koechlin´s twist coefficient on selected mechanical-physical properties (tenacity and breaking elongation), yarn twist take-up, and structural characteristics (yarn diameter, packing density) of two and three-fold twisted multifilament yarns were analyzed.

The results confirmed that twisted multifilament yarn twist take-up increases with increasing twist coefficient. The relationship is polynomial. In our case, the numerical coefficients of this polynomial function probably depend on raw material (PES, PA 6) and structure of single multifilament yarn. From our experiment it results that these numerical coefficients are higher in the case of PA twisted multifilament yarn made of single-end multifilament yarns with interlaced fibrils compared to PES twisted multifilament yarn made of single-end multifilament yarns with protective twist.

The diameter of twisted multifilament yarn is influenced by number of fibrils in the cross-section, size and shape of cross-section of individual fibrils, and number of twists. In our case, the twisted multifilament yarn diameter decreases polynomially with increasing twist coefficient up to the value of twist coefficient 60 - 70 ktex$^{1/2}$.m^{-1}. After this value, the decrease in the yarn diameter is not significant. This phenomenon is in agreement with the course of packing density. Their values fluctuate non-significantly from the level of twist coefficient of 60 $ktex^{1/2}.m^{-1}$ up to higher values. The internal structure of single multifilament yarn (protective twist, interlacing) probably influences the value of maximum packing density recorded in this experiment.

The tenacity of twisted multifilament yarn showed negligible increasing tendency with increasing Koechlin's twist coefficient up to the level approximately equal to α = 50 $ktex^{1/2}.m^{-1}$. From this level, increasing twist coefficient leads to a decrease in yarn tenacity due to higher slope of individual fibers to the multifilament axis. The relationship between coefficient of fiber stress utilization and the angle of peripheral fiber inclination, predicted experimentally as well as theoretically, shows that tenacity decreases from the value of angle β_D = 12°. This phenomenon confirmed previously obtained results [3].

The significant correlation coefficient between experimentally and predicted breaking elongation verified validity of Gégauff's and Neckar's model enabling calculation of breaking elongation of twisted fiber bundle based on the breaking elongation of non-twisted fiber bundle and angle of peripheral fibers to the yarn axis.

We can conclude that observed number of single multifilament yarns in the twisted yarn has not any influence on analyzed properties except tenacity and yarn diameter. When the twisted yarns made of the same raw material have the same twist coefficient, they have also the same or nearly the same angle of slope of single multifilament to the twisted yarn axis and thus the same twist take-up, packing density and breaking elongation.

ACKNOWLEDGEMENT: *This work is supported under Student Grant Scheme (SGS 21249) by Technical University of Liberec, Czech Republic.*

6 REFERENCES

1. Hearle J.W.S., Grosberg P., Backer S.: Structural Mechanics of Fibers, Yarns and Fabrics, New York: Wiley- Interscience, 1969, ISBN 0471366692 9780471366690
2. Neckář B.: Yarn - Forming, structure and properties, Prague: SNTL Prague, 1990
3. Mertová I., Moučková E., Neckář B., Vyšanská M.: Influence of twist on selected properties of multifilament yarn, Autex Research Journal 18 (2), 2018, pp. 110-120, DOI: https://doi.org/10.1515/aut-2017-0018
4. Huang W., Fu T., Zhang Y., Wang, J.: An approach to predict the tensile strength of a two-ply yarn from single multifilament yarn, The Journal of the Textile Institute 108(3), 2017, pp.412-417, https://doi.org/10.1080/00405000.2016.1169010
5. Zimliki D.A., Kennedy J.M., Hirt D. E., Reese G.P.: Determining mechanical properties of yarns and two-ply cords from single-filament data. Part I: Model development and predictions, Textile Research Journal 70(11), 2000, pp. 991-1004, https://doi.org/10.1177/004051750007001110
6. Kilby W. F.: The mechanical properties of twisted continuous filament yarns, The Journal of the Textile Institute 55(12), 1964, pp. T589-T632, https://doi.org/10.1080/19447026408662251
7. Treloar L.R.G., Riding G.A.: A theory of stress-strain properties of continuous-filament yarns, The Journal of the Textile Institute 54(4), 1963, pp. T156-T170, https://doi.org/10.1080/19447026308660166
8. Treloar L.R.G.: The stress-strain properties of multi-ply cords. Part I: Theory, The Journal of the Textile Institute Transaction 56(9), 1965, T447-T488, https://doi.org/10.1080/19447026508662306
9. Treloar L.R.G.: The geometry of multi-ply yarn, The Journal of the Textile Institute Transaction 47(6), 1956, T348-T368,
https://doi.org/10.1080/19447027.1956.10750540
10. Jones J.E., Haddad G.N., Sutton J.N.: Tensile characteristics of twisted continuous-filament glass yarns, Textile Research Journal 41(11), 1971, pp. 900-904,
https://doi.org/10.1177/004051757104101104
11. Hearle J.W.S., Bose O.N.: The form of yarn twisting, Part II: Experimental studies, The Journal of the Textile Institute 57(7), 1966. T294-320, https://doi.org/10.1080/19447026608662372
12. Hearle J.W.S., Hollick L., Wilson D.K.: Yarn texturing technology, Cambridge: Woodhead Publishing Limited, 2001, ISBN 978-1-85573-575-0
13. Neckář B., Das D.: Theory of structure and mechanics of fiber assemblies, (1 edition), New Delhi: Woodhead Publishing India, 2012, ISBN 978-1-84569-791-4
14. Internal Standard No. 46-108-01/01 Recommended procedure for preparation of samples. Soft and hard sections (slices),Technical University of Liberec, Faculty of Textile Engineering, Textile Research Center
15. Internal Standard No. 32-102-01/01. The transverse dimensions of the double-sided yarn and the diameter of the single yarn. Longitudinal views, Technical University of Liberec, Faculty of Textile Engineering, Textile Research Center
16. Gegauff M.C.: Strength and elasticity of cotton threads, Bulletin de la Société Industrielle de Mulhouse 77, 1907, pp. 153-176
17. Das D.: Yarn strength as a stochastic process, Dissertation work, Liberec: Technical University of Liberec, 2005

LONG-SLEEVED SHIRT PATTERN AS GUIDELINES FOR DESIGNING A *SANGGIT* MOTIF BATIK SHIRT

Mulyanto[1], **Nadia Sigi Prameswari**[2], **Mohamad Suharto**[3] **and Narsen Afatara**[3]

[1]*Lecturers of Arts Education Department, Faculty of Teacher Training and Education, Sebelas Maret University, Jl.Ir.Sutami 36A Surakarta, 57216, INDONESIA*
[2]*Lecturers of Fine Art Department, Faculty of Language and Art, Semarang State University, Jl.Sekaran Raya, Gunung Pati, Sekaran, Semarang, 50229, INDONESIA*
[3]*Lecturers of Visual Communication Design Department, Faculty of Art and Design, Sebelas Maret University, Jl.Ir.Sutami 36A Surakarta, 57216, INDONESIA*
mulyanto@staff.uns.ac.id; nadiasigi87@gmail.com; mohamadsuharto@staff.uns.ac.id; narsenafatara@staff.uns.ac.id

Abstract: *The aim of this research is formulating the long sleeved motif pattern of shirt which can be extended into various sizes of long-sleeved batik shirt in which the motif is sanggit patterned. This employed action-participatory research to test the draft pattern by actively involved the batik entrepreneurs, motif designers and tailors. The data were collected through the techniques of observation, interviews, FGDs and document analysis. The result produces a pattern of long-sleeved rectangular shirt motif, 115 cm width and 250 cm length, divided into 12 symmetrical objects of vertical axis. The pattern works to develop the motifs, which can be made into a long-sleeved batik shirt of various sizes (S, M, L, XL and XXL). It is quite effective and efficient to develop random batik asymmetrical motifs and the resulting motif can meet sanggit at the front shirt or buttons, the left, right sides, pocket and specific motifs on cuff and collar parts.*

Keywords*: patterns; motifs; long-sleeved shirts; batik; sanggit.*

1 INTRODUCTION

The textile motifs in patterned such as batik cloth and woven fabrics produced in Indonesia as well as other countries are generally designed according to their function as a long other traditional clothes such as *jarit* and *sarong*. Long cloth pattern, meaning the motif is applied to a piece of cloth without cutting or sewing; i.e., the patterned cloth applied to a traditional model of cloth such as *jarit* for women, as a *sarong* for men, scarves, coconut bundles, *kemben*, sheets, tablecloths, as a *sari* for the Indians, etc. The Solo and Yogya classical batik motifs patterned in general, tend to show the spread motif in all sides, and have geometric motif [1, 2]. Coastal batik products have generally morning-evening patterns, one-headed and two-headed patterns [3]. Long patterned clothes in Indonesia have been adjusted according to the geographical motifs which can be divided into seven types or patterns: *pagi-sore* (morning-afternoon) pattern, the one-headed pattern (the head is located in the middle and the head is located on the edge), the two-headed pattern (similar and different head motifs), oblique patterns or machetes, *ceplok* patterns, upright symmetrical and random patterns.

The *pagi-sore* (morning-afternoon) pattern is designed with 110 cm and 250 cm piece of cloth which has two motifs bounded by a line. This pattern is designed only for *jarits,* traditional long-patterned skirt for women, and if made into shirts, then the motif will be cut off and so the front motif, the left and right sides cannot then be called *sanggit*. One-headed patterned cloth is designed as a piece of cloth 110 cm wide and 250 or 200 cm long which has two motifs, namely head and body motifs. One head patterned cloth of 250 cm long is used for making *jarit* and the head motif is placed in front. While the head pattern cloth of 200 cm long is used for men's wearing *sarongs*, according to the use, the head motif is placed behind. If the one head patterned cloth is made for a shirt, usually the motives cut off and cannot be patterned into *sanggit*.

The two-headed cloth is designed as 110 cm wide piece of cloth and 250 cm long to create *jarit* for women and as a scarf. Slopping patterned clothes are usually designed to create a *jarit* for both women and men. If such slopping patterns are used to create for shirts, then the motifs that can be *sanggit* only at front of the motif, while on the other part of the motifs cannot be *sanggit*.

Ceplok-patterned clothes are usually designed to create a *jarit* for both women and for men. If batik motifs are applied to small-sized *ceplok*-patterned and then the batik cloth is made into a shirt, the motif remains *sanggit*. This is caused by the hape motive which is increasingly geometric and has smaller motive size, then the motifs can be more *sanggit* only if the cloth is made into a shirt.

The upright symmetrical patterned cloth is designed as a wide-sized cloth of 110 cm x long 200 cm or 250 cm which is used for a blouse, dress or robe for women. The making of symmetrical patterned cloth gives emphasis on the efficiency process in drawing motifs on the cloth. If these symmetrical patterned clothes are made into blouses or shirts, then the motifs never may be fully *sanggit*. Random patterned clothes are usually designed only for decoration and beach sarongs. If this random patterned is made into shirts, the motifs will be cut, thus it cannot be *sanggit*.

Such long patterned cloth as mentioned above is designed to create long traditional Javanese dresses such as *jarit* for women and *sarong* for men. In case such long patterned clothes are used as either for a shirt or blouse clothing, then the produced garment shall have motives which cannot be categorized *sanggit* on some of the stitched parts. In fact, one of the criteria of quality patterned clothing (*batik*) lays on "how much *sanggit* the motifs are".

Figure 1 *Pagi-sore* pattern (morning-afternoon)

Figure 2 One-headed pattern

Figure 3 Two-headed pattern

Figure 4 Leaning pattern

Figure 5 *Ceplok* pattern

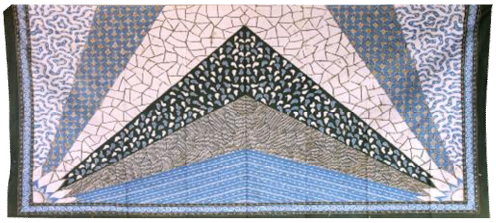

Figure 6 Upright symmetrical pattern

Figure 7 Random pattern

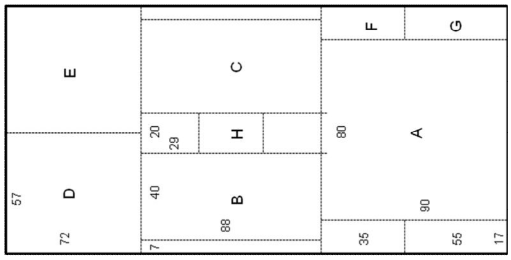

Figure 8 Pola long-sleeved in *sanggit* patterned

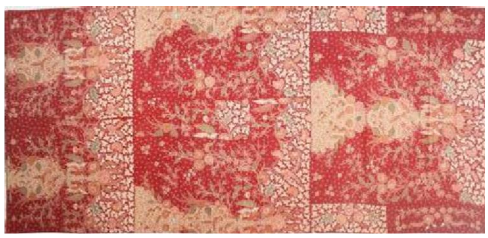

Figure 9 Pola long-sleeved in *sanggit* patterned

Sanggit is a motif for dress and shirts, which is centred at the seams junction fused or met one another, i.e. on the front, the left, right sides and the pocket. Thus, it is creates a long-sleeved blouse or shirt which has *sanggit* motifs, then in the process of making the motif is done on a sheet of cloth that has a long-sleeved shirt patterned. This long-sleeved pattern of shirt is different from the previous seven patterns.

The long-sleeved patterned shirts mean a long-rectangular image used as a guide, a reference to create or develop the batik motifs, additionally the cloth in motifs produced in such a pattern can be made into a shirt or long sleeved-blouse of various sizes (M, L, XL, XXL), which motifs remain *sanggit*. To such pattern of long-sleeved shirt is set the breaking structure pattern according to the components of the long-sleeved shirt like the back side, at the left and the right chest, left and right arms, collar, pocket part and the cuff parts.

The long sleeved shirt patterned by *sanggit* motif is beneficial for some people related to *batik*, among others the batik industry, batik motif designers, batik dyers, batik cloth collectors, convection industries, as wel as the batik consumers.

Benefits for the batik industry, among others:

a. can develop various batik motifs which are managed to be manufactured into batik cloth, which furthermore, batik cloth can be made into long-sleeved shirts of various sizes which motifs remain *sanggit.* Thus, the batik industry can meet the art feel of motifs for consumers and can increase the selling value of batik clothes,
b. can reduce the cost of batik production, save raw materials such as cloth, dyestuff and production cost by adjusting the size of batik cloth motifs produced according to the market demands,
c. can provide information on the pattern of this long-sleeved shirt to the consumer, so they can better understand the form of batik motif from cloth before become clothing.

Benefit for the designer motive is that this pattern further facilitates the work in developing for batik long-sleeved shirt motifs although the undertaken motifs have a high level of difficulty.

Benefit for batik dye artisans is that this pattern is easier to work in putting the colors in accordance with the motif, despite the motif's pairs are located separately.

Benefits will be surely obtained especially for those who work as tailor because on such patterned shirt will be easier to determine ruptured parts of the long-sleeved shirt pattern so for the tailor will be easier to cut the batik cloth to correct long-sleeved clothes. Additionally, the benefits also will be used by society of the batik convection industry, batik agents, batik fashion designers and consumers of batik clothing, who will be able to read and evaluate "the batik motifs" of a long sleeved batik shirt, when the motifs are still fabric sheets, so they can treat and process the batik cloth.

1.1 Review of related literature

There have been a lot of researches on the cloth patterns, both men's and women's clothing. The function of clothing has been researched from its various aspects, for example like by Kang et al. [4] who associate the clothing functions to change the users' moods, while Simoes [5] views the body as the source of the design process and founds the factors from which the discomfort may be resulted by the dressed body while it is in motion. Apart from such views, current research attempts to provide special attention on patterns to develop the cloth motifs, wherein the produced clothes patterned can be made into clothing of *sanggit* motifs patterned which have not yet been found. Some researches were related to dress patterns, e.g. Ghoswatun et al. [6] studied the making of party dress for students of Vocational High School Syafi'i Akrom Pekalongan using a combination of pattern which is deemed to be more effective compared to the use of construction patterns. Effectiveness level of the student group applying a combined pattern reaches 87.40% (very high category), while in control group using construction pattern obtained 79.39% (high category). In the use of combined patterns better clothing is produced and the time required is shorter. The lack of combined pattern is at the draping pattern, since it directly uses the main material, in case there occurred cutting error on cloth, it will be directly impacted on the cost, needed the accuracy in creating a pattern of combination. On the use of a combined pattern with backless model which should be given *kupnat* on the pleated side of the face, so that the fall pleated will result better.

The women's dress making with body modified feels very comfortable compared to the making with non-modification. This is indicated by the difference of respondents' frequencies, namely (1) 47.22% of respondents testified very comfortable and 50% of respondents said comfortable with modifications on the arm part, (2) 55.55% of respondents testified very comfortable and 44.45% respondents said they feel comfortable with modification on neck circumference, and (3) 72.72% respondents informed very comfortable and 27.78% respondents feel comfortable with modification on the back. The results of data analysis on the comfort level of fitting body shows 55.55% of respondents stated very comfortable and 41.66% respondents stated comfortable [7]. Both of these studies examine the pattern of clothing, not the pattern to compose a motif that can be made into clothes.

Researches on motif development for clothing also have been widely practiced. For example, research on coffee and cocoa in the creation of batik motif of Jember type, successfully created six motifs of batik, *uwoh kopi*, *godong kopi, ceplok, kakao* motif, *kakao raja*, *kakao biru*, and *wiji mukti* motif. Of the six motifs, the most favored motif to people of Jember is the *uwoh kopi* motif and the *kakao raja* motif. It shows that superior seeds of a region can be explored and developed into batik motifs that have characteristic of Jember region [8]. In addition, regional art and culture can also be explored and developed for the inspiration of batik motif design.

A research by Salma [9] on the development of Balinese batik motif produced five motifs namely Jepun Alit motif, Jepun Ageng motif, Sekar Jagad Bali motif, Lotus Banji motif, and Poleng Biru motif. Among the five motives, the motifs that many people love are the motive of Jepun Alit, Sekar Jagad Bali motif and the motif of Lotus Banji.

The research by Bimantoro [10], on Dotted-Board Model (DBM) and Extended Local Search (ELS) to optimize the layout of cloth pattern on patterned materials by considering the rules of harmony motif, found the following:

(1) The point of harmony rules can reach the maximum value if the used DBM resolution value is the biggest common factor of the base motif length.

(2) The size of a clothing pattern affects material efficiency and computation time, the larger the size of the clothing pattern, the material efficiency will decrease, but the computation time will be faster.

(3) The efficiency of materials on the orientation of clothing patterns is vertically more efficient when compared with the horizontal clothing orientation pattern, because the orientation of horizontal clothing patterns leads to the use of longer containers, but a lot of free space is freely used by other patterns on the top of the container so it is more wasteful in terms of using the materials.

Thus it can be concluded that the overall mean result of the ELS combination with DBM contributes positively in increasing the computation time, where the computational time of ELS with DBM is about two times faster than just using ELS. The optimal resolution and NMO that can be achieved by the method of integration between ELS and DBM is 5 and 3, with an average of 56% efficiency and an average computational time of 381 seconds. In the research, the motive material used is a material which motif is geometric and repetition, so that the placing motif is more easily harmonious. It will be different if the motif un-geometric or even abstract shaped motif.

Researches on extraction of geometric batik features have been proposed using Cardinal Spline Curve to produce segmentation of klowongan and isen-isen motifs [11]. Batik motifs that vary greatly into problems in laying and cutting patterns of clothing, the problem is known as irregular SPP. Irregular SPP is a common problem in terms of laying and pattern cutting in containers. The respected pattern is an object that has a certain shape. Containers are media where some patterns are placed with certain rules in order to obtain the most optimal container size. The optimal container size is a container that has the least dimension in which there is a non-overlapping pattern and has the least amount of free space left.

One of the SPP Irregular applications is found in the fashion industry. The purpose of Irregular SPP is to minimize the length of the container by optimizing layout of the objects present in condition the absence of overlapping objects [12].

For such researches, there are three main points that have been studied related to the pattern of motifs, namely the pattern of clothing, the development motifs regardless of patterns, and application of fashion patterns. This research combines the three things that are: arrange a pattern on a piece of cloth, placement pattern of clothing fabric for arranged motif can be *sanggit*, and strategy of motif placement (which already exist) in fashion pattern. Thus the produced cloth pattern by this pattern model can be made into a shirt which motif is considered *sanggit*. To formulate a pattern of dress shirts, there are some things that need to be studied, among others, about the various types of shirt pattern breaks, adult body standard size, various standard sizes of cloth as shirt material, various types of motifs, factors that affect the quality of shirt products, and so on.

Various types of brown shirt patterns of adults are associated with the manufacture of long-sleeved shirts, which breaks the body pattern. Broken arm patterned, and broken the collar patterned. The proportions of the adult bodies to be measured are: upper chest circumference, shirt length, arm length, arm circumference, wrist cuff, neck circumference (collar) and pocket size. Actual size used in small, medium, large, x-large and xx-large labels depends on the size and target market of each manufacturer. Manufacturers, who market men's grown products, provide widely clothing sizes than manufacturers who market their products for young men [13]. An example is two standard chest circumference proposed by the British Standards and widely used by factories in the UK.

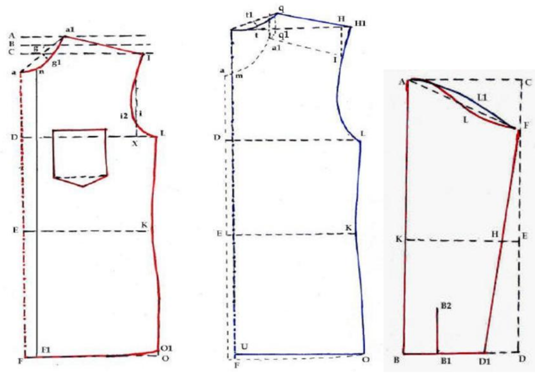

Figure 10 Example of body pattern and long-sleeved pattern of menswear

Table 1 Size [cm] of standard upper chest circumference by British Standards

Consumer Goals	S	M	L	XL	XXL
Young man	<94	97-102	103-109	112-117	119-125
Adult man	94-99	99-107	107-114	114-122	122-130

Table 2 Size [cm] of a broken pattern of men's shirts [13]

Consumer Goals	S	M	L	XL
Top chest circumference	92	100	108	116
Neck circumference	38	40	42	44
Length of the arm	80	82	84	86
The wrist	17	17,8	18,6	19,4
Half width of the back	19	20	21	22

Table 3 Size [cm] of a broken pattern of shirts [14]

Explanation	S	M	L
Low chest	18	22	24
Long shirt	57	66	70
The width of shoulder	33	40	46
Half width of face	22	25	28
The width of shoulder	11	15	16
Long-sleeved length	19	21	23
Arm circumference	28	31	34
Neck circumference	30+2	35+2	37+2

Various types of clothes and the standard sizes are commonly used for shirt materials include primissima cotton f, prime cotton, silk clothes made with non-engine weaving (ATBM) and ATCM twist cotton width 115 cm.

Batik motifs that are considered beautiful on a sheet of cloth does not necessarily look beautiful if the cloth is made into a shirt or blouse clothing. It is caused by the process of making clothes through cutting and sewing cloth. A piece of cloth patterned according to the pattern of clothing then cut and sewn, while the motifs on the part of the clothing connection cannot connect anymore, so the motif does not appear intact or separated or un-*sanggit*. Therefore, batik cloth that will function as quality clothing (known for *sanggit* motif) should be designed in such way in order that the aesthetic value motif can be obtained. Lay out patterns of motifs should be designed based on the type of motifs, broken patterns of dress, production techniques and standard measures of the adult body. There are seven aspects to consider in designing product design: functionally, technically, ergonomically, economically, environmentally, socially, culturally and aesthetically visual [15]. Related to the pattern of motifs, the dominant aspect to note is the aesthetic, the motif can remain *sanggit* although the cloth is made of shirts with various sizes, functional aspects, namely the suitability between the motif and its usefulness. Economical aspect is matched between pattern with requirement of both cloth and motif.

Furthermore, here are several important factors in the process of designing textile products include the products can be produced, marketed used, and then the products are the interesting one [16]. Design patterns of shirt motifs as design is generally a creative industry business distinguished from other cultural industries. Design innovation requires a combination of different knowledge, such as between designer, client and company performance [17].

In formulating the long-sleeved batik shirts pattern, one should understand the process of batik production that will work to create the long-sleeved shirt pattern. The relevant textile (batik) production process undertakes long-sleeved shirt patterns, namely batik production process technique, resin printing or screw printing technique, wax prints and color printing technique (full print). The batik production process involves the preparation of design concepts, sketches of motifs on clothes, the process of batik *klowong*, the first stage staining, the making process of *isen-isen* batik, the second stage staining and *pelorodan* waxing. The printed batik production process is the preparation of design concept, making motif on screen, printing and coloring processes [18]. The resin or printed production process involves the preparation of design concepts, drawing motifs on paper, drawing motifs on the screen, making print dough (resin), staining fabric base, resin printing process with screen on cloth, basic color locking process, batik process, second stage staining and *pelorodan* candle [19].

Types of the batik motifs which are applicable to long-sleeved shirts are all kinds of motifs, not only geometric motifs, but abstract, oblique, random or asymmetrical motifs. Based on the composition and shape, the batik motifs can be classified into four groups: (1) the geometric motifs including *banji, ceplokan, ganggong*, woven, *parang* and *lereng* motifs; (2) cement motifs covering only vegetation motifs; plants and animals; as well as plants, animals and winged animals motifs; (3) bouquet motifs and (4) modern motifs [20]. Based on the shape, the batik motifs can be divided into geometric motifs, *ceplok, parang, lereng*, non-geometric, *lung-lungan*, *buketan* and *pinggiran* (periphery) [21]. While in general, the batik motifs can be divided into numerous motifs such as *parang* motif, geometric, banji, creeping plants, water plants, flowers and animals in their natural lives [22].

2 METHODOLOGY

This research was conducted in two small and medium scale batik and textile industries, which applying various kinds of production techniques, in Central Java Province, Indonesia. The research was conducted using qualitative descriptive approach and participative action study. Qualitative descriptive method to compile the standard draft of long-sleeved shirt pattern for adult size while the method of study uses participatory action to test the draft pattern to the formulated of standard shirt pattern. The textile and batik industries were chosen as a place for training of *batik tulis* and stamped industry of Dewi Ratih and textile industry of nDerbolo of resin printing technique in Sragen regency. The invited tailors cooperated in the test-making shirt is Royal Tailor in Sukoharjo. The used data sources included participants, product documents and events.

Participants included 2 textile entrepreneurs, 3 motive designers, 4 batik, 2 batik dyers, 1 tailor and 2 batik consumers. The documents used primarily patterns of motifs tested, screen, batik motifs and broken long-sleeved shirt patterns. The observed events included all the processes that leading to the "pattern of long-sleeved shirt motifs", which was tested and included the process of designing patterns, designing motifs, making screen motifs, production processes, the process of making long-sleeved shirts, the cutting process of clothes and the process of tailoring into shirts. The data sources were determined based on purposive, snowball and time sampling techniques. The data were collected through observation techniques [23], interviews [24], focus group discussion [25], literature study and then analyzed through flow model [26].

Research stages employed the qualitative-descriptive method, the data collection of research data until the formulated draft shirt patternned. Furthermore the draft shirt pattern was tested through participative action study method. Above the draft shirt pattern was made or developed various types of batik motifs, such as the symmetrical motif, asymmetrical motifs and oblique motif. Then the motif was designed on the draft pattern, which is made median, the draft pattern was processed into batik cloth, batik cloth was processed into long sleeved shirts of various sizes (S, M, L, XL, XXL) and the last motifs on the shirt were analyzed. The *sanggit* motifs on the joints of the seams on a shirt were analyzed by researcher, batik entrepreneurs, motive designers and tailors. When the level of the motif was reached, the draft pattern was standardized; however, if the motive severity level has not been reached then the draft size of the shirt pattern was revised and the draft was retested.

3 ANALYSIS

Before discussing the pattern of long-sleeved shirt of sanggit patterned, first it is needed to set the standard size of the long-sleeved shirt pattern for adults (Indonesia). Based on some references [13, 26, 14, 27] was determined the breaking component size of the long-sleeved shirt pattern for Indonesian adults, as is illustrated in Table 4.

Table 4 The broken part of a long-sleeved shirt of Indonesian adult man [cm]

The broken part pattern	M	L	XL	XXL
Half rear body circumference	54	56	58	60
A quarter of the front body circumference	30	32	34	36
Long shirt	76	78	80	82
The arm circumference	48	50	52	54
Long sleeved length	57	58	59	60
Cuff	38	40	42	44
Collar	17	17,8	18,6	19,4
Pocket	23	23,3	23,6	24
Half rear body circumference	12x14	12x14	12x14	12x14

The pattern of long sleeved shirt motif (Figure 11) is used as a guide to develop a batik motif on a piece of cloth measuring 115 cm x 250 cm, where the resulting batik cloth can be made into a long-sleeved *batik* shirt size S, M, L, XL and XXL which motifs remain sanggit. The resulting motif resilience lies in the front shirt, the right side, the left side seams and the third part of the pocket with the motifs around it. The three pockets are located in the upper left chest, in the lower left abdomen and in the lower right part of abdomen.

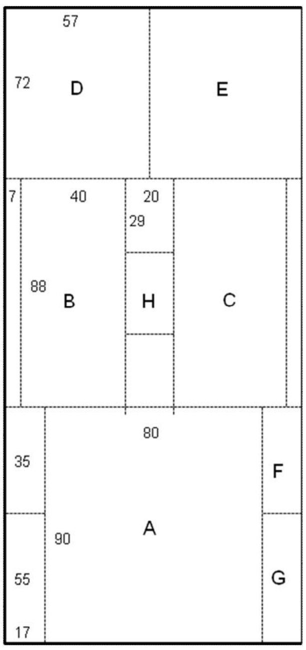

Figure 11 Long-sleeved shirt motif pattern

Figure 12 Batik cloth of long sleeved shirt pattern

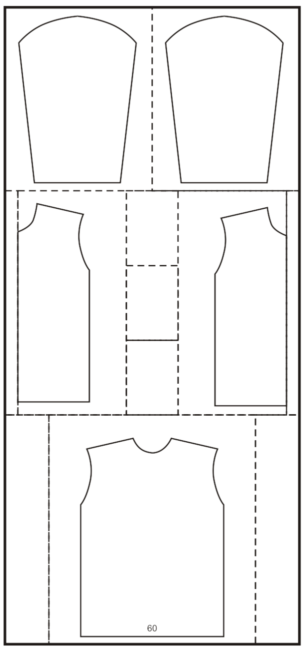

Figure 13 The broken part of a long-sleeved *sanggit* shirt

Figure 14 Long-sleeved shirt is in *sanggit* patterned, symmetrical motif. The shirt motif is *sanggit*: 14a) the front motif of *sanggit*, motif pocket of sanggit with the surrounding motifs, 14b) the front motif is the same as the back, 14c) the left side motif in *sanggit* patterned, 14d) the right side motif of sanggit

The pattern of this long-sleeved shirt motif is identical with the back 80 cm width and the shirt length of 90 cm (code A); quarter circumference of the front body (chest) 40 cm and breast length 88 cm (code B and C); arm circumference 57 cm and hand arm length 72 cm (code D and E); wide collar and cuff width 17-18 cm with length of 90 cm (code F and G); the width of the fold 7 cm buttonhole (the edges B and C); and three pockets each measuring 20x29 cm (H code).

The examples of the symmetrical batik motifs application to long-sleeved shirts (Figure 11) on a silk ATBM twist measuring 115x250 cm fabricated by written technique (Figure 12). Then the batik cloth of long sleeve-patterned shirt is made into a long-sleeved shirt size M. The pattern is then broken into three parts (Figure 13), 1) the upper part is the second part of the long arm; 2) the center of the left chest, the pocket and the right chest; 3) the lower part is the back, cuff and collar. After the cloth is cut according to pattern breaks and is sutured, finally becomes a long-sleeved visible shirt (Figure 14a), which is visible from the front, visible from the back, visible from the left side, and visible from the right side. Motif bagaian front or kacing looks as sanggit, motive of the left side and the right side motive is also sanggit.

The calculation analysis of the use of batik cloth long-sleeved shirt motif patterned made into long sleeve shirt size XXL (Table 5) and made into M size of shirt (Table 6).

Based on Table 5, the pattern relationship (Figure 11) with the XXL size shirt is as follows. Code A, the size of the back rear body circumference on the pattern of size 80 cm while to make the shirt required 64 cm so that there is still cloth remaining 16 cm width. The length of shirt on the pattern of 90 cm while the required length of the shirt is 88 cm so that there is still remaining 2 cm. Code B or C, the sizes of the right or left body circumference ¼ in the size pattern is 40 cm while to create a shirt it is needed 38 cm, thus, there is still 2 cm remaining width of cloth. Thus for the size of entire body circumference there is still the remaining cloth as wide 20 cm (16+2+2 cm). Code D or E, the size on the arm circumference pattern of 57 cm while to make such a shirt it is needed 57 cm, thus will be no remaining cloth. The size for hand arm is 72 cm pattern while the shirt requires about 64 cm, so that there is still the remaining cloth as wide as 8 cm.

Table 5 Size comparison of a long-sleeved shirt pattern with the needs of long-sleeved shirt of XXL size (units in cm)

The broken part pattern	Pattern codes	Kampuh	Body	Total	Remains
1	2	3	4	5=4+3	6=2-5
Half rear body circumference	A-80	4	60	64	16
A quarter of the front body circumference	BC-40	2	36	38	2
Long shirt	A-90	6	82	88	2
The arm circumference	DE-57	3	54	57	0
Long sleeved length	DE-72	4	60	64	8
Cuff	F-35	4	24	28	7
Collar	G-55	4	44	48	7
Pocket	H-20x29	2	13x15	15x17	5x12

Descriptions of Tables 5 and 6, where:

(1) the shattered part of the shirt pattern displayed only breaks the shirt pattern associated with formulation of the shirt patterns only,

(2) code and size of the pattern in question is the code (A to H) on the pattern and size which is the size shown in the pattern (Figure 11),

(3) Kampuh is the edge of cloth which is a place to connect one cloth to other clothes. For example, the circumference of the arm base is given 3 cm excess as a sewing area, ½ rim of the rear body given the right and left advantages 2x2 cm = 4 cm, and the shirt length is given 6 cm excess for seam and stitch,

(4) body is the needed size of a cloth to create a good shirt body size M up to body size XXL,

(5) total means that the required pattern size plus the size of the camp or seams,

(6) the remaining is the size of a cloth pattern minus the total size of the required cloth to create a shirt.

Thus, batik cloth sleeveless long-sleeved shirt patterned made on a cloth sized 115x250 cm simply made into a long-sleeved shirt sized XXL with all along the motifs remain *sanggit*. In addition, batik cloth of long sleeve shirt patterned can also be made into a long-sleeved shirt for large-bodied adults with a maximum body circumference of 152 cm (80+40+4-8 cm).

Code F, collar on the pattern of 17x55 cm, this is considered sufficient to create the XXL shirt collar which requires a cloth approximately 2x(8x48 cm). Code G, the cuff on 17x35 cm pattern is sufficient to create an XXL size shirt cuff that requires a cloth as much as 2x(5x28 cm). Code H, the pocket on pattern with width 20 cm x height 29 cm as much as 3 parts, whereas each pocket section measuring 13x15 cm required cloth size 15x17 cm, thus there is excess width 7 cm and height 14 cm. The excessed pocket is used to provide leeway in placing a pocket between the size of the shirt M, XL size shirt and XXL size shirt so that the motif on pocket size (13x15 cm) can be *sanggit* with the surrounding motifs.

Table 6 Size comparison of a long sleeved shirt pattern with the need for a long sleeved shirt size M (units in cm)

The broken part pattern	Pattern codes	Kampuh	Body	Total	Remains
1	2	3	4	5=3+4	6=2-5
Half rear body circumference	A-80	4	54	58	22
A quarter of the front body circumference	BC-40	2	29	31	9
Long shirt	A-90	6	77	83	7
The arm circumference	DE-57	3	48	51	6
Long sleeved length	DE-72	4	57	61	11
Cuff	F-35	4	23	27	8
Collar	G-55	4	38	44	11
Pocket	H20x29	2	12x14	14x16	6x13

Then, Table 6, the pattern size relationship (Figure 11) with the cloth size required to create the M-size sleeved shirt as follows. Code A, the size of a half-body circumference on a pattern 80 cm while size of the shirt required 58 cm, thus there is still the remaining cloth as wide as 22 cm. The length for the shirt on such pattern is 90 cm while the shirt length is 83 cm and then there is 7 cm leftover. The remaining cloth of 7 cm length will be further discarded, it can be selected top motif or bottom motif to be discarded or motif which parts are used. The used motifs can be selected into top, bottom motifs, or some of the both top motifs and the bottom motifs. In the example of this motif (Figure 12) the used motif is on the middle of the motif, or the discarded motifs on top and bottom motifs, because the middle motif is considered more attractive. Codes B and C, the size of a quarter left or right circumference of the body on a 40 cm-sized pattern whereas the shirt takes 31 cm so that there is still the remaining 9 cm wide cloth. Codes D and E, the size of the arm circumference is 57 cm, while the shirt circumference sleeve required 51 cm so that there is still remaining cloth for 6 cm. The hand arm size on the size pattern is 72 cm while to make a shirt it is needed approximately 61 cm so that the remaining cloth is about 11 cm.

Code F, collar on a pattern of 17x55 cm, which is enough to create M-size shirt collar that requires 2x(7x44 cm) cloth. Code G, cufflinks on a 17x35 cm pattern is also sufficient to create an M size shirt cuff that requires 2x(5x27 cm) of cloth. Code H, pocket on the pattern 20 cm width x 29 cm height as much as 3 parts, whereas each pocket part required size 12x14 cm and 14x16 cm cloth size, thus, there is remaining 6 cm width and 13 cm height. The remaining cloth on pocket size 6 cm and 13 cm is used to provide leeway in placing pockets between M size shirts, XL size shirts and XXL size shirts so that the pocket size motifs (12x14 cm) can be sanggit along with the surrounding motifs.

There are some steps how to apply or develop batik motifs on long-sleeved shirt pattern (Figure 12). The developed motif is made on the broken back pattern (Figure 11, code A) measuring 80x90 cm long. Motif on the back (code A) is referred as the master motif. In Figures 11 or 14b, the master motifs are made upright symmetrical. Then the motif is divided into two with vertical lines into two equal parts, the left half motif is applied to the right broken chest pattern (Figure 11, C code) and the right half of the motif is applied to the left chest rupture (Figure 11, code B). Then the motif is taken up to 57 cm width x 72 cm length at the bottom center, applied to both left and right long arm broken pattern (Figure 3, code D and E). Broken cuff patterns (Figure 11, code F) are taken from the bottom motif, while the ruptured collar pattern is taken by the middle motif or other motifs. Break the third pocket pattern (Figure 11, code H) taken motifs that are located in pocket position.

After the motive is arranged into batik cloth, there are some instructions which need to follow how to read and cut batik cloth made on this long-sleeved shirt pattern (Figure 11). Code A is made back shirt, code B made shirt in left chest, code C made shirt right chest. On the object B and C at front or buttons meet in the line. The objects B and A, on the left side, meet on a vertical line corresponding to the size of the body circumference. The objects C and A, on the right side, also meet on vertical lines according to body size. Hence, the objects D and E are for long-sleeved shirts. Right and left objects F are for the cuff part, and the object G is for the collar. Third object H left for the pocket on the top left, bottom left, and bottom right.

On the pattern of this long-sleeved shirt motif, the cuff position (code F) and collar (code G) can be developed into a different motif design from the shirt's principal motif. In addition, motifs on the cuff can also be made different other motifs located on the collar.

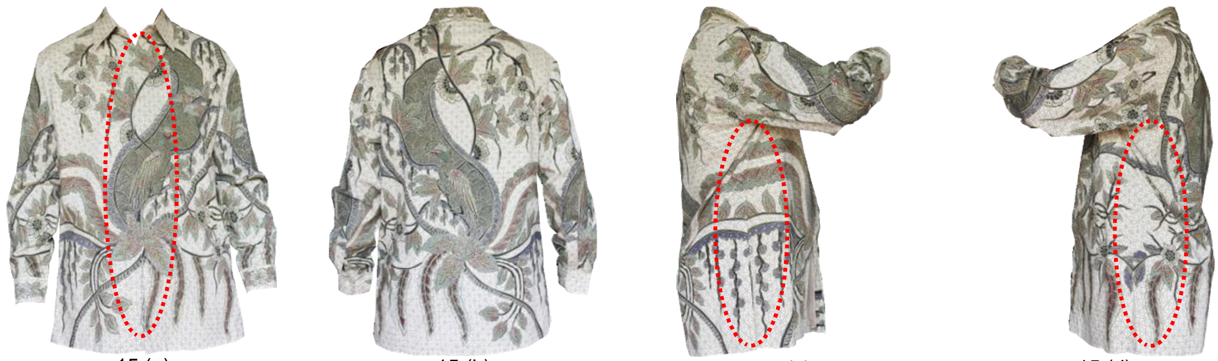

15 (a) 15 (b) 15 (c) 15 (d)

Figure 15 Long-sleeved shirt of symmetrical sanggit pattern: 15a) the sanggit (ness) motif on the front, 15b) the backside motive is opposite to the front motif, 15c) the right side of sanggit, 15d) the left side of sanggit

Here is an example of the batik motifs applications which are asymmetrical on the pattern of long-sleeved shirt. In Figure 15a, the long-sleeved shirt appears from the front of the asymmetrical motif obliquely to the left, whereas in Figure 15b, the shirt appears from the back, the motif is opposite to front motif. Figure 15c shows between the front chest and back of the cloth meets on the right, the motifs meet *sanggit*. Likewise, in Figure 15d, the front cloth motif and the back motif meets on the left side, these occurred to be *sanggit*.

4 CONCLUSION

Based on the research discussion, it can be concluded that one of criteria of quality patterned shirt (*batik*) is at the motif lays on the shirt connections such as the front button, left side, right side and pocket with the surrounding motifs can be categorized as *sanggit*, united or intact. If a batik manufacturer produces batik cloth projected only to create a long-sleeved shirt, a long-sleeved of sanggit pattern shirt can be used as a reference. The pattern of this long-sleeved shirt is 115x250 cm (Figure 11). For that pattern, the resulting batik cloth can be made into long sleeved shirts of various sizes (S, M, L, XL, XXL) which motifs may remain *sanggit*. Motivation sutility lies in the front shirt, the left side, the right side, and the pocket with the surrounding motifs. The front motif of shirt can be made in the same or reverse with the back motif. If the rear motif is different from the front motif, then the motif can be made upside down with the vertical axis. The collar shirts and cuffs can also be created into different motifs from the main.

To the manufacturer of batik cloth, it is advisable that at the time of marketing the long- sleeved shirt of a patterned batik cloth, including the guideline for drawing the long-sleeved broken *sanggit* (Figure 13). Based on the image pattern, this research can be significantly used as a guide for consumers and tailors to easily read the batik motifs in its row material, which also enable the individual to read the motifs in accordance with the broken pattern of long-sleeved shirt. To the batik cloth consumers of long-sleeved shirts patterned, before buying the batik cloth shirts patterned, one should first read and understand the motif, therefore, the purchased batik in accordance individual interests and needs.

ACKNOWLEDGEMENT: *The author wishes to thank the Directorate of Research and Community Service, Directorate General for Research and Development, Ministry of Higher Technology Research and Education, which has funded this research with contract number: 353/UN27.21 / PN/2016 dated February 22, 2016.*

5 REFERENCES

1. Santoso D.: Batik: The Effects of Age and Environment, Surakarta: PT Batik Danarhadi, 2002
2. Van Roojen P.: Batik Design, Amsterdam: The Pepin Press BV, 2001
3. Ishwara H., L.R. Supriyanto Yahya, Moris X.: Indonesian Heritage Coastal Batik, Jakarta: Gramedia, 2011, ISBN: 978-979-91-0338-3
4. Kang J-Y.M., Johnson K.K.P., Kim J.: Clothing functions and use of clothing to alter mood, International Journal of Fashion Design, Technology and Education 6(1), 2013, pp. 43-52, DOI: http://dx.doi.org/10.1080/17543266.2012.762428
5. Simoes I.: Viewing the mobile body as the source of the design process, International Journal of Fashion Design, Technology and Education 6(2), 2013, pp.72-81, http://dx.doi.org/10.1080/17543266.2013.793742
6. Nisa, G., Setyowati E., Musdalifah M.: The effectiveness of the use of combination patterns in the making of students' party dresses for dressing of Syafii SMK Akrom Pekalongan, Journal Teknobuga 2(1), 2015, pp.50-59
7. Irianti A.H.S., Viani A.A., Kusumawardani H., Rahayu S.E.P.: Modification of patterns in the making of women's clothing in the body, Journal TIBBS (Food and Clothing Industry Technology) 3(1), 2012, pp.1-6, http://journal.um.ac.id/index.php/tibbs/article/view/2911

8. Salma I.R., Wibowo A.A., Satria Y.: Coffee and cocoa in typical batik motif creation of jember, Journal Dinamika Kerajinan dan Batik 32(2), 2015, pp.63-72, http://dx.doi.org/10.22322/dkb.v32i2.1362
9. Salma I.R., Masiswo M., Satria Y., Wibowo A.A.: Development of Balinese batik motifs. Journal Dinamika Kerajinan dan Batik 32(1), 2015, pp.23-30, http://dx.doi.org/10.22322/dkb.v32i1.1168
10. Bimantoro F., Suciati N., Arieshanti I.: Dotted-board model and extended local search to optimize the layout of fashion patterns on patterned materials by considering motive harmony rules, JUTI: Scientific Journal of Information Technology 13(1), 2015, pp.75-85, http://dx.doi.org/10.12962/j24068535.v13i1.a390
11. Aris F., Yuniarti A., Suciati N.: Geometric feature extraction of batik image using cardinal spline curve representation, TELKOMNIKA Telecommunication, Computing, Electronics and Control. 12(2), 2014, pp.307-404, http://dx.doi.org/10.12928/telkomnika.v12i2.54
12. Imamichi T.; Yagiura M., Nagamochi H.: An iterated local search algorithm based on non linear programming for the irregular strip packing problem, Discrete Optimization 6(4), 2009, pp.345-361, https://doi.org/10.1016/j.disopt.2009.04.002
13. Aldrich W.: Metric pattern cutting for men's wear, John Wiley & Sons Limited, 2015
14. Kartini: Ikatan Ahli Menjahit Busana Indonesia (IAMBI), Textbooks for Sewing Women and Children's Clothing, 1987
15. Prasetyowibowo B.: The Design of Industrial Product, Bandung: Eight Ten Foundation, 1998
16. Rizali N.: The Review of Textile Design. Surakarta: LPP UNS, 2006
17. Sunley P., Pinch S., Reimer S., Macmillen J.: Innovation in a creative production system: the case of design, Journal of Economic Geography 8(5), 2008, pp. 675-698, https://doi.org/10.1093/jeg/lbn028
18. Mulyanto: Batik design development training as an effort to empower business, Journal of Research on Humanities and Social Sciences 3(6), 2013, pp.22-30
19. Mulyanto, Hartono L.: The production process and batik products are removed, Journal of Language and Arts Education, FKIP UNS Surakarta 5(2), 2009
20. Susanto, Sewan S.K.: Indonesian Batik Art. Jakarta: Research Institute for Batik and Crafts, Ministry of Industry, 1980
21. Hamzuri: Classic Batik, Jakarta: Jambatan, 1981
22. Spradley J.P.: Participant Observation, New York: Holt, Rinehart and Winston, 1980, ISBN 10:0030445019, ISBN 13:9780030445019
23. Bogdan R.C., Biklen S.K.: Qualitative Research for Education: An Introduction to Theory and Methods, USA: Allyn and Bacon, 1982, ISBN 0205076955, 9780205076956
24. Greenbaum T.L.: The Practical Handbook and Guide to Focus Group Research, USA: Lexington Books, 1988, ISBN 10:0669147753; ISBN 13:9780669147759
25. Miles M.B. Huberman A.M.: Qualitative data analysis: A Sourcebook of a New Methods, London: Sage Publications, 1984, ISBN-10:0803922744; ISBN-13:978-0803922747
26. Simanjuntak, Bintang Elly. (t.th.) Basics of pattern making, Jakarta: Vocational Teacher Improvement Development Center
27. Rusli, Kartini & Syahandini: Pattern construction. Jakarta: Depdikbud. Dikjen Dikdasmen, Dikmenjur, 1984

A PROPOSAL FOR DESIGNING KNITTED FABRIC FOR THE“WEAR PROMOTES EXERCISE EFFECT” WITH THE PURPOSE OF IMPROVING COMFORT

Yoshitaka Niimi[1,2], Antonín Havelka[1] and Hiroyuki Kanai[2]

[1]Department of Clothing Technology, Faculty of Textile Engineering, Technical University of Liberec, Studentská 2, 461 17 Liberec, Czech Republic
[2]Department of Advanced Textile and Kansei Engineering, Faculty of Textile Engineering, Shinshu University, 3-15-1 Tokida, Ueda City, 386 8567 Nagano, Japan
k.m.fro.ymg@gmail.com, antonin.havelka@tul.cz, kanai@shinshu-u.ac.jp

***Abstract:** In this paper a study on Compression IW (Inner Wear), the base fabric of TIW (Training Inner Wear), which promotes the exercise effect while walking, will be described. Although the function of clothing is to make and keep a comfortable environment with thermal, compression and tactile comfort, the comfort of TIW has so far not been considered. The main purpose of this research is to recommend TIW, which can be used to make comfortable clothing and maintain the exercise effect in casual wear. Proposed samples of base fabric for TIW were designed by focusing on “material / fineness / density / PU mixing ratio” to improve comfort and maintain function. The thermal properties that are important for clothing comfort were evaluated; especially thermal resistance and water vapor permeability, and tensile properties that are related to fabric stiffness and hoop tension were also measured, because TIW works on the principle of suppressing clothing deformation. These results will be reference values for designing TIW's base fabric.*

***Keywords:** Functional clothing, Compression inner wear, Thermal comfort, Tensile property.*

1 INTRODUCTION

The number of obese Japanese people in the 20s to 70s age range is increasing nowadays and one of the reasons for this problem is a lack of exercise [1]. According to the National Health and Nutrition Survey (2014) by the Ministry of Health, Labor and Welfare, approximately one out of two people in Japan do not spend any time at all exercising; the percentage of these people in their 20s to 40s is especially high [2]. Therefore, they recommend walking 9000 steps (energy consumption: 270 kcal) per day to prevent increasing obesity; however, the average number of walking steps per day (for people in their 20s to 40s) is currently approximately 7400 (energy consumption: 220 kcal). The main reasons why they do not exercise are that they do not have time for it and they usually feel tired after work, both of which are related to the Japanese style of hard work that is forced by long-time labor [3]. Hence, it is efficient to design a product that can promote the exercise effect without spending time exercising in a business situation such as commuting. In a previous research, Training Inner Wear (TIW) was proposed as the wear that promotes exercise effect to the wearer, and it is composed of Low stretch tapes and Compression Inner Wear (IW). The TIW changes wearer’s muscle activity during their walking motion [4]. However, TIW was designed to do this as its main purpose without considering comfort, which is one of the important functions of clothing [5]. Therefore, it is necessary to design and evaluate TIW considering not only its function but also comfort.

2 EXPERIMENTAL SAMPLES

2.1 TIW (Training Inner Wear)

TIW is composed of Low stretch tapes and Compression IW. The tapes have a function of restraining body motion, and the IW is the base fabric to which tapes are attached for TIW. It was already decided how the tapes should be applied to the IW in previous research, as can be seen in Figure1. Each tape has different functions for wearer body. TAPE.01 suppresses a flexion of the knee joint and an extension of the hip joint and TAPE.02/03 suppress a lateral rotation and an abduction of the hip joint. TAPE.04 suppresses an extension of the knee joint and a flexion of the hip joint and TAPE.05 suppress a medial rotation of the hip joint. These tapes have the role of suppressing clothing deformation, which was proposed as a method to obtain the TIW exercise effect; hence the positions in which the tapes were applied were selected according to the level of clothes deformation, which was measured by motion analysis in previous research.

It has been already reported that the exercise effect which means Energy Consumption caused by wearing TIW increased approximately 9% while walking [5].

Figure 1 The tapes which promote exercise effect of TIW

In addition, it was confirmed that the effect depends on the tapes by a result of an exhalation analysis. Therefore, we tried to improve the comfort of TIW by changing the fabric of the IW, which does not relate to the exercise effect and which also contacts the skin directly.

2.2 Proposed sample (base fabric for TIW)

In this research, a new base fabric (IW) is proposed to improve TIW comfort. Polyester, which is normally used as sportswear material, has been used as the base fabric material for TIW until now; however, it causes discomfort from dampness between the skin and the clothing layer because polyester has low moisture content and does not absorb water. As a new base fabric, samples of cotton material were proposed; this is widely used for underwear due to good water absorbency and softness to the touch. Cotton is not generally used in clothing for exercise because cotton does not have quick-drying properties [6]. However, TIW is used in daily situations which do not produce much sweat, which is why cotton was selected as the new base fabric of TIW. Furthermore, it is generally better to constitute TIW base fabric with warp (tricot) knitted fabric, which is widely used as sports innerwear because tricot has excellent elasticity and is comfortable and better fitting [7]. However, natural materials such as cotton are not suitable for warp knitted fabric because it is easy for natural material yarns to break due to the high load that is necessary for warp knitting. Therefore, plain knitted fabric was selected as the TIW base fabric.

However, it easily stretches with this structure, so that, to maintain the TIW's function even after changing the base fabric, we focused on those parameters (fineness / density / PU mixing ratio) that affect fabric rigidity and hoop tension, because the TIW functions by suppressing deformation of clothing. Regarding between IW(C1) and IW(C2), their fineness is different as you can see Table 1; IW(C1)'s is thicker. And, between IW(C2), IW(C3) and IW(C4), their density is different by treating a fulling finish.

These sample's information is given in Table 1 below. Additionally, this IW is made so that course direction is in the circumference direction, while wale direction is in the height direction, as you can see in Figure 2.

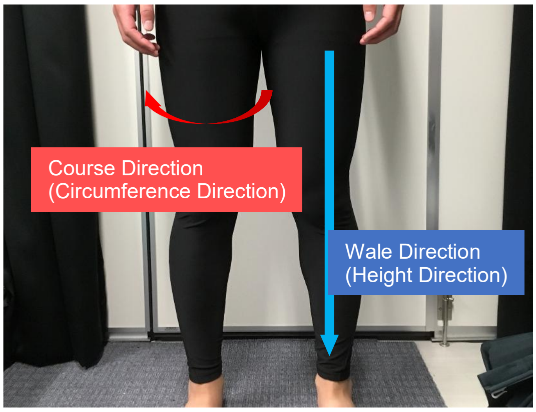

Figure 2 How to knit IW (each direction)

3 METHODS

In proposing a new TIW base fabric (IW), the focus is on two aspects. The first is (1) Maintaining the function of TIW, the second is (2) Improving the comfort of TIW.

Regarding (1), it is necessary to take into account shape stability and displacement by cloth-stretching during the walking motion. The results of motion analysis of TIW show how much deformation each part of IW undergoes, and the tapes attached to the IW must all hold the correct position. It means that it is necessary to confirm the tensile workload and tensile recovery of the IW. Therefore, tensile properties were measured for comparison between each sample.

Table 1 Details of the fabric samples

Sample Name		IW(P)	IW(C1)	IW(C2)	IW(C3)	IW(C4)
		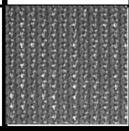	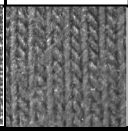	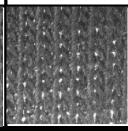	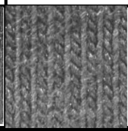	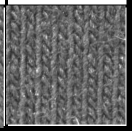
blend ratio [%]	PET	70	0	0	0	0
	Cotton	0	92	95	88	88
	PU	30	8	5	12	12
weight [g/m²]		263.2	224.5	158.2	189.1	214.9
thickness [mm]		0.78	1.03	0.92	0.98	1.00
yarn density	[wales/2.54cm]	66.0	54.0	57.0	62.0	64.0
	[courses/2.54cm]	66.0	38.0	40.0	42.0	45.0
density		66.0	46.0	48.5	52.0	54.5
apparent fineness [tex]		-	21.4	14.5	14.4	15.0
Total volume of pore space [mm³]		0.0631	0.0980	0.336	0.105	0.109
knit construction		Tricot	Plain Stich	Plain Stich	Plain Stich	Plain Stich

Regarding (2), the clothing comfort is composed of three factors which are thermal property, compression property and touch feeling property [8]. In this paper, thermal comfort is discussed as the primary one, as an important function of clothing is to provide aid in maintaining the thermal balance of the human body and ensure that the heat loss, skin temperature, air movement and humidity at the body surface produce a sensation of comfort [9]. Thermal comfort has a relationship with the "clothing climate", which is the climate environment between the human skin and the clothing; this means that Heat transfer, Moisture transfer and Air transfer are important factors [10]. Therefore, the physical properties were measured to confirm the differences in character between samples.

3.1 Tensile property

Tensile property was measured to compare the tensile workload and tensile recovery for each sample, and it was examined by a tensile test with a Tensile and compress testing machine (STA-1225: ORIENTEC) according to Method D (repeated constant elongation method) and Method E (repeated constant load method), which is described in JIS L 1096.

The state where the sample (50×300 mm) was stretched by a constant load was held for a minute, and then it was held again for 3 minutes in a state where it had recovered the position that it had with the initial load. After that process, the grasping interval of the sample was measured under the initial load. Measurement conditions were: Initial load: 29 mN; Grasping interval 200 mm; Grasping width 50 mm; Maximum load 7.25 N; Tensile speed 20 mm/min and the experimental conditions were 23±2°C / 50±4%R.H.

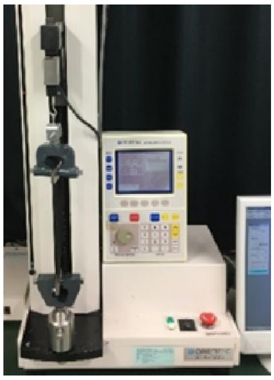

Figure 3 Tensile testing machine (STA-1225: ORIENTEC)

From the Stress [F] - strain [ε] curve (Figure 4) made by the tensile test result, the following values for each feature were calculated.

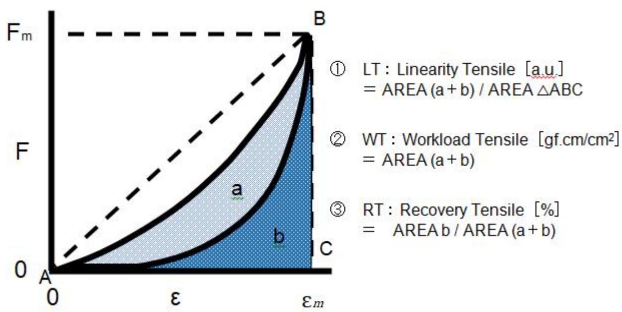

Figure 4 Each feature values from tensile test

3.2 *Thermal property*

As I mentioned, thermal comfort has a relationship with the Clothing Climate environment between the human skin and the clothing, and thermal comfort means that Heat transfer, Moisture transfer and Air transfer are important factors. Especially, Heat transfer and Moisture transfer are important factor for discussing thermal comfort [11]. In addition, air permeability is also important factor, however in the case of having space between skin and clothing [12]. That is why we focus on Heat transfer and Moisture transfer. The method for measuring each physiological property is described below.

Figure 5 Special type thermal characteristic measuring device (NT-H1: KATOTECH)

<u>*Heat transfer*</u>

Heat transfer was measured with special type thermal characteristic measuring device (NT-H1: KATOTECH). It can evaluate Thermal resistance, Thermal conductivity and Q-max. Experimental conditions were 23±2°C and 50±4% R.H. The values could be calculated by the following methods and equations:

$$R_{ct} = (a - b / a) \times 100 \quad (1)$$

where: R_{ct} - Thermal resistance [%], a - Heat flow (no sample) [W], b - Heat flow (each sample) [W].

$$\lambda = (d \times Q)/(A \times \Delta T) \quad (2)$$

where: λ - Thermal conductivity [W/(m.°C)], d - Thickness [m], Q - Heat flow [W], A - Contact area [m^2], T - Temperature [°C]

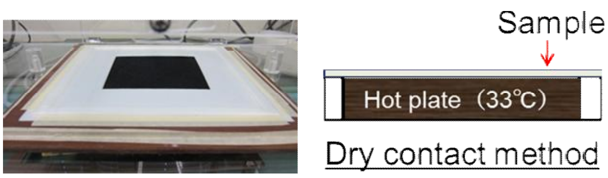

Figure 6 Special type thermal characteristic measuring device (NT-H1: KATOTECH): Thermal resistance

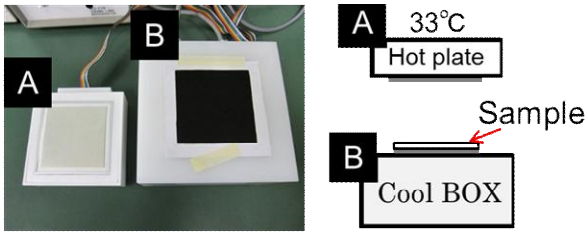

Figure 7 Special type thermal characteristic measuring device (NT-H1: KATOTECH): Thermal conductivity

<u>*Moisture transfer*</u>

The Sweating Guarded Hotplate (SGHP: Thermetrics) was used, often referred to as the Skin Model, to measure water vapor resistance of samples in accordance with ISO 11092. The temperature of the test plate, guard section and bottom plate were maintained at 35±0.5°C without fluctuating more than ±0.1°C during a test. The air temperature was the same as the plate temperature. The relative humidity was 40±4% R.H. and air velocity was maintained at 1.0±0.1 m/s.

$$R_{et} = (P_s - P_a) A / H_E \quad (3)$$

where: R_{et} - Water vapor resistance [kPa.m^2/W], P_s - Water vapor pressure at the plate surface [kPa], P_a - The water vapor pressure in the air [kPa], A - Area of the plate test section [m^2], H_E - Power input [W].

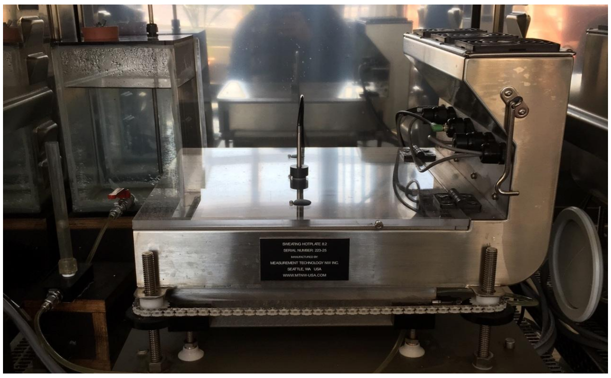

Figure 8 Sweating Guarded Hotplate

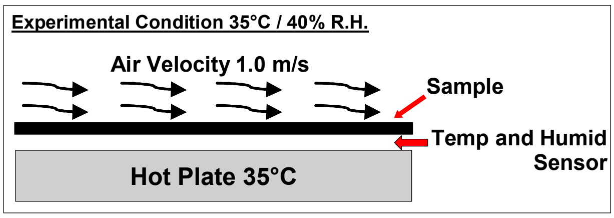

Figure 9 Sweating Guarded Hotplate

4 RESULTS AND DISCUSSION

4.1 *Tensile property*

The analyzed data (WT: Workload Tensile and RT: Recovery Tensile, LT: Linearity Tensile) which were calculated from Stress-strain Curve are shown on

Table 2. Then, it will be described about each result (WT and RT).

Table 2 Physical properties of each sample

Sample		IW(P)	IW(C1)	IW(C2)	IW(C3)	IW(C4)
Density		66.0	46.0	48.5	52.0	54.5
Fineness [tex]		-	21.4	14.5	14.4	15.0
Linearity Tensile [a.u.]	Wale	1.03	0.789	0.659	0.773	0.786
	Course	0.958	0.875	0.758	0.836	0.907
Recovery Tensile [%]	Wale	73.6	36.6	26.7	37.9	40.2
	Course	61.3	37.2	26.6	36.3	39.0
Workload Tensile [gf.cm/cm^2]	Wale	54.4	36.8	36.6	37.1	42.7
	Course	50.8	54.9	68.5	55.4	69.8

WT (Workload Tensile)

It can be recognized from the result whether how much easy to stretch the fabrics and can be seen that there is a different tendency between IW(P) and IW(C) from Figure 10, what IW(C) is lower than IW(P) that is why it describes that fabric of IW(P) is easier to stretch than IW(C), regarding WT of wale direction (Height direction against the body). On the other hand, regarding course direction (Circumstance direction against the body), IW(C) is higher than IW(P) that is why it describes that it is an opposite tendency with wale direction.

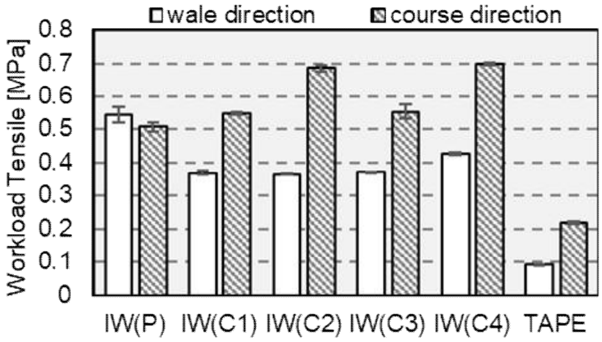

Figure 10 WT (Workload Tensile)

About the human skin deformation during walking, the deformation of a knee that is the main part of a big movement during walking and it is different between wale direction and course direction. It is mentioned that elongation of skin on wale direction has more than course direction about 1.6 times [13]. If it will be mentioned about IW(C), the fabric is not easier to stretch to the height direction (wale direction) that the skin's deformation is high during walking, it might make uncomfortable to the wearer. On the other hand, the fabric is easier to stretch to the circumstance direction (course direction) that is related to hoop tension which effects to a shape stability of clothing, it might make a decreasing clothing stability has related to hoop tension.

RT (Recovery Tensile)

RT of IW(P) and IW(C) is totally different because IW(P) is a warp knitting and be inserted much more PU than IW(C). According to previous research, six IW samples, that are tricot knitted fabric on the general market, are measured their RT by the same method and condition with this experiment, and it is reported that RT average of course direction and wale direction are 57% [5]. Therefore, it can be recognized that it is not enough RT of IW(C) as you can see in Figure 11. The exercise effect of TIW will be not applied if it has not enough RT for IW, because it makes lack of clothing stability. That is why it is necessary to have a sufficient RT for applying to a practical product. It can also be mentioned from the fact that there is a significant correlation between RT and PU mixing ration as you can see Figure 12. It means that the RT will increase if the samples have much PU mixing ration.

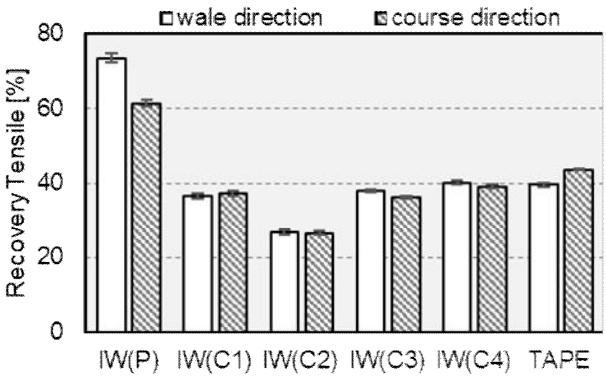

Figure 11 RT (Recovery Tensile)

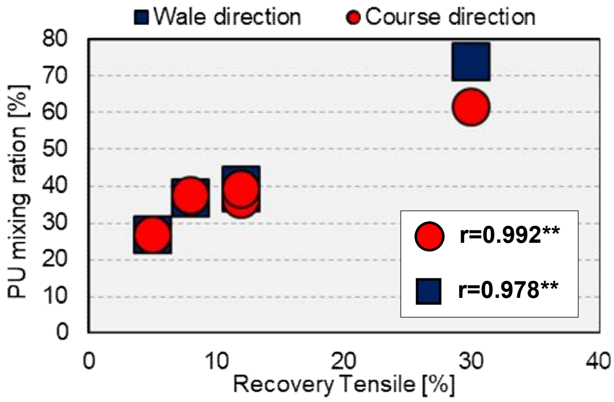

Figure 12 Correlation between RT and PU mixing ratio

4.2 Thermal property

The results, which are shown as Table 3, describe each thermal property that was measured. Measuring of both thermal resistance of clothing and the ability of a fabric to transport the water vapor emitted from the body are important factors in assessing the thermal comfort [11]. Therefore, it is shown the results of important factors below with figure.

Table 3 Thermal physical property of each sample

Sample	*IW(P)*	*IW(C1)*	*IW(C2)*	*IW(C3)*	*IW(C4)*
Thermal Resistance [%]	24.7	29.3	39.7	34.9	34.7
Thermal Conductivity [W/(m.°C)]	0.0591	0.0631	0.0580	0.0604	0.0616
Q-max [W/m^2]	0.0586	0.0502	0.0510	0.0504	0.0482
Air Resistance [kPa.S/m]	0.146	0.824	0.322	0.552	0.756
Water Vapor Resistance [m^2.Pa/W]	3.58	5.01	4.59	4.00	4.29

Table 4 Result of variance analysis

Multiple Comparison (Tukey)			Result				
			(P)	**(C1)**	**(C2)**	**(C3)**	**(C4)**
P Values	**Thermal Resistance**	**(P)**	-	*	**	**	**
		(C1)	0.01	-	**	**	**
		(C2)	0.00	0.00	-	**	**
		(C3)	0.00	0.00	0.01	-	
		(C4)	0.00	0.00	0.01	1.00	-
	Thermal Conductivity	**(P)**	-	**			*
		(C1)	0.00	-	**	*	
		(C2)	0.55	0.00	-	*	**
		(C3)	0.43	0.01	0.03	-	
		(C4)	0.03	0.28	0.00	0.54	-
	Thermal Conductance	**(P)**	-	**	**	**	**
		(C1)	0.00	-			
		(C2)	0.00	0.22	-		
		(C3)	0.00	0.99	0.44	-	
		(C4)	0.00	0.99	0.38	1.00	-

* 5% significant ** 1% significant

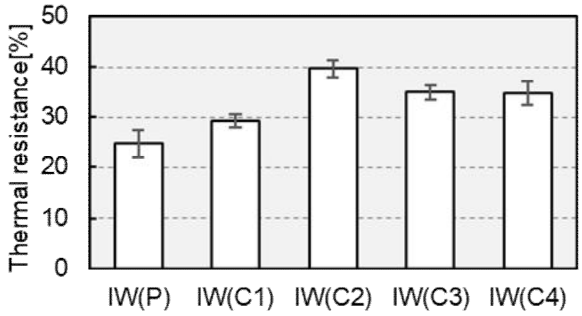

Figure 13 Thermal resistance

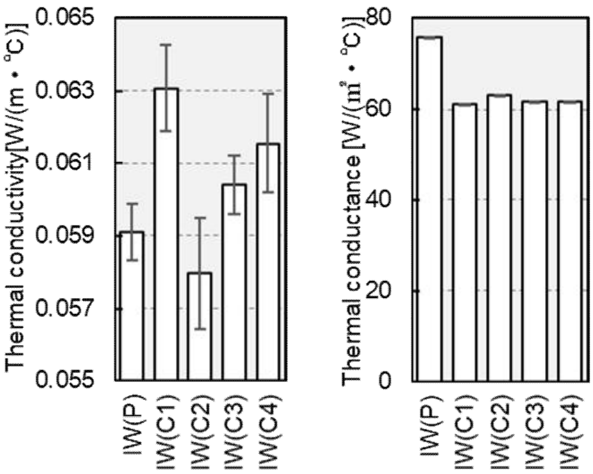

Figure 14 Thermal conductivity / conductance

Heat transfer

It can be recognized the heat transfer features of these samples from Figure 13, what IW(C)'s thermal resistance is significantly higher than IW(P), and each cotton samples have significant different except between IW(C3) and IW(C4). It means that Changing material/fineness, and also Applying fulling relate to thermal resistance. And also, we can say that the result should relates to Total volume of pore space from Table 1 and Figure 13. If a fabric contains much air which is related to thermal conductivity, thermal resistance should be higher under the condition without air flow.

Regarding thermal conductivity, we calculated thermal conductance with removing thickness factor. As you can see in Figure 14 (right), IW(P)'s thermal conductance is significantly higher than IW(C), and each IW(C) samples do not have significant different. On the other hand, as you can see in Figure 14 (left), each cotton sample has different tendency about thermal conductivity. From these results, it can be the thickness factor has the most influence on thermal conductivity.

Water vapor resistance

It is possible to see the result that have different values of Water Vapor Resistance between IW(P) and IW(C). IW(P)'s is lower than IW(C)'s. The reason of the result relates to sample's material; Polyester material feature is a low water content, on the other hand, cotton material has high water absorption. That is why, it is difficult for water to through the cotton fabric.

In addition, in the case of comparing between each IW(C) samples, it is found that the resulting values are larger in the order of IW(C1) > IW(C2) > IW(C4) > IW(C3); it could be guessed that it means the result relates to Cotton Mixing Ration and Density. Although there is a difference between each sample as described above, each sample has excellent in Water Vapor Permeability because it means high Water Vapor Permeability when the value is between 0.0 and 6.0 [14]. That is why these IW samples are suitable for based fabric for TIW in terms of Water Vapor Permeability.

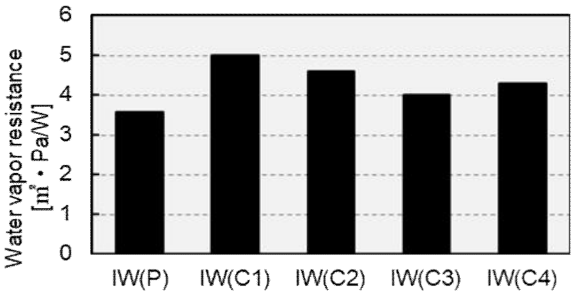

Figure 15 Water vapor resistance

4.3 Summary of the results

About Tensile property

The fabric IW(C) are easier to stretch to the circumference direction that is related to hoop tension which effects to a clothing shape stability, it might make a decreasing clothing stability has related to hoop tension. Furthermore, the fabric IW(P) is easier to stretch to the height direction that is related to mobility which effects to a clothing comfort. Therefore, exchanging the knitted direction should be a good way for applying TIW because the hoop tension and the comfort is going to be increased.

In addition, set RT 57% is a target value for a general tricot knitted, so that it is not enough RT for IW(C) from the result. It is necessary to design TIW again with considering their PU mixing ration.

About Thermal property

1. Compare IW(P) and IW(C)

Thermal properties which are Heat transfer and Water vapor permeability were changed by changing material. IW(C)'s Thermal conductivity is lower than IW(P), while Thermal resistance is higher. IW(C)'s Water vapor resistance is higher than IW(P); however, we could know that both material fabrics have an excellent Water vapor permeability from the reference.

2. Compare each IW(C)

Changing material/fineness, and also Applying fulling relate to thermal resistance. And also, the result should relate to Total volume of pore space. If a fabric contains much air which is related to thermal conductivity, thermal resistance should be higher under the condition without air flow.

Regarding thermal conductivity, most results of comparison between IW(C)'s are significantly different; however, their value of thermal conductance is almost same result. From the result, thickness factor should be the most influence factor on thermal conductivity.

The thickness that is changed by fulling and fineness is most related to heat transfer. In the case of thickness is large, thermal resistance is lower, and then thermal conductivity is higher.

5 CONCLUSION

In this paper we proposed a Compression IW (Inner Wear), the base fabric of TIW (Training Inner Wear) which promotes the exercise effect during walking to improve comfort while maintaining the function. The tensile property and thermal property are measured to confirm physical properties of samples that is changed Material / Fineness / Density / PU mixing ratio to achieve our purpose. From measurement results, we could figure out some positive points, and some negative points as I describe in this paper. Therefore, IW(C) will be re-proposed, and then we will measure the physical properties and to carry out a sensory test to evaluate the objective comfort as next step.

6 REFERENCES

1. Ministry of Health, Labour and Welfare: Health and Nutrition Survey, 2011
2. Ministry of Health, Labour and Welfare: Health and Nutrition Survey, 2014
3. Ministry of Health, Labour and Welfare: Health Japan 21, 2013
4. Kondo Y.: Design and evaluation of TIW to aim improving the amount of energy consumption during walking, Shinshu University, unpublished
5. Kimura K.: Considering pattern of taping and performance requirements for improvement of exercise effect, Shinshu University, unpublished
6. Nakazawa T., Ito M., Yamamoto T., et al.: Psychological effect of Compression garment for sports, Housei University, 2012, pp. 29-34
7. Aoki H., et al.: Joint torque calculation of compression sports spats using anisotropic hyperelastic model, Procedia Engineering 147, 2016, pp. 257-262, doi: 10.1016/j.proeng.2016.06.274
8. Harada T., Toda, K.: Textile materials and comfort, Journal of Textile Consumer Science Association 25(12), 1984, pp. 615-621
9. Ho C.P., Fan J., Newton E., et. al.: Improving thermal comfort in apparel. Improving Comfort in Clothing, Sawson: Woodhead Publishing, 2011, doi: 10.1533/9780857090645.2.165
10. JIS L 1907: Method for testing water absorption of textile products, 2010
11. Greenwood K., Rees W.H., Lord J.: Problems of protection and comfort in modern apparel fabrics, Papers of the Diamond Jubilee Conference of the Textile Institute Manchester, 1970, pp. 197-218
12. Shioda H.: Dumpness and clothing climate·thermal physiology of underwear, Journal of the Japan Research Association for Textile End-Uses 42(5), 2001, pp. 317-321
13. Nannichi T.: Method of determining clothing clearance, Journal of Textile Machinery Society 30(4), 1977, pp. 175-183
14. Glombikova V., Komarkova P.: Study on the impact of dye-sublimation printing on the effectiveness of underwear, Tekstilec 57(2), 2014, pp. 133-138, doi: 10.14502/Tekstilec2014.57.133-138

PREPARATION OF ANTIMICROBIAL NANOADDITIVES AND THEIR CONCENTRATES BASED ON NANO $CaCO_3$, NANO TiO_2 AND NANO ZnO FOR THEIR APPLICATION IN POLYPROPYLENE FIBRES, POLYPROPYLENE AND POLYETHYLENE FOILS

Jozef Šesták[1], Katarína Ščasníková[1], Andrej Dubec[2], Štefan Krivoš[3] and Peter Michlík[3]

[1]VÚTCH-CHEMITEX, spol. s r.o., Rybníky 954, 011 68 Žilina, Slovak Republic,
[2]Faculty of Industrial Technologies in Púchov, Alexander Dubček University of Trenčín I. Krasku 491/30, 020 01 Púchov, Slovak Republic,
[3]Research Institute for Man-Made Fibres a.s., Štúrova 2, 059 21 Svit, Slovak Republic
jozef.sestak@vutch.sk, dubec@fptuni.sk, krivos@vuchv.sk, michlik@vuchv.sk

Abstract: *The paper presents results of the research aimed at development of antibacterial (AMB) nanoadditives prepared by alternative methods using different types of nanocarriers. Results obtained by classical method of preparation-compounding of a carrier and a nanoaditive containing Ag ions, and by so-called progressive method using nanosols incorporating Ag, prepared by sol-gel technology, are compared. The prepared AMB nanoadditives were incorporated in two PP and PE polymer masterbatches with the aim to prepare solid AMB nanodispersions for additivation of PP fibres and PP, PE cast foils. Results from evaluation of antimicrobial efficiency of the AMB nanoadditives, applied on PP fibres and foils, against Escherichia coli CCM, performed according to the methods specified in AATCC 100: 2015 and ASTM E 2149, are reported. Application possibilities of the modified PP fibres and foils are outlined in the conclusion.*

Keywords: *antibacterial nanoadditive, nano$CaCO_3$, nanoTiO_2 and nanoZnO carrier, antibacterial efficiency, antimicrobial nanoadditive, PP masterbatch, color, processing and antimicrobial properties.*

1 INTRODUCTION

Nanoparticles based on silver, copper, titanium or zinc are very interesting for commercial application aimed at achievement of antibacterial activity on fibrous and textile materials. Particular attention is paid to TiO_2 and ZnO carriers with a view to their unique optical, electrical and chemical properties, as well as silver-doped nanoparticles, prepared by sol-gel method [1]. Following methods are used advantageously to analyse nanoparticles trapped / fixed on the carrier surface: scanning electron microscopy (SEM), energy-dispersive X-ray spectroscopy (EDX) or UV-Vis reflectance. Antibacterial, microstructural and fluorescent properties of silver (Ag) – doped TiO_2 nanoparticles were studied to investigate influence of silver on improvement of antibacterial properties of TiO_2. Antibacterial activity of pure TiO_2 and Ag-TiO_2 against gram-negative bacteria *E. coli* and *Pseudomonas aeruginosa* and gram-positive bacteria *Bacillus subtilis* and *S. aureus* was studied by diffusion method in agar medium. It was found that doping with silver increases antibacterial activity of TiO_2. Microstructures of these nanoparticles were studied by transmission electron microscopy (TEM) and atomic force microscopy (AFM) [2].

Attention is paid also to imparting antibacterial properties to polypropylene nonwovens, nonwovens made of cotton/PET blends and cotton woven fabrics, finished by padding – drying - curing as well as by electronic sputtering process. In the first place, surface modification of cotton/PET nonwovens and polypropylene fabrics was made to impart hydrophobic properties using RF plasma system and acrylic acid as monomer. After that silver-doped TiO_2 nanoparticles were prepared by sol-gel technology and processes of chemical reduction using titanium isopropoxide and silver nitrate as precursor. The nanoparticles were applied on the textile samples by padding – drying - curing and by electronic sputtering process. Antibacterial activity of the textile samples against bacteria *E. coli* and *S. aureus* was determined qualitatively and quantitavely according to the AATCC Method 147 and AATCC Method 100. Microstructural characteristics and surface morphology of the textile samples were studied by SEM-EDX and FTIR-ATR. The achieved results confirm, that silver-doped TiO_2 nanoparticles, synthetized by chemical reduction process, imparted good and permanent antibacterial activity to polypropylene nonwovens and to fabrics made of cotton/PET blend as well as to woven cotton fabrics [3].

The other publications present general overview of preparation of functional sols by doping functional materials in sol matrix and methods for modification of textile substrate by sol-gel technology. Combination of chemical and physical modification offers an unlimited potential for development and application of hybrid sol coatings, which can be used to develop functional and smart fabrics.

Structures of organofunctional trialkoxysilane sol-gel precursors are presented and compared with other organic-inorganic silicon-based hybrid materials. Functional properties, e.g. hydrophobicity and oleophobicity, flame-resistancy, antimicrobial properties, electric conductivity and antistatic properties are described in relation to chemical structure of the organic part of the precursor, mechanism and principle of activity of the coating and its washing resistance. Silver nanoparticles were synthetized by sol-gel technology, in the presence of CH_3COONa and hydrazine as reducing agent in water at room temperature. Structure and size of the prepared particles was characterized by SEM method and spectroscopically [4-6].

Functional modifications of chemical fibres imparting protective, hygienic and comfort properties to the fabrics are essential in the textile industry. The functional modifications include mainly permanent antimicrobial (AMB) modification of the fibres [7-10].

Nowadays the market offers AMB additives with average size of the particles in microscopic range (d50 = 2-4 µm) or polymer dispersions of these additives. Application of a nanoadditive as a carrier of an active component with significantly higher specific area than current microadditives is presumed to result in more uniform scattering of the antimicrobial active component on the surface of an inorganic carrier. Besides, antimicrobial efficiency at lower concentrations as compared to microadditives will be achieved.

2 EXPERIMENTAL

2.1 Materials and methods

Philosophy of our research, focusing on preparation of the AMB nanoadditive, is based on two options: so-called classical method and progressive one. The classical method consists of physico-mechanical compounding by means of a separate chemical reaction of the prepared Ag^+ ions in dispersion solution and subsequent doping a nanocarrier surface. This method corresponds to a certain extent with knowledge about methods, currently used in the world, with subsequent preparation of concentrates in powder form and their application to the polymeric systems. The progressive method assumes separate preparation of a silver-containing antimicrobial nanosol using specific procedures. Subsequent process involves compounding of the AMB nanosol with nanocarrier in a solution, under specified conditions, from which powdered nanoadditive suitable for preparation of solid AMB nanodispersion in polymeric matrix is prepared. Another option is application of sol-gel method using selected polysiloxane types in objectified ratio and subsequent incorporation of $AgNO_3$ into the nanosol solution. The prepared solution is then compounded with the powdered nano$CaCO_3$, nanoTiO_2 and nanoZnO nanocarrier. The above-mentioned methods to prepare the AMB nanoadditive (application of sol-gel method, compounding the nanosol with a nanocarrier, preparation of powdered nanoadditive from a solution) has not been described anywhere yet, what points to high topicality of the proposed research solution.

Three types of commercially available nanocarriers, used in the experiments, were as follows:

a) C type: nano$CaCO_3$ content - 98 wt.% $CaCO_3$, particle size 30-70 nm, specific surface 120 $m^2.g^{-1}$,
b) T type: nanoTiO_2 content - 88-92 wt.% TiO_2, particle size 10-12 nm, specific surface 100 $m^2.g^{-1}$,
c) Z type: nanoZnO content – 99.8 wt.% ZnO, particle size 10-30 nm, specific surface 80-100 $m^2.g^{-1}$.

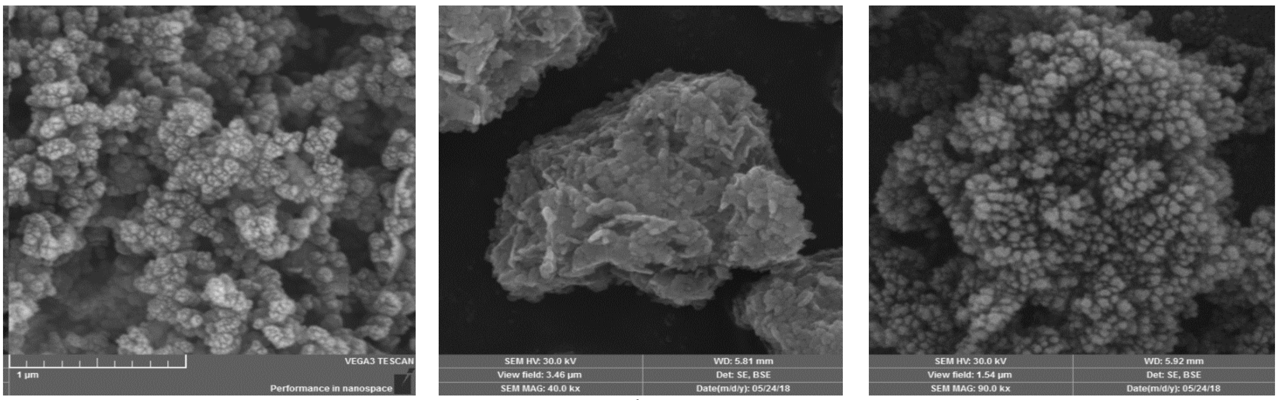

a b c

Figure 1 SEM images of nanocarrier surfaces (a) nano$CaCO_3$, (b) nanoTiO_2 and (c) nanoZnO

The samples were designated according to method used for preparation of the AMB nanoadditive as follows:

a) **KM** - *classical method:*

Preparation of a nanoadditive is based on physico-chemical compounding of the active agent ($AgNO_3$) with selected nanocarrier type: nano$CaCO_3$ or nanoZnO. In the course of compounding, while cold, doping of nanocarrier surface by Ag^+ ions, released in the process of dissociation in the presence of reducing agent (chlorid natrium), takes place (samples designated KM/C and KM/Z, Tables 1-3).

b) **PM** - *progressive methods:*

PM/A - preparation of a nanoadditive by this method is based on physico-chemical compounding of the active agent (antimicrobial nanosol) with selected nanocarrier type: nanoTiO_2 or nano$CaCO_3$. In the course of compounding, while cold, doping of nanocarrier surface by Ag^+ ions, released in the process of dissociation in the presence of reducing agent (citrid acid), takes place (samples designated PM/A/C, PM/A/T, Tables 1-3),

PM/B - development of a nanoadditive by this method is based on preparation of nanosol by hydrolysis of a mixture of selected siloxane precursors (triethoxysilane + vinyltriethoxysilane), subsequent incorporation of an active agent ($AgNO_3$) and compounding with selected nanocarrier type: nanoTiO_2 or nanoZnO. In the course of compounding, while cold, doping of nanocarrier surface by Ag^+ ions (samples designated PM/B/T, PM/B/Z, Tables 1-3).

Selected samples of the prepared AMB nanoadditives and basic data on Ag-content and antimicrobial activity are given in the Table 1.

2.2 Preparation and evaluation of functional properties of PP and PE solid dispersions

Following materials were used to prepare samples of PP and PE masterbatches containing nanoadditives (Table 2):

Isotactic powdered PP (Lyondell Basell Company) with flow index (MFI) 10.2 g/10 min.

PE homopolymer, foil type, with melting flow index 19.6 g/10 min

1) Inorganic AMB nanoadditives:

- **KM/C, PM/A/C** ultrafine calcium carbonate with particle mean diameter 45 nm and surface area 120 $m^2.g^{-1}$ modified by an antimicrobial active component (VÚTCH-CHEMITEX, spol. s r. o).
- **PM/A/T, PM/B/T** nano TiO_2 rutile type with inorganic surface finish with rutile content 88÷92% TiO_2; specific surface 100 m^2/g; inorganic surface finish 8÷11% Al_2O_3 with primary particle size 10÷12 nm modified by an antimicrobial active component (VÚTCH-CHEMITEX, spol. s r.o).
- **KM/Z, PM/B/Z** nano ZnO containing 99.8% ZnO; particle size 10÷30 nm with specific surface 80÷100 m^2/g modified by an antimicrobial active component (VÚTCH-CHEMITEX, spol. s r.o.).

2) Dispersants:

- D1 - PE wax with flow index 520 g/10 min (Clariant Corp.)
- D2 - copolymer of ethylene and acrylic acid with adjusted acid value by zinc salt (Honeywell Corp.)
- D3 - mixture of glycols and aliphatic amines (Clariant Corp.)
- D4 - condensing product of stearic acid and polyethylene glycol (Clariant Corp.)
- D5 - amidated PP wax (Clariant Corp.) with flow index 230 g/10 min (Clariant Corp.)

2.3 Evaluation methods

Functional properties of PP masterbatch

MFI of the masterbatches was evaluated using Dynisco Kayness capillary rheo-viscometer according to the STN EN ISO 1133 standard. The filterability index was evaluated using a filtration single-screw extruder with screw diameter of 25 mm and pore density of the filtration sieve of 16000 pores per cm^2.

Coloristic characteristics of PP fibres

Coloristic characteristics of the drawn PP fibres of 3.0 dtex with concentration of nanoadditives 0.75 wt.% were measured using Hunterlab UltraScan XE under conditions as follows: illumination D65 - daylight with temperature 6500 K, observer 10°, CIELAB color space. The evaluated chromatic characteristics included: L* (CIELAB) D65 10° color gradient light to dark, a* (CIELAB) D65 10° - color gradient red to green, b* (CIELAB) D65 10° - color gradient yellow to blue, WICIE - whiteness index, YIE-313/96 - yellowness index.

Antimicrobial activity

Antimicrobial activity of the PP fibres with concentration of AMB nanoadditives 0.75% and PP and PE foils incorporating 2.25% additives was measured as well.

POY discontinuous technological process and TS-32 equipment was used to prepare 3 dtex PP fibres. Technological conditions of preparation:

PP homopolymer	Flow index 25.4 g/10 min
Melt temperature	220°C
Additivation level	0.75% of the AMB nanoadditive in the fibre
Melt dosage	20 g/min
Spinning nozzle	25×0.3/1.2
Winding speed	1500 m/min

Drawing process:

Temperature of the heater	108°C
Draw ratio	2.0
Winding speed	80 m/min

Influence of the Filterindex parameter (unquantifiable value) became evident during preparation of the fibres, containing PM/A/T and PM/B/T additives, by increase of operating pressure in the die block, what influenced negatively its lifetime.

3 RESULTS AND DISCUSSION

3.1 Results from preparation of the AMB nanoadditives using nanocarriers based on nanoCaCO$_3$, nanoTiO$_2$ and nanoZnO

Table 1 Results of silver content and antimicrobial activity determined on powdered AMB nanoadditives prepared using nanocarriers

Sample	Nanocarrier type	Ag content [wt.%] determined by AAS	Antimicrobial activity (AMA) - determined bacterial reduction R [%]
KM/C	C	0.29-0.59	60-97.1
PM/A/C	C	0.010	88.6
PM/A/T	T	0.06	38.0
PM/B/T	T	0.05	35.6
KM/Z	Z	0.61	98.3
PM/B/Z	Z	0.14	77.4

Notice: 1/ R - mean value of bacterial reduction, AAS - atomic absorption spectroscopy , AMA - antimicrobial efficiency of the nanoadditive against *Escherichia coli CCM 3954* determined according to the ASTM E 2149-13a method.
2/ It was not possible to use the PM/B type technology on application of nanoCaCO$_3$ due to oxidation processes taking place after addition of a mixture of the siloxanes and the additive.

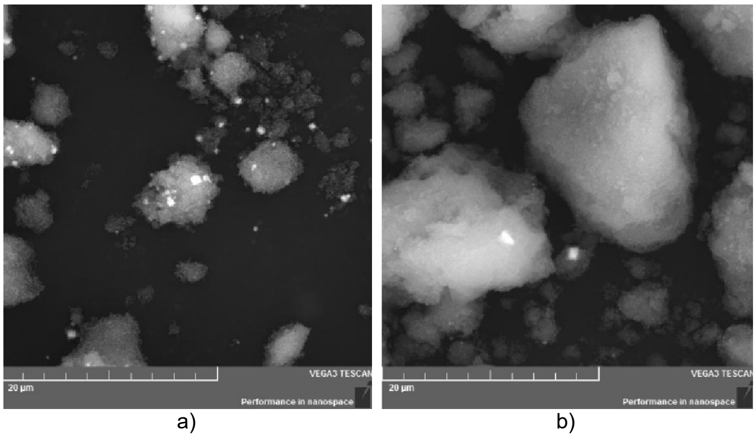

Figure 2 SEM images of surface morphology with 4000x magnification: (a) AMB PM/A/T nanoadditive (nanoTiO$_2$ carrier) and (b) of PM/B/T nanoadditive (nanoTiO$_2$ carrier)

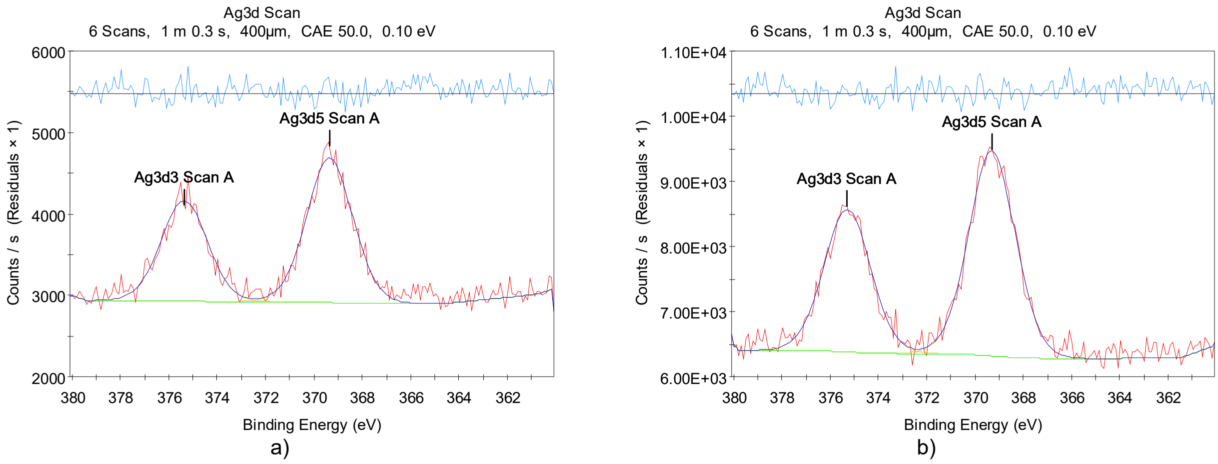

Figure 3 Diagram of XPS analysis of PM/A/T with identified form of Ag at wavenumber of 369.3 eV (a), Diagram of XPS analysis of PM/B/T nanoadditive with confirmation of content of 0.3 % mol. Ag$^+$ ions at wavenumber of 369.3 eV (b)

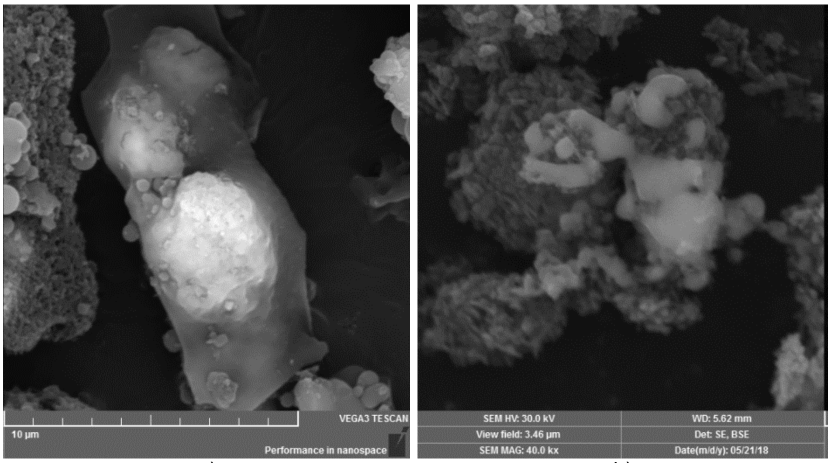

a) b)

Figure 4 SEM image of AMB KM/Z nanoadditive surface with nanoZnO carrier (25 000x magnification) (a), SEM image of AMB PM/B/Z nanoadditive surface with nanoZnO carrier (25 000x magnification) (b)

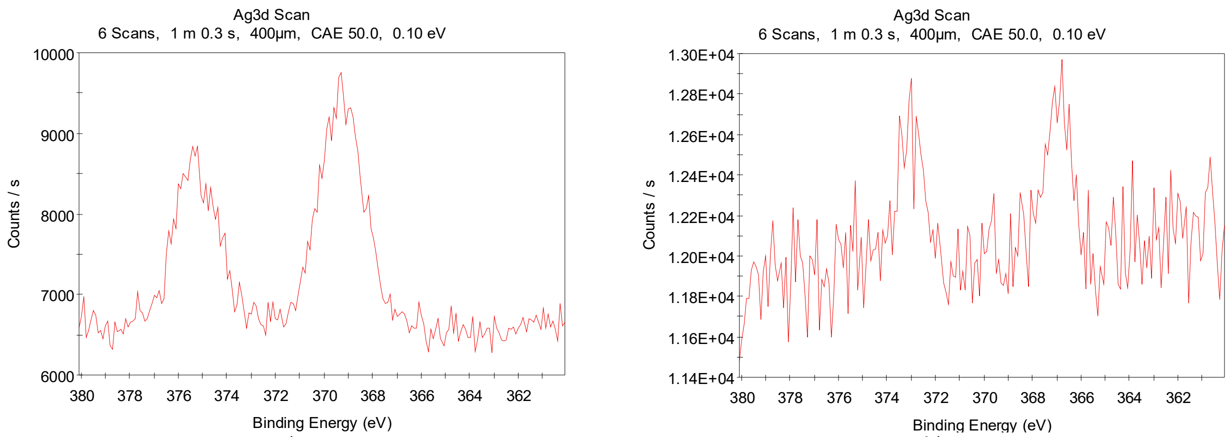

a) b)

Figure 5 Diagram of XPS analysis of KM/Z nanoadditive (nanoZnO carrier) with determined atomic percentage of Ag+ ions 0.1% (a), Diagram of XPS analysis of PM/B/Zn nanoadditive (nanoZnO carrier) with determined atomic percentage of Ag+ ions 0.3-0.4% (b)

3.2 Results from preparation of polymer dispersions containing AMB nanoadditives and their application in PP fibers and PP, PE foils

Composition of PP and PE solid dispersions of AMB nanoadditives is given in the Table 2.

PP masterbatches were prepared from premix o powdery PP, nanoadditive and dispersing system using Werner-Pfeiderer ZDSK 28 twin screw extruder with 28 mm screw diameter. Preparation was performed at constant screw rotating speed 250 min^{-1} and constant extrusion temperature 220°C.

Functional properties of the prepared solid dispersions, describing suitability for their application in fibres and foils, were measured in the laboratory conditions.

Determined functional properties of PP and PE solid dispersions are given in the Table 3.

Preparation of the solid dispersions was trouble free. Functional properties, flow index and melt viscosity are on a level suitable for additivation of PP and PE matter to be used for manufacture of PP and PE foils and PP fibres. The parameter filterindex is non-significant in the case of additivation of PP and PE foils. However, the value of filterindex is important in the case of additivation of PP fibres, because it determines time of functional use of the die block. Unquantifiable filterindex values of PP solid dispersions of AMB nanoadditives with TiO_2 nanocarrier of the antimicrobial component determine very short durability life of the die block.

Table 2 Composition of PP and PE solid dispersions of AMB nanoadditives

Composition of PP solid dispersions of AMB nanoadditives				
nanoadditive	Concentration [%]	Dispersant [%]		Concentration of PP [%]
KM/C	15.0	D3+D4	3+2	80.0
PM/A/C	15.0	D5+D4	3+2	80.0
PM/A/T	15.0	D5+D4	3+2	80.0
PM/B/T	15.0	D5+D4	3+2	80.0
KM/Z	15.0	D2	10	75.0
PM/B/Z	15.0	D2	10	75.0
Composition of PE solid dispersions of AMB nanoadditives				
nanoadditive	**Concentration [%]**	**Dispersant**		**Concentration of PE [%]**
KM/C	15.0	D1	1.5	83.5
PM/A/C	15.0	D1	2.5	82.5
PM/A/T	15.0	D1	1.5	83.5
PM/B/T	15.0	D1	1.5	83.5
KM/Z	15.0	D2	10	75.0
PM/B/Z	15.0	D2	9.4	75.6

Table 3 Functional properties of PP and PE solid dispersions of AMB nanoadditives

Functional properties of PP solid dispersions with concentration of AMB nanoadditive 15 wt.%					
Designation	Flow index [g/10 min]	Cv [%]	Viscosity [Pa.s]	Cv [%]	Filterindex [MPa/kg]
KM/C	15.40	2.74	557.00	2.70	157
PM/A/C	14.72	1.61	582.60	1.60	191
PM/A/T	11.94	2.20	734.50	2.20	Unquantifiable
PM/B/T	12.58	5.05	667.10	5.10	Unquantifiable
KM/Z	12.97	1.87	694.50	2.00	88
PM/B/Z	12.24	2.84	695.00	2.60	2724
Functional properties of PE solid dispersions with concentration of AMB nanoadditive 15 wt.%					
Designation	**Flow index [g/10 min]**	**Cv [%]**	**Viscosity [Pa.s]**	**Cv [%]**	**Filterindex [MPa/kg]**
KM/C	13.50	2.08	666.20	2.10	165
PM/A/C	18.69	1.55	483.10	1.50	689
PM/A/T	13.03	2.42	683.10	2.40	Unquantifiable
PM/B/T	13.64	1.86	614.80	1.90	Unquantifiable
KM/Z	23.19	1.33	398.60	1.30	358
PM/B/Z	15.08	1.03	579.70	1.05	Unquantifiable

Preparation and evaluation of coloristic characteristics of the smooth 3dtex PP fibre

The measured coloristic characteristics of the prepared fibres were compared with those of a standard non-additivated PP fibre. Coloristic properties are given in the Table 4. Very good coloristic characteristics were achieved by additivation of PP fibres with AMB nanoadditives KM/C; KM/Z; PM/A/C and PM/A/T. The fibres show low yellowness (yellowing degree 4÷2) and whiteness nearly on a level of a non-additivated standard (WICIE 66.61÷74.78). Delustring effect represented by RFS parameter is remarkable for AMB nanoadditives KM/Z (998.5) and PM/A/T (594.06) Fibres containing AMB nanoadditives PM/B/T; PM/B/Z achieve coloristic parameters proper to yellow color shades with significant delustring effect.

Preparation of PP and PE cast foils

PP and PE cast foils with thickness 40 μm and 2.25% level of additivation of active substance were prepared on the Plasticizer equipment with screw diameter of 25 mm and temperature regime of 250°C. No negative phenomenons were observed during the preparation.

Table 4 Coloristic of smooth 3 dtex PP fibres with 0.75% concentration of the AMB nanoadditive

AMB nanoadditive	L*	a*	b*	GS	RFS	WICIE	Yellowing degree	YIE313/10
Standard (PP)	**94.23**	**-0.17**	**1.33**	**5.00**	**100.00**	**79.73**	**4.00**	**2.44**
KM/C	92.00	-0.27	1.27	3.00	189.00	**74.78**	4.00	2.29
PM/A/C	95.16	-0.74	4.71	2.50	95.93	**66.61**	2.00	8.31
PM/A/T	**94.22**	-0.15	3.10	3.00	594.06	**71.62**	3.00	5.82
PM/B/T	**87.9**	0.42	12.73	1.00	707.12	**10.27**	1.00	24.83
KM/Z	92.69	0.00	1.93	4.00	998.50	**73.32**	4.00	3.77
PM/B/Z	85.16	-0.10	16.36	1,00	999.99	**-15.04**	1.00	31.49

3.3 Results from application of the prepared AMB nanoadditives using polymeric dispersions of their concentrates in PP fibres, PP and PE foils

Samples of modified PP fibres (smooth fibres, 3 dtex) were prepared with 15 wt.% of the nanoadditive in the concentrate. Content of the AMB nanoadditive in the fibre was 0.75 wt.%. Results of the evaluation are shown in the Table 5.

Different results of antimicrobial activity on the surface of PP fibre have been achieved after addition of the prepared samples of AMB nanoadditives into fibre-forming PP polymer in a form of solid polymeric dispersion (concentrate). The highest efficiency was achieved after application of nanoadditives prepared by the classical method (KM), the lowest efficiency showed additives prepared by the PM/A method. Very good results of antimicrobial efficiency were established on the fibres, where additives prepared by PM/B sol-gel method were applied. When comparing the nanocarriers, the highest antimicrobial efficiency was found with the additive containing nanoZnO (KM/Z and PM/B/Z nanoadditives).

Experimental research in the field of application of the AMB nanoadditives and solid dispersions, made from them, used in polymeric systems designed for preparation of extruded foils, allowed to achieve also sufficient level of AMA in selected types of PP and PE foils.

The experiments have confirmed necessity to increase content of dispersion of the concentrate in the mass up to min. 15 wt.% and to ensure this way at least 2 wt.% content of the nanoadditive in the mass, so that AMA on PP foils close to 50% bacterial reduction could be achieved. In this case PM/A method as well as PM/B alternative have proved the most appropriate for preparation of suitable types of the AMB nanoadditives. Results of AMA evaluation on the samples of PP and PE foils are shown in the Tables 6 and 7.

Antimicrobial efficiency against *E. coli CCM 3954* was evaluated on the modified PP and PE foils according to the ASTM E 2149-13a method. As for AMA evaluation, the highest efficiency with the both types of foils became evident after application of AMB nanoadditives prepared by the classical method (KM/C type), where even bactericidal effect was achieved. Nanoadditives with nanoTiO_2 carrier approved one selves on sufficient bacteriostatic level, the lowest level of antimicrobial efficiency was achieved with the nanoZnO carrier.

Table 5 Results from the analysis of antimicrobial activity (AMA) on selected types of modified **PP fibres** containing 15 wt.% of the nanoadditive in the concentrate

Bacterium	***E. coli CCM 3954,* CFU/sample**					
Sample of PP fibre (containing 15 wt.% of the additive in the concentrate), additive concentration in the fibre 0.75 wt.%	KM/C (C carrier)	PM/A/C (C carrier)	PM/A/T (T carrier)	PM/B/T (T carrier)	KM/Z (Z carrier)	PM/B/Z (Z carrier)
Bacterial reduction [%]	99.9	0.0	0.0	36.0	99.5	84.8

Notice: antimicrobial efficiency against *E. coli CCM 3954* determined according to the AATCC 100: 2015 method; CFU - colony forming unit (number of bacterial colonies in the volume of the inoculum)

Table 6 Results of AMA analysis on selected types of modified **PP foils** containing 15 wt.% of the additive in the concentrate

Bacterium	***E. coli CCM 3954*, CFU/sample**					
Sample of PP foil (15% content of the concentrate), 2.25 wt.% additive content	KM/C (C carrier)	PM/A/C (C carrier)	PM/A/T (T carrier)	PM/B/T (T carrier)	KM/Z (Z carrier)	PM/B/Z (Z carrier)
Bacterial reduction [%]	61.1	9.8	10.1	23.9	9.1	7.3

Table 7 Results of AMA analysis on selected types of modified **PE foils** containing 15 wt.% of the additive in the concentrate

Bacterium	***E. coli CCM 3954,* CFU/sample**					
Sample of PE foil (15% content of the concentrate), 2.25 wt.% additive content	KM/C (C carrier)	PM/A/C (C carrier)	PM/A/T (T carrier)	PM/B/T (T carrier)	KM/Z (Z carrier)	PM/B/Z (Z carrier)
Bacterial reduction [%]	77.0	19.4	18.2	13,4	6.2	9.4

4 CONCLUSION

The achieved level of antimicrobial efficiency in PP fibres exceeds significantly practical requirements related to application of PP fibres in the textiles (sufficient bacteriostatic level) and at the same time it is satisfactory for application in PP foils designed for food packing (bacteriostatic level). It is possible to expect also significant economical benefits whilst maintaining high antimicrobial efficiency in the final products - fibres and foils - regarding comparatively low Ag content in the polymeric mass of PP fibre and PP foil after application of the AMB nanoadditive, prepared using the progressive methods (0.01-0.14 wt.%).

Permanent AMB modification of PP fibres and PP and PE foils is achieved especially by addition of the main AMB additive into the basic polymer during spinning and foil forming. The masterbatch must have at the same time all functional, processing and coloristic characteristics together with the antimicrobial activity. Results presented in this document showed that all above-mentioned preconditions have been fulfilled with PP nanoadditived masterbatches with concentration 15 wt.%, in particular samples of the type: KM/C; KM/Z and PM/A/C with correctly selected dispersing system (D3 - mixture of glycols and aliphatic amines; D2 - copolymer of ethylene and acrylic acid with acid value adjusted by zinc salt; D4 - condensation product of stearic acid and polyethylene glycol) and their mutual combinations. It is possible to state on the base of these observations that the PP nanoadditived masterbatch with concentration 15 wt.%, KM/C; KM/Z and PM/A/C type are suitable for preparation of antimicrobial nanocomposite PP fibres. Bacteriostatic efficiency is sufficient for preparation of antimicrobial PP and PE packing foils. Positive effect of the dispersant D2 - ethylene copolymer and acrylic acid with acid value adjusted by zinc salt was observed for PE solid dispersions. The dispersant D1 - PE wax has limited application in higher concentrations over 2.5%.

ACKNOWLEDGEMENT: *Results presented in the paper were achieved in the frame of elaboration of the research project APVV-15-0016 „Research on antimicrobial nanoadditive for fibres and foils“ supported from financial means of The Slovak Research and Development Agency with the seat in Bratislava, Slovak Republic*

5 REFERENCES

1. Nigussie G., Tesfamariam G., Mekele B., Weldemichel Y., Gebreab T., Gebrehiwot D., Gebremiche G.: Antibacterial activity of Ag-doped TiO_2 and Ag-doped Zn0 nanoparticles, International Journal of Photoenergy, Vol. 2018, Article ID 5927485, 7 pages, https://doi.org/10.1155/2018/5927485
2. Bahadur J., Agrawal S., Panwar V., Parveen A.: Antibacterial properties of silver doped TiO_2 nanoparticles synthetized via sol-gel technique, Macromolecular Research 24(6), 2016, pp. 488-493, https://doi.org/10.1007/s13233-016-4066-9
3. Aksit A., Camlibel N. O., Zeren E. T., Kutlu B.: Development of antibacterial fabrics treatment with Ag-doped TiO_2 nanoparticles, The Journal of the Textile Institute 108(12), 2017, pp. 2046-2056, https://doi.org/10.1080/00405000.2017.1311766
4. Wang C., Yin Y.: Functional modification of fiber surface via sol-gel technology, Active Coatings for Smart Textiles, Woodhead Publishing Series in Textiles, 2016, p.301-328, https://doi.org/10.1016/B978-0-08-100263-6.00013-7
5. Vasiljevič J., Tomšič B., Jerman I., Simončič B.: Organofunctional trialkoxysilane sol-gel presursors for chemical modification of textile fibres, Tekstilec 60(3), 2017, pp. 198-213, DOI: 10.14502/Tekstilec2017.60.198-213
6. Shahjahan M., Rahman H., Hossain M., Khatun M.A., Aminul Islam A., Begum M.H.: Synthesis and characterization of silver nanoparticles by sol-gel technique, Nanoscience and Nanotechnology 3(1), 2017, pp. 34-39, doi: 10.11648/j.nsnm.20170301.16
7. Hongbin L., Dan S., Wang Y., Feng Ch.: Preparation and properties of silver-load chitosan-based antibacterial yarn, Chemical Fibers International 66(2), 2016, pp. 84-85
8. Cox R., Mukherjee A.: Antimicrobial fibers - Technical design and performance challenges, International Fiber Journal 30(5), 2016, pp. 29-31
9. Gerhardt A.: Antimicrobial textiles – Optimizing for performance, safety and efficacy, International Fiber Journal 30(5), 2016, pp. 14-19
10. Espana M.: New functional additive, Man-Made Fiber Year Book 65, 2015, pp. 73-75

CARBON NANOTUBES AS FILLER FOR ELECTROMAGNETIC INTERFERENCE APPLICATIONS

Jan Vácha

Technical University of Liberec, Studentská 2, 461 17 Liberec 1, Czech Republic
jan.vacha@tul.cz

Abstract: *This work examines the electrical properties of composite thermoplastic polymer matrix and carbon nanotubes. As basic matrix polybutylene terephthalate was used, to which nanoparticles in the weight percentage ratio were added. As filler multi-wall carbon nanotubes in various percentages by weight ratio were used. The nanocomposite was made by the Arburg injection molding machine. For evaluation of electrical behavior electromagnetic interference of the final composite materials with and without added nanofillers was measured. In this paper also mechanical properties are evaluated. These results are compared and discussed. Influence of conductive filler (multiwall carbon nanotube) on electrical and mechanical properties is evaluated and valid conclusions are deduced based on these findings.*

Keywords: *carbon nanotubes, nanocomposites, injection molding, electromagnetic interference*

1 INTRODUCTION

In nowadays, one of the most developing technologies is nanotechnology. Now it consists of four main areas - nanomaterials, nanoelectronics, molecular nanotechnology and microscopes working in the scale of nanometers. The same use is also in the high tech of nanocomposite materials, which today has properties that we previously could not imagine [1]. Growing application of these nanocomposites is in electrostatic discharge (ESD), electro-conductive (EC), electromagnetic interference (EMI) and radio frequency interference (RFI) applications. A conductive compound in manufactured products is dominated by injection moulding caused by fast growing demand for electronics goods and automotive components. Due to the ease of processing and improved heat dissipation properties, polymer nanocomposites with carbon nanotubes become attractive in the manufacture of automotive [2]. Carbon nanotubes have a many properties (mechanical and physical) that make them attractive for use in a broad spectrum of applications, especially as filler for nanocomposites. There are two kinds of carbon nanotubes: single-walled carbon nanotubes (SWCNTs) with one graphene layer and multi-walled carbon nanotubes (MWCNTs) with many graphene layers wrapped onto themselves, see Figure 1. Generally, an individual carbon nanotube is in a macromolecular structure with nanosized diameter and micrometer length. The diameter range for the SWNTs is between 0.4 and 5.6 nm [3], while that for MWNTs it is from several nanometers to several hundred nanometers. Their morphology depends very much on the production method and the treatment (for example, for dispersion purpose) before being put into the matrix [4].

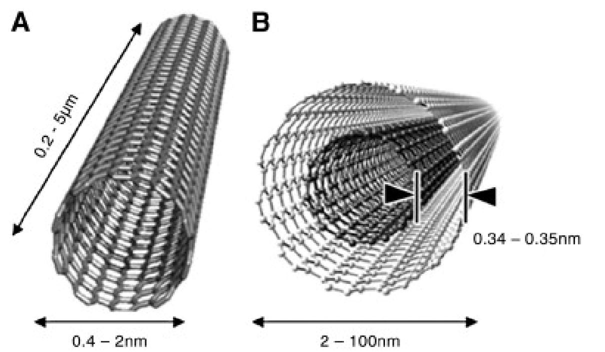

Figure 1 Scheme carbon nanotubes: single-wall carbon nanotube (SWCNT) and multi-wall carbon nanotube (MWCNT) [3]

However, CNTs have large specific surface area, bending fiber-like shape, and strong van der Waals interactions which are easy to make the CNTs agglomerate and entangled, and difficult to disperse in polymer. So, how to enhance the dispersibility of CNTs in polymer matrix has been one of the most concerns in the field of CNTs reinforced polymer-based composite materials. Therefore, functionalization of CNTs is extremely important for their dispersion, stress-transfer, and potential applications in polymer composites [5].

In this work MWCNT are used as filler in polybutylene terephthalate (PBT) polymer matrix and the effect on the nanocomposite is examined using electron microscopy, tensile test and measurement of electromagnetic interference.

2 EXPERIMENT

2.1 Materials

PLASTICYL PBT1501 is a conductive masterbatch based on polybutylene terephthalate loaded with 15% MWCNTs (NC7000™) from Nanocyl Company. For mixing pure polybutylene terephthalate with trade name Celanex 2002-2 from Resinex Company was used. The masterbatch was used as the parent matrix from which mixed polymer blends were created. Following weight ratio of multi wall carbon nanotubes was chosen 1, 2 and 5%. This percentage of the nanotubes was chosen due to satisfactory electrical properties with a relatively small proportion of nanotubes in the matrix. Melting temperature varies around 230°C. The material was dried before processing at 120°C for 4 hours. Surface resistivity of polybutylene terephthalate without MWCNTs is $1x10^{12}$ Ohm.cm. Electromagnetic shielding efficiency of pure matrix PBT is zero on frequency range between 30 MHz and 1.5 GHz.

2.2 Methods

For injection molding the standard column-mounted injection machine ARBURG 270S 400-100 was used. Injection molding technological parameters had to ensure both sample production and also need to avoid degradation of the polymer matrix. It was crucial to set proper plastication and injection moulding parameters (see Table 1) mainly with regard to thermal and shear loading. Aggregate TA3 was used for injection mould tempering. Temperature of melt was 260°C. Injection rate was 30 cm^3/s and size of holding pressure 560 bars. Holding pressure time for the samples was 20 s. Injection mould with central ejector was used for production of testing samples for tensile and impact test which had exchangeable plates according to requirements and individual ISO standards. The mould has cooling channels both on the part of die and part of punch and it was tempered on the temperature 80°C for both sides of injection mould.

Table 1 Injection moulding parameters

Barrel Temperature [°C]					Injection Speed [cm^3/s]
Zone 5	Zone 4	Zone 3	Zone 2	Zone 1	
260	255	250	245	235	30

Measurement of tensile properties of test samples were performed on a multipurpose Hounsfield H10KT tensile machine with the sensor head measuring power up to 10 kN. The measurement procedure was in accordance with standard ČSN EN ISO 527-1, 2. After clamping the sample to the clamping jaws, specimen was tensile loaded. Measurements were taken to the point of test specimen breakage. The loading speed was 50 mm/min.

Electromagnetic interference measurement was carried out according to ASTM D4935-10. This standard works for frequencies from 30 MHz to 1.5 GHz. Electromagnetic interference efficiency of samples was measured on the device consisting of a coaxial sample holder (Electro-Metrics, Inc., Model EM-2107A), see Figure 2 and measuring equipment Rhode & Schwarz ZNC3 circuit analyzer, which was used to generate and receive the electromagnetic signal, see Figure 3. The temperature was 22°C and relative humidity in the room was 55%. The size of the test samples was 150x150x2 mm. Measurement was performed on 10 specimens because of further statistical analysis.

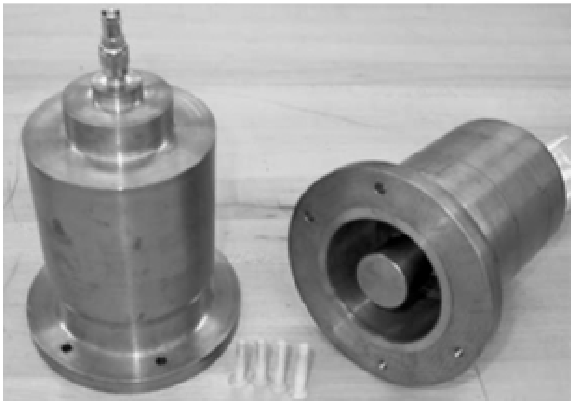

Figure 2 Coaxial sample holder from company Electro-Metrics Inc. model EM-2107A

Figure 3 Electromagnetic shielding efficiency meter with Rhode & Schwarz ZNC3 circuit analyzer

Masterbatch from polybutylene terephthalate with MWCNT in the form of granulates was dried and processed by injection moulding technology to produce testing samples which were evaluated for electromagnetic shielding efficiency and tensile properties. With regard to the fact that nanocomposite melt flow index (MFI) was much lower than MFI of pure PBT, pressure parameters during filling phase and pressure phase for commonly adjusted temperature conditions at injection were quite high: pressure at switch-over was 1000 bars, holding pressure was 560 bars. Adjusted technological parameters for testing samples production were tried out and they were chosen from several testing variants of the technological parameters. Due to the higher viscosity of composite it was necessary to increase the melt temperature from 230°C to 260°C. The structures do not degrade at this temperature. The production parameters were the same for all nanocomposites with different percentage by weight of MWCNT.

At composite processing there was presumption that foliation of the multi wall carbon nanotubes is homogenous as shown in [6, 7]. We can see fracture on surface of nanocomposite PBT with 5% weight of MWCNT after cryogenic freezing and after fracture in Figure 4. There is also shown the homogeneous distribution of MWCNT in the thermoplastic polymer matrix PBT and only small MWCNT agglomerates of maximum size 1 micrometer. Figure 4 also confirms that it is a prerequisite for creating a 3D network that has influence on mechanical, electrical and electromagnetic interference properties.

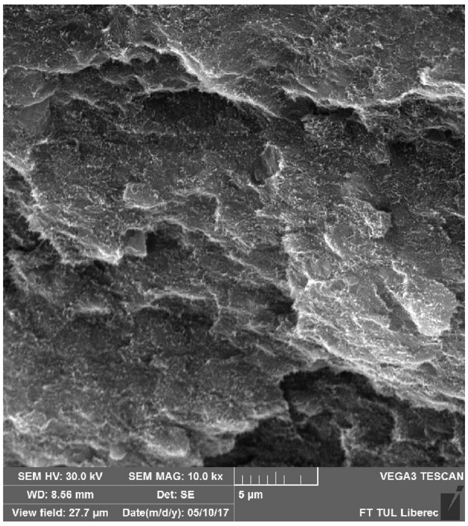

Figure 4 The homogeneous dispersion of MWCNT in PBT nanocomposites with 5% weight ratio of MWCNT

3 RESULT AND DISCUSSION

On 1, 2 and 5 wt.% ratio MWCNT´s in thermoplastic polymer nanocomposites made from masterbatch Plasticyl PBT1501 electromagnetic shielding efficiency was measured. Measurements show us, how appropriate nanocomposites are for electromagnetic interference applications. Table 2 shows the determination of the percentage of electromagnetic shielding effectiveness as written in [8]. Measurements were performed on 10 samples of each nanocomposite with different percentage ratio of MWCNT. The resulting values of electromagnetic shielding efficiency, we can see in Table 3.

Table 2 Determination of percent shielding efficiency

Degree of effectiveness	Electromagnetic shielding efficiency SE	Percentage of shielding effectiveness ES
5 - Excellent	SE>30 dB	ES>99.9%
4 - Very good	30 dB≥SE>20 dB	99.9%≥ES>99.0%
3 - Good	20 dB≥SE>10 dB	99.0%≥ES>90.0%
2 - Moderate	10 dB≥SE>7 dB	90.0%≥ES>80.0%
1 - Poor	7 dB≥SE>5 dB	80.0%≥ES>70.0%

Table 3 Determination of percent shielding efficiency

Electromagnetic shielding efficiency SE [dB] for frequency 1.5 GHz			
	1 wt.% of MWCNT	2 wt.% of MWCNT	5 wt.% of MWCNT
PBT	4.29	6.23	15.5
Standard deviation	0.99	0.68	0.69

The resulting nanocomposites with 1, 2 and 5% ratio of MWCNT indicates that these nanocomposites are conductive plastics. PBT with 5% weight ratio of MWCNT shows good electromagnetic interference - 15 dB for frequency 1.5 GHz. It is 90-99 percentage of shielding effectiveness. These results also indicate that there was a homogeneous dispersion of MWCNTs (as shown Figure 4) and the injection moulding had not a great influence on the electric and electromagnetic properties of the nano-composites. The dependence of the electromagnetic shielding efficiency on the content of the conductive component above the percolation threshold (>1% by weight MWCNT) can be approximated by means of power function [9].

$$SE = SE_P \, CNT^X \tag{1}$$

where SE_P is a shielding efficiency of 1% weight ratio of MWCNT in polymer matrix, CNT is % weight ratio of MWCNT in the thermoplastic polymer matrix and parameter X is dependent on the type of thermoplastic polymer matrix.

Figure 5 shows the dependence of the electro-magnetic shielding effect on the 1.5 GHz frequency with the expressed dependence and the interlaced power function.

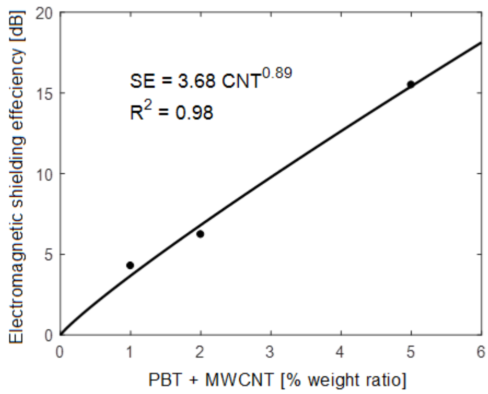

Figure 5 Dependence of electromagnetic shielding efficiency on MWCNT content in PBT interleaved by power function with its expression

The resulting regression models were obtained using the least squares method. Coefficient of determination (denoted as R^2) indicates a high correlation of the measured results.

Measurements of tensile test were performed on 10 specimens for 1, 2 and 5% weight ratio of carbon nanotubes and pure PBT. The resulting values of Young's modulus we can see in Table 4.

Table 4 Young's modulus of pure PBT and PBT with MWCNT

Young's modulus [MPa] - ISO 527-1,2				
PBT	**Neat polymer**	**1 wt.% of MWCNT**	**2 wt.% of MWCNT**	**5 wt.% of MWCNT**
[MPa]	2753.3	3267.5	3535.2	3922.6

The Young's modulus of PBT without carbon nanotubes as fillers is 2753.3 MPa with 5 wt.% ratio MWCNT´s is 3922.6 MPa. From results, an increase in young modulus more than 1200 MPa can be seen. Ductility as also reduced, resulting in increased hardness and brittleness of the final composite. Due to the continually decreasing cost of a CNT application of these fillers to improve the mechanical properties seems to be profitable in future.

4 CONCLUSION

The progression of composites with thermoplastic and carbon nanotubes is a constantly evolving process that will be influenced by expanding number of application possibilities, using not only excellent electrical properties of such composites. These properties and application potentials will be influenced not only by the type and form of nanotubes, their percentage weight ratio, but also the type and kind of the polymer matrix. Picture from SEM and results indicate that there is a homogeneous dispersion of MWCNTs and the injection moulding had not a great influence on the mechanical and electromagnetic properties of the nanocomposites. The test results show an increase in the mechanical properties of young modulus. Due to the decreasing cost of CNT's probably in the future these nanofillers will be used to improve the mechanical properties of composites. Measurements of electromagnetic shielding efficiency show than the PBT nanocomposite with 5% weight ratio have good electromagnetic interference 15 dB for frequency 1.5 GHz which means 90-99 percentage of shielding effectiveness. These properties enable wide use of this nanocomposite, such as applications requiring superior electrostatic discharge (ESD) properties, electrically conductive parts (EC), electrical and electronics (E&E) and electromagnetic interference (EMI) parts. Influence of change of processing parameter will be examined in the near future.

ACKNOWLEDGEMENT: The report has been prepared under the terms of solution of SGS 21 122.

5 REFERENCES

1. Duleba B.: Uhlíkové nanotrubice - materiál budoucnosti (Carbon nanotubes - the material of the future). Košice: Transfer inovacií (Transfer of Innovations) 21, 2011 (in Slovak)
2. Lew C.Y., Dewaghe C., Claes M.: Injection moulding of polymer-carbon nanotube composites, Polymer-Carbon Nanotube Composites, Cambridge: Woodhead Publishing, 2011, doi: 10.1533/9780857091390.1.155
3. Bai J.B, Allaoui A.: Effect of the length and the aggregate size of MWNTs on the improvement efficiency of the mechanical and electrical properties of nanocomposites-experimental investigation, Composites Part A: Appl. Sci. Manuf. 34(8), 2003, pp. 689-694, doi: 10.1016/S1359-835X(03)00140-4
4. Kasaliwal G.R., Villmow T., Pegel S., et. al.: Influence of material and processing parameters on carbon nanotube dispersion in polymer melts, Polymer-Carbon Nanotube Composites, Cambridge: Woodhead Publishing, 2011, doi: 10.1533/9780857091390.1.92
5. Dai L, Sun J.: Mechanical Properties of Carbon Nanotubes-Polymer Composites, Carbon Nanotubes, London: InTech, 2016, doi: 10.5772/62635
6. Pötschke P., Pegel S., Claes M., et al.: A novel strategy to incorporate carbon nanotubes into thermoplastic matrices, Macromolecular Rapid Communication 29(3), 2008, pp. 244-251, doi: 10.1002/marc.200700637
7. Lenfeld P., et. al.: Evaluation of plastication and injection molding influence on the morphology of polyamide with carbon nanotubes, In: Proceedings of The 28th International Conference of Polymer Processing Society (PPS-28), Pattaya, Thailand, 2012, pp 134-138
8. Safarova V., Militky J.: Multifunctional metal composite textile shields against electromagnetic radiation-effect of various parameters on electromagnetic shielding effectiveness, Polymer Composites 38(2), 2017, pp. 309-323, doi: 10.1002/pc.23588
9. Clingerman M., King J., Schulz K.: Evaluation of electrical conductivity models for conductive polymer composites, Journal of Applied Polymer Science 83(6), 2002, pp. 1341-1356, doi: 10.1002/app.10014

ECONOMIC EFFICIENCY OF TEXTILE MATERIALS CUTTING DESIGNER COSTUMES OF HOSPITALITY FACILITIES

Dmytro Yakymchuk[1], Oksana Dzyundzya[1], Valentyna Burak[2], Irina Shvets[3], Yuriy Shvets[3], Nadiia Myrhorodska[4], Polishchuk Oleh[5], Dzmitry Karneyenka[6] and Stanislau Krasner[6]

[1]Kherson State University, 40 rokiv Zhovtnya str., 27, Kherson, Ukraine
[2]Kherson State Agricultural University, Sretenskaya str., 23, Kherson, Ukraine
[3]Financial University, Leningradskij prospekt, 49, Moscow, Russia
[4]Kherson National Technical University, Berislav highway, 24, Kherson, Ukraine
[5]Khmelnytskyi National University, Universytetska str., 11, Khmelnytskyi, Ukraine
[6]Vitebsk State Technological University, Moscow Av., 72, Vitebsk, Belarus
starcon84@gmail.com

***Abstract:** The cutting process of textile materials for costumes of hospitality facilities at the expense of use a new flywheel design is described in the article. A series of experiments was conducted, which allowed to explore the cutting process from point of view of equipment energy efficiency. Maximum values of energy consumption for layers from variety of materials for costume and coat fabrics were determined. Comparison of existing press equipment with improved allowed to establish the economic efficiency of its application.*

***Keywords:** textile materials, cutting, frequency drive, cutting press, flywheel, hospitality facilities, costume.*

1 INTRODUCTION

Textile materials and fabrics are widespread in all spheres of human activity. They are irreplaceable in everyday life of people [1].

Textile materials include wide assortment of materials of various structures: fabrics, nonwoven and knit fabrics, felt, artificial fur. They are made of various types of fibers, threads and yarns. The main characteristics of fabrics quality is the structure and physical-mechanical properties [2].

Depending on the type of yarn distinguish cotton, mixed, woolen, semi-cotton, silk and linen fabrics of various types of interweaving. To get the desired thickness, produce duplicate or three-layer fabrics. Connection of layers is carried out by different methods. The most common types of fabrics are: cotton, mixed, wool, semi-cotton, silk, linen [3].

In industry, during the manufacture of parts from textile materials, use different equipment [4]. The most commonly used equipment is: hydraulic cutting plants; laser cutting complexes; cutting presses; cutting complexes using a knife, which varies with high frequency [5].

Each of the above equipment has advantages and disadvantages. Equipment for hydro-cutting of textile materials is characterized by high cutting efforts and a large number of floorings of fabrics, which can be cut out [6]. However, using a jet of water, which operates under high pressure, leads to a number of disadvantages: fabrics wetting which requires further drying of parts; uneven parts of details with a large number of layers, which make worse their quality; variability of detail edge due to specific conditions of work [7, 8].

Laser cutting complexes are characterized by a large number of advantages. First of all, this is the high quality and precision of details manufacture [9]. Also, great performance, small amount of waste when cutting, high technological capabilities and many others. The disadvantages include the high cost of equipment and slight deterioration edges quality of details during cutting.

That is known application of equipment for the laser cutting of fiber reinforced plastics [10]. A theoretical model is presented considering the spatial distribution of the laser beam, interaction time between the laser and the work material and also other parameters. The obtained results are in good agreement with theoretical calculations.

Cutting presses are the most common in the industry. This is explained to the following factors:

– construction simplicity;
– work reliability;
– equipment low cost;
– high performance characteristics;
– technological construct design of presses;
– final products low cost.

As a rule, they are characterized by a reliable construction of console type with a hydraulic drive. The cutting device returns by worker to required position and technological process of cutting is carried out [11]. For obtain the required detail form the cutters of a certain area are used.

The disadvantages of that specified equipment work are deterioration in the quality of cuttings at the end of cutters service life [12]. This specified disadvantage is eliminated either by replacing the cutter, or its exacerbation to the required level.

The next equipment, which is widespread in textile enterprises there are cutting complexes using a knife that fluctuates with a high frequency [13]. Such complexes characterized of high precision molding materials, wide programming possibilities and computer control of cutting parameters, high productivity and efficiency of work [14]. There are disadvantages such as: deterioration of quality manufactured details with a large number of materials layers; high cost of equipment.

From the above equipment for small and medium enterprises the most rational is the use of cutting presses of console type. Exactly, they provide execution of most operations with materials and correspond to the price-quality indicator.

However, one of significant disadvantages of such equipment is high electricity consumption during continuous work in the work time period. This worsens economic efficiency and increases the value of the final product. This leads to deterioration of economic efficiency and raises the cost of the final product.

Therefore, there is a need to increase economic efficiency of textile materials cutting on such equipment. It will also provide increase in demand on designer costumes of hospitality establishments. This must be taken into account of various factors which directly affect on the process, and also establish an economic effect from the proposed changes.

2 EXPERIMENTAL

2.1 Experimental equipment

Experimental investigations conducted on the Atom SE20C cutting press. This is the most commonly used press at many industries enterprises, which is characterized by high reliability and stability of work. It is also characterized by high-quality cutting of details from textile materials.

The basis of experimental research is the task to increase an economic efficiency of work of press equipment by improving its energy efficiency and durability of work, technical and economic indicators. This is done due to the application of a new flywheel construction and rational use of its kinetic energy.

For conducting researches used frequency converter Altivar 320 ATV320U15N4C by Schneider Electric with the following main characteristics: power 1.5 kW; voltage 380 V; number of phases 3; nominal current 4.10 A; maximum output frequency 600 Hz. The main advantages of using this device are: smooth start of press electric motor which provides reduction of its overload; reduction of electricity consumption from the network; increase of electric motor reliability; service life increase of electric motor; no starting currents.

The given task is solved by the fact that electrohydraulic cutting press with a rotary drummer additionally equipped by improved flywheel of a new design. The main elements of the research equipment include: body, hammer drill, turning mechanism of a striker, electrohydraulic drive.

The flywheel of a new design is placed in special case in vacuum. It provides reduction of friction during flywheel rotation and also accumulation of much more kinetic energy. There is also growing of efficiency coefficient of the drive, load reduction on electric motor and increasing its longevity of work.

Addition to construction of electro-hydraulic press a new developed flywheel allows to reduce drive load during technological process of details cutting. It also increases its energy efficiency due to accumulation and reuse of kinetic energy. It improves the economic efficiency of equipment.

To receive an accurate data of equipment work the measuring unit WB-1 is used [15-18]. It works on the principle of analog-digital signal conversion and obtaining accurate data of measuring values (Figure 1).

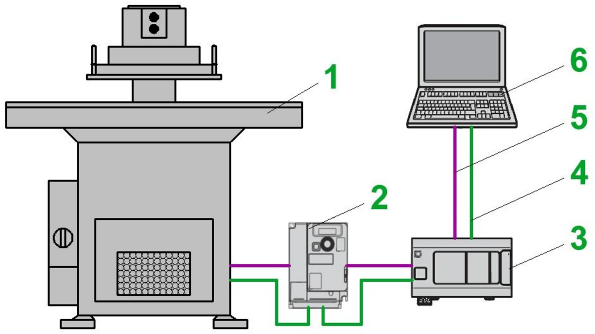

Figure 1 Experimental scheme for parameters investigation of press equipment: 1 – cutting press Atom SE20C; 2 – frequency converter Altivar 320 ATV320U15N4C; 3 – measuring unit WB-1; 4 - line of direct connection; 5 - line of feedback connection; 6 - PC

2.2 Methodology

For conducting experimental research, a suit and coat fabrics were used. Cutting efficiency for single-layer and multilayer flooring of specified materials was tested. In this case, in the case of significant deviation of the indicators, the average values of experimental data were selected. During experimental investigations cutting press worked as follows. When press is turned on, the pump motor does not work. That is, most functional systems work without a load on the network. With switches of control block the required mode operation of frequency converter ATV320U15N4C Altivar 320 and measuring block WB-1 was established. The entire measuring system is connected to a personal computer. It configures necessary software for collecting and processing the necessary data, which in the future will be obtained experimentally way. After that, they are processed in appropriate software products and received necessary characteristics.

Before performing a technological cutting operation, the necessary operating mode is selected, which depends on following parameters:

1) material (type of material directly affects on cutting process as it depends on cutting power);
2) sample form (larger area of detail, which will be cut off, requires more effort to be applied in cutting);
3) number of material layers (for a large number of material layers it is necessary to apply considerable effort, which can lead to deterioration of details).

When pressed on control buttons, the corresponding electrical equipment is turn on and electric motor and hydraulic pump are activated. The oil from hydraulic pump through the corresponding pipelines is sent to the working cylinder of press. After drummer turning into working position under action of oil pressure, the drum jumper drops down, cutting off given material.

At the same time, when cutting, work flywheel of a new design, which accumulates a large quantity of kinetic energy. This happens at the final cutting stage when cutter is immersed in material. When cutting a part of accumulated energy spent on reducing peak load on the drive and equipment as a whole. When cutting is completed, electrical equipment is turned off. The energy of the compressed oil, accumulated in the working cylinder, raises the drummer up. Oil from the pump moves through pipelines and appropriate distributor into the tank. The electric motor of hydraulic pump is turned off and system is ready for next operation (Table 1).

Table 1 Technical parameters of cutting technological process of textile materials

Technical parameter	Marking	One-layer	Many-layer
Cutting effort	N_{vr}	52-70 kH	74-220 kH
Cutting time	t	0.002 s	0.0027 s
Quality of cutting line of parts	k	0.99-1	0.97-0.99
Electric motor maximum power (with a usual flywheel)	W_{max1}	0.43 kW	0.71-0.78 kW
Electric motor maximum power (with a flywheel of new design)	W_{max2}	0.42 kW	0.70-0.76 kW
Efficiency factor of equipment use	α_{eq}	0.81	0.78

During next cutting cycle the flywheel accumulated energy will be reused. This reduces the load on electric motor and equipment, raises energy and efficiency of cutting press.

During conducted research a frequency energy converter Altivar 320 provided a significant improvement of equipment energy performance. At startup, there was a smoothing of peak loads, which reduced engine overload.

During cutting process provides press reliability and its protection from possible breakdowns through the use of following security functions (in accordance with IEC 61508 and ISO/EN 13849-1-2):

1) STO – safety moment shutdown;
2) SLS – safety speed limit;
3) SS1 – safety stop 1;
4) SMS – safety maximum speed;
5) SLS – safety door lock.

Thus, it was provided reliable work of electric motor and his protection from possible stops, breakdowns and failures.

3 RESULTS AND DISCUSSION

During the experiments economic efficiency of cutting textile materials of hospitality establishments' designer costumes was investigated. The results of experiments are presented on appropriate graphic dependencies (Figure 2).

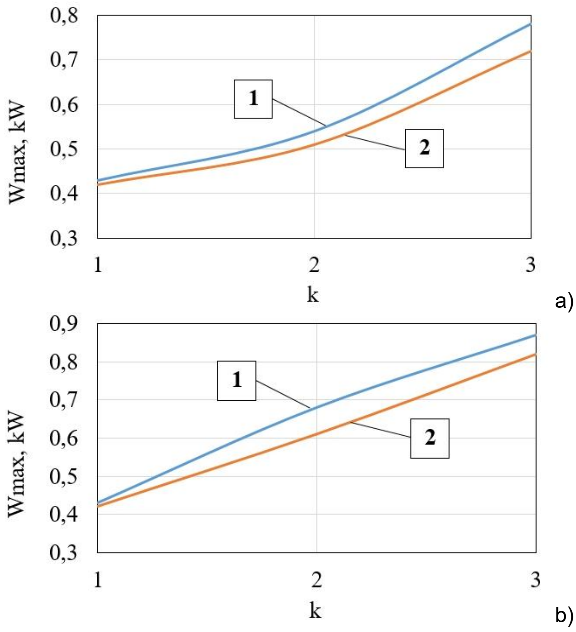

Figure 2 Graphic dependencies of changes the maximum energy consumption *Wmax* from the factor, that takes into account a number of material layers *k*: 1 - press equipment with a standard flywheel; 2 - press equipment with a new flywheel design; a) coat fabric; b) costume fabric

Conducted experimental studies allowed to determine the nature of change in the energy consumption of suit and costume fabrics, depending on flywheel design. We established that when increasing the number of material layers, the energy consumption increases to 2 times (Figure 2). This is explained by emergence of additional resistance forces in system drummer-cutter-material. They hamper the cutting process and impair quality of cut details.

The maximum values of energy consumption were determined: 1) for coat fabrics (W_{max1} = 0.78 kW and W_{max2} = 0.73 kW for a usual flywheel and flywheel of a new design respectively);

2) for costume fabrics (W_{max1} = 0.87 kW and W_{max2} = 0.82 kW for a usual flywheel and flywheel of a new design respectively).

Determined influence character of flywheel accumulated energy on total energy consumption of press equipment during cutting. It was investigated that with increasing the number of fabric layers, efficiency of flywheel accumulated energy increases to 93%. This explained by increased pressure on the press when cutting, especially with final cutter immersion into material.

The economic efficiency application of developed equipment provided with reduced power consumption in comparison with usual equipment. The economic potential of saving energy is 18% for coat fabrics and 15% for costumes.

But, we should note some of drawbacks of conducted researches. The research was carried out only for costume and coat fabrics, which limits the breadth of coverage of other materials. Also, a new flywheel design has an experimental character and requires further improvements from point of view reliability and stability of work. These disadvantages need to be solved in further studies.

4 CONCLUSION

A new flywheel design, which is used in electro-hydraulic cutting presses of console type, was developed.

Conducted experimental research and determined maximum values of energy consumption, which are: for coat fabrics W_{max1} = 0.78 kW for usual equipment and W_{max2} = 0.73 kW for developed equipment; for costume fabrics – W_{max1} = 0.87 kW for usual equipment and W_{max2} = 0.82 kW for developed equipment.

Completed comparison of developed equipment with existing and establish economic effect from its application. It was found that economic potential of saving energy is 18% for coat fabrics and 15% for costumes.

5 REFERENCES

1. Drehulias E.P., Rybalchenko V.V., Suprun N.P.: Textile material science, KNUTD, 2011, p. 430, (in Ukranian)
2. Patlashenko O.A.: Material science of sewing production, Aristei, 2003, p. 288, (in Ukranian)
3. Lazur K.R.: Sewing material science, Svit, 2004, p. 240, (in Ukranian)
4. Suprun N.P.: Material science of sewing products: fibers and threads, Znannia, 2008, p. 183, (in Ukranian)
5. Suprun N.P., Shustov Y.S.: Textile material science basics, KNUTD, 2009, p. 293, (in Ukranian)
6. Savostitskii N.A., Amirova E.K.: Material science of sewing production, “Textbooks, training benefits” series, Pheniks, 2002, p. 288, (in Russian)
7. Miller R.: Waterjet Cutting: Technology and Industrial Applications, Fairmont Press, 1991, p. 154
8. Orel V., Shchetinin V., Salenko A., Yatsyna N.: The use of controlled cracking to improve the efficiency of waterjet cutting, Eastern European Journal of Enterprise Technologies 1(7), 2016, pp. 45-56, DOI: https://doi.org/10.15587/1729-4061.2016.59907
9. Li M., Li S., Yang X., Liang Z.: Fiber laser cutting of CFRP laminates with single- and multi-pass strategy: A feasibility study, Optics and Laser Technology 107, 2018, pp. 443-453, DOI: 10.1016/j.optlastec.2018.06.025
10. Cenna A.A., Mathew P.: Analysis and prediction of laser cutting parameters of fibre reinforced plastics (FRP) composite materials, International Journal of Machine Tools and Manufacture 42(1), 2002, pp. 105-113, DOI: 10.1016/S0890-6955(01)00090-6
11. Bol’shakov A.N.: The theory of discontinuous cutting, Russian Engineering Research 38(5), 2018, pp. 358-359, DOI: 10.3103/S1068798X18050040
12. Volkova A.N., Toroptseva E.L., Ambrosimov S.K.: The relationship between the change in the conditions of discontinuous cutting, the structure, and microhardness of the cut layers, Fundam. Prikl. Probl. Tekh. Tekhnol. 3(299), 2013, pp. 61-65
13. Krowatschek F., Nestler R.: Automatic cutting machines for single- and multiple-ply lays, Knitting Technology 20(6), 1998, pp. 266-267
14. Phakphonhamin V., Chudokmai M.: Optimizing the performance of the LECTRA automatic fabric cutting machine, In: Proceedings of 5th International Conference on Business and Industrial Research: Smart Technology for Next Generation of Information, Engineering, Business and Social Science, ICBIR 2018, Thailand, 2018, pp. 282-287, DOI: 10.1109/ICBIR.2018.8391207
15. Yakymchuk D.M., Karmalita A.K.: Features of use energy efficient drives of light industry machines, Materials of All-Ukrainian Scientific and Practical Conference of young scien. and stud. “Resource-saving technologies of light, textile and food industry”, Khmelnytskyi, 2013, pp. 50-51, (in Ukranian)
16. Karmalita A.K., Yakymchuk D.M.: Experimental study of influence a drummer turning mechanism on work efficiency of electrohydraulic press equipment, Herald of Khmelnitskyi national university 3, 2013, pp. 106-109, (in Ukranian)
17. Yakymchuk D.M.: Improving work efficiency of cutting presses of light industry, Herald of Khmelnitskyi national university 1, 2011, pp. 46-50, (in Ukranian)
18. Karmalita A.K., Yakymchuk D.M.: Investigation of energetic parameters of electro-hydraulic press equipment, Herald of Cernihiv state technological university 42, 2010, pp. 265-269, (in Ukranian)

PROVISION OF THE QUALITY OF DECORATION OF SEMI-FINISHED FASHIONABLE CLOTHES, MADE OF SUITING FABRICS WITH COTTON CONTENT (DENIM TYPE)

Olga Yezhova[1], Kalina Pashkevich[2], Marina Kolosnichenko[2], Oksana Abramova[1] and Liudmyla Nazarchuk[3]

[1]Volodymyr Vynnychenko Central Ukrainian State Pedagogical University
Shevchenko Street 1, 25006 Kropyvnytskyi, Ukraine,
[2]Kyiv National University of Technologies and Design, Nemirovich-Danchenko Street 2, 01011Kyiv, Ukraine,
[3]Lutsk National Technical University, Lvivska Street 75, 43018 Lutsk, Ukraine
oyezhova70@gmail.com, kalina.pashkevich@gmail.com, nlv_29@ukr.net

Abstract: *The article is devoted to the problem of provision of the quality of decoration of semi-finished fashion products from the fabrics of suiting group of denim type, embroidered by a machine method. Standard methods of the research of geometric properties of textile materials (thickness, surface density), as well as rupture characteristics at constant-rate-of-extension (CRE) testing machine (force at rupture, extension) are used. The embroidery of the samples is made using the Brother Innovis 750S machine. As a result of the analysis of 7 samples of the materials of suiting group, "stretch-denim" type, it is found that elongation at rupture in weft of all of the samples exceeds the value of such indicator in warp and reaches 37.5%, and the samples with elastane and polyamide content have higher value of the indicator. The conducted correlation analysis showed a strong correlation between weight and force at rupture in warp (r = 0.84), as well as between weight and thickness (r = 0.74). All samples of denim-like fabrics are conventionally divided into 3 groups in accordance with their elongation at rupture in weft: 1) 30 - 40%; 2) 20 - 30% 3) 15 - 20%. Classification of the defects of embroidered semi-finished products is improved. All defects are divided into: 1-dimensional (stitch defects); 2-dimensional (defects of setting the fabric in the embroidery frame, embroidery defects); and 3-dimensional (deformation of the embroidered area; deformation of the area, adjacent to the embroidered area; deformation of the materials along the embroidery frame line). The method of evaluation of the quality of semi-finished products embroidery using the 4-point scale (where 0 - unsatisfactory, 3 - no identified defects) is proposed. Evaluation of embroidery with a complex design is recommended to be carried out separately for each area of the image. The use of a duplicate glutinous material for stabilization of semi-finished products, made of denim-like fabrics, for machine embroidery is recommended. The research is a contribution to the development of fashion design of the products, made of denim-like fabrics, decorated with machine embroidery.*

Keywords: *fashion design, decoration, denim, fabric, machine embroidery, quality, stabilization of semi-finished product.*

1 INTRODUCTION

The development of the design of modern clothes begins with the selection of the materials: basic, applied, decorative etc. When choosing the parameters of the design and the methods of processing and decoration of the product, it is necessary to consider the properties of the materials: fiber composition, physical and mechanical properties, technological features etc. That is why the study of the properties of the materials at the pre-design stage takes an important place in design-projecting of the modern clothes. Recently, designers and users of the fashion clothes have turned their attention to the products from suiting and dressing assortment range, which are made of denim and denim-like materials: trousers, shorts, skirts, dresses, jackets, vests. The author of the article [1] considers that «we're in an exciting era of reinvention for denim». An up-to-date decoration of such products is embroidery. Modern and effective way of embroidery for semi-finished products is embroidery on computerized machines using the double-thread lock stitch (machine embroidery). This process requires a reasonable selection of technological modes of execution of embroidery operation and selection of stabilizing materials, depending on the properties of the main material of the product. Embroidery of the fabrics with stretch effect (elongation) requires special care, since such materials can deform the most during the embroidery, sewing and operation. Thus, selection of the optimal models of machine embroidery on the elastic suiting materials of "stretch-denim" type is an actual task, the solution of which can ensure the quality of embroidered semi-finished products.

The purpose of the article is the development of recommendations regarding the provision of the quality of semi-finished products, made of the fabrics of suiting group, denim type, embroidered by machine, taking into account the properties of the materials. For this purpose, the following tasks should be solved:

- determination of composition and indexes of physical and mechanical properties of the materials of suiting group of “stretch-denim” type;
- development of methodology of evaluation of the quality of embroidery on semi-finished products;
- selection of the optimal package of materials for stabilization of the materials for machine embroidery;
- development of recommendations regarding machine embroidery on the materials of suiting group of “stretch-denim” type.

2 LITERATURE REVIEW

The problem of determining the physical and mechanical properties of suiting materials (denim type) with the cotton content is at the center of attention of a number of researches.

In the research [2], tensile properties of elastic denim fabrics are studied using the KES-F system. In particular, it has been found that the fabrics with higher polyester content and lesser cotton content recover better after stretching. In the research [3], as a result of the analysis of suiting fabric with cotton fibers, it has been identified that the main physical and mechanical characteristics that have an effect on the shape and design of the clothes are thickness, surface density (weight), rigidity and drapeability of the fabric. The influence of the characteristics of denim on its sewing properties is studied in the study [4]. The author has developed and implemented the method of forecasting the quality of stitching, depending on the properties of denim and the parameters of the stitch.

In the article [5], the author has selected the most suitable washing treatment for denim-like knitted fabrics to prevent the loss of strength. In the study [6], the denim for the clothes for motorcycle riders is developed. Such created material has the increased tensile strength and abrasion resistance in comparison with the classic denim. The assessment and provision of the quality of the embroidered semi-finished products have become the subject of the scientific research of the researches. In the study [7], the dependence of the embroidery machine vibration on the parameters of the embroidery pattern is identified. In the article [8], it has been found the following dependence: the higher the level of heat gathered in the thread, the higher the risk of thermal damage. The study [9] is dedicated to the synergism of design and technology in order to optimize the quality of the embroidered elements. The technique of designing and analysis of the design for the machine method of embroidery is discussed in the following publications.

In the article [10], the technology of creation the embroidery design by means of the universal CAD system is considered. In the paper [11], an automated analysis system for Tatami embroidery fabric images is proposed.

At the same time, we could not find any publications in which the scientifically grounded recommendations regarding the technology of stabilization of the fabric during the machine embroidery are described. Therefore, the problem of the choice of stabilizing materials for machine embroidery is not sufficiently researched and needs to be considered.

3 MATERIALS AND METHODS

In accordance with the aim and the objectives of the researches, 7 samples of suiting elastic fabrics of denim type with cotton twill weave, which differ as to their geometric and physical and mechanical properties, have been selected for the experiment (Table 2, Columns 1, 2). In order to characterize the fabrics, the following indicators have been selected. General properties are determined by the fibrous composition (%) and the structure of the interweaving (for all of the samples it is twill). Geometrics parameters are described using such indicators as thickness and surface density. The main characteristic that distinguishes the selected materials among the other suiting fabrics of denim type is elasticity. In this regard, mechanical tensile characteristics have been determined, such as: force at rupture *Pr* [N], relative force at rupture P_{rel} [Nm/g], breaking extension *Lr* [mm] and relative breaking elongation *Er* [%]. Depending on the values of these indicators, assortment range and design of the product, technology of its manufacture and decoration are determined.

Testing of the properties of materials has been carried out in accordance with the current normative documents, observing the regulations to the objects of the experimental research; the processing of the results of the measures has been made using the mathematical apparatus of statistical analysis of data. The test has been conducted in climatic conditions in accordance with ISO Standard 139:2005 [12]. Before the test, each sample is kept in climatic conditions (relative humidity of 65±4% and temperature of 20±2°C) not less than 24 hours. Thickness is measured under the pressure of 1 kPa according to ISO standard 5084-1996 [13]. Weight *Ms* in g/m^2 is determined in accordance with ISO standart 3801:1977 using the formula (1):

$$Ms = \frac{m \times 10^4}{L \times b} \qquad (1)$$

where *Ms* – weight [g/m^2]; *m* – mass of the point sample [g]; *L* – length of the sample [mm]; *b* – width of the sample [mm].

The mechanical characteristics of elongation are determined by standard strap method in accordance with ISO standard 13934-1:2013 [14]. From each sample, 6 test samples with a size of 350x50 mm are taken, 3 in warp and 3 in weft. The study has been carried out at a tensile-test machine (Figure 1) with a constant rate of extension (CRE) 100 mm per min. The gauge length of the samples is 200±1 mm.

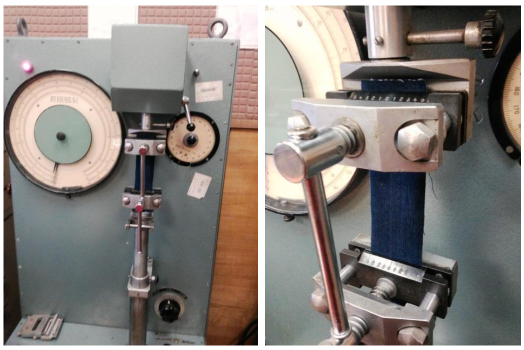

Figure 1 The research of rupture characteristics

The following characteristics are measured: force at rupture *Pr* [N], and breaking extension *Lr* [mm].

In order to compare the properties of the fabrics of various mass, the relative force at rupture P_{rel} [Nm/g] is determined using the formula (2):

$$P_{rel} = P_r / M_s b \tag{2}$$

where *Pr* - force at rupture [N]; *Ms* – weight of the fabric [g/m^2]; *b* – width of the sample of the fabric [m].

In order to compare the breaking extension of the materials regardless of the squeezed length of the sample, the relative breaking elongation *Er* [%] is determined using the formula (3):

$$Er = 100 \times Lr / L_0 \tag{3}$$

where L_0 – the initial length of the sample.

During the evaluation of the properties of the samples, the recommended values of indicators for suiting cotton fabrics, including denim, have been taken into account (Table 1).

Table 1 Oriented values of the properties of suiting fabrics of denim type in accordance with [15]

Indicator	Units	Recommended value		
		Total	In warp	In weft
Thickness	mm	0.5-0.9	-	-
Weight	g/m^2	150-300	-	-
Force at rupture	N	-	785-981	392-589
Elongation at rupture	%	-	15-20	15-20

4 RESULTS

As a result of the conducted experimental research, the properties of 7 samples of suiting fabrics (denim type) have been determined, which have different raw material composition, thickness, surface density and other physical and mechanical properties. All identified characteristics are generalized in Table 2.

To illustrate the results of the measures of thickness and surface density of denim-like fabrics, the diagram (Figure 2) is constructed, where the samples are ranged as to the growth of their weight values.

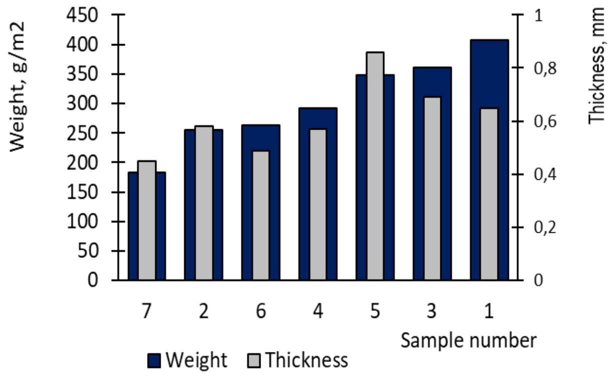

Figure 2 The interdependence between weight and thickness of the denim-like fabrics

The thickness of the fabric depends on the linear density of the yarn and its twist, the structure of the threads weaving, the density and the nature of processing of the fabric. Samples 3 and 5 have the largest thickness (0.69 and 0.86 mm respectively). Samples 6 and 7 have the lowest thickness (0.49 and 0.45 mm respectively). Consequently, the thinnest sample has the thickness almost 2 times smaller than the thickest one. Surface density depends on the thickness of warp and weft threads, on the density of the fabric and on the type of processing. Sample 1 has the maximum weight (407 g/m^2), sample 7 – the minimum weight (183 g/m^2).

In order to illustrate the results of the measurements and calculations of the elongation at rupture for denim-like fabrics, a diagram (Figure 3) is constructed, in which the samples are located on the basis of the elongation at rupture growth in warp. Characteristics of material elongation at rupture depend on the fiber composition, on the density and the structure of threads and fabric.

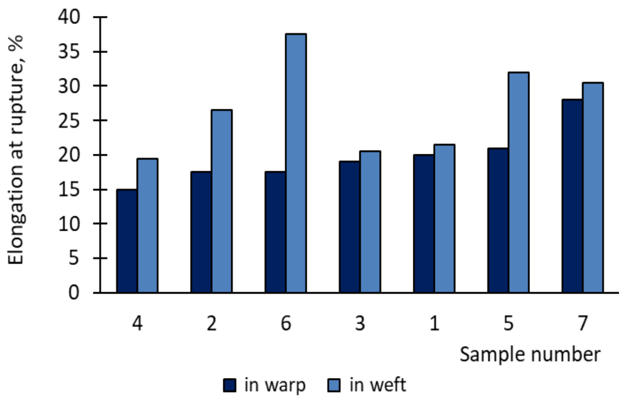

Figure 3 The interdependence between the elongation at rupture in warp and in weft for denim-like fabrics

Table 2 Generalized characteristics of denim costume fabrics

№	Fiber composition	Weight [g/m^2]	Thickness [mm]	Elongation at rupture [%]		Force at rupture [N]		Relative force at rupture [Nm/g]	
				warp	weft	warp	weft	warp	weft
1	98% cotton, 2% elastane	407	0.65	20.0	21.5	1410	1481	69.3	72.8
2	97% cotton, 3% elastane	255	0.58	17.5	26.5	674	1280	52.9	100.4
3	9 % cotton, 3% elastane	361	0.69	19.0	20.5	1405	1455	77.8	80.6
4	95% cotton, 5% elastane	292	0.57	15.0	19.5	978	1155	67.0	79.1
5	90% cotton, 6% PE, 4% elastane	348	0.86	21.0	32.0	943	1558	54.2	89.5
6	84% cotton, 10% PE, 6% elastane	263	0.49	17.5	37.5	1117	1827	84.9	138.9
7	71% cotton, 15% PE, 9% rayon, 7% elastane	183	0.45	28.0	30.5	597	641	65.2	70.1

In order to increase these indicators, such material as elastane can be added, in particular, to the weft threads. As can be seen from the Figure 3, sample 4 has the lowest value of elongation at rupture in warp (15%), when sample 7 has the largest one (28%). Sample 4 also has the lowest value of elongation at rupture in weft (19.5%), when sample 6 has the largest value of such indicator (37.5%). In this case, all samples have elongation at rupture in warp less than in weft, but not less than the recommended minimum values for suiting fabrics (15 - 20%). It should also be noted that the value of elongation at rupture in weft greater than 30% is found for samples 5, 6 and 7, the raw material composition of which, along with cotton and elastane, contains polyester.

In order to illustrate the results of the force at rupture measurements for denim-like fabrics, a diagram (Figure 4) is constructed, in which the samples are located on the basis of the force at rupture growth in warp.

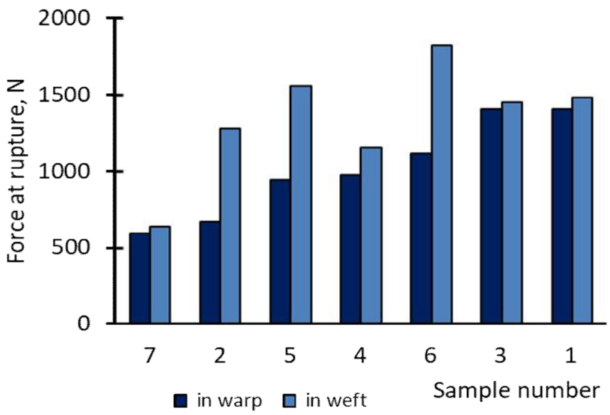

Figure 4 The interdependence between the force at rupture in warp and in weft for denim-like fabrics

As provided at the Figure 4, all samples have the force at rupture in warp less than in weft. Samples 2 and 7 have the lowest force at rupture in warp (674 and 597 N accordingly), which is less than the standard minimum for denim fabrics (785 N), but corresponds to the standard value for cotton and mixed fabrics (490 - 785 N) in accordance with GOST 21790-2005 [16]. Samples 1 and 3 have the largest force at rupture in warp (1.410 and 1.405 N accordingly). Sample 7 has the lowest force at rupture in weft (641 N), and sample 6 has the largest value of this indicator (1.827 N).

In order to illustrate the results of the relative force at rupture calculations for denim-like fabrics, a diagram (Figure 5) is constructed, in which the samples are located on the basis of the relative force at rupture growth in warp.

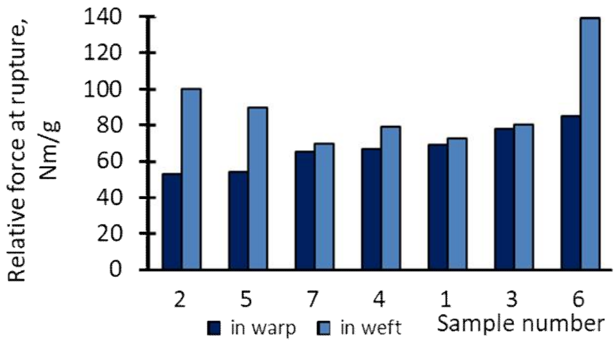

Figure 5 The interdependence between the relative force at rupture in warp and in weft for denim-like fabrics

As provided at the Figure 5, all samples have the relative force at rupture in warp less that in weft. Samples 2 and 5 have the lowest value of the relative force at rupture in warp (52.9 and 54.2 Nm/g accordingly), and sample 6 has the largest value (84.9 Nm/g). Samples 1 and 7 have the lowest value of the relative force at rupture in weft (72.8 and 70.1 Nm/g accordingly), and sample 6 has the largest value of this indicator (138.9 Nm/g).

In order to identify the degree of the interdependence between the physical and mechanical characteristics of the analyzed samples of dress fabrics, correlation coefficients between each pair of indicators are determined. The results of the correlation analysis are presented in the Table 3.

The conducted correlation analysis has showed a strong connection (r = 0.7 - 0.9) of the weight with the force at rupture in warp (r = 0.84), as well as of the weight with the thickness (r = 0.74).

Table 3 Correlation coefficients between the values of physical and mechanical characteristics of denim-like fabrics

Indicator	Direction	Weight	Thickness	Elongation at rupture in warp	Elongation at rupture in weft	Force at rupture in warp	Force at rupture in weft	Relative force at rupture in warp
	Direction	-	-	in warp	in weft	in warp	in weft	in warp
Thickness	-	0.74	-	-	-	-	-	-
Elongation at rupture	in warp	-0.31	-0.10	-	-	-	-	-
	in weft	-0.41	-0.13	0.47	-	-	-	-
Force at rupture	in warp	0.84	0.36	-0.31	-0.33	-	-	-
	in weft	0.59	0.43	-0.47	0.26	0.63	-	-
Relative force at rupture	in warp	0.09	-0.39	-0.14	0.08	0.60	0.37	-
	in weft	-0.21	-0.21	-0.31	0.66	-0.01	0.66	0.38

The interdependence between the indicated values is shown in the graphs (Figures 6 and 7). The graphs are supplemented with trend lines and linear regression equations. The average connection (r = 0.5 - 0.7) has been found between five pairs of indicators. The corresponding cells in Table 3 are painted.

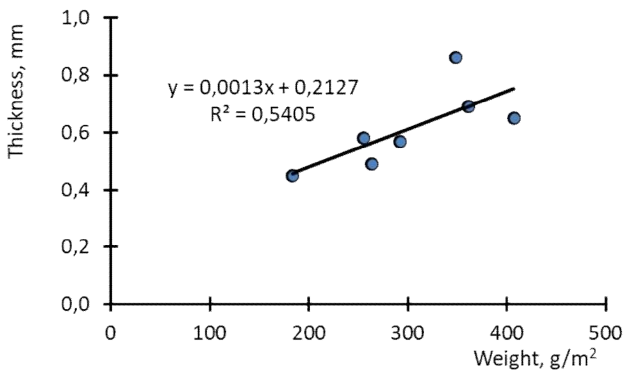

Figure 6 The interdependence between the weight and the thickness for denim-like fabrics

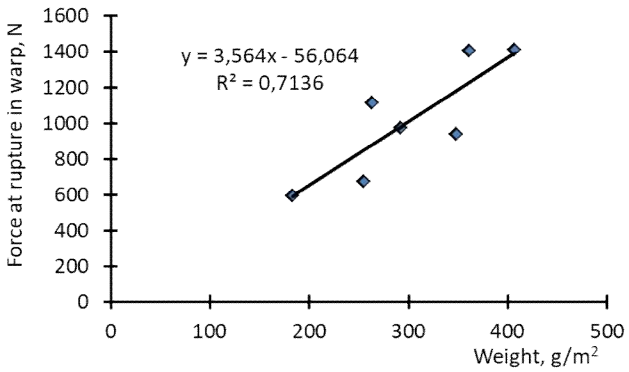

Figure 7 The interdependence between the weight and the force at rupture in warp for denim-like fabrics

Thus, as a result of the conducted experimental researches, the samples of denim-like fabrics can be divided conveniently into 3 groups as to their elongation at rupture, and recommendations regarding the selection of stabilizing materials for embroidery for each group can be developed. So, the first group with a large elongation at rupture (30 - 40% in weft) consist of samples 5, 6 and 7; the second group with a medium value (20 - 30% in weft) – of samples 1, 2 and 3; the third group with a low value (15 - 20%) – of sample 4.

4.1 Method of evaluation of the quality of embroidered semi-finished products

At the next stage the ways of stabilization of semi-finished products for the machine embroidery, depending on the properties of the materials, have been analyzed. In order to evaluate the effectiveness of stabilization clear-eyed, the method of evaluation of the quality of embroidered semi-finished products has been developed.

Defects of the embroidered fabrics are formed at the next stages: design of embroidery image; connection of the main material with the stabilizer; setting the package of the materials in the embroidery frame; embroidery; removal of stabilizing material. At the design stage, the following defects are formed: fragments of the image that are not closed by the embroidery; excessive density of covering of the image fragments with embroidery stitches; inconsistency of the neighboring areas or layers of embroidery; asymmetry of the fragments of image that has a symmetry axis. The types of the defects of embroidery fabrics are determined in accordance with the research [17]: 1-dimensional, 2-dimensional and 3-dimensional. Our article specifies and completes the list of these defects:

1-dimensional – defects of the stitch: slip stitching, thread breaking; excessive or insufficient tension of threads; interweaving of the needle and the shuttle thread on the front side of the product; cutting of the material with a needle;

2-dinemsional: defects of the setting the fabric in the embroidery frame (skewness of the package of materials, displacement of the elements of image after the repeated setting the fabric in the embroidery frame); embroidery defects (tightness, stretching of the embroidered area);

3-dimensional: deformation of the embroidered area (bulge, cavity, buckles); deformation of the area, adjacent to the embroidered area (bulge, cavity); deformation of the materials along the embroidery frame line (bulge, cavity).

The size of the tightness is evaluated as the value of reduction of the linear size of embroidered area. The size of the bulge, cavity or buckles is evaluated as the highness of the relief of the deformed area in relation to the flatness of the main material. Since at the various parts of the image the defects are presented to different extents or even absent, the assessment of the quality was carried out separately on the fragments of embroidery, the locations of which are indicated by the figures at the Figure 8.

Quantitative characteristics do not always fully assess the impact of a certain defect on the quality of semi-finished product. Visual perception of the defect as essential or unessential for the quality of the product depends on the geometric and optical parameters of the embroidery fragments. Depending on the ratio of the defect area and the area of the corresponding embroidery fragment, as well as on the color, shine and texture of the material, certain defect may be perceived as such that affects the quality of semi-finished product essentially or unessentially. With this connection, quantitative evaluation of the defect is supplemented with the expert evaluation in points, 4-point scale is used:

3 – defects are absent or almost invisible;

2 – defect is barely noticeable and somewhat affects the quality of semi-finished product;

1 – defect is very noticeable and significantly affects the quality of semi-finished product;

0 – semi-finished product cannot be used.

Figure 8 Location of the embroidery fragments for evaluation of the quality of semi-finished products

Table 4 Embroidery Quality Rating Card

Material			Main sample 4		cotton - 95%, spandex - 5%		
			Stabilizing		flizelin PE - 100%, 35 g/m^2		
Method of connection of the main and stabilizing materials					agglutination		
Threads					PE - 100%, №125		
Size of the embroidery frame [mm]					255*175		
Size of the embroidery pattern [mm]					152*118		
Fragment	**Size [mm]**	**Type of the stitch, backstitch**	**Type of the fragment defect, [number of bends]**	**Size of the defect [mm]**	**Type of the defect near fragment**	**Size of the defect [mm]**	**Evaluation of the fragment [points]**
1	40 *30	Straight, multiline 2nd layer - zigzag	~ 4	2	-	0	2
2	40*35	Straight, multiline 2nd layer - straight, multiline 3rd layer - straight, one-line	~ 2	2.5	⌢	2.5	2
3	25*3	Straight, one-line 2nd layer - zigzag 3rd layer - zigzag	-	0	-	0	3
4	38*25	Straight, multiline 2nd layer - straight, multiline 3rd layer - straight, one-line	~ 2	2.0	⌢	2.5	2
5	67*65	Straight, multiline 2nd layer - straight, multiline 3rd layer - zigzag	~ 2	3.0	-	0	2
6	20*4	Straight, one-line 2nd layer - zigzag 3rd layer - zigzag	~ 1	3.0	⌢	2.0	2
7	40*24	Straight, multiline 2nd layer - straight, multiline 3rd layer - straight, one-line	‿ 1	1.0	⌢	2.0	2
8	40*24	Straight, multiline 2nd layer - straight, multiline 3rd layer - straight, one-line	-	0	-	0	3
	Average evaluation of the sample						2.3

The quality of the embroidered semi-finished product has been evaluated after 30 minutes of rest after the removal from the embroidery frame. An assessment of the quality of the embroidered semi-finished products is made by the group of 6 experts. All experts have a higher education in the design of the clothes, 4 of them have a Ph.D. in Technical Sciences, 2 of them have a Doctor of Technical Sciences, all of them have the experience in the fashion industry and fashion education for at least 10 years. For a comprehensive assessment of the quality of the embroidered semi-finished product, Embroidery Quality Rating Card is developed (Table 4). The experts have been asked to evaluate the quality of each piece of the embroidery separately. The valuation of the embroidered semi-finished product is calculated as an average valuation of all its fragments by the formula (4):

$$Q=\sum q_i/i \tag{4}$$

where q_i – evaluation of the i-th fragment; i – number of the fragments of embroidery.

In case if any fragment of embroidery is evaluated as unsatisfactory, the quality of the entire embroidered semi-finished product is considered unsatisfactory.

4.2 Method of selection of the optimal method of stabilization of embroidered semi-finished product

To eliminate the possible defects of embroidery, connected with the deformation of semi-finished product, it is necessary to stabilize fabric and to set it in the frame of the embroidery machine with a small tension. In order to choose the optimal method of stabilization of elastic denim-type fabric, a method of successive improvement of the initial solution has been used, in accordance with [18]. At the same time, stabilization method, which allows getting the quality of embroidered semi-finished product that is evaluated almost of about 3 points, is considered as the optimal one. To reduce a number of factors that affect the quality of the embroidered semi-finished product, the same image of embroidery is used for all samples (Figure 8). The embroidery is done at the computerized embroidery machine Brother Innovis 750S (Figure 9).

Figure 9 Embroidering at the computerized embroidery machine

First, the method of the “blind search” is used, when every next step is done regardless of the previous one [18]. Sample 4 without stabilizer is taken as a zero point of the experiment. Sample 4 is selected because it meets all the requirements for suiting denim fabrics and has the lowest elongation at rupture in warp and in weft, so it can be expected that such sample almost doesn’t need additional stabilization. Setting the fabric in the embroidery frame in accordance with the instruction to the machine (set in the embroidery frame – tighten the screw on the embroidery frame slightly – pull the material – reset again – tighten the screw to the stop) did not allow getting sufficient tension of the material in the embroidery frame. An attempt to embroider a sample as such has led to the breakage of the thread and breakage of the needle already in the beginning of the embroidery, which gives a reason to consider the embroidery of elastic denim without additional stabilization unacceptable. In this regard, zero point of the experiment is defined as unsatisfactory. The material has been set in the embroidery frame using the additional tightening of semi-finished product by hand. Such method allows for the acceptable quality of semi-finished product (Table 5) but cannot be recommended for use because of the possible breakdown of the fabric threads and embroidery frames.

Based on the analysis of the embroiderers` experience by interviewing the specialists, and the analysis of the messages at the embroidery masters sites, three main ways of stabilization of semi-finished product for embroidery aims have been identified: provision on the main material with additional rigidity; setting the main material in the embroidery frame together with the stabilizing non-stretch material; duplication of the main material with non-stretch glutinous material. All three methods are tested at the “blind search” stage.

For additional rigidity, a method of gelatinization is applied. The material is kept in gelatin water (25 g of gelatin per 0.5 l of water), dried, ironed and set in the embroidery frame. However, the use of gelatin has not allowed to achieve better quality of semi-finished product than with the use of additional tightening of semi-finished product by hand (Table 5). The method of gelatinization also has its disadvantages: 1) it is hard to set the gelatinized semi-finished product in the embroidery frame because of the excessive rigidity; 2) such semi-finished product requires washing after embroidery in order to remove gelatin. Consequently, such method of stabilization is not recommended for denim-like fabrics. Setting the main fabric in the embroidery frame with the stabilizing non-stretch material (non-woven fabric polyester 100%, 50 g/m^2) did not allow obtaining sufficient tension of the main material in embroidery frame.

Sample 3 Sample 4 Sample 5 Sample 6

Figure 10 Samples of the embroidery products made of denim-like fabrics

Table 5 Comparable analysis of the methods of stabilization of embroidered semi-finished product at the "blind search" stage (sample No. 4)

No. of experiment	Method of stabilization	Average score of the experts	Recommendations regarding the use
1	None	0	Not recommended
2	Additional tightening of semi-finished product	2.0	Not recommended because of the possible destruction of the fabric and embroidery frames
3	Gelatinization	1.8	Not recommended because of the difficult setting of the fabric in the embroidery frame and the need for the further washing
4	Setting the fabric in the embroidery frame together with non-glue stabilizing material	0	Not recommended
5	Duplication with interfacing fabric	2.3	Recommended, needs further research – selection of the duplicate material

At the beginning of the embroidery, the thread was torn several times, in connection with that the attempt was defined as unsuccessful. Such method of stabilization is not recommended for denim-like fabrics.

In accordance with the results of the study, the following method of stabilization of the material for embroidery is chosen – duplication with glutinous non-woven fabric (flizelin). Such method has allowed to obtain embroidered semi-finished product of satisfactory quality. This method received the average experts` score 2.3 points out of 3 possible (Table 5). The results of the experiment on selection of the optimal method of stabilization of denim-like fabrics for machine embroidery are summarized in Table 5. So, as a result of the experiment, the recommendation as to the use of duplicate glutinous material for stabilization of denim-like fabrics for machine embroidery is scientifically grounded at the "blind search" stage.

Using the developed recommendations, denim products, made from samples 3, 4, 5 and 6, have been embroidered (Figure 10). For the materials of the first group in regard to their elasticity (sample 6, elongation at rupture is more than 30 - 40%) additional duplication with the second layer of non-woven fabric (flizelin) has been applied at the embroidery image area, without the second layer has fallen under the embroidery frame.

5 CONCLUSIONS

1. As a result of the analysis of 7 samples of the materials of suiting group of "stretch-denim" type, is has been found that elongation at rupture in weft of all of the samples exceeds the value of such indicator in warp and reaches 37.5%, and the samples with elastane and polyamide content have higher value of the indicator. The conducted correlation analysis showed a strong correlation between weight and force at rupture in warp (r = 0.84), as well as between weight and thickness (r = 0.74). Thus, as a result of the conducted experimental researches, the samples of denim-like fabrics are conventionally divided

into 3 groups in accordance with their elongation at rupture in weft: 1) with a large value 30 - 40%; 2) with a medium value 20 - 30%; 3) with a low value 15 - 20%.

2. The classification of the defects of embroidered semi-finished products is improved. All defects are divided into: 1-dimensional: defects of the stitch, 2-dimensional: defects of setting the fabric in the embroidery frame, embroidery defects; and 3-dimensional: deformation of the embroidered area; deformation of the area, adjacent to the embroidered area; deformation of the materials along the embroidery frame line.
3. The method of evaluation of the quality of semi-finished products embroidery using the 4-point scale (where 0 – unsatisfactory, 3 – no identified defects) is proposed. Evaluation of embroidery with a complex design is recommended to be carried out separately for each area of the image.
4. As a result of the selection, received during the “blind search”, the use of duplicate glutinous material for stabilization of denim-like fabrics for machine embroidery is recommended. Using the developed recommendations, products made of denim-like fabrics have been embroidered.
5. Further researches will be aimed at optimization of the composition and parameters of duplicating materials in order to stabilize denim-like fabrics for the machine embroidery.

6 REFERENCES

1. Wojciechowska I.: The changing face of denim, AATCC Review 17(4), 2017, pp. 26-31, DOI: https://doi.org/10.14504/ar.17.4.1
2. Ancutiene K., Koldinska M., Havelka A.: Investigation of tensile resilience properties of stretch denim fabrics, Indian Journal of Fibre & Textile Research (IJFTR) 42(2), 2017, pp. 175-182
3. Pashkevich K.L., Kolosnichenko M.V., Ostapenko N.V.: Research of some physical and mechanical characteristics of suiting fabrics for designing the clothes, Vlakna a Textil 23(1), 2016, pp. 3-8
4. Malek S., Khedher F., Jaouachi B., Cheikrouhou M.: Determination of a sewing quality index of denim fabrics, The Journal of The Textile Institute 109(7), 2018, pp. 920-932, DOI: 10.1080/00405000.2017.1385968
5. Değırmencı Z.: Study on the loss of strength of denim-like knitted fabrics after different washing treatments, Fibres & Textiles in Eastern Europe 25(3), 2017, pp. 98-105, DOI: 10.5604/12303666.1237244
6. Kurtulmuş O., Güner S., Akkaya M. S., Kayaoğlu B.K.: Design and development of denim fabrics with improved strength and impact abrasion resistance for motorcyclist clothing, Fibres & Textiles in Eastern Europe 26(1), 2018, pp. 53-58, DOI: 10.5604/01.3001.0010.7797
7. Suteu M.: Analysis of embroidery pattern influence on the working mode of "Happy" embroidery machine by using the vibration measurement technique, Industria textila 67(4), 2016, pp. 250-255
8. Suteu M., Indrie L., Gherghel S., Timofte A.: Identifying the points that represent potential defects in embroidery machines using infrared thermography, Industria textila 66(1), 2015, pp. 39-42
9. Daukantiene V., Laurinaviciute I.: The synergism of design and technology for the optimisation of embroidery motifs in clothing, International journal of clothing science and technology 25(5), 2013, pp. 350-360, DOI: 10.1108/IJCST-03-2012-0007
10. Indrie L.; Kazlacheva Z., Ilieva Ju., Gherghel S.: Embroidery - from digital designing to fine art, Industria textila 68(5), 2017, pp. 366-369
11. Shih C.Y., Kuo CFJ., Cheng JH.: A study of automated color, shape and texture analysis of Tatami embroidery fabrics, Textile Research Journal 86(17), 2016, pp. 1791-1802, DOI: 10.1177/0040517515609253
12. ISO 139:2005. Textiles - Standard atmospheres for conditioning and testing
13. ISO 5084-1996. Textiles - Determination of thickness of textiles and textile products
14. ISO 13934-1:2013 Textiles - Tensile properties of fabrics - Part 1: Determination of maximum force and elongation at maximum force using the strip method
15. Buzov B.A., Rymiantseva G.P.: Materials for clothes. Fabrics, Moscow, Forum Infra-M, 2012, pp. 108-116
16. GOST 21790-2005. Cotton and mixed fabrics for garment. General specifications
17. Chung-Feng Jeffrey Kuo, Yun Juang.: A study on the recognition and classification of embroidered textile defects in manufacturing, Textile Research Journal 86(4), 2015, pp. 393-408, DOI: https://doi.org/10.1177/0040517515590410
18. Tikhomirov V.B.: Planning and analysis of the experiment, Moscow, Legkaya industriya, 1974

DEFINING THE MAIN FEATURES OF CLOTHING TO APPLY DEEP LEARNING IN APPAREL DESIGN

Oksana Zakharkevich, Anna Selezneva, Svetlana Kuleshova, Alla Slavinskaya, Julia Vovk and Galina Shvets

Khmelnitskyi National University, Department of Clothing Design and Technology
Institytska str. 11, 29016 Khmelnitskyi, Ukraine
zbir_vukladach@ukr.net, sellannyshka@gmail.com

Abstract: *The paper is devoted to defining the features of clothing to apply deep learning in apparel design. The images of women's outerwear were selected with the help of reverse image search. The images of women's duffle coats, coats and suit jackets were selected. The selected material was sampled for the next categorical principal components analysis and general assessment of differences that are caused by specific features of garments. It was revealed that similarity search might be used to perform the selection of models to define the typical design solutions. However, a process of defining the solutions cannot be automated yet. The indicators of clusters, which were revealed in the result of the categorical principal components analysis, define the structure of the database for the deep learning. Based on the results of performed online survey, it was considered advisable to use as labels specific features of the particular garment type rather than its name. Each label refers to one of the main features of a garment type.*

Keywords: *deep learning; garment type; features of garment; similarity search.*

1 INTRODUCTION

Although clothing design is one of the most creative realms in the contemporary world; it is a highly developed technological industry as well. However, the great part of designer's work is not performed with the help of computers. Whether it is because of considerable creative part of design process or equivocal information about clothing, the fact remains to be.

Internet shopping has incredibly increased in the last years, and fashion created an interesting application field for image understanding and retrieval, since hundreds of thousands images of clothes constitute a challenging dataset to be used for automatic or semi-automatic colour analysis, texture analysis, similarity retrieval and so on [1]. Such tasks are performed with methods of machine learning, part of which is deep learning. Deep learning trains a computer to perform human-like tasks, such as recognizing speech, identifying images or making predictions [2]. Instead of organizing data to run through predefined equations, deep learning sets up basic parameters about the data and trains the computer to learn on its own by recognizing patterns using many layers of processing.

Fashion is an entirely new direction for machine learning, but it is far from to be an exception from the list of possible applications. The opportunities for deep learning in the fashion domain are very versatile. Researches all over the globe work with algorithms of machine learning, which are universal and therefore, it is possible to use them for the purposes of apparel design and fashion industry. For example, the results, which were described in [3], allow the user to translate the image into the text that might as well be interpreted as a description of the garment, based on its sketch.

Authors of [4] suggest that in the domain of visual search, with a focus on image similarity for online shops, understanding images of clothing means more than just classifying them into coarse categories. In order to get a meaningful description of the whole image, one needs to decompose the image into its parts. In addition, to train the machine to recognize the clothes, it is required to use a large dataset because of the great number of apparel categories [5]. Furthermore, in contrast to other domains, fashion images are usually annotated with one or more categories (labels) since these pictures are often used directly in some kind of online shop or catalogue website or fashion portal. The report [6] says that the number of global online shoppers will grow by 50% from 2013 to 2018, from 1.079 billion to 1.623 billion. Clothing is the most frequently purchased online category of goods. Furthermore, according to [7] the growth of the global women's apparel market will accelerate, driven by a shift to the faster growing, emerging markets. It shows that there is a wide range of possibilities to develop the online searching techniques. Thus, fashion industry is the market, which has great future in the area of computer vision [8, 9].

However, fashion and apparel design are not exactly the same. Apparel design focuses on the garment manufacturing while fashion is concentrating on the clothing distribution. Hence, the application of deep learning in apparel design means to be of help for a patternmaker while deep learning in fashion is a help for a consumer or a fashion retailer. Thus, available fashion search engines are to be examined in order to determine the extent of their possible applications in domain of apparel design rather than fashion.

Fast and accurate fashion item detection model, based on deep neural networks, was proposed in [9]. Results, obtained by authors, make it possible to use their model for the task of fashion item detection and recognition, followed by visual similarity search.

To design clothes, one should know and understand the mechanisms of fashion: causes and spreading of the trends, principles of cyclic repetition and evolution patterns. Considering all of the above, designers develop the fashion of tomorrow. The authors of [4] suggest that now the task of designing or predicting trends can be simplified, thanks to a new class of neural networks. These networks can automatically allocate shapes, elements and types of clothing and further combine them.

The dashboard, developed by [5], allows seeing “how frequently a particular type of garment appears per day, what kind of apparel is popular within a certain age range, how people match their garments, etc.” Authors [5] developed the graph showing the predictions of how popular certain types of garments would be over the next season that could be up to five months. This kind of analysis aims to help fashion retailers plan sales and avoid any surplus.

Snap Fashion [11, 12] is one of the first projects in this area. It has already been several years on the market. The accuracy of search is low though. It is based mostly on the item’s colour.

Project ASAP54 [11, 13] allows one to find an item by its colour taking into account several additional characteristics, which are to be ascribed by user.

IPhone App "Take pictures of clothes" [14] allows one to search the items by computer vision technologies developed by Yandex. The process is as follows: an algorithm defines the garment in the image, and then it compares similar pictures, which are available in the web, and at last, it provides the user with the images of items, which have the most similar appearances to the original image.

«GETSARAFAN» [11, 15] is the project that is still under development. The main issue of the project is so called semantical gap. It means there is a difference between machine perception of an image and human perception of the same image. The main idea of the project is to label an enormous set of garment images with specific labels, teach the classificator, and to classify the segmented images in that way.

Above mentioned projects have a common purpose, that is so called «similarity search», which allows finding the images that are similar to the original image by its general characteristics such as dimension, number of pixels, colour.

The result of such search is the list of items, which make the same impression as the original garment. However, these items differ by their design characteristics. Therefore, they even might belong to different garment types [16, 17]. It is unacceptable situation for the clothing designer.

2 DISCUSSING IDEAS

Modern pattern design systems relay the functions of clothing designer to a computer user. Presence of two design subsystems in such software, the first one aims at creating the sketch and the other one at drafting the garment construction, allows designing the garment in complete accordance with the original idea.

In the era of global digital technologies, most of the sketch creating subsystems most likely can be used for searching through the catalogues of apparel garments in the Web as well as for the review of online fashion shows in order to forecast the fashion tendencies and retrieving of the most frequently used elements of the fashionable outfits. Google Images is a search service owned by Google. It allows users to search the Web for image content and most likely can be used for the garment search as well. According to [2], the question of differences between the specific garments types might cause misunderstandings in design process due to the ambiguous definitions that lead designers to the completely different appearances of the garments.

Deep learning is a popular means of new era of technology that provides ability to exclude human factor and differences in experts’ opinions from specific steps of design process. The supervised learning is the task of inferring a function from labelled training data that consist of a set of training examples. Deep learning in apparel design means that the training examples are labelled pictures of garment types. Differences in definitions of garments types especially in different languages are the obstacles in the way of successful online search, preparing technical documentation [18], development and implementation of expert systems and other elements of artificial intelligence in apparel design [19]. Therefore, in order to make a qualified fashion review or perform an online searching of specific garments with keywords, it is necessary to determine the description of each garment type and its main features.

3 METHODS

In order to investigate the possible applications of deep learning in domain of apparel design, it was determined to use the methods of online surveys as well as methods of statistical analysis and data mining. A set of images, which display a particular garment type, was obtained with Google reverse image search. Consumer impressions from clothes, which were found by similarity search with tools of Google Images, were assessed with the help of method of semantic differential, which is described in [18, 21]. Categorical principal components analysis was used to graphically display the relationship between the garment features that result in significant differences in appearances or impressions of the garments, which were found by similarity searching. The chosen method optimizes distances between objects and it is very useful for the primary interest is difference or similarity between the objects.

4 EXPERIMENTAL

Online survey that was performed through social networks in order to determine the name of the specific garment type, which is a duffle coat, shows that experts, whose area of expertise is clothing design, are not able to perform the task unanimously or even within statistical error (Figure 1). The expert group consisted of 67 experts.

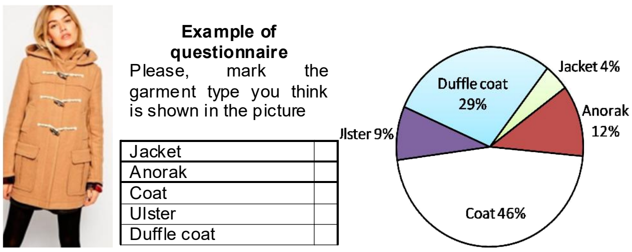

Figure 1 Results of the survey in the social media

As it can be seen in the Figure 1, only 29% of examined group were able to recognize a duffle coat in the image. Hence, it is advisable to use as labels specific features of the particular garment type rather than its name because the features are standard and can be determined specifically.

In order to reveal the prospects of utilizing the similarity search in the domain of apparel design actual image search was performed by tools of Google Images (Figure 2). The original image of duffle coat is the same that was used for the online survey (see Figure 1). Original images of coat and suit jacket are presented in the Figure 3. As it is displayed in the Figure 4, only half of the found images might be of any aid for the designing purposes, for the other half contains the images of different types of women's coats that are not the duffle coats.

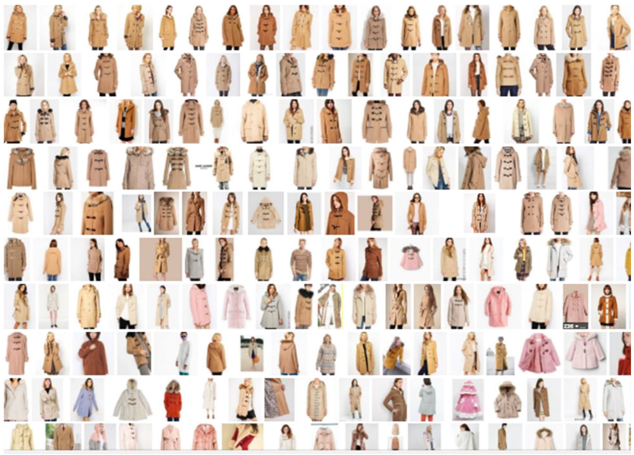

Figure 2 Results of the search by image algorithm of Google images (a fragment)

Figure 3 Original images of coat and suit jacket

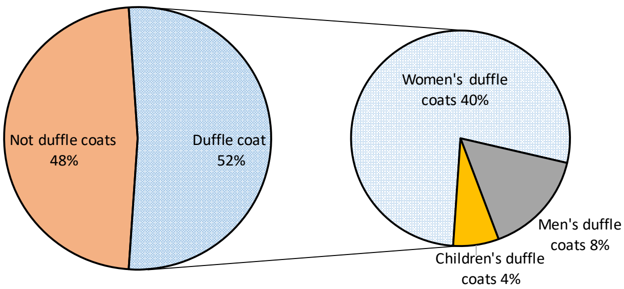

Figure 4 Quantity analysis of the images

While searching images of coats, it was discovered that only 53.9% meet the requirements, and actually, are coats. Among them 97.4% of images are women's garments, 1.55% – men's garments, 1.05% – clothes for children. Among presumably images of suit jackets, only 70.61% are actually women's suit jackets, 27.19% – men's suit jackets, 2.2% – clothes for children.

For the next step of current research, the number of examined items decreased to the number of actual women's duffle coats. In order to use categorical principal components analysis, which would be performed with tools of the package PASW Statistics [22], every single garment was described with a code, which consisted of Arabian numerical codes of certain features of the garment (Table 1). The list of the considered features is as follows: silhouette (S), length (L), form (F), toggle-fastenings (TF), fastenings (Fs), yoke (Y), pockets (P), hood (H), trimming (T), collar (C), seams (Ss), Cut (Cut). A garment, which was the origin of the search, has a code like follows: 1.2.1.2.1.1.5.1.6.1.1.1. The other ones were coded according to the developed code system, example of which is displayed in the Table 1.

Table 1 Example of the Code System

Code	Collar	Code	Hood	Code	Form
1	No collar	1	Stitched hood	1	Rectangular
2	Convertible collar	2	Stitched hood with fur	2	Trapezoid (long base down)
3	Standing straight collar	3	Removable hood	3	Oval
…	…	4	Removable hood with fur	4	X-shaped
…	…	5	No hood	…	…

The list of considered features of coats is as follows: silhouette (S), length (L), form (F), buttons (B), Cut (Cut), collar (C), pockets (P), seams (Ss), additional details (AD), fastening (Fs), hood (H). Considered features of suit jackets are as follows: silhouette (S), length (L), form (F), buttons (B), Cut (Cut), collar (C), pockets (P), seams (Ss), additional details (AD), fastening (Fs). Each feature is presented in the numerical codes of garments' images.

The procedure of categorical principal components analysis simultaneously quantifies categorical variables while reducing the dimensionality of the data. Two most important components, which show the combined impact of all considered features, were selected out as dimensions for the graphical visualization of the results of the current research. The most important dimension 1 refers to the component 1 that is "form" (for the duffle coats, coats, and suit jackets) and the second one, dimension 2, refers to the component 2 that means "fastenings" (for the duffle coats) or "buttons" (for the coats and suit jackets).

Besides that, photos of clothes were valued using valuation factors in bipolar scales defined by verbal antonyms of Kansei words, which were described in [18, 21]. Thus, each image was represented as a list of the average meanings of the estimated coefficients of semantical differential, which is called psychographic profile, for six pairs of Kansei words: symmetry - asymmetry (SA), bright – soft (BS), casual – smart clothes (CS), transparent – non-transparent (TN), folk – modern clothes (FM), trapezoid shape (long base down) – trapezoid shape (long base up) (TdTu). The garments, which were the origins of the search, have profiles like follows: -3.0.-1.3.-2.-3 (duffle coat), -3.1.0.3.-2.3 (coat), -3.-2.0.3.-1.3 (suit jacket). The procedure of categorical principal components analysis allowed selecting two dimensions as well as estimating the loadings of the principal components (table 2). The components are TdTu and BS (for the duffle coats), CS and TN (for the coats), and CS and TdTu (for the suit jackets).

Table 2 Loadings of the Principal Components (Impressions)

Component	TdTu	BS	FM	CS	TN	SA
1	0.970	-1.240	1.191	1.354	-0.437	0.280
2	-0.885	0.538	0.947	0.518	1.489	1.243

5 RESULTS

Objects plots (Figure 5) display the differences between clusters of images. Objects are labelled by the category indicator values. One object plot is produced per variable, which is the feature of garment.

Each graph in the Figure 5 displays two clusters that differ significantly by one of the follows features: F, SS, C, or H. The form and the style seams are the features that cause the change of garment draft and the style. Particularities of the collar and hood cause differences in assembly techniques and a marker for the cutting. The size of each cluster that differs is considerable in comparison to the general size of the examined population of images. The number of items, which differ by features of the collar and hood, is 26 garments that is about 25% of the population of examined images of the duffle coats. The number of items, which differs by features of the form and style seams, is lesser. It is only four items for the form and eight items for the style seams, which compose a small cluster of ten images. It is about 10% of the population of the duffle coats. However, because of all these differences a considerable part (about 72%) of the original population of the search results, which are displayed in the Figure 6, is no use for the garment industry.

Similar results were obtained for the other garment types. About 19% of images differ from the majority by the feature "silhouette", 13.8% – by the feature "form", and 25% – by the feature "cut". About 22.4% of images of suit jackets differ by the feature "silhouette", 14.9% - by the feature "form", and 11.8% – by the feature "buttons". On the other hand, the graphs in the Figure 6 display that all found images of the duffle coats cause the similar consumer's impressions from clothes. Several items, which differ from the main cluster by certain impression like TN "transparent – non-transparent" (Figure 6a) or "trapezoid shape (long base down) – trapezoid shape (long base up)" (Figure 6b), compose a small proportion that is insignificant in the general population of examined images. The part of each one is about 3% and 2% respectively. The same goes to the results of analysis the images of suit jackets and coats (Figures 7 and 8).

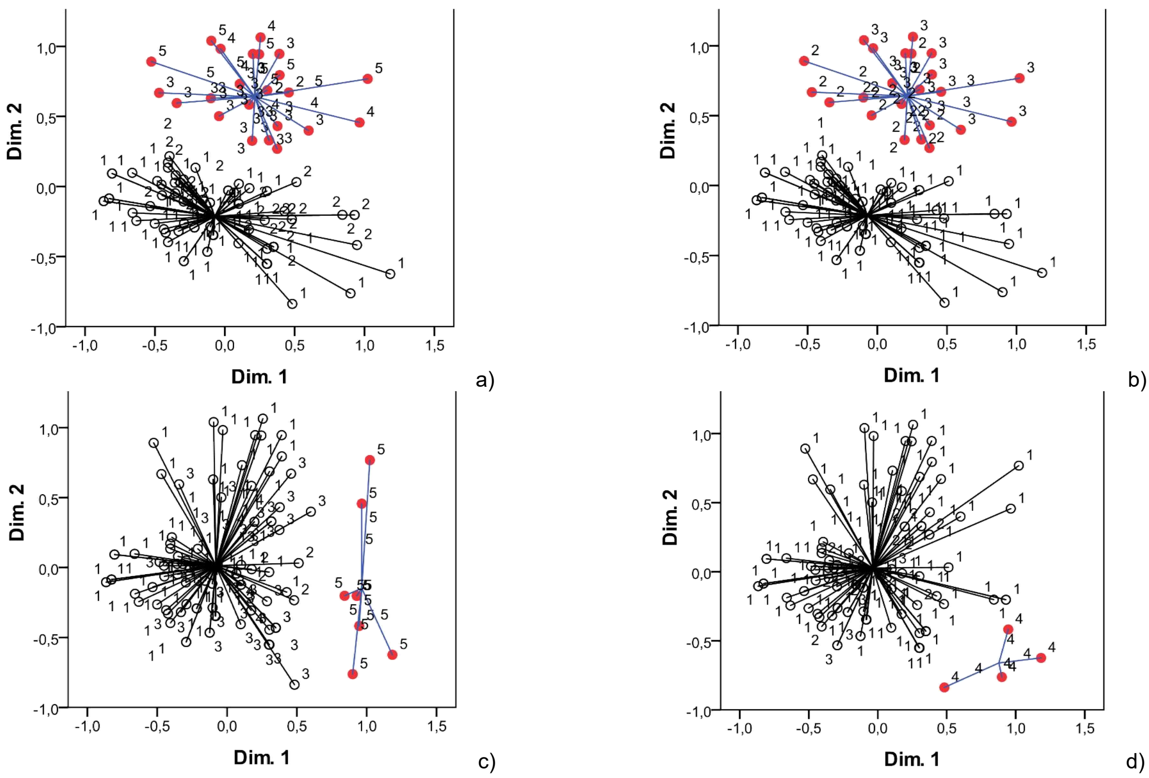

Figure 5 Results of the Categorical principal components analysis based on codes of garments: a) hood; b) collar; c) style seams; d) form

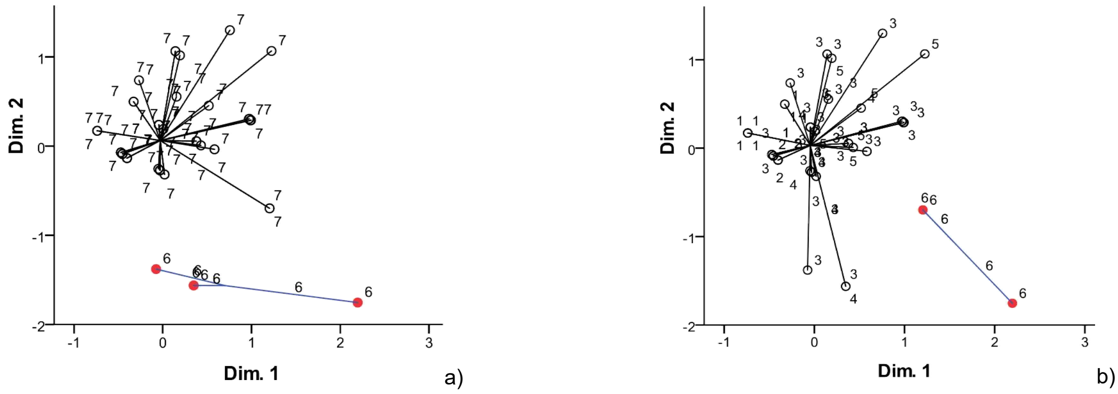

Figure 6 Results of the Categorical principal components analysis based on consumer's impressions of duffle coats images: a) TN; b) TdTu

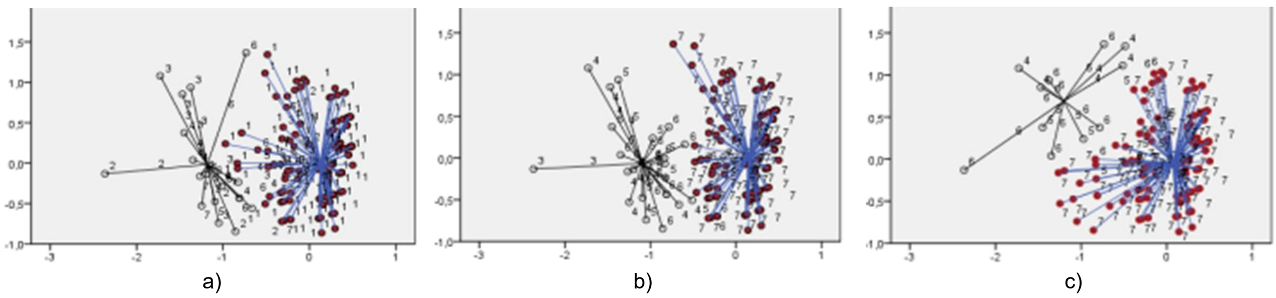

Figure 7 Results of the Categorical principal components analysis based on consumer's impressions of coats images: a) SA; b) TN; c) FM

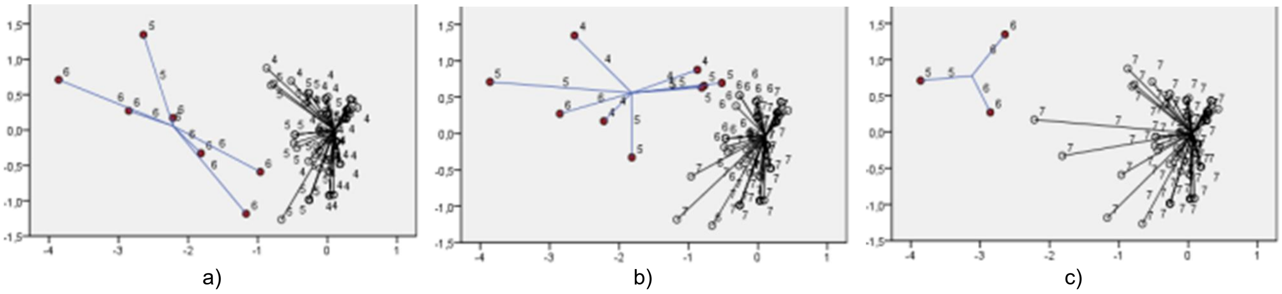

Figure 8 Results of the Categorical principal components analysis based on consumer's impressions of suit jackets images: a) TdTu; b) TN; c) FM

Therefore, it is impossible to disagree with the statement of [22] about the need to consider every single fashion item as a whole concept that has to do with human perception of contemporary world.

6 CONCLUSIONS

As a result of the current research, it was displayed that the task of organizing the database of properly labelled images of garments is the first step to performing automatic fashion reviews, online searching and forming descriptions of garments. Based on the results of performed online survey, it was considered advisable to use as labels specific features of the particular garment type rather than its name because the features are standard and can be determined specifically.

Analysis of images of outerwear, which were obtained with the help of reverse image search, was conducted. The images of women's duffle coats, coats, and suit jackets were selected. The selected material was sampled for the next categorical principal components analysis and general assessment of differences that are caused by specific features of garments.

It was determined that less than 30% of original population of images were sampled with required level of accuracy. However, all found images of the certain clothing types cause the similar consumers' impressions. Hence, although it is certain that deep learning has great future in domain of apparel design, for now it can be used only for the purposes of similarity search for the online shops, which are oriented to the consumers' impressions rather than to retrieving the features of fashionable outfits.

Similarity search might be used to perform the selection of models to define the typical design solutions. However, a process of defining the solutions cannot be automated yet.

Thus, there is a need to form a database for the deep learning in apparel design. Such database must consist of the images, which are labeled with a set of labels. Each label refers to one of the main features of a garment type. Furthermore, it is important to form different databases for the different garment types. The structure of such databases must correspond to the indicators of clusters, which were revealed in the result of the categorical principal components analysis.

ACKNOWLEDGMENT: *The results shown in the paper resulted from the Scientific Project "Development of the Principles of Heuristic Clothing Design to Develop a Prototype of the Expert System for Rapid Change in Production of Clothes", Grant of the Ministry of Education and Science of Ukraine № 0117U003889.*

7 REFERENCES

1. Grana C., Manfredi M., Calderara S., Cucchiara R.: Garment Selection and Color Classification, 2015, Available: http://imagelab.ing.unimore.it/imagelab2015/researchactivity.asp?idAttivita=18 [2017-08-03]
2. What is deep learning? SAS, Available: https://www.sas.com/en_za/insights/analytics/deep-learning.html [2017-08-08]
3. LeCun Y., Bengio Y., Hinton G.: Deep Learning, Nature 521, 2015, pp. 436-444,
   doi: https://doi.org/10.1038/nature14539
4. Firman T., Getmanskyi V.: Designing Apparel with Neural Style Transfer, 2016, Available: http://labs.eleks.com/2016/09/designing-apparel-neural-style-transfer.html [2017-08-03]
5. Romaniuk O.: Fashion and Technology: How Deep Learning Can Create an Added Value in Retail, 2017, Available: http://labs.eleks.com/2017/05/fashion-technology-deep-learning-can-create-added-value-retail.html [2017-08-03]
6. Evans K.: The number of global online shoppers will grow 50% by 2018, 2015, Available: https://www.digitalcommerce360.com/2015/03/31/number-global-online-shoppers-will-grow-50-2018/
7. Lu S.: Unleashing Fashion Growth City by City - FASH455 Global Apparel & Textile Trade and Sourcing, 2014, Available: https://shenglufashion.wordpress.com/2014/10/17/unleashingfashion-growth-city-by-city/
8. Pogrebnyak M.: Why (and what for) we taught the neuron web to recognise dresses and shoes, Rusbase, 2016, Available: https://rb.ru/longread/neirony/

9. Smirnov E., Kulinkin A., Ivanova K., Pogrebnyak M.: Deep Learning for Fast and Accurate Fashion Item Detection, 2016, Available: https://kddfashion2016.mybluemix.net/kddfashion_finalSubmissions/Deep%20Learning%20for%20Fast%20and%20Accurate%20Fashion%20Item%20Detection.pdf [2017-08-03]
10. Search for images with reverse image search – Google Search Help, Available: https://support.google.com/websearch/answer/1325808?hl=en [2017-08-07]
11. Computer vision: recognition of clothing in pictures with help of mobile app / Blog of Anetika Company / Habrahabr, 2014, Available: https://habrahabr.ru/company/anetika/blog/241343/
12. Snap Fashion – Shop Fashion in a Snap, 2017, Available: https://www.snapfashion.co.uk/
13. Asap54 / Fashion Search / Fashion Price Comparison, Available: https://www.asap54.com/
14. Bogoliubov L.: Take pictures of clothes: clothing search based on its image, App Tractor, 2016, Available: http://apptractor.ru/info/news/snimite-odezhdu poiskodezhdyi-po-fotografii.html
15. Sarafan – Clothing search based on photo, Available: https://getsarafan.com/
16. Sviruk L., Kurochka S., Zakharkevich O., Kuleshova S.: Application of deep learning in apparel design, International Conference on Technics, Technologies and Education ICTTE 2017, Yambol, Bulgaria, October 19-20st, 2017, pp. 83-91
17. Vlasyuk N., Zakharkevich O., Dzyuba J.: Computer recognition of garment types based on their images, Resource-Saving Technologies of Light, Textile & Food Industry: Proceedings of Ukrainian Scientific-Practical Internet-Conference of Young Scientists & Students, November 16-17, 2017, Khmelnytskyi: KhNU, 2017, pp. 71-72
18. Vovk Y.V., Slavinska A.L.: Working out unification of transformation type of the base design of the female skirt in the base design of trousers, Proceedings of higher education institutions, Textile industry Technology 6(354), 2014, pp. 84-89
19. Yakymchuk D., Yakymchuk O., Chepeliuk O., Myrhorodska N., Koshevko J., Orlenko O.: Study of cutting presses in designing a women's costume for hospitality industry, Eastern European Journal of Enterprise Technologies vol.5, no 1 (89), 2017, pp. 26-36, DOI: https://doi.org/10.15587/1729-4061.2017.110962
20. Kuleshova S.G., Zakharkevich O.V., Koshevko J.V., Ditkovska O.A.: Development of expert system based on Kansei Engineering to support clothing design process, Vlakna a Textil 24(4), 2017, pp.30-41
21. Kurochka S., Sviruk L., Kuleshova S., Zakharkevich O.: Method of analyzing images of clothes based on Kansei Engineering, International Conference on Technics, Technologies and Education ICTTE 2017, Yambol, Bulgaria, October 19-20st, 2017, pp. 92-99
22. IBM SPSS Statistics – Essentials for Pyton 24.0 [Windows XP]. Available: https://www.ibm.com/us-en/marketplace/statistical-analysis-and-reporting [2017-08-03]
23. Picalica Blog Deep Learning Opportunities in Fashion, 2014, Available: https://www.picalike.com/blog/2014/02/20/deep-learning-opportunities-in-fashion/ [2017-08-03]

INSTRUCTIONS FOR AUTHORS

The journal ,,**Vlákna a textil**” (**Fibres and Textiles**) is the scientific and professional journal with a view to technology of fibres and textiles, with emphasis to chemical and natural fibres, processes of fibre spinning, finishing and dyeing, to fibrous and textile engineering and oriented polymer films. The original contributions and works of background researches, new physical-analytical methods and papers concerning the development of fibres, textiles and the marketing of these materials as well as review papers are published in the journal.

Manuscript

The original research papers are required to be written in English language with summary. The advertisements will be published in a language according to the mutual agreement.

The first page of the manuscript has to contain:

The title of the article (16 pt bold, capital letters, centred)

The full *first name* (s) and also *surnames* of all authors (11 pt, bold, centred).

The complete address of the working place of the authors, e-mail of authors (9 pt, italic, centred)

Abstract (9 pt, italic)

Key words (9 pt, italic)

The manuscript has to be written in A4 standard form, in **Arial, 10 pt**.

The text should be in ***double-column format*** *(width 8.1 cm)* ***in single line spacing***.

Page margins: up and down 2.5 cm; left and right 2.0 cm.

Do not number the pages and do not use footnotes. Do not use business letterhead.

Figures, tables, schemes and photos (centered) should be numbered by Arabic numerals and titled over the table and under the figure or picture.

Photos and schemes have to be sufficiently contrastive and insert in text as pictures.

Figures, tables, schemes and photos, please, send in separate file.

Mathematical formulae should be centred on line and numbered consecutively on the right margin.

Physical and technical properties have to be quantified in SI units, names and abbreviations of the chemical materials have to be stated according to the IUPAC standards.

References in the text have to be in square brackets and literature cited at the end of the text. References (9 pt), have to contain names of all authors.

[1] Surname N., Surname N.: Name of paper or Chapter, In Name of Book, Publisher, Place of Publication, YYYY, pp. xxx-yyy

[2] Surname N., Surname N.: Name of paper, Name of Journal Vol. (No.), YYYY, pp. xxx-yyy

[3] Surname N., Surname, N.: Title of conference paper, Proceedings of xxx xxx, conference location, Month and Year, Publisher, City, Surname N. (Ed.), YYYY, pp. xxx-yyy

[4] Surname N., Surname N.: Name of Paper, Available from http://www.exact-address-of-site, Accessed: YYYY-MM-DD

The final template of manuscript is available on **http://www.vat.ft.tul.cz**

Authors are kindly requested to deliver the paper (in Word form) to be published together with information about at least 3 recommended reviewers from institutions others than the parent (name, e-mail, institution, department) by e-mail: marcela.hricova@stuba.sk

After successful review procedure there is charged fee (article processing charge) of EUR 100. All articles after review process are freely available online and this fee helps to cover the costs of taking a manuscript and turning it into a finished article.

Address of the Editor Office:

Marcela Hricová

Faculty of Chemical and Food Technology,

Slovak University of Technology in Bratislava

Radlinskeho 9

812 37 Bratislava,

Slovakia